Technische Universität München
TUM School of Engineering and Design

Multiple links in a common constellation: A ranging and time reference based on satellites

Stefan Marz

Vollständiger Abdruck der von der TUM School of Engineering and Design der Technischen Universität München zur Erlangung des akademischen Grades eines

Doktors der Ingenieurwissenschaften (Dr.-Ing.)

genehmigten Dissertation

Vorsitz: Prof. Dr.-Ing. Florian Seitz

Prüfende der Dissertation:

1. Prof. Dr. phil. nat. Urs Hugentobler
2. Prof. Dr.-Ing. Susanne Glaser

Die Dissertation wurde am 25.03.2024 bei der Technischen Universität München eingereicht und durch die TUM School of Engineering and Design am 13.08.2024 angenommen.

Abstract

This dissertation evaluates the impact of the combination of different observation techniques for Precise Orbit Determination (POD) and clock synchronization of satellites in a future GNSS (Global Navigation Satellite System) satellite constellation. The aim is to develop a concept for establishing a GEodesy and Time Reference In Space (GETRIS) based on satellites. GETRIS shall able to carry out ranging and time transfer to satellites not only in the near-Earth environment, but also in deep space – up to lunar distances and beyond. Precisely determined orbits and synchronized clocks are key features for the progress in many satellite applications as well as Earth science and deep space missions. In order to be able to use satellites in a constellation as a GETRIS, the orbits are aimed to be known at least at the same level as possible for ground stations – at about 1-3 mm, comparable to the accuracy requirement of GGOS (Global Geodetic Observing System). Satellite clocks shall be synchronized at the picosecond level.

To conduct a POD simulation study, we defined three basic aspects forming three key pillars that have to be taken into account: Instrumentation, geometry and modelling. By analyzing the key pillars, two observations techniques were selected to be used together with GNSS L-band measurements to build the measurement network for a GETRIS: Optical Inter-Satellite Links (OISL) and the ground-space oriented counterpart OTWL (Optical Two-Way Links). Both techniques were chosen as they are the most complementary to L-band observations. While OISL enhances the measurement geometry, OTWL supports L-band in measuring to the ground. Thereby, L-band and OTWL are collocated in space and on ground. The intention is that due to the complementarity, the advantages of each observation technique can compensate disadvantages of the other technique(s). L-band measurements are independent of the weather and establish multiple one-way links. OTWL and OISL are operated as two simultaneous one-way links, representing a two-way measurement concept. The optical links can be calibrated regularly, are less influenced by systematic errors and clocks can be largely synchronized, as they are two-way links. The link types are combined in several ways – L-band+OISL, L-band+OTWL and L-band+OTWL+OISL – and are compared with each other as well as to L-band-only solutions. For L-band and OTWL observations, a small ground station network consisting of 16 stations is used. First, the analysis is carried out for a satellite constellation built on Medium Earth Orbit (MEO) satellites. Second, the constellation is expanded by geosynchronous orbit (GSO) satellites – inclined geosynchronous orbit (IGSO) and geostationary orbit (GEO) satellites. Furthermore, it is shown that the parameter decorrelation (e.g. between satellite altitude, time synchronization and troposphere zenith delays) due to the complementary use of the link types, allow the estimation of additional orbit modelling parameters. By analyzing the orbit modelling errors, empirical parameters are selected that are estimated in addition to the Empirical CODE Orbit Model 2 (ECOM2) parameters. It is investigated how well the different link combinations can handle the parameter correlations and to what extent the expanded empirical parameter model can improve the orbit solution. For a satellite clock analysis, all scenarios are simulated with respect to two different clock types. The first type of clock is the PHM (Passive Hydrogen Maser), which is already used in current GNSS satellites. The ACES (Atomic Clock

Ensemble in Space) clock is selected as a clock type of high stability for comparisons. It is investigated how well the PHM clocks contribute to establish a GETRIS and to what extent ACES clocks can improve the accuracy of the clock solution.

The outcome of this dissertation is the finding that the optical links greatly support L-band in combined use – they help to largely reduce systematic errors, such as e.g. multipath, phase center variations and troposphere parameters, and to synchronize the clocks. It is shown that for MEO, IGSO and GEO satellites an orbit accuracy at the low millimeter level and a picosecond clock accuracy can be achieved in our simulations. Thereby, the best link scenario is the L-band+OTWL+OISL scenario. The analysis points out that not only a complementary use of all the three observation techniques is possible but also that the synergy of a combined use of OTWL and OISL has a substantial impact on the achievable orbit and clock solutions, compared to L-band+OTWL and L-band+OISL scenarios.

Zusammenfassung

Diese Dissertation untersucht den Einfluss von Kombinationen verschiedener Beobachtungstechniken zur präzisen Bahnbestimmung (POD, *Precise Orbit Determination*) und Uhrensynchronisation von Satelliten in einer zukünftigen GNSS-Satelliten-Konstellation. Ziel ist die Entwicklung eines Konzepts zur Etablierung einer Geodäsie- und Zeit-Referenz im Weltraum (GETRIS, *GEodesy and Time Reference In Space*) basierend auf Satelliten. GETRIS soll Entfernungsmessungen und Zeittransfer zu Satelliten nicht nur in der erdnahen Umgebung, sondern auch im Weltraum – bis hin zu Mondentfernungen und darüber hinaus – durchführen können. Präzise bestimme Satellitenbahnen und synchronisierte Uhren sind Schlüsselmerkmale für die Weiterentwicklung bei vielen Satellitenanwendungen sowie erdwissenschaftlichen und Weltraummissionen. Um Satelliten in einer GETRIS Konstellation nutzen zu können, sollen die Satellitenbahnen mindestens auf dem gleichen Level bekannt sein, wie es für Bodenstationen möglich ist – etwa 1-3 mm, vergleichbar mit den Genauigkeitsanforderungen von GGOS (*Global Geodetic Observing System*). Satellitenuhren sollen auf Pikosekunden-Genauigkeit synchronisiert werden können.

Um eine POD Simulationsstudie durchzuführen, haben wir drei Aspekte definiert, die drei Grundpfeiler bilden, die berücksichtigt werden müssen: Instrumentierung, Geometrie und Modellierung. Durch die Analyse der Grundpfeiler wurden zwei Beobachtungstechniken ausgewählt, die zusammen mit GNSS L-Band-Messungen das Messnetzwerk für ein GETRIS bilden: Optische Intersatellitenverbindungen (OISL, *Optical Inter-Satellite Links*) und das Boden-Weltraum gerichtete Gegenstück OTWL (*Optical Two-Way Links*; optische Zweiwegverbindungen). Beide Techniken wurden ausgewählt, weil sie sich am besten mit L-Band Beobachtungen ergänzen. Während OISL die Messgeometrie verbessert, unterstützt OTWL das L-Band bei der Messung zum Boden. Dabei sind L-Band und OTWL sowohl im Weltraum als auch am Boden kollokiert. Die Intention ist, dass durch die Komplementarität die Vorteile jeder Beobachtungstechnik die Nachteile der anderen Technik(en) kompensiert werden. L-Band Messungen sind wetterunabhängig und stellen mehrere Einwegverbindungen her. OTWL und OISL werden als zwei simultane Einwegverbindungen betrieben, was ein Zweiwegmesskonzept darstellt. Die optischen Verbindungen können regelmäßig kalibriert werden, sind weniger von systematischen Fehlern beeinflusst und Uhren können weitgehend synchronisiert werden, da es sich um Zweiweg-verbindungen handelt. Die Linktypen werden auf mehrere Weisen kombiniert – L-Band+OISL, L-Band+OTWL und L-Band+ OTWL+OISL – und miteinander sowie mit einer reinen L-Band Lösung verglichen. Für L-Band und OTWL Beobachtungen wird ein kleines Bodenstationsnetzwerk bestehend aus 16 Stationen verwendet. Zunächst wird die Analyse für eine Satellitenkonstellation durchgeführt, die aus Satelliten auf mittleren Erdumlaufbahnen (MEO, *Medium Earth Orbit*) aufgebaut ist. Zweitens wird die Konstellation um Satelliten in geosynchronen Umlaufbahnen (GSO, *geosynchronous orbit*) erweitert – Satelliten in inklinierten geosynchronen (IGSO, *inclined geosynchronous orbit*) und geostationären Umlaufbahnen (GEO, *geostationary orbit*). Darüber hinaus wird gezeigt, dass die Parameterdekorrelation (z.B. zwischen Satellitenflughöhe, Zeitsynchronisation und Troposphären-Zenit-Verzögerungen), aufgrund der Verwendung der komplementären Linktypen, die Schätzung von zusätzlichen Bahnmodellierungsparametern ermöglicht. Durch die Analyse der Bahnmodellie-

rungsfehler wurden empirische Parameter ausgewählt, die zusätzlich zum *Empirical Code Orbit Model 2* (ECOM2) geschätzt werden. Es wird untersucht, wie gut die verschiedenen Linkkombinationen mit den Parameterkorrelationen umgehen können und inwieweit das erweiterte empirische Parametermodel die Bahnlösung verbessern kann. Für eine Analyse der Satellitenuhr werden alle Szenarien bezüglich zwei verschiedenen Uhrentypen simuliert. Die erste Uhr ist der passive Wasserstoffmaser (PHM, *Passive Hydrogen Maser*), der bereits in aktuellen GNSS-Satelliten verwendet wird. Die ACES (*Atomic Clock Ensemble in Space*) Uhr wird für Vergleiche als hochstabiler Zeitgeber ausgewählt. Es wird untersucht, wie gut die PHM-Uhren zum Aufbau von GETRIS beitragen und inwieweit die ACES-Uhren die Genauigkeit der Uhrenlösungen verbessern können.

Das Ergebnis dieser Dissertation ist, dass die optischen Links im kombinierten Einsatz eine große Unterstützung für das L-Band bieten – sie tragen dazu bei systematische Fehler, wie z.B. Mehrwegseffekte, Phasenzentrumsvariationen und Troposphären-Parameter, weitgehend zu reduzieren und die Uhren zu synchronisieren. Es wird gezeigt, dass in unseren Simulationen eine Bahngenauigkeit im niedrigen Millimeterbereich und eine Uhrgenauigkeit im Bereich von Pikosekunden für MEO-, IGSO- und GEO-Satelliten erreicht werden können. Das beste Link-Szenario ist dabei das L-Band+OTWL+OISL Szenario. Die Analyse hebt hervor, dass nicht nur eine komplementäre Nutzung aller drei Beobachtungstechniken möglich ist, sondern auch, dass die Synergie einer kombinierten Nutzung von OTWL und OISL einen erheblichen Einfluss auf die erreichbare Bahn- und Uhrlösung hat, verglichen mit den L-Band+OTWL und L-Band+OISL Szenarien.

Contents

Preface

This cumulative dissertation is based on the following four publications:

P-I Schlicht, A.; Marz, S.; Stetter, M.; Hugentobler, U.; Schäfer, W. (2020)
Galileo POD using optical inter-satellite links: A simulation study.
Advances in Space Research, 66(7): 1558-1570. doi: 10.1016/j.asr.2020.06.028.

P-II Marz, S.; Schlicht, A.; Hugentobler, U. (2021)
Galileo precise orbit determination with optical two-way links (OTWL): a continuous wave laser ranging and time transfer concept.
Journal of Geodesy, vol. 95, art. 85. doi: 10.1007/s00190-021-01534-4.

P-III Marz, S.; Schlicht, A.; Hugentobler, U. (2023)
Geosynchronous Satellites Expanding a Future GNSS Satellite Constellation: A Precise Orbit Determination Study.
Advances in Space Research, 71(1): 624-644. doi: 10.1016/j.asr.2022.11.009.

P-IV Marz, S.; Schlicht, A.; Hugentobler, U. (2023)
Toward a Geodesy and Time Reference in Space (GETRIS): A Study of Apparent Satellite Clocks of a Future GNSS Satellite Constellation.
Geosciences, vol. 13(6), art. 173. doi: 10.3390/geosciences13060173.

The four papers are peer-reviewed and are already published. The accepted versions of the papers are included in full-text at the end of this dissertation. Elsevier, the publisher of P-I and P-III, allows that authors can include their articles in full in a dissertation for non-commercial purposes, according to their permission guidelines. P-II, published by Springer, and P-IV, published by MDPI, are open access articles under a Creative Commons Attribution 4.0 International License. This allows the author to include the articles in full in a dissertation.

Before presenting the publications, Section 1 explains the motivation to write this dissertation. Section 2 highlights the structure of the dissertation, explains the approaches for each paper and highlights the relationship between the publications. The state-of-the-art of satellite-ground, satellite-satellite links and clocks are addressed as well. Section 3 summarizes the content of the publications. This includes explanations for the simulation and the estimation setup as well as an overview of important results. In Section 4, additional analyses of the results are shown, with focus on the precision of the links and possible bad weather conditions. Section 5 summarizes the main conclusions from the publications, addresses open questions and provides an outlook.

1 Motivation

Space missions and applications can be subdivided into two main areas of interest: the near-Earth environment and deep space. Although applications in both areas pursue their own goals, they increasingly benefit from a combination of each other. The observation techniques used in each area e.g. have systematic errors, which can be detected and minimized by combining them. Therefore, the two areas of interest will continue to grow together in the future.

For the near-Earth environment, goals such as the improvement of the Terrestrial Reference Frame (TRF) are pursued. With the Global Geodetic Observing System (GGOS), the flagship of the International Association of Geodesy (IAG), the aim is to determine a precise TRF with 1 mm accuracy and a stability of 0.1 mm/year (Plag and Pearlman, 2009). In order to achieve these goals, various types of geodetic observation techniques are foreseen to be combined, coordinated and optimized to improve the understanding of the dynamic Earth system. One vision of GGOS is to connect the different layers from the ground-based infrastructure to satellites at all altitudes, to the Moon and up to extragalactic objects such as quasars. The major involved observation techniques in GGOS are among others: VLBI (Very Long Baseline Interferometry), SLR (Satellite Laser Ranging), LLR (Lunar Laser Ranging), GNSS (Global Navigation Satellite System) measurements, radar observations, ISL (Inter-Satellite-Links) and gravity acceleration measurements. Future planned satellite missions such as Genesis (Delva et al., 2023) target the GGOS goals of realizing an accurate and stable TRF. Studies show that a combination of GNSS observations and precise optical ISL measurements already result in a significant improvement in the accuracy and stability of the TRF (Glaser et al., 2020). Furthermore, objectives for the near-Earth environment include ongoing studies of the Earth, for example in the areas of altimetry and gravity field measurements. Key drivers for such Earth studies are especially socially relevant topics such as climate change.

Interests concerning deep space are mainly driven by the goal ‘to the moon and beyond’ (Parker, 2019). Starting with the Artemis program (Smith et al., 2020) by NASA (National Aeronautics and Space Administration), mankind is scheduled to return to the Moon’s surface as early as 2026. To provide precise navigation on the Moon, many works aim to bring GNSS to the Moon, either through an expansion of the Space Service Volume (SSV; Bauer et al., 2006; UNNOSA, 2021), to receive GNSS side-lobe signals from the Earth up to Highly Elliptical Orbit (HEO) or cislunar satellites (Winternitz et al., 2017; Ashman et al., 2018, Enderle et al., 2018; Parker et al., 2018; Parker et al., 2022; Guan et al., 2022). An alternative concept is to establish an own GNSS satellite constellation around the Moon (Di Benedetto et al., 2022; Pereira et al., 2022; Gil et al., 2023). Therefore, the implementation of a lunar time system is also necessary to enable a precise navigation on the Moon. There is discussion about either defining an own lunar time standard or to synchronize the lunar time with UTC (Universal Time Coordinated) on the Earth (Gibney, 2023). Synchronization of Earth-Moon clock is only possible through time transfer between clocks on or around the Earth and clocks on or around the Moon. Therefore, connecting the near-Earth environment and deep space is of increasing importance.

With the aim of strengthening the connection between the near-Earth environment and deep space as well as the combination of different orbital layers, as envisaged by GGOS or the extended SSV, the idea of realizing a GEodesy and Time Reference In Space (GETRIS; Schäfer et al., 2013; Schlicht et al., 2014) arose. Stepping up from a TRF based on ground stations, the implementation of a reference system realized by satellites might be a valuable extension to the TRF. The GETRIS can not only contribute to achieve the GGOS goals for the precise TRF, but can also substantially enhance the interaction with satellites up to lunar distances and beyond. In order to use a satellite network as a GETRIS, the orbits have to be determined with a similar precision to that of ground stations – about 1-3 mm. Furthermore, GETRIS envisages installing high-precision clocks onboard of the satellites, with the target of a time transfer accuracy at ps-level. In terms of both the accuracy of the orbit and the clock, the state of the art is still far from achieving such a level of precision. Similar to GGOS, the aim of GETRIS is to realize the reference system through combinations of observation techniques with a synergetic use.

While the installation of a GETRIS is still far from being realized, the target of this dissertation was to build up a satellite constellation and measurement network concept based on simulations that will help to get towards a GETRIS. The concept shall provide the potential to fulfill the GETRIS goals in terms of satellite Precise Orbit Determination (POD) at the low mm-level and clock accuracy at the ps-level. The focus is on a synergetic use of different advanced measurement techniques with the capabilities to do high-precision ranging and time transfer.

2 Introduction

This section is intended to present the ideas and to explain the approach of creating a concept for a GETRIS, to achieve the goal of precisely determined satellite orbits at the low mm-level as well as clock accuracy at the ps-level. The essential steps of the concept creation then form the basis of the papers of this cumulative dissertation (see the Preface). The detailed content of the papers is discussed in Section 3, together with an introduction to the specific simulation and estimation setups as well as the summary of the main outcomes.

In order to build a satellite constellation and measurement concept in the sense of a simulated POD study, we have defined three key pillars that have to be considered. The first is the instrumentation, which comprises the measurement noise and the characteristics of the observation technique. The second is the geometrical configuration given by the satellite constellation and ground station network designs as well as the observation network. The third covers the modelling of orbit and observation parameters. A detailed description of the three key pillars can be found in Section 2.1. Taking into account the characteristics of the three key pillars helps in making the final decisions for the satellite constellation as well as the observation network design to be used.

A scheme of the final GETRIS concept developed in this dissertation is shown in Figure 1. The approach to realize the concept is highlighted below and explained in more detail in Section 2.2.

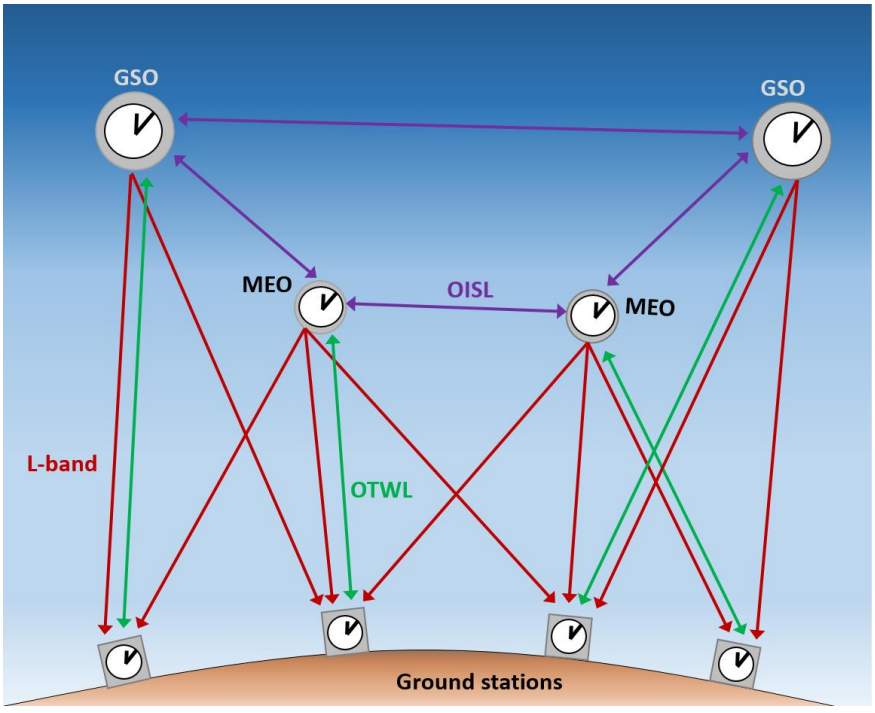

Figure 1: Scheme of the targeted satellite constellation and measurement network design.

A Medium Earth Orbit (MEO) GNSS satellite constellation is already a well-integrated satellite network for satellite POD. By using GNSS L-band measurements, POD for all current satellite missions as well as navigation on ground is provided. Therefore, in this dissertation a MEO GNSS satellite constellation is preferred as a fundamental satellite network for a GETRIS. A GNSS L-band link is a space-ground oriented one-way measurement. A main advantage of L-band is the huge amount of measurement that are available: per epoch, one ground station can track all visible satellites and many ground stations can receive signals from the same satellite. Therefore, L-band by itself has a good ranging geometry. As a result of the connection of one ground clock to the many satellite clocks, the ground clock can be synchronized. However, the microwave one-way link comes along with some systematic errors. These errors are in particular multipath and phase center variations. Clock and troposphere parameters – mainly the wet tropospheric zenith delay –, together with the orbital altitude and station height, are correlated with each other.

Adding another measurement technique to the concept can help to significantly reduce the systematic errors. In order to achieve the goal of a synergetic use, the measurement technique has to be complementary to L-band. In terms of the instrumentation (see Section 2.1.1), is a two-way or dual one-way link in the optical domain is the best complement to L-band.

Using a space-ground oriented measurement technique with a good ranging geometry, satellite-to-satellite links, also known as ISL, are the obvious complementary measurements to enhance the geometry of the observation network (see Section 2.1.2). The impact of a combination of L-band and optical ISL (OISL) measurements for POD of satellites in a GNSS MEO satellite constellation was analyzed in P-I (see Section 3.1). As the goal of GETRIS is to achieve satellite orbits at the level of 1-3 mm, the precision of the optical links has also to be at that level. With a selected link precision of 1 mm for OISL in this work, the precision assumption is at the level of state-of-the-art techniques such as SLR / ELT (European Laser Timing; Schreiber et al., 2010) (see also Section 2.2.2). A more detailed explanation of the approach for P-I can be found in Section 2.2.1.

As a second analysis of this dissertation, the idea was to use the same observation technique as used for OISL but pointed from the satellites to the ground and vice versa. This observation technique is named OTWL (Optical Two-Way Link). The combination of two observation techniques at one ground station is known as co-location on the ground. Through the co-location of observation techniques, there is the potential to tighten the space segment to the ground segment, which can also be interpreted as a geometrical enhancement of the observation network design (see Section 2.1.2). The impact of OTWL, as an alternative measurement technique to OISL in a combination with L-band, was analyzed in P-II (see Section 3.2). In addition, scenarios were also carried out in which all three measurement techniques were combined. The L-band+OTWL+OISL scenario synergizes the advantages of all three measurement techniques. A more detailed explanation of the approach for P-II can be found in Section 2.2.2.

Aside from adapting the measurement network, as discussed in P-I and P-II, geometry can also be improved by expanding the satellite constellation (see Section 2.1.2). In P-III (see Section 3.3) the impact of additional geosynchronous orbit (GSO) satellites in the constellation was analyzed for GSO and for MEO POD. GSO satellites were selected to expand the satellite constellation as GETRIS aims a connection with satellites in the deep space. In Section 2.2.3, the approach for P-III is covered.

The up to now three papers of this dissertation focus on satellite POD. As GETRIS also aims to build up a reference in space to perform accurate time transfer as well, P-IV (see Section 3.4) was written to analyze the satellite clock synchronization. The approach for P-IV is explained in more detail in Section 2.2.4.

Although using optical links at the state-of-the-art level of 1 mm precision (Schreiber et al., 2010; Luceri et al., 2019), it might be challenging to implement such optical dual one-way links for the real purposes. In particular, unknown sources of errors or model errors can limit the utilization of the full potential of precision. Therefore, an additional analysis using lower link precision was performed in Section 4. Section 5 provides conclusions and an outlook.

2.1 Key pillars of a POD simulation study

For our POD simulation study, we have defined the key pillars of instrumentation, geometry and modelling that need to be taken into account (see Figure 2). Thereby, all three key pillars are interlinked with each other:

- The selection of the instrumentation together with the modelling of the measurements leads to the observations to be simulated.
- The analysis of the instrumentation together with the geometry defines the observation network design.
- The geometry together with the orbit modelling are the basis for the satellite constellation design.

The key pillars are described in more detail in the following sections.

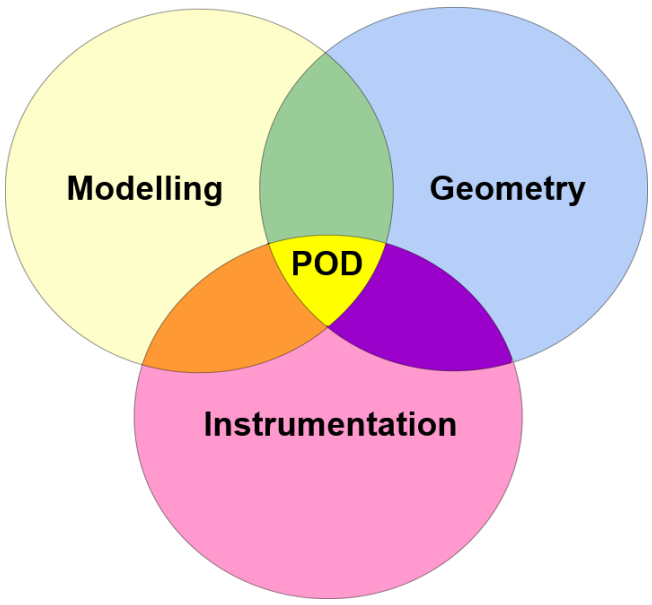

Figure 2: Key pillars of a POD simulation study.

2.1.1 Instrumentation

The instrumentation defines the type of the observation technique and therefore the ranging and time transfer method. This includes the following points:

- Measurement errors
  - Noise (stochastic error)
  - Systematic errors
- Measurement characteristics
  - One-way / two-way / dual one-way
  - Microwave / optical

The measurement errors describe the stochastic and systematic errors that the measurements show. The error and thus the final link precision generally depends on the measurement characteristics, the technological progress and the costs.

An overview scheme of different measurement characteristics is shown in Figure 3. The figure faces the above listed characteristics and names the most common advantages and disadvantages.

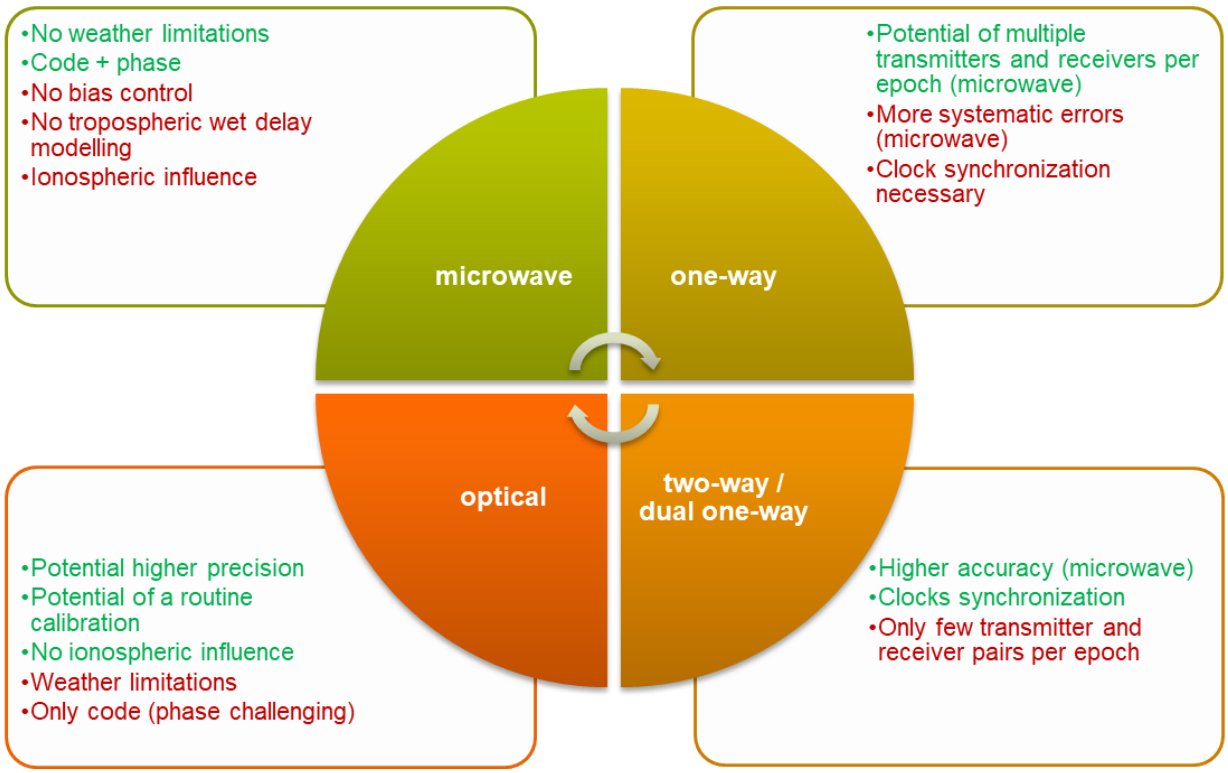

Figure 3: Types of ranging and time transfer methods. Some advantages (green) and disadvantages (red) of each type are listed in simplified form.

Microwave measurements are always performed as phase modulated signals. Code and phase can be analyzed. Furthermore, a measurement in the microwave domain is generally not limited by cloudy weather conditions. Disadvantages are a dependence on the tropospheric wet delay and an ionospheric influence. However, the ionospheric influences can be largely eliminated by measuring with two different frequencies and building the ionosphere-free linear combination. The modelling of the wet part of the troposphere is very difficult but can be estimated as unknown. A microwave link also offers no ability to control changing biases. The distance until microwave signals reach the far field is too large, so calibrations in the short range are challenging.

Measurements in the optical domain can be performed either as pulsed signals or phase modulated. We only focus on optical code measurements. Phase measurements in the optical domain are possible, but very demanding for an initial concept (Giorgi et al., 2019). An optical link provides the ability for routine calibration over short distances as done in SLR and allows the determination of measurement and changing hardware biases. Much higher modulation rates are possible for a phase modulated optical link because the wavelength of an optical link is shorter compared to a microwave link. Hence, there is the potential to achieve a higher precision when using links in the optical domain, as the higher modulation rate allows more measurements per unit of time. In addition, optical links are not influenced by the ionosphere, but are limited in cloudy weather conditions.

The advantage of a one-way link performed in the microwave domain is the possibility to have multiple transmitters and receivers per epoch. This improves the geometrical configuration of the observations. To have multiple transmitters and receivers is not possible with an optical one-way link due to the sharp focusing of a laser. Disadvantages of the one-way ranging technique compared to a two-way link are more systematic errors and the necessity for a clock synchronization.

A two-way or dual one-way link directly synchronizes the clock. With a two-way / dual one-way microwave link, it is possible to achieve a higher accuracy compared to a one-way link. However, due to the nature of the two-way / dual one-way ranging techniques, a measurement is performed only between few transmitter and receiver pairs per epoch. This restricts the geometrical configuration of the observations. Combining the different characteristics lead to state-of-the-art, but also possible future observation techniques. A detailed comparison of several different observation techniques can be found in the P-II paper of this dissertation.

A main part of this dissertation is the analysis of the impact of combinations of observation techniques for POD of a GNSS satellite constellation. The most common observation technique for POD of a GNSS satellite constellation is the classical GNSS L-band tracking and represents the basis for the combinations of observation techniques analyzed in this work. GNSS POD solutions using only L-band measurements serve as a reference for the results of this dissertation and the papers. GNSS L-band combines the characteristics of microwave and a space-ground oriented one-way link.

The most complementary observation technique to L-band is a two-way or dual one-way link in the optical domain. Thus, all four instrumentation characteristics (see Figure 3) are covered and the advantages of all the different techniques can be combined. This even compensates some disadvantages of certain measurement methods and exploits the synergetic aspects. Therefore, it was decided to combine GNSS L-band with an optical two-way or dual one-way link for the simulations in this dissertation and the papers. The optical observation techniques to be finally selected are related to the geometrical part of the key pillars, which is explained below.

2.1.2 Geometry

The geometrical configuration used in a simulation study is based on three designs:

- Satellite constellation design
- Ground station network design
- Observation network design

The satellite constellation design and the ground station network design determine the relation and orientation between satellites and ground stations, but also between all satellites in a constellation itself. This is the basis for the observation technique design.

The observation network design is defined by the type of the participating entities and the scheduling of all the measurements. The precision and accuracy of a measurement depends on the measurement errors and the instrumentation (see Section 2.1.1).

For this dissertation, it was decided to first enhance the geometry through the observation network design (see Section 2.1.2). As described in Section 2.1.1, the L-band measurements shall be supported by an optical observation technique. A geometrical enhancement comes from the use of additional satellite-to-satellite links. The geometry can also be improved by co-location of different observation techniques. This particularly refers to links that directly connect the ground and space segment. The observation techniques have the potential to support each other. This tightens the space segment to the ground segment, which can be interpreted as an improved geometrical configuration.

Secondly, the geometry is enhanced by adapting the satellite constellation design. With respect to the GETRIS goals (see Section 1), it was decided to expand the MEO satellite constellation by GSO satellites in this dissertation (see Section 2.2.3).

To quantify the geometry contribution and white noise of a POD solution, we use the formal orbit uncertainties. The formal orbit uncertainties can be taken directly from the covariance matrix of the estimated parameters of an adjustment. The formal orbit uncertainties shall not contain systematic errors.

2.1.3 Modelling

Two types of errors are distinguished here concerning a satellite POD simulation study:

- Orbit modelling errors
- Delay modelling errors

Orbit modelling errors arise when the models do not exactly represent the gravitational and non-gravitational accelerations. The gravitational accelerations include the Earth gravity fields,

ocean and solid Earth tides as well as influences from third bodies (Sun, Moon, planets). The main non-gravitational force affecting MEO, GSO and HEO satellites is Solar Radiation Pressure (SRP). The true orbit with additional orbit modelling errors defines the mismodeled orbit and, accordingly, the initial orbit for the adjustment to obtain a satellite POD solution. The latter is called the adjusted orbit. To quantify the a-posteriori orbit modelling errors, we define the so-called best possible orbit:: empirical SRP parameters are estimated directly to the true satellite trajectory to improve the mismodeled orbit. Therefore, no measurements are used in the estimation process of the best possible orbit. By analyzing the best possible orbit, the SRP model can be optimized by estimating different or more SRP parameters.

Two of the most commonly used empirical SRP models for GNSS are the Empirical CODE Orbit Model (ECOM; Beutler et al., 1994) of the Center for Orbit Determination in Europe (CODE) and ECOM2 (Arnold et al., 2015). Equations for ECOM (see Eq. (1)) and ECOM2 (see Eq. (2)) are given below. Both distinguish in the type of periodic parameters in the directions D (pointing from the satellite to the Sun), Y (the direction along the solar panels), and B to complete the right-handed orthogonal satellite-fixed system. Δu is the argument of latitude with respect to the Sun. A main part of this dissertation is the analysis of the true orbit modelling errors and, finally, to optimize the SRP model with regard to the findings.

(1)
$$D(\Delta u) = D_0 + D_{1c}\cos(\Delta u) + D_{1s}\sin(\Delta u)$$
$$Y(\Delta u) = Y_0 + Y_{1c}\cos(\Delta u) + Y_{1s}\sin(\Delta u)$$
$$B(\Delta u) = B_0 + B_{1c}\,cos(\Delta u) + B_{1s}\sin(\Delta u)$$

(2)
$$D(\Delta u) = D_0 + D_{2c}\cos(2\Delta u) + D_{2s}\sin(2\Delta u) + D_{4c}\cos(4\Delta u) + D_{4s}\sin(4\Delta u)$$
$$Y(\Delta u) = Y_0$$
$$B(\Delta u) = B_0 + B_{1c}\,cos(\Delta u) + B_{1s}\,sin(\Delta u)$$

In the adjustment, the SRP parameter estimation is correlated with the measurements – the measurement geometry (see Section 2.1.2) and errors. Therefore, the ability to benefit from an optimized SRP model depends on the observation techniques used and their instrumentation (see Section 2.1.1).

The second error type describes modelling errors that cause a delay in the measurements, e.g. a troposphere modelling error introduced by the use of different troposphere models. The model types have to be selected according to the instrumentation (see Section 2.1.1). In the case of microwave measurements, influences of the ionosphere are predominately removed by building the ionosphere-free linear combination.

2.2 GETRIS concept development

As explained in Section 2.1.1, the aim for the GETRIS concept is to combine L-band observations with optical links and to make use of the synergy of those links. When aiming at point-to-point connections, optical links are a perfect technique and can be used for data transfer, communication, ranging and clock synchronization. As the links in the optical domain have shorter wavelength compared to microwaves, operations with higher modulation rates are possible – up to hundreds of MHz for microwave links compared to several GHz for optical links. Higher modulation rates lead to higher data rates when using the links for communication and allow for a higher precision in ranging applications. However, although there is a theoretical advantage over microwave links in this context, it has been a difficult task in the recent years to achieve the same precision or better with the optical links as it was already possible with microwave links. A main issue for ground-space oriented optical links were turbulences in the troposphere. To compensate for the turbulences, the development of adaptive optics was necessary (Weyrauch and Vorontsov, 2004). Hemmati (2020) provides an overview of developments for optical communication links in space. Today, optical terminals that offer Gbit/s modulation rates over several ten thousands of kilometers are already operative, as e.g. the TESAT-Spacecom terminal used for the European Data Relay System (EDRS) with modulation rates of up to 1.8 Gbit/s (Zech et al, 2015; Calzolaio et al., 2020). But optical links allow even higher modulation rates up to about 10 GHz to be used for future applications. Pribil and Hemmati (2020) provide an overview of active, tested and planned optical transmitters. In Giorgi et al. (2019) possible optical communication and timing technologies for a space-based clock synchronization are reviewed.

In the following sections, the steps to achieve the final GETRIS concept (see Figure 1) developed in this dissertation is explained. From these steps, the papers of this cumulative dissertation are derived (see the Preface). Thereby, we first introduced two different types of optical links for a combination with L-band, with the goal of improving geometry by expanding the observation network design (P-I and P-II). Then we aim to expand the satellite constellation design (P-III). After selecting the link types for a synergetic use (instrumentation) and covering different types to enhance the geometry, we also aim to improve the orbit modelling in these papers. While all three papers focus on satellite POD, we finally analyze the impact on the clock errors for the created GETRIS concept (P-IV). A more detailed approach for each paper is described below. The detailed content and the summary of the papers can be found in Section 3.

2.2.1 Approach for P-I

With L-band, a space-ground oriented measurement technique with a good ranging geometry is the basis for the GETRIS observation network design. In a first step, the aim is to enhance the geometry by an adaption of the observation network (see Section 2.1.2). The obvious geometric complement to L-band are ISL measurements. ISL is one of the next generation observation techniques for many

satellite constellations. In general, ISL enhances the ranging geometry within the satellite constellation and allows a synchronization of all satellite clocks of a constellation. BeiDou is already using Ka-band ISL in their third generation of GNSS satellites and demonstrated the advantages in terms of POD and satellite clock synchronization (Yang et al. 2020; Zhang et al., 2021). Missions such as GRACE-FO (Gravity Recovery And Climate Experiment – Follow On; Abich et al., 2019) and the Laser Interferometer Space Antenna (LISA) Pathfinder (McNamara et al., 2008) use inter-satellite optical frequency ranging. EDRS uses its optical carriers for data transfer and communication between GEO and LEO satellites, but these very high modulated optical signals have the potential to be used for ranging and time transfer, too.

With the goal of combining the L-band measurements with two-way or dual one-way optical links, it was decided to implement ranging and time transfer capable EDRS-like links, as expected to be available in future and already motivated for use for GETRIS (Schäfer et al., 2013; Schlicht et al., 2014). This optical ISL ranging and time transfer measurement technique is in the following named OISL (Optical Inter-Satellite Link). Similar to the EDRS links, OISL shall operate with dual one-way continuous wave signals that use phase modulation. Therefore, active transponders are needed onboard of the satellites.

P-I (see Section 3.1) focuses on the combination of L-band and OISL (Figure 4), covering the impact for POD of satellites in a GNSS MEO satellite constellation. In this work it is assumed that OISL measurements are pre-processed pseudo-ranges, resulting in a range and clock difference measurement. We also simulated many stochastic and systematic errors for the optical link such as a colored measurement noise, distance dependent effects as well as constant and variable link biases. We assumed a link precision of about 1 mm for OISL in this work. Thus, the precision assumption is still moderate and at the level of state-of-the-art techniques such as SLR / ELT (see also Section 2.2.2), not exhausting the potential of phase modulated optical links within this dissertation.

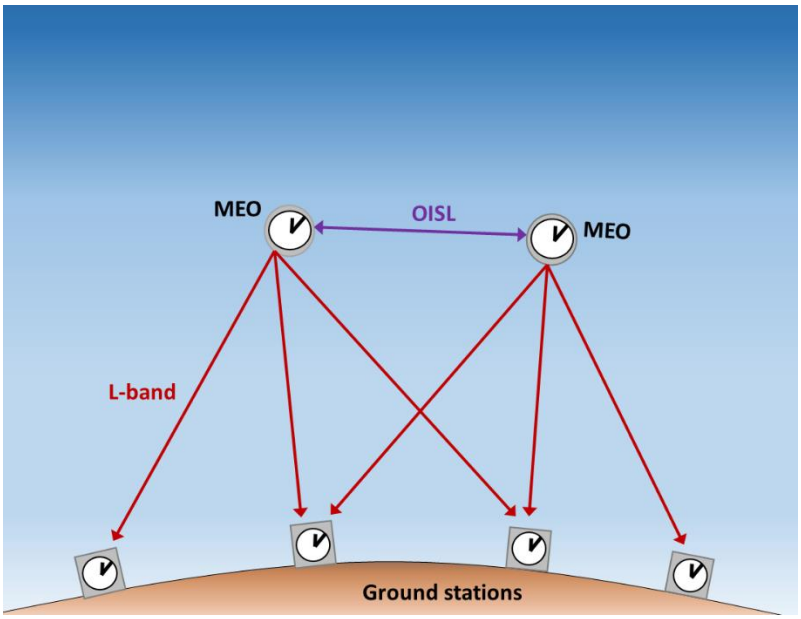

Figure 4: Combining L-band and OISL measurements.

2.2.2 Approach for P-II

While ISL can determine the relative positions of the satellites very well, the satellite constellation itself has some freedoms to be rotated around the geocenter. Therefore, links to connect the satellites to the Earth's surface are needed in addition to ISL. The GNSS L-band measurements are one candidate for a combination with ISL. Due to the good geometry offered by the GNSS L-band measurements, the relative positions of the satellites are tied to the Earth's surface. However, as GNSS L-band has a level of systematic errors, it is unable to tie a satellite constellation tightly enough to the Earth's surface for a GETRIS. Hence, depending on the precision of the space-ground links, there are still rotational freedoms between the satellite constellation and the ground station network per epoch. By co-locating L-band with an equally directed high-precision observation technique, the space segment can be tightened to the ground segment by local and clock ties. If the high-precision technique can perform ranging and time transfer measurements, not only the orbit will benefit from this technique, but also the clock synchronization. Due to troposphere modelling errors, the relative positions and the satellite clocks are not as well determined from ground than by ISL from space.

Links between ground stations and satellites are used since a long time for ranging and time transfer to support GNSS observations or, for instance, for geodetic and geophysical applications. The most common ground-space oriented observation technique is SLR. This technique is operated by ground stations and makes use of retroreflectors carried by the satellites, leading to a two-way (round-trip) range measurement. The LTT (Laser Time Transfer; Meng et al., 2013), T2L2 (Time Transfer by Laser Link; Samain et al., 2014) and the upcoming ELT (European Laser Timing; Schreiber et al., 2010) as part of the ACES (Atomic Clock Ensemble in Space; Cacciapuoti and Salomon, 2009; Cacciapuoti et al., 2020), combine pulsed one-way and two-way optical links to offer ranging and time transfer. ELT is expected to achieve a time transfer and ranging precision of 1 mm. Examples for techniques in the microwave domain are the two-way TWSTFT (Two-way Satellite Time and Frequency Transfer; Tang et al., 2016) and the two-way MWL (MicroWave Link; Delva et al., 2012) of ACES. MWL uses phase modulation and operates in the Ku-band with a modulation rate of 100 MHz and achieves a ranging precision of about 0.2 mm for the phase at 30 s integration time. For comparisons, GNSS L-band uses signals with a modulation rate of about 10 MHz and achieves a ranging precision of about 1.5 mm for the phase.

For P-II of this dissertation (see Section 3.2), the idea was to use OTWL (Optical Two-Way Link) alongside L-band for the measurement network (Figure 5 left). OTWL uses the same observation technique as used for OISL, but is pointed from the satellites to the ground and vice versa. With the high precision and the dual one-way phase-modulated optical link nature, OTWL is the perfect candidate for a co-located use with GNSS L-band. Theoretically, measurement techniques such as SLR or ELT can also be used as an alternative to OTWL, but the idea of OTWL is to have a standardized system that uses the same hardware at all ground stations. This is currently not the case for SLR. In addition, OTWL is a phase modulated link with the potential to use much higher modulation rates than MWL. Therefore, even higher link precision can potentially be expected than with a pulsed link such as SLR or the phase modulated MWL. For OTWL, we assumed the same precision and systematic errors as for OISL. The only additional measurement error of OTWL is a

tropospheric delay. P-II analyzes the impact of OTWL in a combination with L-band for the POD of GNSS MEO satellites, using OTWL as an alternative measurement technique to OISL. Scenarios combining all three measurement techniques were analyzed as well (Figure 5 right). This L-band+OTWL+OISL measurement network design combines the strength of OISL – well determined relative satellite positions and a synchronization of the satellite clocks – with the strength of the L-band+OTWL combination to tighten the satellite constellation to the Earth's surface and to synchronize the satellite and the ground station clocks.

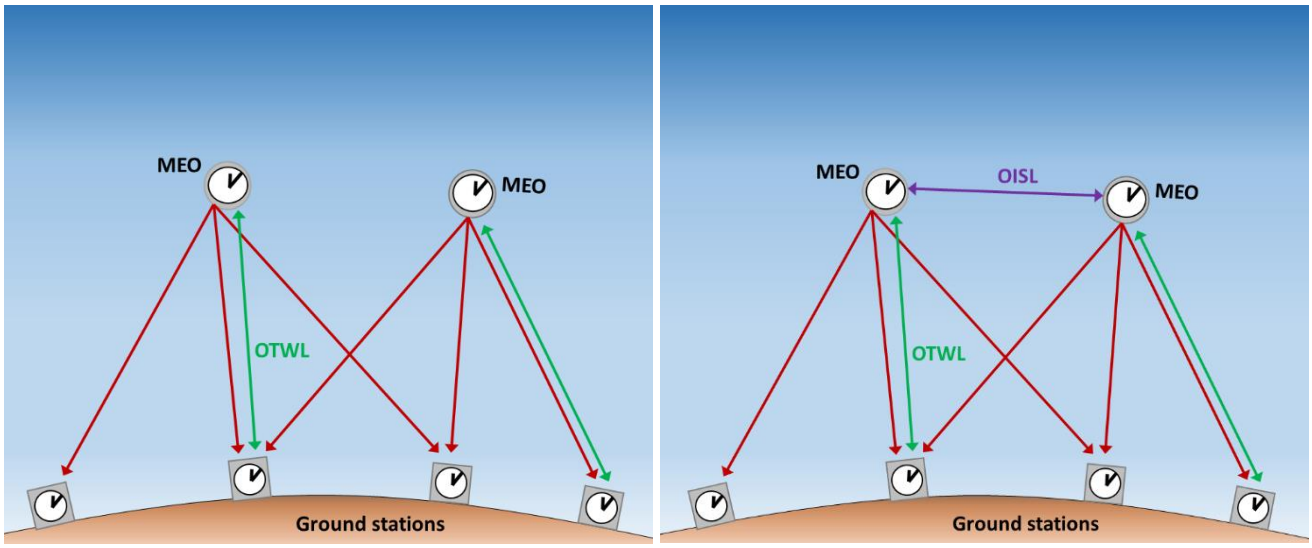

Figure 5: Combining L-band and OTWL measurements (left) as well as all three measurement types (right).

2.2.3 Approach for P-III

P-I and P-II focus on the observation network design to enhance the geometrical configuration. Geometry can also be improved by adapting the satellite constellation design (see Section 2.1.2). Two orbit types come into question for the satellites used for the GETRIS alongside MEO satellites: the LEO (Low Earth Orbit) and the geosynchronous orbit (GSO). While satellites in LEOs are mainly involved in geodetic missions, the GSO satellites also become more and more important. As part of a GNSS constellation, a regional enhancement is provided within the tracking system. In addition, the accuracy and reliability of the user positioning is increased. The current best example of embedding GSO satellites in a MEO GNSS constellation is the BeiDou satellite navigation system. Navigation satellite systems such as QZSS (Quasi-Zenith Satellite System) and IRNSS (Indian Regional Navigation Satellite System) are purely regional and are built entirely on GSO satellites. Other GSO satellite constellations such as SBAS (Satellite Based Augmentation Systems; Walter, 2017), including the European Geostationary Navigation Overlay Service (EGNOS; Ventura-Traveset et al., 2015) or the US-American Wide Area Augmentation System (WAAS; Walter et al., 2018), aim to support GNSS systems with regional services and information.

With the European Data Relay System (EDRS; Zech et al, 2015; Calzolaio et al., 2020) very advanced optical carriers with a very high modulation rate were developed and are used for data transfer and communication between geostationary orbit (GEO) satellites and LEO satellites. These data transfer links can be used synergistically for ranging. As GETRIS aims a connection with satellites in the deep space, GSO satellites are favorable compared to LEO satellites. A connection between MEO and LEO satellites by optical links was analyzed in the Kepler concept (Michalak et al., 2021).

In P-III (see Section 3.3), the POD of GSO satellites was analyzed when the GSO satellites are used together with MEO satellites in the constellation. Considering the observation network design as derived in P-II, several scenarios with combinations of observation techniques were simulated. In addition, the impact on MEO POD was analyzed using the MEO+GSO satellite constellation.

2.2.4 Approach for P-IV

GETRIS aims to build up a reference in space not only for ranging but also to perform accurate time transfer. While P-I, P-II and P-III focus on satellite POD, P-IV (see Section 3.4) analyzes the satellite clock errors from the simulations of P-III. These simulations were performed using Passive Hydrogen Masers (PHM) carried by all satellites in the constellations. PHM clocks are used in state-of-the-art GNSS satellites, besides Rubidium Atomic Frequency Standards (RAFS). The PHM clocks have a frequency stability at the level of some 10^{-15} at one day.

Compared to PHMs, more stable types of clocks are in preparation or have already been tested in space. Clocks based on iodine cells and using optical frequency standards target a frequency stability at the level of few 10^{-15} for sample intervals between 100 s and 10000 s (Schuldt et al., 2017; Giorgi et al., 2019; Schmidt et al., 2022). NASA developed a trapped-ion atomic clock named Deep Space Atomic Clock (DSAC; Tjoelker et al., 2016). DSAC demonstrated a frequency stability of $2 \cdot 10^{-15}$ at 1 day and $3 \cdot 10^{-15}$ at 23 days (Tjoelker et al., 2016; Burt et al., 2021). The ESA mission ACES, scheduled to launch in April 2025, will test a clock concept that combines an Active Hydrogen Maser (AHM) and the PHARAO (Project d'Horloge Atomique à Refroidissement d'Atomes en Orbite), a laser-cooled Cesium clock. The targeted frequency stability of the ACES clock is at the level of $3 \cdot 10^{-15}$ at 300 s, $3 \cdot 10^{-16}$ at 1 day and $1 \cdot 10^{-16}$ at 10 days (Cacciapuoti and Salomon, 2009; Laurent et al., 2015; Cacciapuoti et al., 2020). While these highly stable clocks are still challenging high costs and a complex manufacturing, they are candidates to be carried by future GNSS satellites. To analyze the benefit of using such a highly stable clock onboard of the satellites in our simulations, we repeated the simulations with ACES clocks carried by all satellites in the constellation. In our simulations, we estimate epoch-wise clock corrections. Therefore, more stable clocks are not expected to improve the clock error for estimation intervals, but they are beneficial for clock prediction.

2.3 Scientific questions

From the step by step build up GETRIS concept of this dissertation, the following scientific questions derived.

Different observation techniques and combinations - impact on orbit modelling:

Q1: What impact does the co-located combination of high-precision OISL and L-band measurements have for MEO POD?

Q2: What is the best connectivity scenario for OISL in terms of satellite POD?

Q3: Co-location of two observation techniques (L-band+OTWL): How does it compare to L-band+OISL in terms of MEO POD?

Q4: What is the synergy in terms of MEO POD when combining L-band+OTWL+OISL?

Optimization of the empirical orbit modelling:

Q5: Gain in geometry through link combinations: Is it possible to optimize the orbit modelling by estimating additional model parameters?

Expanding the space segment: Improved geometry by the constellation design

Q6: What is the impact on POD of all involved satellite types when expanding a MEO constellation by GSO satellites?

Impact on clock estimation:

Q7: What is the impact on the clock error in the different measurement scenarios (L-band-only, L-band+OTWL, L-band+OISL and L-band+OTWL+OISL)?

2.4 Methodology: From the simulation design to the result analysis

This dissertation and the papers build on a simulation study of a future GNSS satellite constellation that will use OISL and/or OTWL measurement in addition to L-band measurements for MEO satellite POD. The impact of POD and clock errors for GSO satellites are also evaluated.

A major advantage of a simulation in general is the knowledge of the true case, which is the basis for a simulation study. This true case includes the true orbits as well as error-free measurements from a certain observation technique. Based on this true case, step by step more errors can be included in the simulation to approach reality. This also provides an opportunity to understand the influence of a single error for the final solution by comparing it with the true case.

Generally, a POD simulation study is beneficial to

- understand POD results by studying individual error contributions
- investigate future observation techniques
- investigate future satellite constellations

It must be understood that in a simulation environment the complexity of the physical reality can never be fully covered and only known systematic errors and orbit perturbations can be included in the simulations. Hence, simulations have to be carried out either to the best knowledge – but the correctness and quality of the simulated results can only be proven by comparing with (future) real results – or by simulating only relevant errors and models to answer a certain scientific question.

Based on the assumptions made in the study (see also Section 2.2), the following main implementations have to be addressed:

- Generation of satellite orbits and accordingly the satellite constellations (MEO and GSO).
- Implementation and simulation of the OISL and OTWL measurement types: In general, these measurement types are pseudo-ranges. For the use in this dissertation, we assume a pre-processing of the measurements, leading to range and clock difference measurements.
- Simulation of the measurement errors (L-band, OISL and OTWL).
- Implementation of scheduling algorithms for the observation types (OISL and OTWL).
- Implementations of adaptions to the orbit modelling (parameter estimation).
- Implementation of algorithms to analyze the results and the creation of figures.

The methodology to finalize this dissertation can be split into three main steps, which are described in the following.

Step 1: Implementations in the Bernese and Matlab software

This simulation study was carried out using the Bernese GNSS Software Version 5.2 (Dach et al., 2015). Before starting the dissertation, the software version available at the Technical University of Munich (TUM) was able to simulate and estimate GNSS code and phase measurements as well as SLR range observations. A sub-version of the TUM Bernese software version was partly capable of using additional OISL range measurements. In this sub-version, the Bernese implementation for SLR range observation was reused and adapted for ranging between satellites. The implementations in the Bernese software described in the following, which enable analysis of OTWL and OISL measurements, were carried out by the author.

The Bernese implementations for SLR and OISL were reused and extended by the author of this dissertation to be able to process OTWL range measurements as well. For clock difference measurements of OTWL and OISL, a separate implementation was necessary within the Bernese software. An option to set a flag in the Bernese observation files allows to differentiate between SLR, OTWL or OISL measurement inputs in the software, as well as whether range or clock difference measurements should be processed. These were the main software changes that enabled the analysis of OTWL and/or OISL measurements in addition to GNSS L-band with the TUM Bernese software version.

The simulation of the OTWL and OISL measurements scheduling was solved using externally created scenario files – defining the sampling as well as the transmitter and receiver of an OTWL or OISL measurement. These scenario files were generated using the Matlab software by MathWorks. An additional column in the scenario files can be used to define measurement errors for the range and clock difference observations. It was implemented so that the scenario file can be read by the Bernese simulation program. Bernese observations files are written according to the scheduling and measurement errors specified by the files. For OISL, several different connectivity schemes were generated and compared with each other in the simulation study. A detailed description of the different schemes can be found in Section 3.1. For OTWL measurements, a scheduling algorithm was developed for the used satellite constellation and the ground station network. The OTWL measurement scheduling is described in more detail in Section 3.2.

The evaluation program required implementing the option to select the use of OTWL and/or OISL measurements for the least-squares adjustment. Estimation parameters had to be adapted according to the OTWL and OISL measurement types. Additionally, it should be possible to estimate a clock synchronization and a range bias for each satellite or station, as well as separately for OTWL and OISL. The bias estimation was implemented into the least-squares adjustment performed in Bernese.

As an additional option, the Bernese software should be able to estimate additional empirical orbit parameters. The basic SRP models in Bernese are the ECOM (see Eq. (1)) with up to nine parameters, and ECOM2 (see Eq. (2)) with a total amount of nine parameters as well. The baseline scenario for the simulations of this work should be ECOM2. The author implemented an option to estimate up to 13 empirical parameters. Therefore, changes had to be made in the orbit generation and estimation program.

The correctness of the implementations was checked by null-tests, where error-free measurements and satellite orbits have to be adjusted to error-free solutions. The results of the null-tests were in the range of numerical uncertainties.

Step 2: Definition, simulation and computation of scenarios

After the implementations, different simulation scenarios were defined, as already highlighted in Section 2.2. The main simulation and computation steps are listed below.

- The L-band measurements were generated according to the selected ground station network and the satellite constellation. L-band-only solutions were estimated with Bernese.
- Different OISL measurement scenarios were simulated and estimated in combination with L-band measurements with the Bernese software.
- OTWL measurements were simulated. L-band+OTWL and L-band+OTWL+OISL solutions were estimated with Bernese.
- The steps were repeated with an expanded satellite constellation: Geostationary orbit (GEO) and inclined-geosynchronous orbit (IGSO) satellites were included in addition to the MEO satellites.
- Selected scenarios were repeated using a more precise and stable clock type for comparisons.

Step 3: Analysis and evaluation of the results

The analysis and evaluation of the results as well as the creation of figures were carried out using the Matlab software. The outcome of the various scenarios described above was analyzed step by step and published in the attached papers of this dissertation.

The impact on satellite POD was analyzed on the basis of the formal orbit uncertainties (see also Section 2.1.2) and the orbit errors. The results are published in the papers P-I, P-II and P-III. Clock errors were evaluated and summarized in P-IV.

3 Content of publications

This chapter provides an overview of the publications as part of this cumulative dissertation (see the Preface). The four papers are included in full-text at the end of the dissertation. Below, each of the papers are briefly introduced and summarized by giving the most important results. In the conclusions section the main outcomes are addressed. The individual contribution of the author of this dissertation is described as well.

3.1 P-I: Analysis of OISL measurements

P-I Schlicht, A.; Marz, S.; Stetter, M.; Hugentobler, U.; Schäfer, W. (2020)
Galileo POD using optical inter-satellite links: A simulation study.
Advances in Space Research, 66(7): 1558-1570. doi: 10.1016/j.asr.2020.06.028.

Introduction

ISL is one of the next generation observation techniques used alongside GNSS L-band to improve the relative positions of the satellites and the clock synchronization. Section 2.2.1 gave an introduction to ISL in general. As explained in Section 2.1.1, the best complement to L-band would be an optical two-way / dual one-way link. This paper analyzes the potential of additional optical ISL measurements, named OISL (see Section 2.2.1), used in a 1st generation Galileo satellite constellation as of 2019. The constellation builds on 24 MEO satellites: 21 Full Operational Capability (FOC) satellites – including two satellites in eccentric orbits – and three IOV (Initial Orbit Validation) satellites. The ground station network for the L-band measurements consists of 16 stations, similar to the Galileo Sensor Station (GSS) network. OISL observations are generated as range and clock difference measurements (see also the Sections 2.2.1 and 2.4). For the simulations, it is assumed that L-band and OISL measurements are performed to the same epoch with 60 s sampling each. In reality, the L-band and OISL observations will have slightly different measurement epochs. In an adjustment, the measurements then need to be interpolated to the evaluation epoch. This leads to additional errors that are not taken into account in this dissertation. The analysis comprises an interval of 10 days and the processing of 1-day-arc solutions. An overview of the simulated measurement errors for L-band and OISL can be found in Table 1. A more detailed description can be found in the full version of the paper P-I.

In this paper, three different OISL connectivity scenarios are simulated and their advantages and disadvantages are compared. The first is an any-to-any connectivity scenario with dual one-way links between all satellites of the constellation after a certain amount of epochs. In this case, every satellite

of the constellation has to be equipped with one optical terminal. This means that one satellite can connect to one other satellite per epoch, building a linking pair. With 24 satellites in the constellation, there are 12 observations per epoch. New satellite pairs are formed in each epoch. After 24 epochs the scheme starts from the beginning. The connecting algorithm used in the paper for the any-to-any scenario is derived from the connectivity scheme by Fernández (2011). In the case that the satellites of a linking pair cannot see each other, e.g. when the link is occulted by the Earth, the measurement is treated as missing. A benefit of the any-to-any scenario is that for each satellite a bias can be estimated. Scenarios with two terminals per satellite were not tested because the software is unable to process two different optical terminals in an any-to-any scenario and estimate biases.

Table 1: Overview of simulated measurement errors for L-band and OISL in P-I.

	L-band	OISL
White noise	**Yes** 15 cm (1-sigma) for code, 1.5 mm (1-sigma) for phase	**Yes** up to 0.5 mm (1-sigma)
Flicker-phase noise (distance dependent)	**No**	**Yes** 0.1-1.5 mm (1-sigma)
Troposphere	**Yes**	-
Phase Center Variations (PCV)	**Yes**	**No**
Constant bias	**Yes** up to 5 mm (1-sigma)	**Yes** between ±0.5 mm (1-sigma)
Variable bias	**Yes** up to 5 mm (1-sigma)	**Yes** between ±0.5 mm (1-sigma)

The second connectivity scenario is a static bidirectional ring configuration, also called closed ring scenario. Every satellite is equipped with two terminals and only tracks its two direct neighbors in the same orbital plane. The advantage is that within a ring information can be immediately transmitted without data interruptions. The permanent monitoring and synchronization of the clocks in a ring is interesting for L-band navigation, as a synchronized set of satellite clocks is available all over the globe.

The third configuration is a broken ring scenario. Overall, this scenario is similar to the closed ring scenario, but at some epochs – in our case every 30 minutes or every two hours – two neighboring satellites from each of the orbital planes break their intra-orbital-plane connection and link to a satellite from another orbital plane. From this configuration some benefits due to a synchronization and data transfer between the different planes are expected.

L-band+OISL scenarios according to the three connectivity schemes are compared to L-band-only scenarios to evaluate the POD impact of OISL in our simulations. We also compared results computed with different processing strategies: a code-only processing as well as a code and phase processing with float or fixed ambiguities. E.g. for cost reduction, all scenarios were computed with either 16 or 7 ground stations, to investigate the effect of a reduced station availability for L-band measurements. In our simulations the ground station coordinates are estimated. An overview of the

estimated parameters for L-band and OISL can be found in Table 2. A more detailed description can be found in the full version of the paper P-I.

In addition to analyzing different link configurations, initial tests were carried out regarding the possibility to estimate additional empirical SRP parameters when using L-band+OISL instead of a L-band-only. An extended SRP parameter analysis was performed in P-II. The results and findings are presented in more detail in Section 3.2.

Table 2: Overview of estimated parameters for L-band and OISL in P-I.

	L-band	OISL
Station specific tropospheric zenith delays	Yes	-
Ground station coordinates	Yes	-
Satellite initial state vectors and empirical SRP parameters	Yes	Yes
Epoch-wise satellite and ground station clock parameters	Yes	Yes
Phase ambiguities (float)	Yes and No	-
Range and clock biases (OISL: any-to-any / closed-ring / broken-ring)	No	Yes / No / No

Summary

The weighting of the different measurement techniques in a combination of observations techniques is very important for the achievable results. In a simulation study, the question of which weight best represents a real scenario is difficult to answer. In our case, we weighted according to the lowest achievable orbit error with each scenario. This allows a conclusion to be made about the POD potential of each scenario. Section 4.1 of this dissertation contains an extended description of the weight analysis.

Starting with the analysis of the results, we first had a look at the formal orbit uncertainties – focusing on the stochastic errors and the geometry of the measurements. Overall, the formal orbit uncertainties are significantly reduced when OISL measurements are used in addition to L-band, compared to a L-band-only solution. The improvement is by a factor of 14. This already shows the strength of inter-satellite observation in terms of improving the measurements geometry. The effect is underlined when comparing the 16 and 7 stations scenarios. While the availability of more stations has a large positive impact on the solution in the L-band-only scenario, the L-band+OISL scenarios show only minor improvements. When comparing the code-only and the code+phase scenarios, the additional L-band phase measurements significantly help to improve the solution. The phase fixed scenario results in even lower formal orbit uncertainties than the float solution, as expected. However, the phase fixed scenario must be viewed as an overly optimistic scenario. When comparing

the different OISL link configurations, the any-to-any scenario produces the best results in terms of POD uncertainties, followed by the broken ring and the closed ring scenario.

Analyzing the orbit errors, focusing on the impact of the systematic measurement errors and the orbit modelling, the findings align with the ones concerning the formal orbit uncertainties. The relative improvement in orbit error of a 16-station phase-float solution is a factor of about 7 when using additional OISL observations compared to only L-band measurements in our simulations – achieving orbit errors of about 20 cm using L-band-only and 2.8 cm using L-band+OISL.

In a first test, we also compared solutions using a different number of empirical SRP parameters in the least-squares adjustment. While the L-band-only scenario shows an increase in the orbit error when estimating additional empirical SRP parameters, the orbit errors resulting from the L-band+OISL scenario decrease slightly. This shows that a measurement system combining L-band and OISL can handle the estimation of additional empirical SRP parameters, leading to an enhanced compensation of orbit modelling errors. Recently, Lv et al. (2024) compared BeiDou-3 MEO satellite orbit errors resulting from solutions using either a reduced 5-parameter ECOM or ECOM2 (Eq. (2)) empirical SRP parameter estimation. The contribution of Ka-band ISL for the estimation of ECOM2 D_0 is significant for beta angles smaller than 40° as correlations between parameters could be improved.

Individual contribution: The idea of analyzing the impact of OISL measurements in addition to L-band measurements was of Urs Hugentobler and Wolfgang Schäfer. Anja Schlicht and Monika Stetter designed the structure of the paper. The Matlab and Bernese implementations to process OISL range and clock difference measurements were started by Monika Stetter and finalized as well as improved by the author of this dissertation. The generation of the orbits, the simulation of the observations, the computation of the L-band-only and L-band+OISL scenarios as well as the generations of the figures shown in the paper were carried out by the author of this dissertation. The idea of estimating additional ECOM parameters was of the author of this dissertation and Anja Schlicht. The author of this dissertation implemented the possibility to estimate more empirical SRP parameters in Bernese. Anja Schlicht took the first authorship as project manager. Anja Schlicht mainly wrote the paper. The sections 4.1 and 4.2 were written by the author of this dissertation. All co-authors reviewed the paper.

Conclusions

The any-to-any OISL scenario overall offers best solution of the different scheduling types. This answers Q2. The ambiguity float solution provides the best and most realistic results overall for an orbit error analysis. As expected, the OISL measurements significantly expand the geometry of the observation network. This is reflected in a reduction of the formal orbit uncertainties by a factor of 14. The improvement for the orbit error is by a factor of about 7. Both results answer Q1. Initial tests to estimate more empirical SRP parameters were successful for a L-band+OISL scenario. This is a first indication to answer Q5, but is investigated in more depth in following paper P-II.

3.2 P-II: Introduction of OTWL measurements

P-II Marz, S.; Schlicht, A.; Hugentobler, U. (2021)
Galileo precise orbit determination with optical two-way links (OTWL): a continuous wave laser ranging and time transfer concept.
Journal of Geodesy, vol. 95, art. 85. doi: 10.1007/s00190-021-01534-4.

Introduction

In this paper, the optical dual one-way ground-space counterpart of OISL is analyzed, called OTWL (see Section 2.2.2). The idea is to use the same link technology for OTWL as used for OISL. Due to the ground-space link it is a co-located measurement technique to GNSS L-band, while OISL connects and stabilizes the satellite constellation itself and thus improves the geometry of the observation network. The same satellite constellation and ground station network as in P-I was used. The analysis comprises four simulation periods, each with an interval of 10 days. The selection of four simulation periods served to analyze dependencies on the beta angle - the sun elevation angle above the orbital plane. 1-day-arc solutions are processed. An overview of the simulated measurement errors for L-band, OTWL and OISL can be found in Table 3. A more detailed description can be found in the full version of the paper P-II.

Table 3: Overview of simulated measurement errors for L-band, OTWL and OISL in P-II.

	L-band	OTWL	OISL
White noise	**Yes** 15 cm (1-sigma) for code, 1.5 mm (1-sigma) for phase	**Yes** up to 0.5 mm (1-sigma)	**Yes** up to 0.5 mm (1-sigma)
Flicker-phase noise (distance dependent)	**No**	**Yes** 1.2-1.4 mm (1-sigma)	**Yes** 0.1-1.5 mm (1-sigma)
Troposphere	**Yes**	**Yes**	-
Phase Center Variations (PCV)	**Yes**	**No**	**No**
Constant bias	**Yes** up to 5 mm (1-sigma)	**Yes** between ±0.5 mm (1-sigma)	**Yes** between ±0.5 mm (1-sigma)
Variable bias	**Yes** up to 5 mm (1-sigma)	**Yes** between ±0.5 mm (1-sigma)	**Yes** between ±0.5 mm (1-sigma)

The scheduling of OTWL can be interpreted as an any-to-any scenario, but was optimized according to the visible satellites for a ground station per epoch. Analogously to OISL, the sampling of OTWL is 60 s in the simulations of this paper. It is only allowed that each satellite connects to one station per epoch and vice versa. At each epoch, a station connects to the satellite that is the closest in

azimuth and elevation in terms of the previous station-satellite link to avoid excessive slewing. In the case that this satellite is already connected to another station, the next nearest satellite is chosen for linking. The skipped satellite is then considered for a connection in one of the upcoming epochs. Double observations of a satellite in successive epochs or a suspending of the station for one epoch is allowed, but is avoided as much as possible.

The L-band+OTWL scenarios are compared to the L-band+OISL scenarios in terms of satellite POD and are evaluated against a L-band-only scenario. Furthermore, a scenario that combines all three observation techniques (L-band+OTWL+OISL) and a scenario that only uses the optical measurements (OTWL+OISL) are analyzed. In addition, we analyze the orbit modelling errors and run scenarios using additional empirical SRP parameters in the estimation. While first analyzing scenarios with estimation of ground station coordinates, we alternatively compute scenarios with fixed ground station coordinates. An overview of the estimated parameters for L-band, OTWL and OISL can be found in Table 4. A more detailed description can be found in the full version of the paper P-III.

Table 4: Overview of estimated parameters for L-band, OTWL and OISL in P-II.

	L-band	OTWL	OISL
Station specific tropospheric zenith delays	Yes	No	-
Ground station coordinates	No	No	-
Satellite initial state vectors and empirical SRP parameters	Yes	Yes	Yes
Epoch-wise satellite and ground station clock parameters	Yes	Yes	Yes
Phase ambiguities (float)	Yes	-	-
Range and clock biases	No	Yes	Yes

Summary

We started our study with an analysis of the orbit modelling. Therefore, we extracted the acceleration differences acting on the mismodelled orbit compared to the true orbit in the DYB directions – D points from the satellite to the Sun, Y is in the direction along the solar panels and B completes the right-handed orthogonal system. From the Power Spectral Density (PSD) of the acceleration differences, we analyzed the SRP impact in the DYB directions with respect to multiples of the orbital period. In addition to the ECOM2 parameters (see Eq. (2)), we noticed a large influence of the parameters of three and five times of the orbital period in B direction. Furthermore, we analyzed the empirical accelerations as a function of the beta angle. In particular, the B1, B3, D2, and D4 parameters show a large dependence on the beta angle, while the B5 parameters only have an impact when the beta angle is lower than about 35°. From the analysis of the acceleration differences, we

finally defined the empirical models we compare in our scenarios. While the ECOM2 (Eq. (2)) represents the reference case, we additionally perform scenarios with an SRP modelling according to ECOM2+B3 (Eq. (3)) and ECOM2+B3+B5 (Eq. (4)).

(3)
$$D(\Delta u) = D_0 + D_{2c}\cos(2\Delta u) + D_{2s}\sin(2\Delta u) + D_{4c}\cos(4\Delta u) + D_{4s}\sin(4\Delta u)$$
$$Y(\Delta u) = Y_0$$
$$B(\Delta u) = B_0 + B_{1c}\,cos(\Delta u) + B_{1s}\,sin(\Delta u) + B_{3c}\,cos(3\Delta u) + B_{3s}\,sin(3\Delta u)$$

(4)
$$D(\Delta u) = D_0 + D_{2c}\cos(2\Delta u) + D_{2s}\sin(2\Delta u) + D_{4c}\cos(4\Delta u) + D_{4s}\sin(4\Delta u)$$
$$Y(\Delta u) = Y_0$$
$$B(\Delta u) = B_0 + B_{1c}\,cos(\Delta u) + B_{1s}\,sin(\Delta u) + B_{3c}\,cos(3\Delta u) + B_{3s}\,sin(3\Delta u) + B_{5c}\,cos(5\Delta u) + B_{5s}\,sin(5\Delta u)$$

One of the main outcomes of this paper is the dependence of the results on whether estimating or fixing ground station coordinates. The scenarios including OTWL measurement can handle the estimation of ground station coordinates very well. This is due to the strong tying of the satellite to the ground station by the high OTWL precision. However, from the analysis of this paper it is clear that the results of the L-band+OISL scenario depend heavily on whether ground station coordinates are estimated or fixed. When estimating the station coordinates, the additional freedoms of the satellite constellation with respect to the Earth's surface restricts the geometry within the L-band+OISL measurement combination. If we first focus on a SRP modelling according to ECOM2, we notice about twice as large formal orbit uncertainties compared to the L-band+OTWL scenario. Nevertheless, the improvement of the formal orbit uncertainties of L-band+OISL with respect to L-band-only is by a factor of about 13 and accordingly a factor of about 26 for L-band+OTWL. A similar behavior can be found for the orbit errors (see Table 5), with an improvement by a factor of about 18 for L-band+OTWL and a factor of about 9 for L-band+OISL compared to the L-band-only solution. With a L-band+OTWL+OISL observation network, the orbit error improvement is approximately a factor of two compared to L-band+OTWL. The L-band+OISL combination benefits significantly from the fixing of the ground station coordinates and thus the tightening to the Earth's surface (see Table 6). While L-band+OTWL and L-band+OTWL+OISL measurement networks achieve similar results whether fixing or estimating station coordinates, the L-band+OISL scenario achieves similar orbit errors as the L-band+OTWL scenario when fixing ground station coordinates. The formal orbit uncertainties of a L-band+OISL scenario improve to the same level as L-band+OTWL as well. This indicates, that the geometrical benefit achieved with either OTWL or OISL is similar. The lowest formal orbit uncertainties are for the L-band+OTWL+OISL scenario, combining the synergies of both OTWL and OISL with L-band.

A second main outcome of this paper is the possibility of estimating additional empirical parameters when using combinations of observation techniques. While a L-band-only solution cannot handle the estimation of additional empirical parameters - resulting in an increased orbit error (see Table 6) - the combinations of observation techniques benefit from the additional empirical parameters

estimated. In a scenario with fixed ground station coordinates, all three types of combinations of observation techniques now achieve sub-centimeter level orbit error results in our specific simulations: about 6 mm with L-band+OISL, about 4.5 mm with L-band+OTWL and 3 mm with L-band+OTWL+OISL (see Table 6). A similar behavior can be found for the formal orbit uncertainties.

Finally, we analyzed the impact of a reduced number of available ground stations for OTWL measurements, representing scenarios with possible cloudy weather conditions or a station network that is not fully equipped with OTWL terminals. By reducing the number of available OTWL stations, the relative improvement of the L-band+OTWL scenarios continually decreases. With 7 OTWL stations in the ground segment, the degradation is at about a factor of 1.6, and with 3 available stations it is a factor of about 4.7 compared to the full network with 16 ground stations. Hence, the orbit errors behave almost directly proportional to the amount of available OTWL stations.

Table 5: MEO satellite orbit errors from solutions with estimating ground station coordinates, with respect to different combinations of observation techniques and SRP modelling.

	L-band-only [mm]	L-band + OTWL [mm]	L-band + OISL [mm]	L-band + OTWL + OISL [mm]
ECOM2	234.8	13.3	25.4	6.2
ECOM2+B3	275.1	3.6	21.6	3.4
ECOM2+B3+B5	294.9	3.6	21.9	3.4

Table 6: MEO satellite orbit errors from solution using fixed ground station coordinates, with respect to different combinations of observation techniques and SRP modelling.

	L-band-only [mm]	L-band + OTWL [mm]	L-band + OISL [mm]	L-band + OTWL + OISL [mm]
ECOM2	260.4	12.8	10.8	5.8
ECOM2+B3	311.9	4.3	5.8	3.0
ECOM2+B3+B5	329.5	4.5	5.9	2.9

Individual contribution: The idea of analyzing the impact of OTWL measurements in addition to L-band measurements was first developed in a talk between Anja Schlicht, Urs Hugentobler, the author of the dissertation and the company Tesat-Spacecom. The Matlab and Bernese implementations to be able to simulate and estimate OTWL measurements were carried out by the author of this dissertation. After the publication of initial results in Schlicht et al. (2019), the author of this dissertation continued the analysis with more depth together with Anja Schlicht and Urs Hugentobler. The author of this dissertation and Anja Schlicht designed the structure of this paper. The generation of the orbits, the simulation of the observations, the estimation of all scenarios as well as the generations of the figures and tables shown in the paper were carried out by the

author of this dissertation. The author of this dissertation, as the first author, wrote the paper. All co-authors improved the paper by their comments and correction.

Conclusions

Co-location of observation techniques, namely the combination of L-band and OTWL in our case, leads to a similar improvement as L-band+OISL in our simulation scenarios. This answers Q3. Moreover, the observation network benefits from the combination of L-band+OTWL+OISL, exploiting the synergy of all three observation techniques. This answers Q4. Through combinations of observation techniques, it is possible to estimate more empirical SRP parameters in the least-squares adjustment, thereby optimizing the orbit modelling. In our specific simulations, the orbit error improves significantly in the scenarios with the estimation of ECOM2 and additional B3 and/or B5 parameters compared to the ECOM2-only SRP modelling. This answers Q5.

Furthermore, we can conclude from the simulations that the results concerning OISL strongly depend on the fixing of the ground station coordinates. Therefore, to fully exploit the potential of a L-band+OISL scenario, we do not estimate the ground station coordinates in all following simulations. L-band+OTWL, on the other hand, already tightens the space segment to the Earth's surface due to the co-location of the observation techniques, driven by the high precision of the OTWL measurements.

3.3 P-III: POD with additional GSO satellites

P-III Marz, S.; Schlicht, A.; Hugentobler, U. (2023)
Geosynchronous Satellites Expanding a Future GNSS Satellite Constellation: A Precise Orbit Determination Study.
Advances in Space Research, 71(1): 624-644. doi: 10.1016/j.asr.2022.11.009.

Introduction

In P-I and P–II, the measurement techniques OISL and OTWL were introduced to the simulation study and analyzed. Both observation techniques in combination with L-band improve the geometry of the measurement and satellite constellation, leading to a more stabilized system and an improved POD. Another solution to improve the geometry is by including other satellite types - in different altitudes than the MEO satellites - to the constellation. While such satellites could be also LEO satellites, GSO satellites were chosen for this dissertation, leaning towards the goal of the GETRIS concept.

In this work, the expansion of a GNSS MEO satellite constellation with GSO satellites is analyzed. Therefore, either four GEO or four IGSO satellites are included in the MEO satellite constellation. For this paper, we switched the real Galileo constellation used in P-I and P-II into a simulated Walker

constellation, with each eight satellites on three orbital planes. The used orbital elements and information is based on 1st generation Galileo FOC satellites. The four simulated GSO satellites are equally distributed around the Earth. This allows analysis regarding the impact of the amount of visible ground stations for the GSO POD. For IGSO satellites, an inclination of 52° proved the best visibility with the ground station network. Similar to the MEO satellites, the GSO satellites are treated as GNSS satellites. For OTWL observations, the GSO satellites are directly integrated into the scheduling procedure (see Section 3.2). For OISL, the GSO satellites are integrated into the any-to-any connectivity scheme such that GSO satellites do not directly follow one another in the satellite list used for the scheme. Furthermore, the viewing angle of the GSO satellites is restricted to ± 90° around nadir and the maximum ranging distance is limited to 60000 km. The latter is to avoid a low signal-to-noise ratio from long distance signals.

In the paper, we discuss not only the POD capabilities for the GSO satellite in the different linking networks, but also for the MEO satellites in the MEO+GSO satellite constellations, compared to results of a MEO-only satellite constellation. The analysis is carried out for two simulation periods, each with an interval of 10 days. 1-day-arc solutions are processed.

Summary

As for the MEO satellites in P-II, we began with an analysis of the orbit modelling errors of the IGSO and GEO satellites. The SRP accelerations acting on the IGSO satellites are similar to those on the MEO satellites. While the MEO and IGSO satellites are in the nominal yaw-steering attitude mode, the GEO satellites are in orbit normal mode. In orbit normal mode, the solar panel is not oriented perpendicular to the Sun-satellite direction. Therefore, we use the $\overline{DYB}$ frame for the GEO satellites: $\overline{Y}$ is perpendicular to the orbital plane, $\overline{B}$ perpendicular to $\overline{Y}$ and the Sun-satellite direction, and $\overline{D}$ completes the right-handed orthogonal system. The analysis of the SPR accelerations impacting the GEO satellites led to Eq. (5), which was used as a GEO optimized empirical SRP parameter model in this paper.

$$\begin{aligned}(5)\qquad \bar{D}(\Delta u) &= \bar{D}_0 + \bar{D}_{1s}\sin(\Delta u) + \bar{D}_{2c}\cos(2\Delta u) + \bar{D}_{3s}\sin(3\Delta u) + \bar{D}_{4c}\cos(4\Delta u)\\ \bar{Y}(\Delta u) &= \bar{Y}_0 + \bar{Y}_{1s}\sin(\Delta u) + \bar{Y}_{2c}\cos(2\Delta u)\\ \bar{B}(\Delta u) &= \bar{B}_0 + \bar{B}_{1c}\cos(\Delta u) + \bar{B}_{2s}\sin(2\Delta u) + \bar{B}_{3c}\cos(3\Delta u) + \bar{B}_{4s}\sin(4\Delta u)\end{aligned}$$

First, we analyzed the formal orbit uncertainties. In general, the formal orbit uncertainties decrease significantly when L-band observations are combined with the optical measurements compared to the formal orbit uncertainties of a L-band-only scenario. In the case of a L-band+OISL scenario, the MEO formal orbit uncertainties improve by about 25% when a MEO+IGSO or MEO+GEO constellation is present compared to a MEO-only constellation. With L-band+OTWL, a MEO+IGSO constellation cannot achieve any improvement over the MEO-only constellation. The reason is that the clocks are already well synchronized in the MEO-only constellation due to the co-located observation network of L-band and OTWL. However, with GEO satellites in the constellation, the

formal orbit uncertainties improve due to the continuous observation of the same ground station clocks. The IGSO and GEO formal orbit uncertainties behave similar to the formal orbit uncertainties of the MEO satellites, as analyzed in the paper P-II. The main findings are that the formal orbit uncertainties in a L-band+OTWL scenario behave indirect to the total number of OTWL observations with respect to each GSO satellite. As soon as OISL measurements are part of the observation network, the errors are similar for all the GSO satellites.

When analyzing the orbit error, we first investigate the impact for the MEO POD in a MEO+GSO compared to a MEO-only satellite constellation. For the L-band-only scenario, where about 26 cm is achieved with the MEO-only constellation, we obtain 1-2 cm lower MEO satellite orbit errors with the MEO+GSO constellations. For all the scenarios in our specific simulations using combinations of observation techniques, we achieve a sub-centimeter POD level. The L-band+OTWL scenario does not show a significant difference in MEO POD when adding IGSO or GEO satellites to the constellation. With L-band+OISL, the MEO orbit error improves by about a factor of 1.5 with IGSO or GEO satellites in the constellation. For the L-band+OTWL+OISL scenario, we again notice no difference between a MEO-only, MEO+IGSO or MEO+GEO satellites constellation for MEO POD. However, the orbit error is already close to the best possible orbit error (see Section 2.1.3) of our simulations.

For IGSO POD in a MEO+IGSO satellite constellation we notice a dependence on the number of visible ground stations for each IGSO satellite. This means that a ground station network consisting of only 16 stations is not sufficient to achieve the same POD results four all for IGSO satellites in our simulated constellation for scenarios with only ground-space directed links (L-band-only and L-band+OTWL). For the L-band-only scenario, the best IGSO satellite achieves an orbit error of about 38 cm, which is by about a factor of 1.5 larger than the average orbit error of the MEO satellites. However, using a L-band+OTWL measurement network, the best observed IGSO satellite achieves the same POD level as the MEO satellites. Once OISL measurements are added in the observation network, all four IGSO satellites achieve about the same POD results, which are a factor of about two worse than the MEO POD results from the L-band+OISL scenario. With a L-band+OTWL+OISL observation network, the IGSO POD improves by a factor of about two compared to the L-band+OISL scenario, but the POD result is about 2 times worse than achieved for the MEO satellites in the same scenario.

Analyzing the POD results concerning GEO satellites, the best GEO satellite can only be determined to about 5 m using L-band-only. This is a much worse orbit error compared to the MEO and IGSO satellites. Using the combination of L-band with OTWL and/or OISL, the orbit error results behave similar to those of the IGSO satellites. These results show that the support of L-band by at least one of the optical observation techniques is indispensable to achieve useful GEO POD results with a small ground station network.

Individual contribution: The idea of analyzing the impact of GSO satellites as an extension for a GNSS MEO satellite constellation was of author of the dissertation. The author of this dissertation and Anja Schlicht designed the structure of this paper. Anja Schlicht simulated the PHM satellite clocks used for the scenarios. The generation of the GSO orbits, the simulation of the additional observations, the estimation of all scenarios as well as the generations of the figures and tables shown in the paper were carried out by the

author of this dissertation. The author of this dissertation, as the first author, wrote the paper. All co-authors improved the paper by their comments and correction.

Conclusions

For MEO POD, the expansion of a MEO-only constellation by either IGSO or GEO satellites only results in an improvement in a L-band+OISL scenario. This is due to an improvement of the geometry. With OTWL measurements in the observation network, the clocks are already well synchronized due to the co-location of L-band and OTWL measurements. Therefore, scenarios combining L-band and OTWL measurements do not show a further improvement of the MEO POD when expanding the constellation by GSO satellites. For GSO POD, similar orbit error results than for MEO satellites can be achieved when using the combinations of observation techniques. However, for scenarios without OISL measurements, the GSO POD depend heavily on the number of ground stations each GSO satellite can see and connect to. Here, a ground station network of 16 stations is not sufficient to achieve the same orbit errors for all the GSO satellites in the simulated satellite constellation. This answers Q6.

3.4 P-IV: Analysis of the satellite clocks

P-IV Marz, S.; Schlicht, A.; Hugentobler, U. (2023)
Toward a Geodesy and Time Reference in Space (GETRIS): A Study of Apparent Satellite Clocks of a Future GNSS Satellite Constellation.
Geosciences, vol. 13(6), art. 173. doi: 10.3390/geosciences13060173.

Introduction

This paper analyses the clock errors from the simulation scenarios performed in P-III. The scenarios of P-III were originally computed with PHM clocks carried by all satellites. We simulated the PHM clocks with white frequency noise at the level of $1 \cdot 10^{-12}$ and random walk at the level of level of $3.9 \cdot 10^{-16}$, when integrating over one second. We did not simulate a quadratic phase drift for the PHM clocks. For comparisons, we recomputed the scenarios using ACES clocks. While the PHM is a clock type that is already used in GNSS satellites, the ACES clock represents a future type of clock with significantly higher stability. The ACES clock is a combination of an Active Hydrogen Maser (AHM) and a laser-cooled Cesium clock, called PHARAO (see also Section 2.2.4). The AHM was simulated with flicker phase noise at the level of $1.4 \cdot 10^{-13}$, white frequency noise at the level of $3 \cdot 10^{-14}$ and flicker frequency noise at the level of $1.35 \cdot 10^{-15}$, when integrating over one second. We simulated PHARAO with white frequency noise at the level of $1 \cdot 10^{-13}$, when integrating over one second. For the ACES clock always the lowest noise dominates. The ACES clock is not expected

to have a quadratic phase drift as PHARAO is a frequency standard. The clock analysis is done not only for the estimated simulation interval, but also for the prediction of the clocks.

Summary

We analyzed the estimated (apparent) satellite clock errors by the mean error and the standard deviation for the different observations technique combinations L-band+OTWL, L-band+OISL and L-band+OTWL+OISL as well as the L-band-only scenario, for comparisons.

As the estimation of the clock synchronization biases leads to a rank-deficient normal equation matrix in our simulations, we had to introduce constraints for the bias estimation. Therefore, we first analyzed different constraints for the clock synchronization bias concerning OTWL observations. A constraining of the clock synchronization biases with respect to OISL measurements is not necessary as the any-to-any inter-satellite link scheduling allows to estimate the satellite clock synchronization biases. We analyzed a scenario with a tight constraining of the clock synchronization biases at the level of the OTWL measurement precision of 1 mm, and a scenario using five times looser constraints. The outcome is, that the mean errors of the estimated clocks from scenarios including OTWL measurements are already up to a factor of 10 worse when using the loose constraints compared to tight constraints. We processed all following solutions by using the tight constraints as the goal is to realize a time and ranging reference based on the satellites. Nevertheless, this shows that the OTWL measurement concept, as used in the papers, can still be optimized to be more robust in terms of the estimation of the clock synchronization bias. However, this may only be possible by using e.g. two OTWL terminals per satellite.

While the estimated satellite clocks have substantial mean errors at about 21 cm on average when using only L-band, the additional use of OTWL measurements helps to reduce the mean errors to the sub-centimeter level. The reason for this is that OTWL largely compensates the systematic errors that are no longer absorbed by the clock. Similar to L-band-only, the biases per satellite still vary in the case of L-band+OTWL. In our simulations, the maximum value of the mean error of the estimated clocks is at about 50 cm for L-band-only and about 3.8 cm for L-band+OTWL. In the L-band+OISL scenario, the OISL measurements help to uniformly distribute the mean errors on an average error with respect to each satellite. However, as OISL does not have a direct relation to the reference station, the mean errors of the estimated clocks are still substantial at about 18 cm on average. Hence, the strength of OISL is to uniformly distribute the mean errors of the estimated clocks, while the strength of OTWL is the compensation of the mean errors with respect to the reference clock. The L-band+OTWL+OISL scenario combines both advantages of OTWL and OISL, leading to a mean error of the estimated clocks in the low millimeter levels for all satellites. MEO, IGSO and GEO satellites all show a similar behavior for the mean errors of the estimated clocks.

Analyzing the standard deviation of the estimated clocks, the L-band-only scenario shows a high variability with about 3 cm for the minimum and 18 cm for the maximum value. With combinations of observation techniques, the standard deviations of the estimated clocks of all three kinds of combinations are at sub-centimeter level for all constellations.

The above described errors of the estimated clocks are similar for using either PHM or ACES clocks. This is expected as the clocks are estimated epoch-wise. The advantage of the ACES clock compared to the PHM is the much higher frequency stability. To analyze the stability for the different combinations of the observation techniques, we computed the Allan deviation. With PHM clocks, the estimated clocks from all three scenarios of combinations of the observation techniques show a similar stability and reach the stability of the true PHM clock almost for all averaging times. This means that the noise of the clock synchronization is smaller than the noise of the PHM clocks. With ACES clocks, the separation in achievable frequency stability between the combinations of the observation techniques is more pronounced. The L-band+OTWL and L-band+OISL scenarios benefit from the ability to achieve a higher frequency stability, but only the L-band+OTWL+OISL results reach the true ACES clock for intervals larger than about 20000 s.

The frequency stability of a clock is also important for the prediction of the clocks. Therefore, we analyzed the prediction of the clocks and showed the differences for all the scenarios processed either with PHM or ACES. Generally, the remaining mean errors from the estimation dominates the prediction of the clocks for short prediction times. This especially impacts L-band-only and L-band+OISL in our simulations. From the best possible analysis of the prediction of the true PHM clocks, the 95% percentile of the clock prediction errors decreases from the low centimeter level at short prediction times to about 1 m at 1-day prediction. As already shown with the analysis of the Allan deviation, the results of the clock prediction errors from a scenario using L-band-only do not reach the stability of the PHM clocks. On the other hand, the scenarios using the combinations of observation techniques are strongly limited by the PHM frequency stability. Performing a best possible analysis of the prediction of the true ACES clocks, only a minor degradation of the clock prediction error up to about 1-2 cm can be noticed up to a 1-day prediction. A similar behavior of a clock error degradation can be found for all the four measurement scenarios.

Individual contribution: The idea of analyzing the clock errors from the simulation scenarios of P-III was of the author of the dissertation, Anja Schlicht and Urs Hugentobler. The author of this dissertation designed the structure of this paper and decided, together with Anja Schlicht, to analyze the impact of high-precision satellite clocks for comparisons. Anja Schlicht simulated the ACES satellite clocks. The author of this dissertation, as the first author, processed the scenarios with the ACES clocks, wrote the paper and generated the figures and tables shown in the paper. All co-authors improved the paper by their comments and correction.

Conclusions

With the analysis of this paper, Q7 was answered. Measurement scenarios including OTWL measurements are able to largely compensate the mean errors of the estimated clocks with respect to the reference clock on ground compared to the L-band-only solution. While OTWL is unable to synchronize the clocks between the satellites, the use of OISL observations allows to do so. By synchronizing all the satellite clocks within the constellation, the OISL measurements help to generate a kind of common clock error for the entire satellite constellation, which is almost uniformly distributed across all satellites. The disadvantage of OISL is that there is no direct relation to the reference clock on ground. Hence, the mean clock error estimated with L-band between ground and

space is also only distributed between the satellites in the solution. The high-precision OTWL or OISL measurements help to reduce the standard deviation of the clock error to the sub-centimeter level, compared to about 8 cm at the mean for L-band-only. A combination of the two optical measurement techniques together with L-band allows to benefit from the advantages of OTWL and OISL. Finally, the L-band+OTWL+OISL scenario achieves clock errors at the millimeter level in our simulations, which transfers to a picosecond level clock accuracy.

4 Additional orbit error analysis

4.1 Extended analysis of the weight selection

It was mentioned in Section 3.1 that the weight between L-band and the optical links is important for the final orbit error results. As it is difficult to select a weighting that optimally represents reality, we decided to weight each scenario according to the best achievable orbit error. This weighting procedure thus provides the maximum potential that each link combination can accomplish in each scenario. Figure 6 shows the orbit error results for L-band+OTWL, L-band+OISL and L-band+OTWL+OISL – in a MEO-only constellation and using 16 ground stations – when varying the weights of the optical links with respect to L-band phase ($\frac{\sigma^2_{\text{L-band}}}{\sigma^2_{\text{OTWL/OISL}}}$). Scenarios with different empirical SRP parameter estimation are compared as well. In the L-band+OTWL+OISL scenario, OTWL and OISL are weighted equally. As we achieved orbit errors of about 260 mm using L-band-only, the orbit errors from the scenarios with the combinations of observation techniques are still much lower despite of the weighting of OTWL/OISL in the analyzed weight interval.

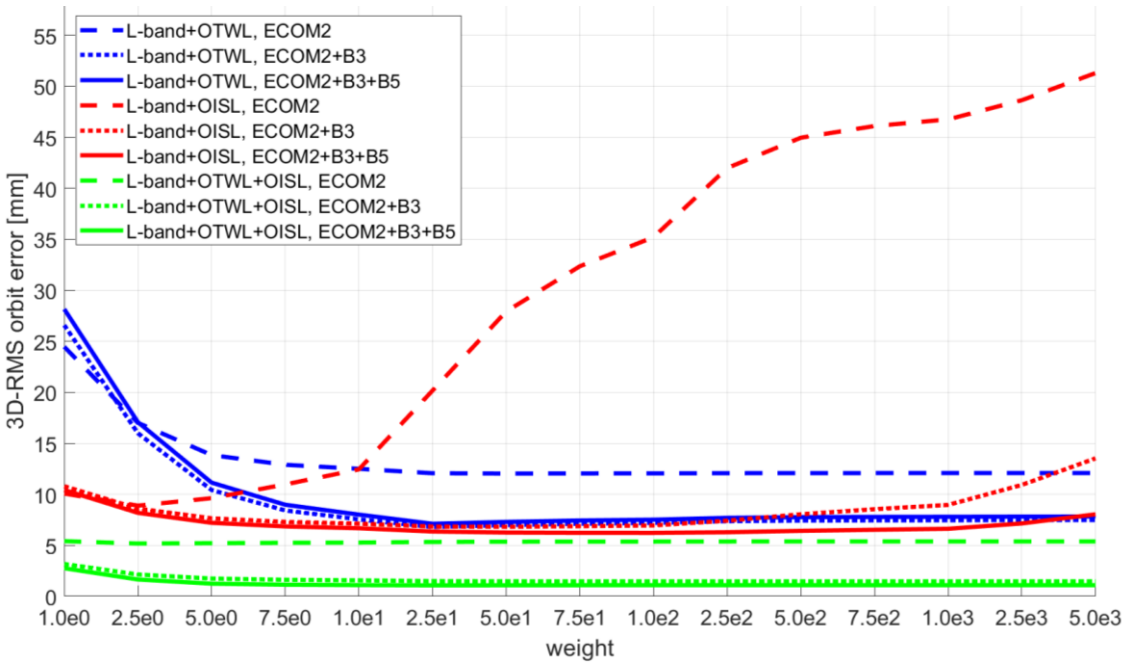

Figure 6: Orbit error results of scenarios using observation technique combinations as well as a different empirical SRP parameter estimation with respect to the weight of OTWL/OISL to L-band phase ($\frac{\sigma^2_{\text{L-band}}}{\sigma^2_{\text{OTWL/OISL}}}$). For L-band+OTWL+OISL, OTWL and OISL are weighted equally. For comparisons, L-band-only orbit error results are at the level of about 260 mm.

The L-band+OISL measurement network with empirical parameter estimation according to ECOM2 is the most sensitive in terms of weighting. In this case the optimal weight to get the minimum orbit error is in a quite small range. Deviation from this optimal weight already gives much worse results. If OISL is weighted to high with respect to L-band phase, the orbit errors show a tremendous increase. Therefore, it is very important for this scenario to be close to the optimal weight, otherwise the true quality of a L-band+OISL link combination can be largely misinterpreted. However, as soon as more empirical parameters are estimated, the range around the optimal weight is much more tolerant. This effect is even more pronounced when estimating B5 parameters in addition to ECOM2+B3. L-band+OTWL scenarios provide stable orbit error results for all scenarios when the weighting ratio OTWL/L-band is 25 or larger. An orbit error difference between the ECOM2 scenario and the scenarios with estimating more than nine parameters is well pronounced. For lower weights, the orbit error shows an increase. In our case, a weight of 1-2.5 does not indicate an orbit error improvement when estimating more empirical parameters. For the L-band+OTWL+OISL scenario, the orbit error result is similar regardless of the selected weighting. This is especially noticeable for the scenario with estimating parameters of the standard ECOM2 model.

L-band measurements provide the multiple linking between satellites and ground stations, as well as compensate for measurement outages of OTWL. This could be a reason for the stable behavior of the orbit error regardless of a higher weighting of OTWL. For very high weighting for OTWL with respect to L-band we expect an increase in orbit errors, as the influence of the epoch-wise linking of L-band is necessary. OISL itself cannot tighten the satellite constellation to the Earth's surface and therefore relies heavily on L-band measurements. Thus, L-band must not be weighted to low with respect to OISL. However, OISL allows to estimate additional empirical SRP parameters in a L-band+OISL scenario and therefore supports L-band to compensate systematic errors. An argument for this conclusion is that if L-band is weighted to high with respect to OISL, there is no supportive effect of estimating additional empirical parameters. The same argument is valid for L-band+OTWL.

Overall, we can conclude that the estimation of more than nine empirical parameters does not only help to get better orbit error results but also make the link combinations, especially L-band+OISL, less sensitive to the selection of the weight. Procedures such as a Variance Component Estimation (VCE) are used to determine the weighting in a least-squares adjustment. Depending on the total number of estimation parameters, a VCE can lead to much longer least-squares adjustment run times. But with the link combinations and the ability to estimate additional empirical parameters to ECOM2, the shown stability of the orbit error results with respect to the weight indicates that even just a constant weighting could be chosen, as commonly done for the L-band code to phase weighting.

4.2 Dependence on the precision of the optical links

For the results shown in the papers of this dissertation, we assumed a link precision of 1 mm for OTWL and OISL measurements. From a theoretical perspective, the technology to operate an optical link with such a high precision already exists, as shown for SLR in terms of ranging and time transfer with the upcoming ELT experiment. These ground-space optical links with 3 mm or a higher precision are well realizable (Schreiber et al., 2010; Luceri et al., 2019). For OISL measurements, it

is expected that the same link precision can be achieved. In this section, the orbit error results are analyzed with respect to the link precision of OISL and OTWL measurement. For comparisons to the high-precision link, link precisions as low as centimeter level are simulated. Questions to be answered are: How sensitive are the orbit error results on less precise optical measurements? How does the estimation of additional empirical parameters behave with less precise optical links?

4.2.1 L-band+OISL

First, the combination of L-band observations with OISL measurements is analyzed for different OISL precisions. Figure 7 shows the orbit error results according to the optimal weighting for each scenario with different OISL precisions.

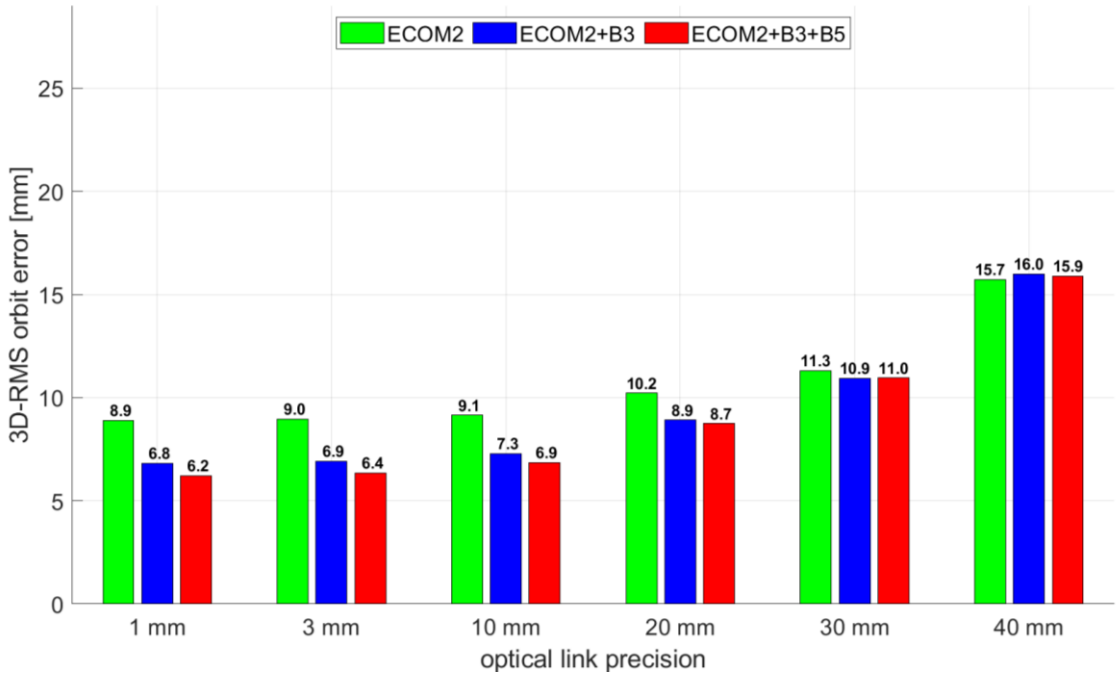

Figure 7: L-band+OISL orbit error results according to different OISL measurement precisions. For comparisons, orbit errors results using L-band-only are at the level of 260 mm.

For OISL precisions of 1 cm and higher, the ECOM2 scenario delivers almost the same orbit error results. For the scenarios with the estimation of more empirical parameters, the orbit error only increases by about 0.5 mm when the precision decreases from 1 mm to 1 cm. If the link precision deteriorates further, the orbit error increases more distinctly. To this effect, the discrepancy between the ECOM2 scenario and the scenarios with estimating more than nine empirical parameters is continuously getting smaller. With a OISL precision of about 4 cm, the ECOM2 scenario finally delivers slightly better results. Nevertheless, even OISL links with a 4 cm precision still result in an orbit error improvement by a factor of about 16 compared to L-band-only solution in our simulation

environment. As for an optical link we expect much higher link precisions than a few centimeters, the estimation of more empirical parameters will always lead to beneficial orbit error results.

4.2.2 L-band+OTWL

In this section, the combination of L-band observations with OTWL measurements according to the OTWL precision is analyzed. The used ground station network consists of 16 stations with a 100% measurement success rate. In reality, due to weather limitations or maintenance work, a 100% measurement yield from all 16 ground stations cannot be expected. Nevertheless, such a 100% scenario indicates the potential of the measurements network design. Therefore, we provide an additional analysis on weather limitations for OTWL in Section 4.3.1.

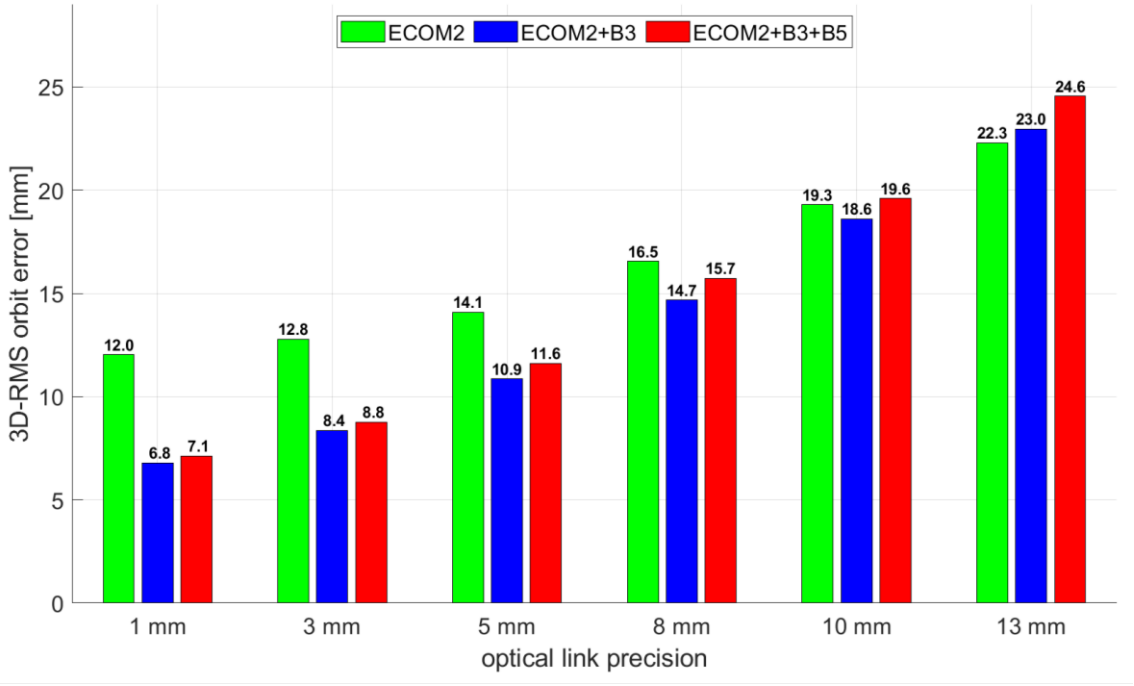

Figure 8: L-band+OTWL orbit error results according to different OTWL measurement precisions. For comparisons, orbit errors results using L-band-only are at the level of 260 mm.

Figure 8 shows the orbit error results for the scenarios using different OTWL precisions. The orbit error results are much more sensitive to the OTWL precision compared to OISL. Here, with a precision of 3 mm, the orbit error is already reduced by about 0.8 mm for the ECOM2 scenario and by 1.6 mm for the scenarios with the estimation of more than nine empirical parameters. Similar to OISL, the discrepancy between the ECOM2 scenario and the scenarios with estimating additional empirical parameters is continuously decreasing when lowering the OTWL precision. For OTWL precisions between 10-13 mm, the ECOM2+B3 and ECOM2+B3+B5 scenarios would finally be not

beneficial to ECOM2. It is worth mentioning that even a cm-level precision of OTWL measurements supports L-band to achieve orbit errors that are by a factor of about 12 lower compared to L-band-only solutions. However, state-of-the-art ground-space optical links already achieve precisions between 1-3 mm (SLR/ELT). Therefore, similar to L-band+OISL, it can be stated that estimating additional empirical parameters in a L-band+OTWL measurement combination is beneficial.

4.2.3 L-band+OTWL+OISL

The combination of L-band, OTWL and OISL uses the synergy of all three measurement techniques. Figure 9 shows the orbit error results of the L-band+OTWL+OISL scenarios with respect to different OTWL and OISL precisions. Again, it is assumed that we can measure with the full ground station network (16 stations) and a 100% measurement success rate. An analysis on the weather limitations can be found in Section 4.3.2.

The difference between 1 mm and 3 mm precision for both optical link types is negligibly small. Only when the OISL precision is further reduced to 1 cm, the orbit error begins to increase. However, the orbit error is still by a factor of about 2.5 smaller than achieved for the L-band+OTWL and L-band+OISL measurement networks with an optical link precision of 1 mm. This again underlines the strengths of the synergetic use of OTWL and OISL.

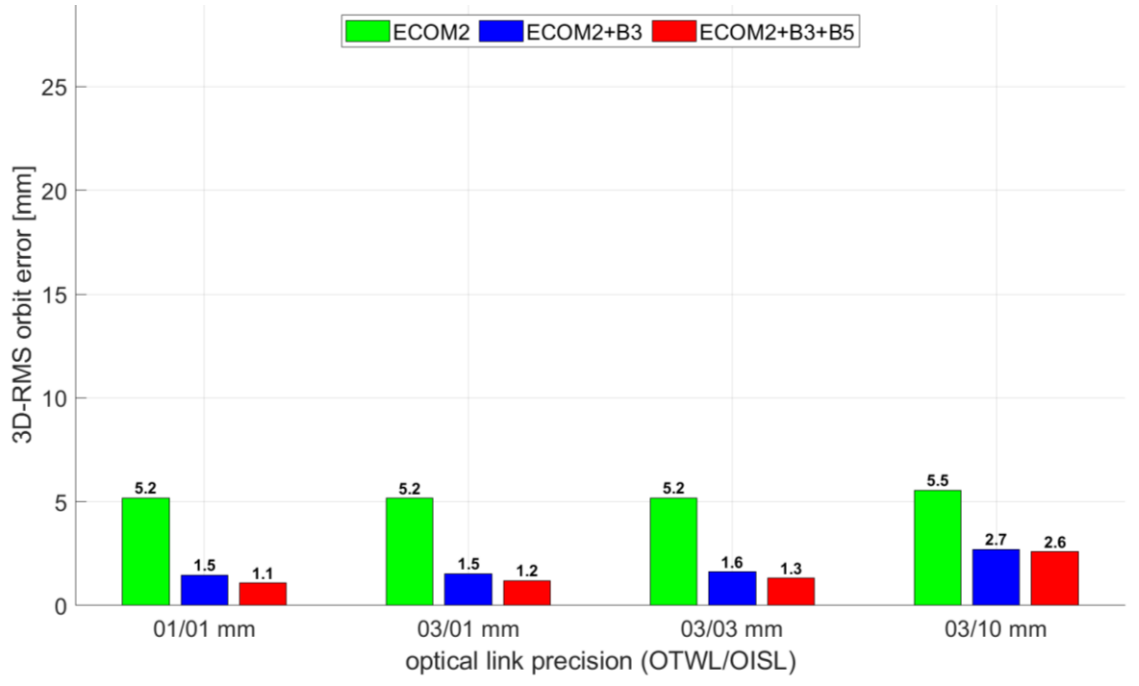

Figure 9: L-band+OTWL+OISL orbit error results with different OTWL/OISL measurement precisions.

4.3 Dependence on bad weather conditions

For the previous analysis, we mainly assumed perfect weather conditions for the OTWL measurements. A brief analysis with a reduced number of stations available for OTWL observations was given in the paper P-II of this dissertation. The aim was to simulate a scenario where either not all of the stations are equipped with hardware to perform OTWL measurements or stations cannot measure due to 100% cloudy weather conditions per day. In the following, we expand the analysis to include the influence of less precise OTWL measurements – 3 mm instead of 1 mm – (for L-band+OTWL). Furthermore, we investigate cases where the remaining stations in the network only have a OTWL measurement success rate of 30% (only for L-band+OTWL+OISL). The latter scenario indicates a worst-case scenario in terms of bad weather conditions.

4.3.1 L-band+OTWL

If we reduce the total number of available OTWL stations to seven as shown in Figure 10 – considering a 100% measurement success rate of the remaining stations –, we already notice an

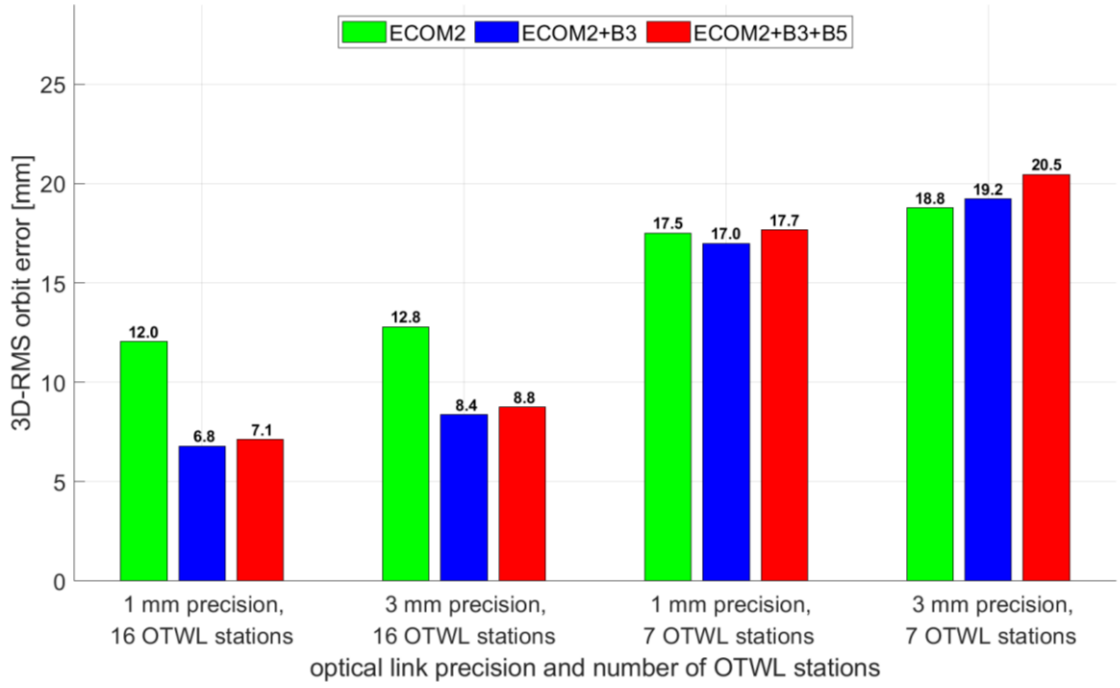

Figure 10: L-band+OTWL orbit error results with respect to the total number of OTWL stations. The remaining stations are assumed to have a 100% measurement success rate. For L-band measurements, the ground station network still consists of 16 stations. For comparisons, orbit errors results using L-band-only are at the level of 260 mm.

increase in orbit error by a factor about 1.46 for the ECOM2 scenario. This implies that reducing the number of available stations by a factor of two results in a worsening of the orbit error of about a square-root of two, which is expected. For the scenarios with estimating more parameters, the orbit error results increase by a factor of 2.5 with seven compared to 16 stations. This shows that the total number of OTWL measurements as well as the ground station geometry is not sufficient to handle the estimation of more empirical parameters. While for the seven stations and 1 mm OTWL precision scenario the ECOM2+B3 still delivers slightly better results than the ECOM2 scenario, for 3 mm OTWL precision the ECOM2 scenario is the best. We can conclude, that a L-band+OTWL scenario depends heavily on the number of available ground stations for OTWL measurements.

4.3.2 L-band+OTWL+OISL

In the following, we simulate scenarios with a reduced number of available stations to perform OTWL measurements in the case of a L-band+OTWL+OISL scenario. The results are shown in Figure 11. The scenarios are simulated with a measurement precision of 1 mm for OTWL and for OISL. From Figure 9 we learned that the resulting orbit errors from scenarios using 1 mm or 3 mm precision are almost identical in the case of a L-band+OTWL+OISL scenario. First, we assume a measurement success rate of 100% for the remaining stations. The orbit errors from scenarios with down to only four available stations is the same as we get for the 16 ground station scenario. Compared to the L-band+OTWL scenario, the additional inclusion of OISL measurements help to compensate for the reduced number of OTWL measurements and the less well geometrical distribution of ground stations. When only 3 stations are available for OTWL measurements, we gradually notice an increase in orbit error. However, the impact is only an increase in orbit error by around 12-15%, translating to a degradation of around 0.2 mm for the ECOM2+B3 and ECOM2+B3+B5 scenarios, which is negligibly small. An extreme scenario with the use of only one OTWL station – the reference station – leads to an increase in orbit error by a factor of about two for the ECOM2+B3+B5 scenario, while for the ECOM2 scenario there is no noticeable difference compared to the scenario with three available OTWL stations. This shows that theoretically only one OTWL station would be sufficient to support the L-band+OISL scenario by a precise tightening of the satellite network to the Earth's surface, resulting in a factor of 2.4 lower orbit errors compared to the best L-band+OISL scenario.

Up to now, we assumed a measurement success rate for the available stations of 100%. This represents the best-case scenario in terms of weather conditions with a reduced ground station network. In the following, we limit the success rate to 30% to show the impact of bad weather conditions at the available stations. This is done in a simple way by randomly removing OTWL measurements for each of the available stations – also for the reference station. The orbit errors with 30% measurement success rate is shown in Figure 12.

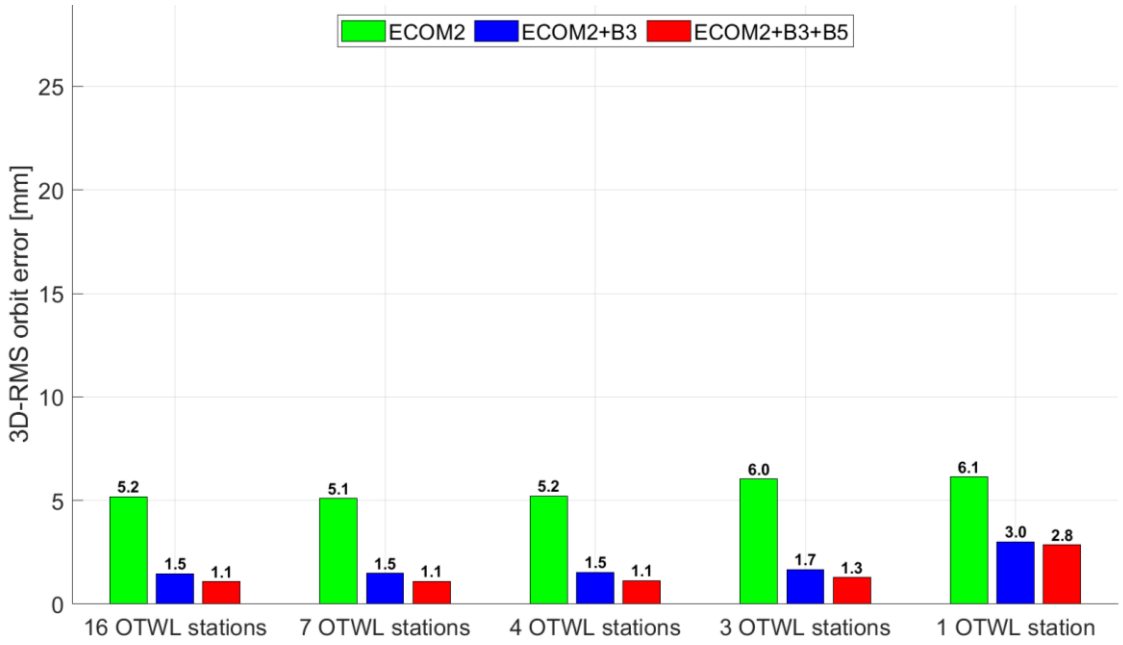

Figure 11: L-band+OTWL+OISL orbit error results with respect to the total number of OTWL stations; 1 mm OTWL and OISL measurement precision; 100% measurement success rate. For L-band measurements, the ground station network still consists of 16 stations.

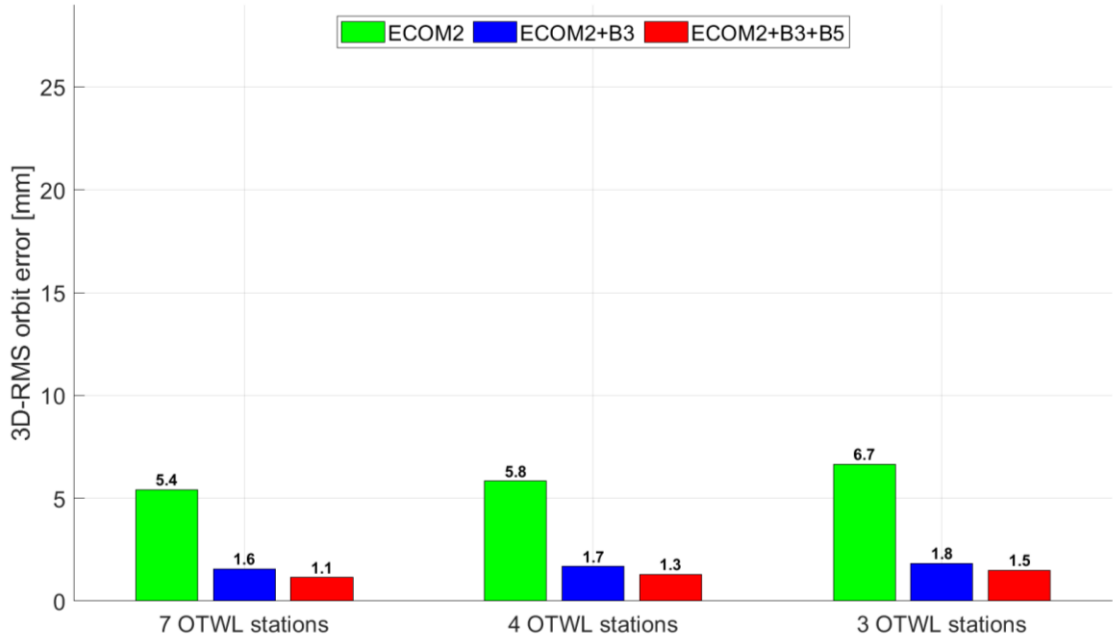

Figure 12: L-band+OTWL+OISL orbit error results with respect to the total number of OTWL stations; 1 mm OTWL and OISL measurement precision; 30% measurement success rate. For L-band measurements, the ground station network still consists of 16 stations.

For the scenario with 7 stations and 30% measurement success rate we still get similar results as for the scenario with 100%. Reducing the total number of available stations to four and having 30% measurement success rate leads to similar results as for the scenario with 3 stations and 100% measurement success rate. With 3 stations and a measurement success rate of 30%, similarly to the solution with measurement success rate of 100%, we observe a larger increase in orbit error of about 0.7 mm in the ECOM2 scenario compared to the 4-station solution. For the ECOM2+B3+B5 scenario we only have an increase of 0.2 mm. This means that in a worst-case scenario where 3 stations only have a measurement success rate of 30% per day and 13 station cannot measure at all, the orbit errors increase by around 22-27% compared to the best-case scenario with 16 stations and 100% measurement success rate. For the ECOM2+B3+B5 scenario, this degradation translates to an increase in orbit error of only 0.4 mm, which can be considered as rather small. We can conclude that only a small ground station network – even under bad case weather conditions – could be enough to support a L-band+OISL scenario to achieve significantly better orbit error results, when estimating additional empirical parameters for ECOM2.

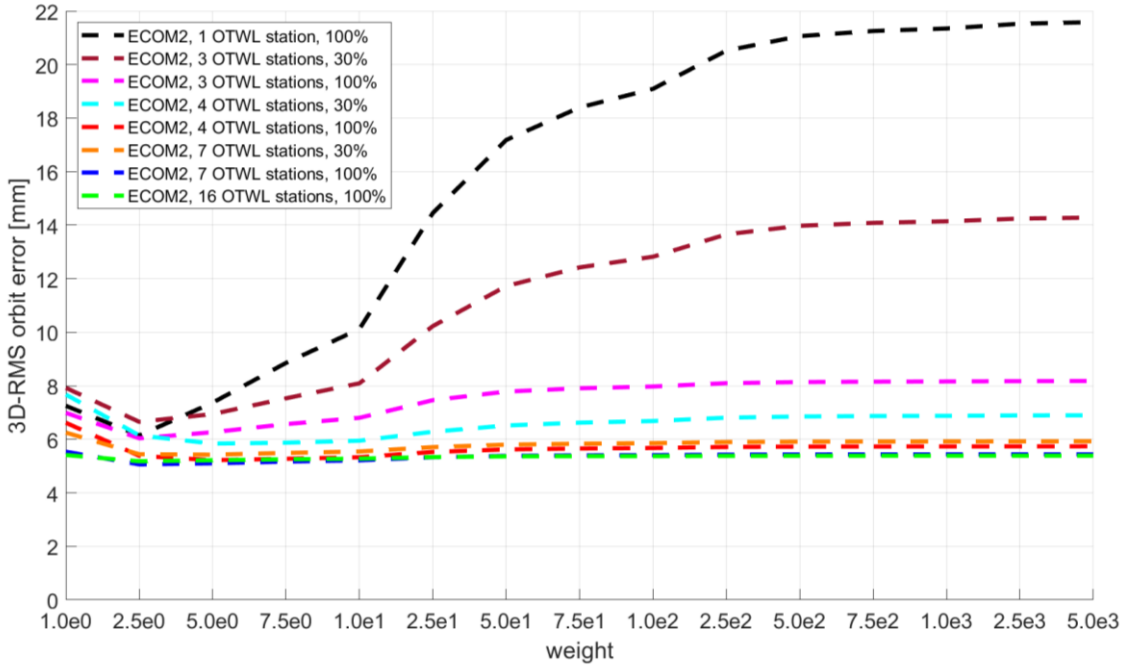

Figure 13: L-band+OTWL+OISL orbit error results with respect to the weight of OTWL/OISL to L-band phase ($\frac{\sigma^2_{\text{L-band}}}{\sigma^2_{\text{OTWL/OISL}}}$) for scenarios with an SRP modelling according to ECOM2. OTWL and OISL measurements are weighted equally. 1 mm OTWL and OISL measurement precision is used. The scenarios differ in the total number of available OTWL stations as well as the measurement success rate (100% or 30%).

Figure 13 shows the behavior of the orbit error results with respect to the weighting of the optical measurements to the L-band phase of the above given scenarios with SRP modelling according to ECOM2. Figure 14 shows the same for the ECOM2+B3+B5 scenarios. When analyzing the behavior

of the ECOM2 scenarios (see Figure 13), we noticed an increasing similarity to the behavior of the weight of the L-band+OISL scenario (compare Figure 6) when reducing the number of available stations for OTWL measurement and/or decreasing the measurement success rate. The reason for this behavior is again the decreasing support of OTWL for L-band to tighten the satellite constellation to the Earth's surface when reducing the number of OTWL stations or measurements. For the optimal weighting of about 2.5, the different scenarios achieve quite similar orbit errors, while a too high weight leads to a substantial discrepancy between the different scenarios.

For the ECOM2+B3+B5 scenarios shown in Figure 14, the behavior is opposite. Low weighting of the optical links result in a distinct orbit error difference of up to 5 mm, while with a weight of about 25 or larger almost the same orbit errors are achieved for the different scenarios with three or more available stations for OTWL.

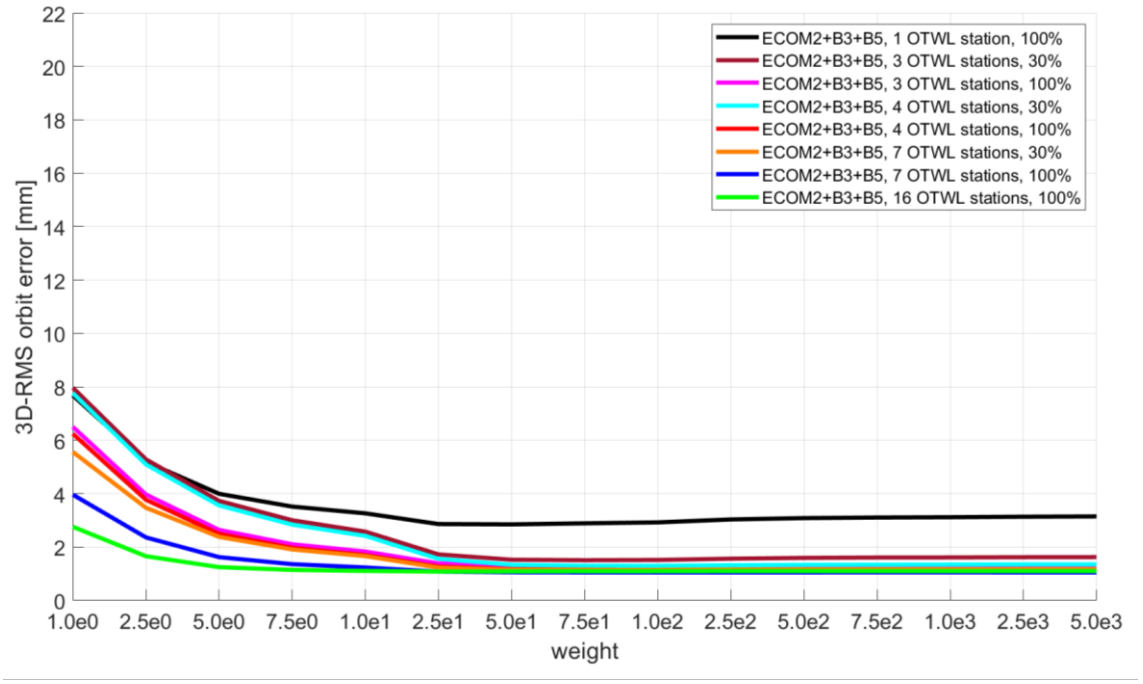

Figure 14: L-band+OTWL+OISL orbit error results with respect to the weight of OTWL/OISL to L-band phase ($\frac{\sigma^2_{\text{L-band}}}{\sigma^2_{\text{OTWL/OISL}}}$) for scenarios with an SRP modelling according to ECOM2+B3+B5. OTWL and OISL measurements are weighted equally. 1 mm OTWL and OISL measurement precision is used. The scenarios differ in the total number of available OTWL stations as well as the measurement success rate (100% or 30%).

5 Conclusions and outlook

5.1 Conclusions

In this dissertation, we built up a concept for a GEodesy and Time Reference In Space (GETRIS). The focus of the concept is on the measurement network to be used and on the satellite network, which should be based on a classical GNSS MEO constellation expanded by GSO satellites. We analyzed the impact on the satellite orbits and the clock synchronization for the GETRIS concept. With the goal to achieve satellite orbits at the level of 1-3 mm and a ps-level clock accuracy, we expanded the concept step-by-step in terms of the measurement and satellite types. This procedure allowed a comparison of different measurement scenarios and the impact on satellite POD.

For the design of the measurement network, we studied the impact of two different optical measurement types when using them in addition to GNSS L-band observations. The first optical link concept is the two-way satellite-to-satellite tracking OISL, the second the two-way ground-space oriented OTWL. Both optical techniques are assumed to use the same measurement technology. Thereby, an advantage for the satellite-to-satellite link is that no troposphere error is influencing the observations. The analysis was carried out for a MEO-only satellite constellation as well as for the MEO satellite constellation expanded by GSO satellites. With the goal to achieve satellite orbits down to 1 mm precision, the overall precision of the optical observations is assumed to be also 1 mm. This precision is still comparable to state-of-the-art pulsed SLR and ELT measurement techniques, although continuous wave measurement concept such as OTWL and OISL are able to reach much higher modulation rates and therefore have the potential for an even higher link precision.

Overall, it can be concluded that the additional use of the optical measurement techniques OTWL and OISL helps to significantly reduce the orbit and clock errors of satellites compared to L-band-only solutions. One of the most important findings from the analysis is that more empirical parameters can be estimated when using precise optical measurements in addition to L-band. This helps to reduce the orbit errors because orbit modelling errors, mainly affected by SRP, could be better compensated (answer to Q5). Furthermore, dependencies of the results on the beta angle – the sun elevation angle above the orbital plane – have been largely eliminated. As shown in the additional analysis in Section 4.2, the ability to estimate more empirical parameters depends on the precision of the optical link. However, state-of-the-art optical link precisions of about 3 mm at the maximum are not affected.

In P-I we analyzed the impact of OISL measurements used in addition to L-band. A main part of P-I was to show the impact of different OISL connectivity schemes on the MEO orbit errors. The result was that an any-to-any connectivity scheme provides the lowest orbit errors (answering Q2). The POD results of P-I showed that L-band+OISL significantly reduces the orbit errors compared to L-band-only. While still estimating ground station coordinates to achieve the results of P-I, we have

noticed from a solution using fixed ground station coordinates (performed in P-II) that L-band+OISL can still be improved. The fixing of the station coordinates helps L-band+OISL to tighten the satellite constellation to the Earth's surface. In P-II we also introduced OTWL measurements as a ground-space alternative to OISL for a combination with L-band. We compared L-band-only, L-band+OTWL, L-band+OISL and L-band+OTWL+OISL measurement scenarios for a MEO-only constellation. While P-I and P-II build on a real Galileo MEO satellite constellation (as of 2019), we switched alongside P-III to a simulated GNSS MEO satellite constellation. This allowed us to perform the simulations for a fully equipped Walker constellation based on 1st generation Galileo MEO satellites.

To draw conclusions, Figure 15 shows the orbit error results of a time interval of 10 days of our simulations for MEO POD. The total orbit error is also split into the main contributing errors analyzed in this work: remaining orbit modelling errors – represented by the best possible orbit error –, formal orbit uncertainties and systematic errors.

With L-band only, the orbit error is at around 26 cm in our simulations. Thereby, systematic errors have a contribution of almost 90% to the orbit error. In the following, the orbit error results for the combinations of observation techniques are concluded by referring to the associated questions as of Section 2.3.

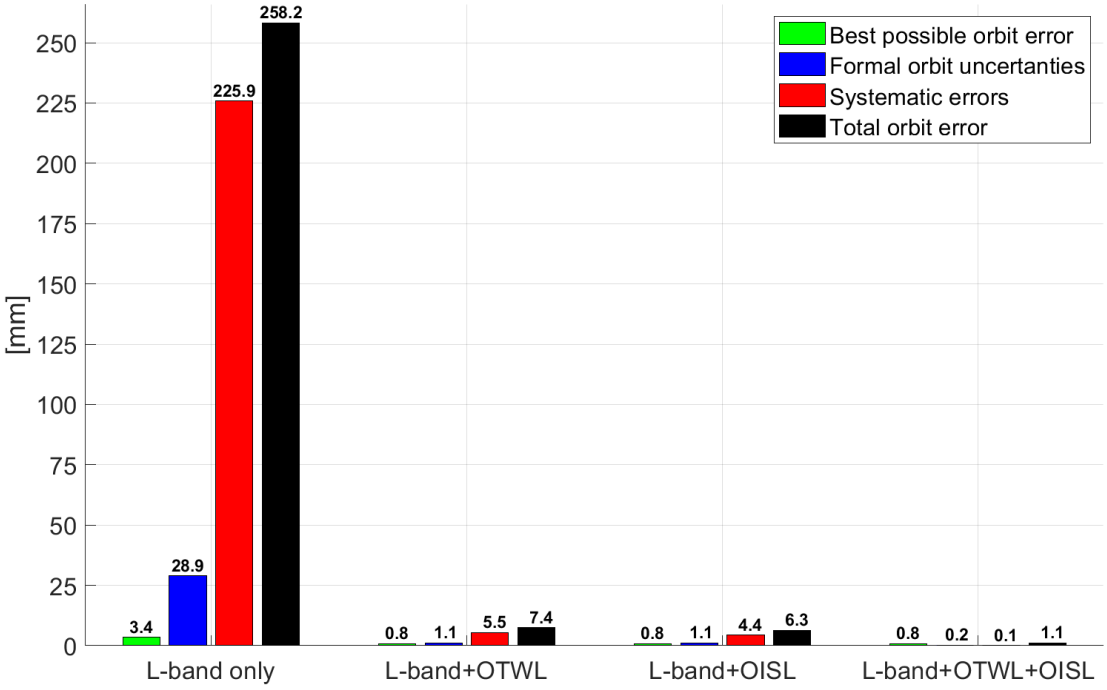

Figure 15: Summary of MEO orbit error results from P-III.

- Q1: Using L-band+OISL, we achieve MEO satellite orbit errors at the level of about 6-7 mm. Compared to L-band-only, all of the analyzed error contributions are significantly reduced. With a share of about 60%, systematic errors have still the largest contribution to the orbit error. The OISL measurements help to enhance the geometrical design, leading to formal

orbit uncertainties at the level of about 1 mm. As the estimation of more empirical SRP parameters is possible in a L-band+OISL scenario compared to L-band-only, the remaining orbit modelling errors – shown by the best possible orbit error – reduce by a factor of about 4.

- Q3: Achieving MEO orbit errors of about 7 mm with L-band+OTWL, the results are at a similar level as L-band+OISL. Remaining orbit modelling errors and formal orbit uncertainties behave similar for L-band+OTWL as for L-band+OISL. The L-band+OTWL orbit errors are also dominated by systematic errors. Depending on the analyzed simulation period, small variation in the systematic errors could be noticed for L-band+OTWL but also for L-band+OISL orbit error solutions, giving periods where L-band+OTWL achieved lower orbit errors than L-band+OISL in our simulations. This indicates that both measurement combinations are affected by differently simulated systematic errors of the optical links per simulation period. Furthermore, even though OTWL measurements are additionally influenced by troposphere errors, while OISL measurements are not, no significant impact on the orbit error could be found for L-band+OTWL compared to L-band+OISL.

  As shown in the additional analysis of Section 4.3.1, the total number of available OTWL stations can represent a major limitation for the ability to estimate more empirical parameters with a L-band+OTWL scenario. While MEO POD largely gained from the estimation of more parameters when using a ground station network consisting of 16 stations, the scenario with seven OTWL stations showed that there is almost no benefit with an extended empirical parameter model. However, the overall improvement of a L-band+OTWL scenario is still significant compared to a L-band-only scenario – reducing the MEO satellite orbit errors by a factor of about 14 in our simulation scenarios.

- Q4: Using the synergy of all three measurement techniques L-band+OTWL+OISL, the impact of the systematic errors and the formal orbit uncertainties decrease to the low sub-millimeter level. Achieving MEO orbit errors of about 1 mm in our simulations, the remaining orbit modelling errors have the largest contribution to the orbit error. It can be concluded, that only the L-band+OTWL+OISL measurement network has the potential to achieve the goal of a GETRIS to have satellite orbits with a precision at the level of 1-3 mm.

  From the additional analysis for the L-band+OTWL+OISL scenario in Section 4.3.2 it could be shown, that the reduction of the number of available OTWL stations is nearly negligible. In principle, using only one station for OTWL gives a better result compared to an L-band+OISL. Overall, it suggests that OISL should be the preferred measurement technique to complement L-band when there are only a few ground stations available. However, the additional use of OTWL measurements alongside OISL manifests its complementarity due to an enhanced geometry. The synergy shows up in the case of a co-located use. While OISL is capable of determining relatively satellite positions and synchronizing all satellite clocks to one another, L-band is not precise enough to well determine the absolute satellite positions with respect to the Earth centered frame. Here, the high-precision OTWL measurements help to tighten the satellite network. This underlines the synergetic aspects of OISL and OTWL,

and recommends a common use of OISL and OTWL for future satellite constellations in terms of precise orbit and clock determination.

Furthermore, in P-III we expanded the MEO satellite constellation by each four IGSO or GEO satellites. Figure 16 provides a summary of the IGSO satellite orbit error analysis. The figure shows the results for the IGSO satellite with the lowest total orbit error that we achieved in our simulations. The same applies to GEO satellites in Figure 17.

Achieving orbit errors of about 40-50 cm for IGSO and 4-5 m for GEO satellites when using only L-band measurements, we can conclude that the GSO orbit errors significantly improve when using a combination of L-band as well as OTWL and/or OISL. Overall, the best IGSO and GEO satellite achieve similar total orbit errors than the MEO satellites for all the combinations of the observation techniques. Moreover, remaining orbit modelling errors, formal orbit uncertainties and systematic errors behave similar to the MEO satellite orbit error results. The systematic errors contribute the most to the orbit errors that we achieve with L-band+OTWL and L-band+OISL measurement combinations. The dominant contributor in the case of L-band+OTWL+OISL are the remaining orbit modelling errors. With GSO orbit errors at the level of about 2 mm in the case of L-band+OTWL+OISL, we can conclude that the GETRIS goals can also be fulfilled for GEO and IGSO satellites. The analysis answered Q6.

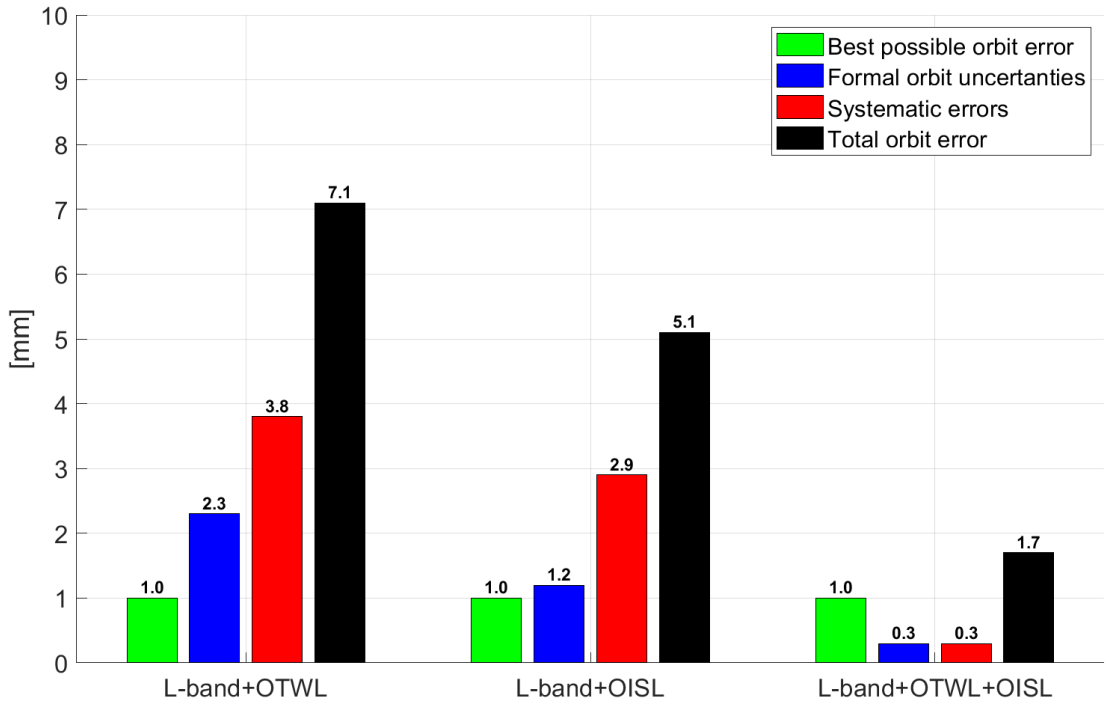

Figure 16: Summary of IGSO orbit error results from P-III. The graphic shows the results for scenarios using the combinations of observation techniques. For each scenario, the errors regarding the best determinable IGSO are given. For comparisons, the L-band-only results are at the level of about 40-50 cm, with systematic errors making the largest contribution to the total orbit error.

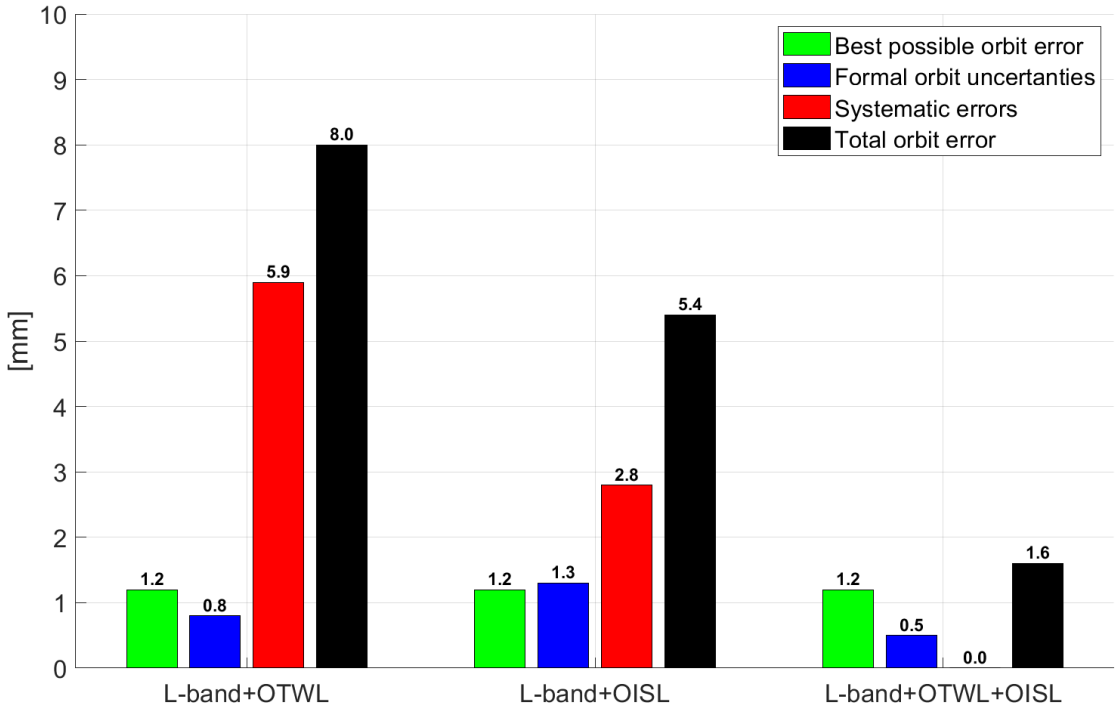

Figure 17: Summary of GEO orbit error results from P-III. The graphic shows the results for scenarios using the combinations of observation techniques. For each scenario, the errors regarding the best determinable GEO are given. For comparisons, the L-band-only results are at the level of about 4-5 m, with systematic errors making the largest contribution to the total orbit error.

To complete the goals of a GETRIS in terms of creating also a time reference, in P-IV we analyzed the satellite clocks from the simulation performed in P-III. Overall, the errors of the satellite clock are significantly reduced when using the combinations of observation techniques compared to L-band-only. For measurement network designs including OISL observation, we can conclude that all satellite clocks are synchronized to a common clock of the satellite constellation – achieving almost uniformly distributed clock errors between all satellites. However, with a L-band+OISL measurement network, the synchronization between the reference clock on ground and the satellite clocks occurs via L-band. Therefore, the mean error of the estimated clocks is much larger than possible to achieve with a L-band+OTWL measurement network. The high-precision OTWL measurements largely compensate for the mean errors of the estimated satellite clocks with respect to the reference clock on ground. However, OTWL is unable to synchronize all the satellite clocks in the constellation. Using L-band+OTWL+OISL, the advantages of all three measurement techniques can be combined. In our simulation, we finally achieved a picosecond level clock accuracy using L-band+OTWL+OISL. The analysis answered Q7.

In this dissertation it could be shown, especially with a L-band+OTWL+OISL measurement concept and an optimized empirical parameter estimation, that orbits of MEO, IGSO and GEO satellites can be determined at the low millimeter level and that clock achieve a picosecond accuracy. This fulfills the introduced requirements of a GETRIS and indicates, that such a measurement concept could possibly contribute to the installation of a GETRIS in the future.

5.2 Open questions

From this dissertation, some new questions arise or questions remain open, as they are not covered by this dissertation. In the following, these questions are listed with respect to the three key pillars (see Figure 2). The questions are closely related to the measurement network and satellite constellation design used in this dissertation, but also leave room for a more general interpretation.

5.2.1 Modelling

Orbit modelling

In our simulations, the optimized orbit modelling included B3 and B5 empirical parameters in addition to ECOM2. Dependent on the orbit modelling, the empirical parameters that are estimated might be adapted and optimized to different satellite types, constellations or applications. While L-band-only cannot handle the estimation additional empirical SRP parameters due to parameter correlations, the combination of L-band with OTWL and/or OISL allows to do so. With the ability to estimate more empirical SRP parameters using combinations of observation techniques, estimation of other kind of parameters without obtaining parameter correlations might also be possible.

O1: How are the results of scenarios using combinations of complementary observation techniques affected when more complex orbit modelling errors such as thruster leakage, thermal imbalances, attitude errors or center of mass variations are taken into account?

O2: In addition to the estimation of empirical SRP parameters, what are the implications of estimating additional parameters such as radiator or attitude parameters in scenarios that use combinations of complementary observation techniques?

The different instruments used for ranging and time transfer are influenced by Center of Mass (CoM) variations. With these different types of ranging instruments, it may be possible to estimate the CoM variations. Here it might be necessary to have e.g. two terminals for OISL measurements or in addition other measurement types alongside L-band, OTWL and OISL.

O3: What are the implications of estimating CoM errors in scenarios using combinations of complementary observation techniques?

Estimation of Earth Orientation Parameters (EOPs) and geocenter coordinates

The estimation and handling of EOPs and geocenter coordinates can be investigated as well. Commonly, for the estimation of EOPs in L-band-only solutions, a ground station network containing some hundreds of stations is used. Uncertainties in modelling non-gravitational forces, especially SRP, impede an accurate estimation of Earth's geocenter variations using only L-band measurements in a MEO-only constellation (Meindl et al., 2013). Glaser et al. (2020) show that a combination of L-band and precise optical ISL measurements as well as the use of a large ground station network is able to significantly improve the estimation of EOPs and geocenter coordinates. Through combinations of complementary observation techniques, a much smaller ground station network could be sufficient to accurately estimate EOPs and geocenter coordinates.

O4: Is it possible to accurately estimate EOPs when using combinations of complementary observation techniques and a small ground station network of e.g. 16 stations?

O5: Which observation network configuration is required to accurately estimate the Earth geocenter variations?

O6: What is the minimum number of ground stations required to accurately estimate the EOPs in scenarios using combinations of complementary observation techniques?

Troposphere modelling

We use L-band and OTWL as co-located measurements. We make use of the local and clock ties, but not the tropospheric ties. As one is performed in the microwave and the other in the optical domain, both are sensitive to the same troposphere in different ways. Microwave delays are sensitive to the wet and dry part, whereas optical delays depend on the dry part only.

O7: To what extent can the troposphere modelling be improved by using co-located L-band and OTWL measurements?

O8: Can a common troposphere be estimated from the combination of microwave and optical measurements?

O9: Can several precise local troposphere models be connected by measurement types such as OISL to a precise global model?

Clock modelling

In our current simulation, clock corrections are estimated epoch-wise. Hence, there is no difference for the clock estimation when using PHM or the more stable ACES clocks.

O10: What is the impact of a non-epoch-wise clock estimation – e.g. estimation of daily clock offset and drift parameters – compared to an epoch-wise clock estimation?

5.2.2 Geometry

The results achieved in this dissertation show that it is possible to estimate the orbits of MEO and GSO satellites at a similar level. An additional expansion of the satellite constellation by other satellite types is possible. This could further improve the geometry.

Constellation expansion by LEO satellites

The inclusion of LEO satellites to the satellite constellation could e.g. be realized by optical links between the LEOs and several GSO satellites as well as with additional L-band tracking from the GNSS MEO satellites. An alternative would be the direct linking of LEO and MEO satellites by optical measurements, as already envisaged in the Kepler concept (Michalak et al., 2021). The impact of a GETRIS-like infrastructure with ISL between either MEO and LEO or GEO and LEO satellites on gravity field recovery has already been discussed by Hauk et al. (2017).

O11: What impact does the use of a L-band+OTWL+OISL measurement network and a MEO+GSO+LEO satellite constellation have on LEO POD?

O12: Can the orbits of GSO and MEO satellites be further improved if LEO satellites are included in the constellation and a L-band+OTWL+OISL measurement network is used?

Constellation expansion by satellites in the deep space

While LEO satellites are representatives for a constellation expansion in the near-Earth environment, the satellite constellation could be expanded by satellites in the deep space, too. These can e.g. be HEO satellites, satellites at the Lagrange points, satellites in lunar transfer orbits or GNSS satellites inserted around the Moon.

O13: What is the POD impact for deep space satellites when such satellites are integrated into a MEO+GSO satellite constellation and combinations of complementary observation techniques are used?

5.2.3 Instrumentation

With L-band, OTWL and OISL three types of observation techniques were covered in this dissertation. E.g. with the aim of GGOS to combine, coordinate and optimize several types of measurement techniques, the measurement network can be further expanded. This could allow additional compensation of systematic measurement errors remaining in the observation network.

Fiber links in a ground station network

OISL helps to establish a kind of common clock for the satellite network. Using OTWL or ELT, the space clock can be synchronized with ground station clocks. However, the clocks within the ground station network are not synchronized. Concepts and applications using fiber links between the ground stations will help to synchronize clocks within a ground station network. As this might lead to several local networks on different continents, an intercontinental clock comparison through the satellite network might be possible.

O14: What impact does the integration of fiber links between ground stations have in addition to the discussed satellite constellation and measurement concept design?

O15: What is the advantage of synchronizing the clocks of different local fiber networks through a satellite network using measurement techniques such as OISL and OTWL?

Radio interferometry from satellites

There is discussion about implementing VLBI-type transponders on satellites that transmit signals that are detected by ground stations. Through the additional spatial and positioning information of the radio interferometry measurements, additional systematic errors within the measurement network might be detected and compensated. Moreover, it might be possible to estimate more parameters to further improve the modelling.

O16: What are the implications on POD if using VLBI type transponders carried by the satellites alongside the discussed measurement concept design?

5.2.4 Establishing a GEodesy and Time Reference In Space (GETRIS)

With a precisely determined MEO and/or GSO satellite network with orbit errors at the level of 1-3 mm and high-precision clocks, the basis for a GETRIS would finally be accomplished. Such a GETRIS can be used for ranging, time transfer as well as data transfer, and interact in addition to the ground station reference network.

Advantages of a GETRIS over the reference based on ground stations would be that there is no troposphere that has to be crossed when connecting to the satellites. The connection between the near-Earth environment and deep space is much easier. Data can be directly shared from the satellite network all over the globe. Furthermore, the clocks used in satellites are generally much more stable than the clocks used on ground. Hence, time transfer and measurements from a GETRIS would overall enhance the measurement quality. Nevertheless, to achieve precise determined satellite orbits for a GETRIS, the connection to the ground stations by links such as L-band or OTWL are of great importance.

O17: It is possible to install and operate a GETRIS with the satellite constellation and measurement concept design discussed?

5.3 Outlook

Precisely determined satellite orbits as well as synchronized precise and stable clocks are the basis for several future application and missions in space research, geophysics, geodesy and fundamental physics. The foundation for the determination of satellite orbits at the low millimeter level are the combination of different observation techniques (geometry), a high precision of used measurement techniques such as OISL and OTWL (instrumentation), but also the optimization of the modelling. For instance, improvements in the latter category is often only possible when using the synergy of different observation techniques to solve problems with parameter correlations. This again shows the connection between the three key pillars. Progress in all three categories is needed to achieve the future goals of the above mentioned application fields.

As an example in the field of geodesy, GGOS aims exactly at progress and combination in all three key pillars that we have defined for this study. The work of this dissertation gave ideas and showed a possible implementation to use the synergy of different observation techniques as well as how to optimize the determination procedure. The achievement of extensively better modelled orbits can help to e.g. remove signals with a draconitic period from the geodetic parameters. This might allow GNSS to contribute to the geocenter determination alongside observation techniques such as SLR. This offers the opportunity to eventually further improve the stability of the International Terrestrial Reference Frame (ITRF). Low millimeter level orbit accuracies or the installation of a GETRIS might be indispensable to accomplish the goals of GGOS – achieving a precise terrestrial reference frame with 1 mm accuracy and a stability of 0.1 mm/year.

6 Bibliography

Abich, K.; Abramovici, A.; Amparan, B.; Baatzsch, A.; Okihiro, B. B. et al. (2019) In-Orbit Performance of the GRACE Follow-on Laser Ranging Interferometer. In: Physical Review Letters 123(3):031101. doi: 10.1103/PhysRevLett.123.031101.

Arnold, D.; Meindl, M.; Beutler, G.; Dach, R.; Schaer, S.; Lutz, S.; Prange, L.; Sosnica, K.; Mervart, L.; Jäggi, A. (2015) CODE's new solar radiation pressure model for GNSS orbit determination. J Geod 89:775-791. doi: 10.1007/s00190-015-0814-4.

Ashman, B. W.; Parker, J. J. K.; Bauer, F. H.; Esswein, M. (2018) Exploring the Limits of High Altitude GPS for Future Lunar Missions. 41st Annual AAS Guidance & Control Conference (AAS/GNC 2018), Breckenridge, Colorado, USA, February 2-7th, 2018. https://ntrs.nasa.gov/search.jsp?R=20180001247.

Bauer, F.H.; Moreau, M.C.; Dahle-Melsaether, M.E.; Petrofski, W.P.; Stanton, B.J.; Thomason, S.; Harris, G.A.; Sena, R. P.; Temple, L. P. III (2006): The GPS Space Service Volume. In: Proceedings of the ION GNSS 2006, Fort Worth, Texas, USA. 2503–2514.

Beutler, G.; Brockmann, E.; Gurtner, W.; Hugentobler, U.; Mervart, L.; Rothacher, M.; Verdun, A. (1994) Extended orbit modeling techniques at the CODE processing center of the International GPS Service for geodynamics (IGS): theory and initial results. Manuscr Geod 19(6):367–386.

Burt, E.A.; Prestage, J.D.; Tjoelker, R.L.; Enzer, D.G.; Kuang, D.; Murphy, D.W.; Robison, D.E.; Seubert, J.M.; Wang, R.T.; Ely, T.A. (2021) Demonstration of a trapped-ion atomic clock in space. Nature 2021, 595, 43–47. https://doi.org/10.1038/s41586-021-03571-7.

Cacciapuoti, L.; Salomon, Ch. (2009) Space clocks and fundamental tests: The ACES experiment. Eur. Phys. J. Spec. Top. 172(1): 57-68. doi: 10.1140/epjst/e2009-01041-7.

Cacciapuoti, L.; Armano, M.; Much, R.; Sy, O.; Helm, A.; Hess, M. P.; Kehrer, J.; Koller, S.; Niedermaier, T.; Esnault, F. X.; Massonnet, D.; Goujon, D.; Pittet, J.; Rochat, P.; Liu, S.; Schaefer, W.; Schwall, T.; Prochazka, I.; Schlicht, A.; Schreiber, U.; Delva, P.; Guerlin, C.; Laurent, P.; Le Poncin-Lafitte, C.; Lilley, M.; Savalle, E.; Wolf, P.; Meynadier, F.; Salomon, C. (2020) Testing gravity with cold-atom clocks in space. Eur. Phys. J. D 74, 164. doi: 10.1140/epjd/e2020-10167-7.

Calzolaio, D.; Curreli, F.; Duncan, J.; Moorhouse, A.; Perez, G.; Voegt, S. (2020) EDRS-C - The second node of the European Data Relay System is in orbit. Acta Astronautica, vol. 177, pp. 537–544. doi: 10.1016/j.actaastro.2020.07.043.

Dach, R.; Lutz, S.; Walser, P.; Fridez, P. (Eds) (2015) Bernese GNSS Software Version 5.2. User manual, Astronomical Institute, University of Bern, Bern Open Publishing. doi: 10.7892/boris.72297, ISBN: 978-3-906813-05-9.

Delva, P.; Meynadier, F.; Wolf, P.; Le Poncin-Lafitte, C.; Lauraent, P. (2012) Time and frequency transfer with a microwave link in the ACES/PHARAO mission. 2012 European Frequency and Time Forum, pp. 28-35. doi: 10.1109/EFTF.2012.6502327.

Delva, P.; Altamimi, Z.; Blazquez, A.; et al. (2023) GENESIS: co-location of geodetic techniques in space. Earth Planets Space, vol. 75, art. 5. doi: 10.1186/s40623-022-01752-w.

Di Benedetto, M.; Boscagli, G.; De Marchi, F.; Durante, D.; Santi, F.; Sesta, A.; Plumaris, M.; Fienga, A.; Linty, N.; Sośnica, K.; Belfi, J.; Iess, L. (2022) An architecture for a lunar navigation system: orbit determination and time synchronization. 8th International ESA Colloquium on Scientific and Fundamental Aspects of GNSS, Sofia, Bulgaria.

Enderle, W.; Gini, F.; Boomkamp, H.; Parker, J. J.K.; Ashman, B. W.; Welch, B. W.; Koch, M.; Sands, O. S. (2018) Space User Visibility Benefits of the Multi-GNSS Space Service Volume: An Internationally-Coordinated, Global and Mission-Specific Analysis. Proceedings of the 31st International Technical Meeting of the Satellite Division of The Institute of Navigation (ION GNSS+ 2018), Miami, Florida, USA, September 2018, pp. 1191-1207. doi: 10.33012/2018.15966.

Fernández, F.A. (2011) Inter-satellite ranging and inter-satellite communication links for enhancing GNSS satellite broadcast navigation data. Adv. Space Res. 47: 786-801. doi: 10.1016/j.asr.2010.10.002.

Gibney, E. (2023) What time is it on the Moon? Nature 614, 13-14. doi: 10.1038/d41586-023-00185-z.

Gil, A. D. A.; Renwick, D.; Cappelletti, C.; Blunt, P. (2023) Methodology for optimizing a Constellation of a Lunar Global Navigation System with a multi-objective optimization algorithm. Acta Astronautica, vol. 204, pp. 348–357. doi: 10.1016/j.actaastro.2023.01.003.

Giorgi, G.; Schmidt, T. D.; Trainotti, C.; Mata-Calvo, R.; Fuchs, C.; Hoque, M. M.; Berdermann, J.; Furthner, J.; Günther, C.; Schuldt, T.; Sanjuan, J.; Gohlke, M.; Oswald, M.; Braxmaier, C.; Balidakis, K.; Dick, G.; Flechtner, F.; Ge, M.; Glaser, S.; König, R.; Michalak, G.; Murböck, M.; Semmling, M.; Schuh, H. (2019) Advanced technologies for satellite navigation and geodesy. Adv. Space Res. 64: 1256-1273. doi: 10.1016/j.asr.2019.06.010.

Glaser, S.; Michalak, G.; Männel, B.; König, R.; Neumayer, K.H.; Schuh, H. (2020) Reference system origin and scale realization within the future GNSS constellation “Kepler“. J Geod 94, art. 117. doi: 10.1007/s00190-020-01441-0.

Guan, M; Xu, T., Li, M; Gao, F., Mu, D (2022) Navigation in GEO, HEO, and Lunar Trajectory Using Multi-GNSS Sidelobe Signals. Remote Sens., 14(2), art. 318. doi: 10.3390/rs14020318.

Hemmati, H (2020) Near-Earth Laser Communications. In: Hemmati, H. (ed) Near-Earth Laser Communications, Second Edition. CRC Press, Boca Raton. ISBN: 978-1-498-77740-7.

Laurent, P.; Massonnet, D.; Cacciapuoti, L.; Salomon, C. (2015) The ACES/PHARAO space mission. Comptes Rendus Phys. 2015, 16, 540–552. https://doi.org/10.1016/j.crhy.2015.05.002.

Luceri, V.; Pirri, M.; Rodríguez, J.; Appleby, G.; Pavlis, E. C.; Müller, H. (2019) Systematic errors in SLR data and their impact on the ILRS products. J Geod 93, 2357–2366. doi: 10.1007/s00190-019-01319-w.

Lv, Y.; Geng, T.; Zhao, Q. et al. (2024) Contribution of intersatellite link measurements to ECOM solar radiation pressure estimation on BDS-3 MEO satellite. GPS Solut 28, art. 47. doi: 10.1007/s10291-023-01588-1.

Meindl, M.; Beutler, G.; Thaller, D.; Dach, R.; Jäggi, A. (2013) Geocenter coordinates estimated from GNSS data as viewed by perturbation theory. Adv. Space Res. 51(7), 1047-1064. doi: 10.1016/j.asr.2012.10.026.

Meng, W.; Zhang, H.; Huang, P.; Wang, J.; Zhang, Z.; Liao, Y.; Ye, Y.; Hu, W.; Wang, Y.; Chen, W.; Yang, F.; Prochazka, I. (2013) Design and experiment of onboard laser time transfer in Chinese Beidou navigation satellites. Adv. Space Res. 51, 951-958. doi: 10.1016/j.asr.2012.08.007.

McNamara, P.; Vitale, S; Danzmann, K. (on behalf of the LISA Pathfinder Science Working Team 2008) (2008) LISA Pathfinder. Classical and Quantum Gravity, 25(11). doi: 10.1088/0264-9381/25/11/114034.

Michalak, G.; Glaser, S.; Neumayer, K.H.; Koenig, R. (2021) Precise orbit and Earth parameter determination supported by LEO satellites, inter-satellite links and synchronized clocks of a future GNSS. Adv. Space Res., 68(12), 4753-4782. doi: 10.1016/j.asr.2021.03.008.

Parker, J. J. K.; Bauer, F. H.; Ashman, B. W.; Miller, J. J.; Enderle, W.; Blonski, D. (2018) Development of an Interoperable GNSS Space Service Volume. Proceedings of the 31st International Technical Meeting of the Satellite Division of The Institute of Navigation (ION GNSS+ 2018), Miami, Florida, USA, September 2018, pp. 1246-1256. doi: 10.33012/2018.15968.

Parker, J. J. K. (2019) New Frontiers in Space Use of GNSS: Moon and Beyond. 7th International ESA Colloquium on Scientific and Fundamental Aspects of GNSS, Zurich, Switzerland.

Parker, J. J. K.; Dovis, F.; Anderson, B.; Ansalone, L.; Ashman, B.; Bauer, F. H.; D'Amore, G.; Facchinetti, C.; Fantinato, S.; Impresario, G.; McKim, S. A.; Miotti, E.; Miller, J. J.; Musmeci, M.; Pozzobon, O.; Schlenker, L.; Tuozzi, A.; Valencia, L. (2022) The Lunar GNSS Receiver Experiment (LuGRE). Proceedings of the 2022 International Technical Meeting of The Institute of Navigation, Long Beach, California, USA, pp. 420-437. doi.: 10.33012/2022.18199.

Pereira, F.; Reed, P. M.; Selva, D. (2022) Multi-objective design of a lunar GNSS. NAVIGATION, 69(1). doi: 10.33012/navi.504.

Plag, H.-P.; Pearlman, M. (eds) (2009) Global Geodetic Observing System: meeting the requirements of a global society on a changing planet in 2020. Springer, Berlin. doi: 10.1007/978-3-642-02687-4. ISBN: 978-3-642-02686-7.

Pribil, K.; Hemmati, H. (2020) Laser Transmitters: Coherent and Direct Detection. In: Hemmati, H. (ed) Near-Earth Laser Communications, Second Edition. CRC Press, Boca Raton. ISBN: 978-1-498-77740-7.

Samain, E.; Vrancken, P.; Guillemot, P.; Fridelance, P.; Exertier, P. (2014) Time transfer by laser link (T2L2): characterization and calibration of the flight instrument. Metrologia, 51: 503-515. doi: 10.1088/0026-1394/51/5/503.

Schäfer, W.; Flechtner, F.; Nothnagel, A.; Bauch, A.; Hugentobler, U. (2013) Geodesy and Time Reference in Space – GETRIS. ESA Study AO/1-6311/2010/F/WE Final Report GETRIS-TIM-FR-0001.

Schlicht, A.; Hugentobler, U.; Stetter, M.; Schäfer, W. (2014) Concept for a Geodetic and Time Reference in Space. Proceedings of the International Laser Ranging Service, Annapolis, USA.

Schlicht, A.; Hugentobler, U.; Marz, S.; Seel, S.; Biller, P. (2019) Concept for continuous wave laser ranging and time transfer to Galileo using optical two-way links. In: Proceedings of the 7th international colloquium on scientific and fundamental aspects of GNSS, Zurich, Switzerland, 4-6 September 2019.

Schmidt, T.D.; Schlüter, S.; Schuldt, T.; Gohlke, M.; Calvo, R.M.; Lüdtke, D.; Dauth, M.; Lezius, M.; Michaelis, C.; Brzoska, A.; et al. (2022) COMPASSO: In-orbit Verification of Optical Key Technologies for Future GNSS. In Proceedings of the 53rd Annual Precise Time and Time Interval Systems and Applications Meeting, Long Beach, CA, USA, 25–27 January 2022; pp. 158–182. https://doi.org/10.33012/2022.18286.

Schreiber, K. U.; Prochazka, I; Lauber, P.; Hugentobler, U.; Schäfer, W; Cacciapuoti, L; Nasca, R. (2010) Ground-based demonstration of the European Laser Timing (ELT) experiment. IEEE Transactions on Ultrasonics, Ferroelectrics and Frequency Control 57 (3): 728-737. doi: 10.1109/TUFFC.2010.1471.

Schuldt, T.; Döringshoff, K.; Kovalchuk, E.; Keetman, A.; Pahl, J.; Peters, A.; Braxmaier, C. (2017) Development of a compact optical absolute frequency reference for space with 10−15 instability. Appl. Opt. 2017, 56, 1101–1106. https://doi.org/10.1364/AO.56.001101.

Smith, M.; Craig, D.; Herrmann, N.; Mahoney, E.; Krezel, J.; McIntyre, N.; Goodliff, K. (2020). The Artemis Program: An Overview of NASA's Activities to Return Humans to the Moon. IEEE Aerospace Conference, Big Sky, MT, USA, pp. 1-10, doi: 10.1109/AERO47225.2020.9172323.

Tang, C.; Hu, X.; Zhou, S.; et al. (2016) Improvement of orbit determination accuracy for Beidou Navigation Satellite System with Two-way Satellite Time Frequency Transfer. Adv. Space. Res. 58(7), 1390-1400. doi: 10.1016/j.asr.2016.06.007.

Tjoelker, R.L.; Prestage, J.D.; Burt, E.A.; Chen, P.; Chong, Y.J.; Chung, S.K.; Diener, W.; Ely, T.; Enzer, D.G.; Mojaradi, H.; et al. (2016) Mercury Ion Clock for a NASA Technology Demonstration Mission. IEEE Trans. Ultrason. Ferroelectr. Freq. Control 2016, 63, 1034–1043. https://doi.org/10.1109/TUFFC.2016.2543738.

UNNOSA (2021) The Interoperable Global Navigation Satellite Systems Space Service Volume (2nd edition). ISBN: 9789211304367.

Ventura-Traveset, J.; López de Echazarreta, C.; Lam, J. P.; Flament, D. (2015) An Introduction to EGNOS: The European Geostationary Navigation Overlay System. In: Nurmi, J.; Lohan, E.; Sand, S.; Hurskainen, H. (eds) GALILEO Positioning Technology. Signals and Communication Technology, vol. 182, pp. 323-358. Springer, Dordrecht. doi: 10.1007/978-94-007-1830-2_14.

Walter, T. (2017) Satellite Based Augmentation Systems. In: Teunissen, P.J., Montenbruck, O. (eds) Springer Handbook of Global Navigation Satellite Systems. Springer Handbooks. Springer, Cham. doi: 10.1007/978-3-319-42928-1_12.

Walter, T.; Shallberg, K.; Altshuler, E.; Wanner, W.; Harris, C.; Stimmler, R. (2018) WAAS at 15. J Inst Navig 65(4):581-600. doi: 10.1002/navi.252.

Weyrauch, T.; Vorontsov, M. A. (2004) Free-space laser communications with adaptive optics: Atmospheric compensation experiments. In: Majumdar, A. K.; Ricklin, J. C. (eds) Free-Space Laser Communications. Optical and Fiber Communications Reports, vol 2. Springer, New York, NY. doi: 10.1007/978-0-387-28677-8_5, ISBN: 978-0-387-28652-5.

Winternitz, L. B.; Bamford, W. A.; Price, S. R. (2017): New High-Altitude GPS Navigation Results from the Magnetospheric Multiscale Spacecraft and Simulations at Lunar Distances. Proceedings of the 30th International Technical Meeting of The Satellite Division of the Institute of Navigation (ION GNSS+), Portland, Oregon, September 25th, pp. 1114-1126, 2017. https://ntrs.nasa.gov/search.jsp?R=20170009487.

Yang, Y.; Yang, Y.; Hu, X. et al. (2020): Inter-Satellite Link Enhanced Orbit Determination for BeiDou-3. Journal of Navigation, 73(1), 115-130. doi: 10.1017/S0373463319000523.

Zech, H.; Heine, F.; Tröndle, D.; Seel, S.; Motzigemba, M.; Meyer, R.; Philipp-May, S. (2015) LCT for EDRS: LEO to GEO optical communications at 1,8 Gbps between Alphasat and Sentinel 1a. Proc. SPIE 9647, Unmanned/Unattended Sensors and Sensor Networks XI; and Advanced Free-Space Optical Communication Techniques and Applications, 96470J (29 October 2015). doi: org/10.1117/12.2196273.

Zhang, R.; Tu, R.; Zhang, P.; Fan, L.; Han, J.; Lu, X. (2021) Orbit determination of BDS-3 satellite based on regional ground tracking station and inter-satellite link observations. Adv. Space Res., In Press, Corrected Proof, Available online 1 March 2021. doi: 10.1016/j.asr.2021.02.027

Acknowledgements

First of all, I would like to thank Urs Hugentobler for giving me the opportunity to do my doctorate under his supervision. I would also like to thank Susanne Glaser for being reviewer of this dissertation. I would like to thank the responsible reviewers and editors who contributed to the papers with their comments and suggestions.

I greatly appreciate the time that Urs Hugentobler invested in discussions and helped me to understand the Bernese GNSS Software. I am very thankful for his comments and suggestions related to the papers and this dissertation, as well as for sharing his expertise with me. My warmest thanks go to Anja Schlicht for being my mentor. I really appreciate the time she invested in discussions related to issues of this dissertation, for her helpful ideas and her guidance. I am very grateful that she introduced me to the GETRIS concept, which forms the basis for the work of this dissertation. I would also like to thank Stefan Seel and Philipp Biller from Tesat-Spacecom for sharing with us the idea of using the OISL terminals and links in ground-space directions as well. This concept named OTWL helped to achieve the set goals of the dissertation. Many thanks also to my current and former colleagues for their comments on my work in the doctoral seminar.

During my time at TUM I had the opportunity to work on several projects. I particularly appreciated the close collaboration with Anja Schlicht, Christoph Bamann and Peter Vollmair in the ACES/ELT project, as well as the close collaboration with Urs Hugentobler, Anja Schlicht and Manik Reichegger in the G2G project. Working on these projects helped me greatly in my professional development.

Finally, I would like to thank my family for their constant support in all aspects of my life and for always believing in me.

Appendix A

P-I Schlicht, A.; Marz, S.; Stetter, M.; Hugentobler, U.; Schäfer, W. (2020)
Galileo POD using optical inter-satellite links: A simulation study.
Advances in Space Research, 66(7): 1558-1570. doi: 10.1016/j.asr.2020.06.028.

P-II Marz, S.; Schlicht, A.; Hugentobler, U. (2021)
Galileo precise orbit determination with optical two-way links (OTWL): a continuous wave laser ranging and time transfer concept.
Journal of Geodesy, vol. 95, art. 85. doi: 10.1007/s00190-021-01534-4.

P-III Marz, S.; Schlicht, A.; Hugentobler, U. (2023)
Geosynchronous Satellites Expanding a Future GNSS Satellite Constellation: A Precise Orbit Determination Study.
Advances in Space Research, 71(1): 624-644. doi: 10.1016/j.asr.2022.11.009.

P-IV Marz, S.; Schlicht, A.; Hugentobler, U. (2023)
Toward a Geodesy and Time Reference in Space (GETRIS): A Study of Apparent Satellite Clocks of a Future GNSS Satellite Constellation.
Geosciences, vol. 13(6), art. 173. doi: 10.3390/geosciences13060173.

Available online at www.sciencedirect.com

ScienceDirect

Advances in Space Research 66 (2020) 1558–1570

ADVANCES IN SPACE RESEARCH (a COSPAR publication)

www.elsevier.com/locate/asr

Galileo POD using optical inter-satellite links: A simulation study

Anja Schlicht [a,*], Stefan Marz [a], Monika Stetter [a], Urs Hugentobler [a], Wolfgang Schäfer [b]

[a] Technical University of Munich, Arcisstr, 21, 80333 Munich, Germany
[b] TimeTech GmbH, Curiestrasse 2, 70563 Stuttgart, Germany

Received 17 December 2019; received in revised form 18 June 2020; accepted 20 June 2020
Available online 30 June 2020

Abstract

In this simulation study the benefit of optical two-way inter-satellite links (OISL) between the Galileo satellites for orbit determination is discussed. Different link scenarios are analyzed in combination with Global Navigation Satellite System (GNSS) observations and a ground station network of seven or 16 stations, respectively. Great importance was attributed to the simulation of systematic effects in the different measurement techniques as realistically as possible. For GNSS observations this is multipath, errors in tropospheric delays and phase center variations on transmitter and receiver side as well as variable biases. For ISL this is colored link noise, a variable offset in the phase lock loop and a distance dependent noise. Modelling errors also have to be considered to avoid unexpectedly good orbit solutions in all scenarios. We study formal errors together with the influence of the systematic errors and the weighting of the measurement techniques relative to each other. The main focus lays on the comparison between the different inter-satellite link scenarios and only secondarily we looked on the gain these additional measurements have on the precise orbit determination of Galileo satellites. Inter-satellite links can be used for different purposes, such as data transfer, increasing autonomy, reducing costs and higher accuracy in orbit determination and clock synchronization. Especially for optical inter-satellite links data transfer capabilities rise and the scenarios preferring stable link configuration are discussed more and more. The question answered by this study is whether or not closed link topologies have a valuable contribution to precise orbit determination. In different sub-scenarios the precision of Galileo processing is increased from worst case to unexpected precision, and the benefit of the additional optical tracking is analyzed.

Keywords: Simulation study; Galileo; Inter-satellite link

1. Motivation

Inter-satellite link (ISL) is the connection of two or more satellites by the exchange of electromagnetic signals. These can be microwave signals with modulated code or the code modulated on an optical carrier generated by a laser. Inter-satellite links can fulfill different purposes: they can allow data transfer like in the case of optical two-way links between the European Data Relay Satellites (EDRS) to the Sentinel satellites transferring data from the low Earth orbiter to the geostationary satellite. This allows high data rates and up to continuous tracking. In gravity field recovery, where two low orbiting satellites fly one after the other measuring the distance between them, inter-satellite links come into play, too. These satellites exchange microwave signals like in GRACE (Gravity Recovery And Climate Experiment) and GRACE FO or optical signals as installed on GRACE FO for demonstration purposes. In GNSS two-way links can be used for time synchronization, distance measurements and data transfer. Different purposes prefer different link scenarios. As in permanent link scenarios continuous data exchange between satellites is feasible, it is possible to achieve very short time to alerts.

* Corresponding author.
E-mail addresses: anja.schlicht@tum.de (A. Schlicht), s.marz@tum.de (S. Marz), urs.hugentobler@tum.de (U. Hugentobler), Wolfgang.Schaefer@timetech.de (W. Schäfer).

https://doi.org/10.1016/j.asr.2020.06.028
0273-1177/

Whereas in an any-to-any scenario ranging biases can be estimated and the changing ranging geometry will allow a more accurate orbit determination and clock synchronization. As in the discussion of optical inter-satellite links the focus on data-transfer rises as data rates rise, ring scenarios are discussed in more detail (Michalak et al., 2018).

How much will orbit determination suffer from a ring scenario? If the rings are broken up and the orbital planes connected from time to time, does the orbit accuracy increase? Inter-satellite links can be used to reduce costs due to a reduction in the number of ground stations. Is the benefit different in different scenarios? Biases cannot be estimated in fixed scenarios, but optical links can be calibrated to a high extend. What influence does this have on orbit determination? The geometry of the measurements gets better when ranging from satellite to satellite and not only from ground: Can this help estimating solar radiation pressure parameters? The analysis in this paper will show: Permanent links are, due to the biases, range-rate measurements and not range measurements.

These are the main questions answered in the following simulation study, addressing three major benefits of inter-satellite links, which are a priori expected for orbit determination: The ability of clock synchronization should allow a higher consistency between clocks and orbit. Orbit determination and modelling will further benefit from better tracking geometry and more accurate ranges. Tracking cones from ground are limited. Optical two-way links between satellites do not go through the troposphere and show neither phase center variations, nor multipath or problems due to ambiguity fixing.

2. Introduction

Many different topics are discussed for future developments in the GNSS systems. The use of accelerometers on board satellites (Vespe, 2014; Lucchesi et al. 2016) as well as optical time transfer and ranging from the ground (Shargorodsky et al., 2013; Wang et al., 2012; 2014), with developments in Europe like T2L2 (Time Transfer by Laser Link) (Samain et al., 2014) and ELT (European Laser Timing) (Schreiber et al., 2010). Optical two-way time and range measurements support the one-way microwave measurements by separating the clock synchronization from station height and tropospheric influences. Inter-satellite links are mostly discussed in the microwave regime (Sánchez et al., 2008). The benefits of ISL are manifold and range from real-time clock synchronization and better GNSS orbits (Fernández et al., 2010; Gill, 1999; Michalak et al., 2018), to on-board orbit solutions close to real-time and enhanced accuracy of broadcast information (Abusali et al., 1998; Rajan, 2002; Rajan and Orr, 2003; Fernández, 2011). Data exchange between the satellites for shorter time to alert (Xu et al., 2012), potential reduction of the ground station network associated with a reduction in cost, operator work load is as important as the robustness against ground station unavailability (Han et al., 2011). The Chinese Beidou system performs already inter-satellite ranging (Yang et al., 2018; Zhou et al., 2018).

Inter-satellite ranging in the optical will have some further advantages like no regulations in this frequency band, no danger for jamming and interference, higher bandwidth for commercial services and data exchange, and the ability for implementing swarm intelligence. With the possibility to have high data rate inter-satellite links between GNSS satellites a discussion about a permanent linking of all or a group of GNSS satellites started. Such a constellation would be preferred for real-time exchange of data, permanent system control and hazard monitoring. In this work, we analyze three different permanent link scenarios with an any-to-any scenario. The focus lays on the comparison of these scenarios for precise orbit determination. How much accuracy and precision do we lose when we integrate permanent structures in inter-satellite ranging? Does a breaking-up of permanent structures from time to time help enhancing the performance? On the other hand, permanent ring scenarios bring benefit for clock synchronization inside the ring. They allow the combination of all clocks to a common clock, as well as elimination of malfunctioning clocks in real time. In a ring structure with permanent two-way links the concept would allow a reduction of clock redundancy on each satellite without losses of autonomy, if desired. This also means integrating one high performance clock in a ring will constrain all other clocks.

For the comparison, we discuss different GNSS processing strategies, different sizes of the ground station network and the problem of the weighting of the two-way inter-satellite link measurements with respect to the one-way Galileo measurements.

3. Simulation set-up

For validating the impact of OISL observations in a typical Galileo orbit solution, we simulated 10 days of OISL and GNSS observations. We used a modified version of the Bernese GNSS Software (Dach et al., 2015) for simulation and analysis. Different systematic effects are simulated externally and were then integrated into the simulation process. We parameterized the satellite orbits with six initial conditions and nine or more parameters for an empirical solar radiation pressure model, based on the ECOM2 model (Arnold et al., 2015). For the solution epoch-wise satellite and ground station clocks were estimated as well as L-band phase ambiguities and station specific tropospheric zenith delays every two hours. The errors in modelling the troposphere were introduced using an accurate weather model in the simulation and a less accurate model in the analysis. The accurate model was the gridded VMF based on real weather data and the less accurate model was the GMF model (Boehm et al., 2006). We eliminated to a great extend effects due to the ionosphere, by building the ionosphere free linear combination.

The coordinate system in which the solar radiation pressure parameters (SRP) are estimated are the direction from

satellite to sun (e_D), the direction pointing along the solar panels (e_Y) and the direction completing the orthogonal system (e_B). The acceleration of the satellite is a Fourier series in these direction in multiples of once per revolution. Despite the constant term, every other term has a sine and cosine time evolution. Table 1 shows which parameters we estimated in addition to the constant terms in B, D and Y. The *best possible* orbit shows the importance of the different estimated parameters (see Fig. 1).

In simulation studies, four different orbit types are relevant. Setting-up the simulated reality a further called *true* orbit is necessary. To get as realistic Galileo orbits as possible the Walker constellation (56°:24/3/1) was simulated and adjusted with a force model including the Earth gravity field up to degree and order 12 and direct tides from third bodies (Sun, Moon, Venus, Mars, Jupiter), ocean and solid Earth tides as well as solar radiation pressure. The solar radiation pressure model was a Galileo box-wing model (Duan et al., 2019). The least-squares adjustment needs an *initial* orbit. We slightly changed some parameters of the solar radiation pressure model to get this orbit. We modified the x body plane surface by +20%, the y surface by −10%, and the z surface by +10%. All three optical parameters of the surfaces, the wings sizes as well as wings optical parameters of the satellites remained unchanged. The *initial* orbit is wrong by 14.7 cm. The least squares adjustment to the simulated measurements delivers the *adjusted* orbit. To analyze the modelling error we introduce into our simulation, the estimation of a *best possible* orbit shows the maximum achievable accuracy. This procedure fits the empirical solar radiation parameters to the *true* orbit. The *best possible* orbit represents the modelling error we introduced in the simulation: No solution of our simulations can result in better orbits than these. The orbit accuracy of the *best possible* orbit is some millimeters in root mean square in all three dimensions (3D RMS). Table 2 shows the differences in the empirical models. Estimating more parameters leads to better *best possible* orbits. In most cases, the radial direction suffers the most from SRP mismodelling. In scenario 2, estimating B3 but not B1, large errors in cross-track occur, too.

The OISL measurements are based on 24 h observations with one minute sampling. The laser technology in mind is based on the EDRS data transfer links. Within the study three basic ISL-configurations have been considered (compare Fig. 2).

- Bidirectional links between all satellites (“any-to-any”)
  The satellites are equipped with one terminal and are linked in pairs so that for every observation epoch and 24 satellites in the constellation 12 links per epoch are realized. Every epoch the links are broken up and new pairs are built. The pairs are chosen in a way that after a minimum amount of time all possible satellite pairs in the constellation have been formed. In this connectivity scheme each satellite derives range observations to all other in-view satellites, in a sequence of single links. Following an algorithm, which is derived from the connectivity scheme shown by Fernández, 2011, the satellite pairs are changing every epoch with a given fixed connection timeline. If the satellites cannot see each other, this link is missing. Our software is not able to simulate two terminals in an any-to-any scenario and to estimate a bias for each. To get a good guess what the benefit of an additional terminal is, we simulated a doubled measurement rate and left the precision unchanged. As we fixed the clock of one ground station and adjusted clocks epoch-wise, we also had to double the Galileo L-band measurements in this case.
- A static bidirectional ring configuration which is called “closed ring”.
  In this configuration only neighboring satellites in the same orbit plane are linked. The links are permanent and each satellite carries two terminals measuring two nearest neighbors. With bidirectional OISLs information can be transmitted around the ring in clock-wise and counter clock-wise direction. The advantage of this scenario mainly resides in uninterrupted data transfer. Each satellite is permanently monitored and anomalies can be detected and located very rapidly. For L-band navigation the permanent monitoring of the clocks in the ring is of interest. The deployment of ISL full operational capability may in practice last many years and during this transient phase it may not always be possible to establish a permanent ring topology. In our simulations, we have foreseen a ranging capability to the next nearest neighbor.
- A broken bidirectional ring configuration (“broken ring”)
  For most of the measured epochs the “broken ring” will correspond to a “closed ring” scenario. At some epochs two neighboring satellites from each of the three rings will establish links between the orbital planes. Here we expect some benefit for orbit determination from the ranging between the orbital planes. Analyzing two different scenarios we studied how the frequency at which a ring is opened influences the orbit quality. The ring was opened every 30 min or every two hours.

The OISL-observations are two-way pseudorange measurements. The observation is a code measurement

Table 1
The empirical solar radiation pressure model consists of different Fourier components in the different scenarios. The number represents the order of the Fourier component and the letter the direction. D is the direction from the satellite to the sun, Y the direction along the solar panels and B completes the orthogonal system.

Estimated SRP parameters	Parameters
Scenario 1	D2, D4, B1
Scenario 2	D2, D4, B3
Scenario 3	D2, D4, B1, B3
Scenario 4	D2, D4, B1, B3, B5

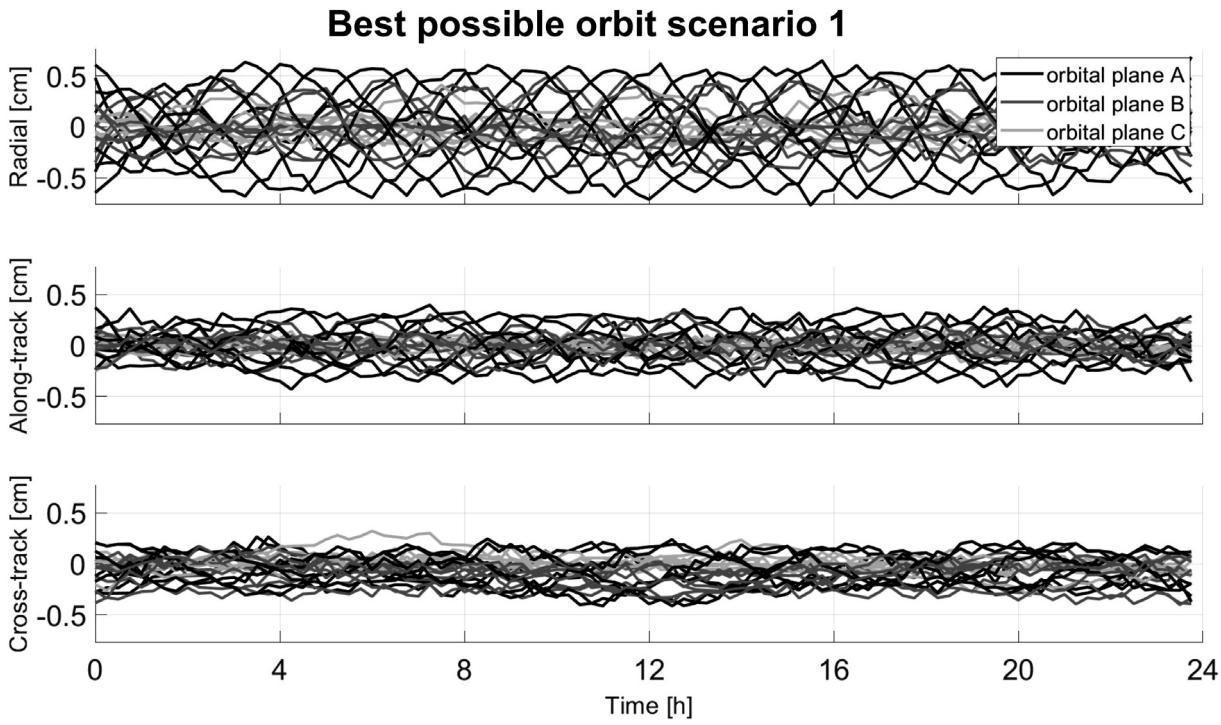

Fig. 1. Orbit differences between the *true* orbit and an orbit modelled with changed box-wing parameters and additionally adjusted ECOM parameters. The modelled parameters relate to scenario 1. These differences represent the *best possible* orbit, the error due to solar radiation pressure modelling.

Table 2
Root mean square (RMS) errors of the *best possible* orbit in the different scenarios.

Orbit errors Best possible [mm]	3D-RMS	Mean RMS per axis	Radial RMS	Along-track RMS	Cross-track RMS
Scenario 1	3.4	2.0	2.8	1.4	1.5
Scenario 2	16.4	9.5	6.2	4.2	14.5
Scenario 3	1.1	0.5	0.8	0.5	0.6
Scenario 4	0.9	0.4	0.7	0.4	0.5

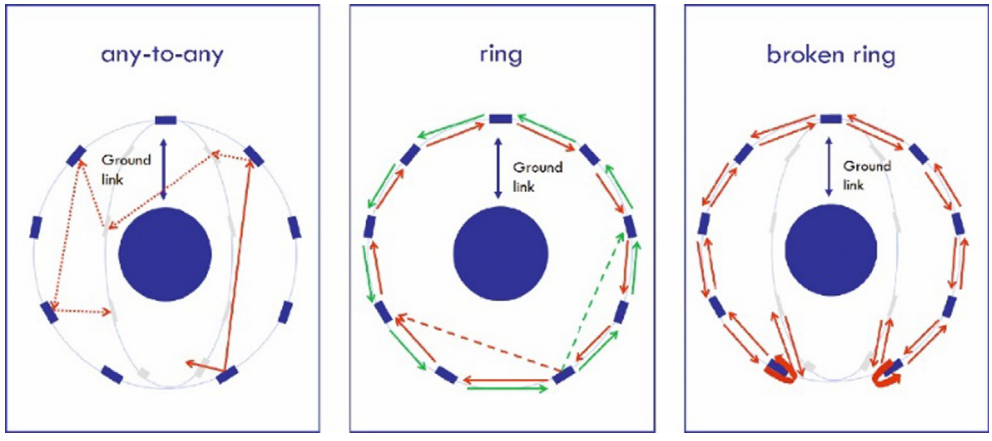

Fig. 2. This study discusses three scenarios for optical inter-satellite links. In the case of any-to-any OISL measurements, every satellite has only one terminal and can see one other satellite at a time. The other scenarios are ring scenarios where each satellite has two terminals measuring to the two next neighbors in the orbital plane. In the broken ring the configuration is opened at regular time intervals to connect the orbital planes.

of a microwave signal modulated onto an optical carrier. The signal is transmitted simultaneously by each of the two connected satellites and is subsequently received by the other. The combined OISL ranging observation between the satellite j and k can be written as

$$ISL_{Sj,Sk} = \frac{1}{2}\left(\left|\vec{r}^{\,k}\left(t^k_{res}\right) - \vec{r}^{\,j}\left(t^j_{send}\right)\right| + \left|\vec{r}^{\,j}\left(t^j_{res}\right) - \vec{r}^{\,k}\left(t^k_{send}\right)\right|\right) + \delta\rho^{j,k}_{clk} + \delta\rho^{j,k}_{rel} + \epsilon^{j,k}. \quad (1)$$

Here, $\vec{r}^{\,j}\left(t^j_{send}\right)$and $\vec{r}^{\,k}\left(t^k_{send}\right)$ are the position vectors of the satellites at the signal transmission times t^j_{send} and t^k_{send}. $\vec{r}^{\,j}\left(t^j_{res}\right)$and $\vec{r}^{\,k}\left(t^k_{res}\right)$ are the satellite positions at the signal reception times t^j_{res} and t^k_{res}. $\delta\rho^{j,k}_{rel}$ are the relativistic corrections and $\delta\rho^{j,k}_{clk}$ geometrical corrections due to clock errors. The parameter $\epsilon^{j,k}$ refers to the measurement error, consisting of three parts:

1. The measurement noise.
2. An offset due to the so-called repeatability of the link.
3. An additional offset related to the quality of absolute equipment delay calibrations.

The first part of the error $\epsilon^{j,k}$, the measurement noise , can be modeled as the product of:

- the noise due to the jitter of the Phase Locked Loop (PLL) which is used to recover the phase of the microwave signal and
- flicker-phase noise (Riley, 2008).

Flicker phase noise occurs in all electronic devices, induced by several effects, e.g. trapping of charge carriers in semiconductors. In the simulation a flicker noise floor of 0.5 mm has been used. The noise due to the PLL-jitter standard deviation depends on the ranging distance. It can be modeled by computing the PLL-jitter for every OISL observation and subsequently multiplying the resulting time series with white noise drawn from a standard normal distribution (Riley, 2008). The PLL-jitter σ_{PLL} of a single OISL observation as described above can be written following (Holmes, 1990) as

$$\sigma_{PLL} = \frac{1000c}{\pi f}\sqrt{\frac{B}{2C/N_0}} \quad (2)$$

in which c is the speed of light, f is the frequency after mixing, B is the noise bandwidth in Hz of the PLL, and C/N_0 is the signal-to-noise density ratio of the received signal. The C/N_0 is dependent on the distance as the received power of a divergent laser is a function of the distance. It can be defined as

$$C/N_0 = C/N_{0,min}\frac{P(r)}{P_{min}} \quad (3)$$

With a distant dependent power of (Degnan, 1993)

$$P(r) = \frac{P_t\eta_t G_t A_r \eta_r}{4\pi r^2} \quad (4)$$

Here $C/N_{0,min}$ is the minimum C/N_0 at maximum link distance, $P(r)$ is the received signal power at distance r, P_{min} is the minimum received power at maximum link distance, P_t is the transmitted power from the transmitter, η_t the transmission efficiency coefficient (attenuation, mispointing, etc.),$A_r$is the effective area of the receiver telescope and η_r the efficiency of the receiver. For this study we took a receiving telescope with a diameter of 70 mm and a maximal ranging capability of 46,000 km in case of ring scenarios and up to 60,000 km in case of any-to-any scenarios. The gain G_t of the transmitter is dependent on the divergence of the telescope and is here the diffraction limit of a 70 mm diameter transmission telescope at a wavelength of 1064 nm. Furthermore a signal frequency after mixing f of 80 MHz and a $C/N_{0,min}$ of 65 dBHz have been used in the simulations. The efficiencies are taken as 1. The noise at maximal link distance is then 1.5 mm.

The second part of the error $\epsilon^{j,k}$ is an offset due to the so-called repeatability of the link. The repeatability refers to the fact that the PLL can lock the phase of the carrier with an accuracy of 1° to 0.1°. This effect implies that within following signal acquisitions the phase-tracking in the PLL steady-operation is biased, and that this bias would be trial-dependent even if the controllable conditions are unchanged. The bias component would exist for any trial, independently from whether the link stays fixed or is broken afterwards. Therefore, it would need to be accounted in all scenarios as a contributor to the ranging error budget. Differently from flicker-noise and white-noise, mitigation by averaging over time would only partly be possible in the any-to-any scenario. Please note that the bias-error power is expected to be about the white-noise error power. The effect has been taken into account by adding a random phase difference in lock within the range of $+-0.5$ mm (white noise) changing with every break-up of a link.

The third part of the error $\epsilon^{j,k}$ is a bias. We assumed this bias to be constant and randomly distributed value between -0.5 and 0.5 mm for each satellite. The biggest disadvantage of all ring scenarios is the fact that biases cannot be estimated from ISL observations. This leads to a significant error contribution in these scenarios. The only way out of this dilemma is an in-flight calibration capability. With optical two-way tracking short distance calibrations are in principle possible. Such calibrations are regularly performed in pulsed optical satellite laser ranging at ground stations. For the calibration the telescope has to point to a retroreflector, which reflects a small part of the transmitted signal back into the telescope. Depending on the realization of the inter-satellite links, an additional frequency shift maybe necessary (accustom-optical modulators). Otherwise, the calibration has to be performed with a shared aperture, where the sending and the receiving path use different parts of the telescope. At least the procedure is difficult and may not lead to calibration accuracies better than the 0.5 mm we have assumed in this study. In an any-to-any scenario, the biases are estimated relative to

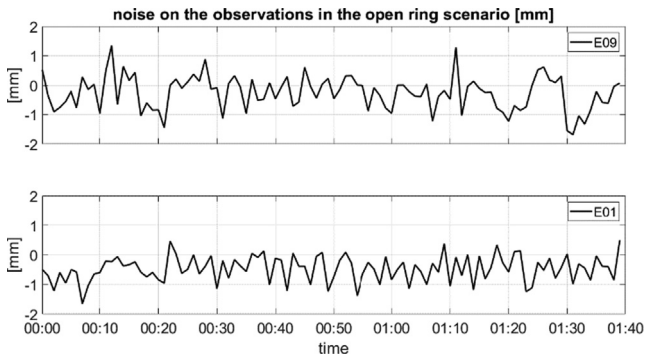

Fig. 3. Noise of two satellites in the open ring scenario. Satellite E09 is the one who opens the optical measurements in the ring and connects to satellites in the other two rings every 30 min. Satellite E09 has a higher noise level, as with every changing connection the offset changes. Satellite E01 stays always connected with its two next neighbors.

one bias, and have therefore less systematic influence. We will further see that it is in some cases better to take the measurements in the ring scenario as range-rate measurements. Then the bias is not relevant.

Fig. 3 shows the resulting noise for a typical optical link of two satellites in the open ring scenario. The satellite responsible for the connection to the other rings shows some higher variation due to opening and closing links, whereas the satellite always connected with its neighbors in the ring shows a constant offset.

For up to 16 ground stations (Galileo FOC network) two frequency GNSS code- and phase-observations with a sampling rate of 60 s were simulated. The station network is shown in Fig. 4. For one day about 32,988 OISL observations are simulated in the any-to-any scenario with 60 s and twice as many in the 30 s scenario, 34,560 in the ring scenarios compared to 408,416 GNSS observations in Code and phase with 16 stations and 180,546 with 7 ground stations (marked stations in Fig. 4). The code measurements have a 15 cm white noise for each frequency and the phase measurements a 1.5 mm white noise. Building the ionosphere-free linear combination eliminates the errors due to delays in this part of the atmosphere (the noise levels in phase measurements lead to 4.5 mm white noise in the combination). The satellite clocks are simulated masers and the ground clocks are polynomials of order four. Epoch-wise offsets are estimated for all clocks in the analysis. This procedure needs one fixed ground clock. We analyzed different phase center variation patterns of IGS antennas and took 16 showing signatures comparable to multipath. Fig. 5 shows the phase center variation for one station. For the code measurements we took the same pattern and multiplied the influence by a factor of 50. This should represent a worst case scenario. The transmitter has a phase pattern, too. We also introduced a factor of 50 in case of code measurements here. The Galileo measurements have a bias of up to 5 mm and a variation with once per revolution of up to 5 mm representing the temperature dependence. Both values are random per satellite.

To have a broad basis for discussion, we examined three different GNSS analysis strategies: one where GNSS tracking is not optimally used, one quite realistic, and one much too optimistic. In the low performance scenario only the code measurements are used for the Galileo tracking. This scenario is called *code only*. The much too optimistic scenario we call *ambiguity fixed*. Here a 100% correct ambiguity fixing rate is assumed while this is not realistic for a 16 ground station network. Systematic measurement effects are still present through simulated multipath errors. If in this case inter-satellite links can contribute to orbit determination, this can help to evaluate the benefit of those additional measurements. The *ambiguity float* is the most realistic scenario. It represents the analysis where in the least-squares estimation float ambiguities are estimated and no ambiguity-fixing is attempted.

The weighting of the different measurements in a combination of two or more techniques is a very critical task. For real data the optimum weighting may be assessed by

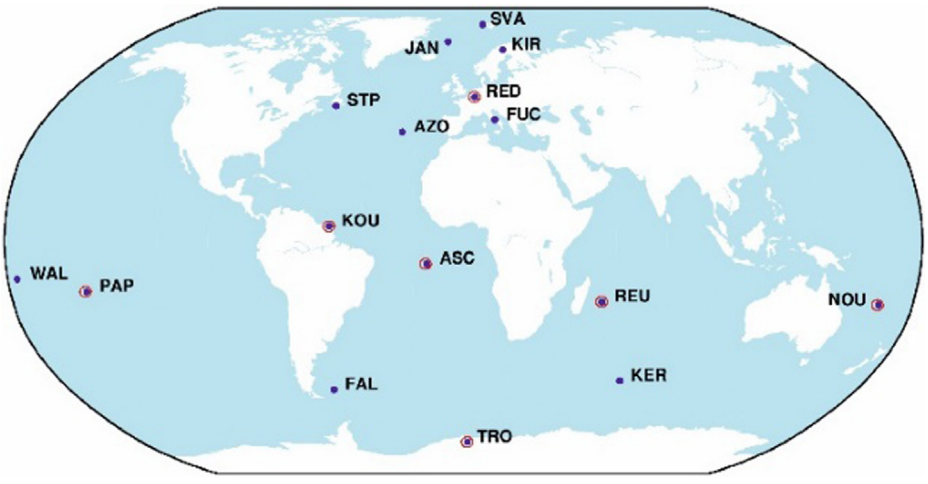

Fig. 4. FOC Galileo ground station network. The seven stations, which represent a reduced network, are marked in red. (For interpretation of the references to colour in this figure legend, the reader is referred to the web version of this article.)

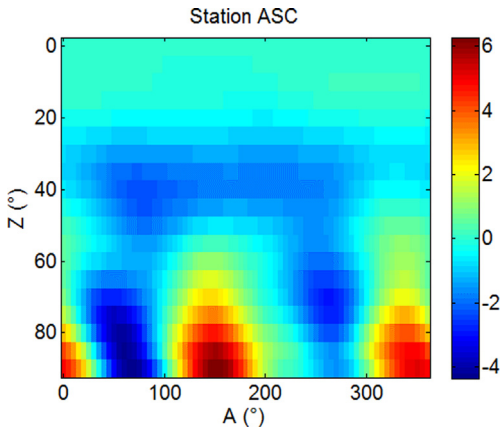

Fig. 5. This figure shows one example of a phase center variation in azimuth and elevation. The error is in millimeter.

minimizing residuals from an independent measurement technique, e.g., Satellite Laser Ranging. In our case the optimum weight between L-band and ISL observations was assessed by minimizing the difference of the *adjusted* to the *true* orbit. Although this is not possible in practice, it shows the best achievable solution.

In Table 3 the different weighting factors are shown. Very interesting is the observation that the weighting of the OISL measurements in the ring configurations is very high. This is due to the fact, that these measurements are very precise range-rate measurements with low systematic errors. The any-to-any scenario on the other hand represents range measurements contaminated with the mentioned systematic influences. If the ring opens and the L-band measurements have a low quality, like for *code*, the weighting of the OISL is high. From the *code* to the *ambiguity fixed* scenario the OISL measurements lose weight. The optimal weighting was independent of the day analyzed.

4. Results

Having found the right weights, we now can discuss the results of the simulation study. First, we have a look on the formal errors: They represent the covariance information of the *adjusted* orbit parameters propagated in along-track, cross-track and radial direction. Second, we analyze the deviation of the *adjusted* orbit from the *true* orbit. The formal error represents the stochastic errors in combination with the geometry information of the measurements whereas the orbit differences show the influence of the systematic modelling errors in the orbit. The plots present the individual components of the orbit: radial, along-track and cross-track, for the different scenarios with 16 or 7 ground stations, and for different data processing strategies, namely *code only* processing and code and phase processing with float or fixed ambiguities. The table lists the 3D RMS for all the scenarios as a 10 days mean of all satellites.

4.1. Formal error

Discussing the scenarios by means of the formal error focuses the analysis on the stochastic errors and the geometric strength of the measurement. Table 4 collects the results for all simulated scenarios. The second sub-table represent all SRP modelling scenarios with the *ambiguity float* solution. Within each table the OISL scenarios are compared to each other and the L-band-only solution. The right hand side of the first sub-table shows the solution for 16 stations, the left hand side for the 7 stations network with all Galileo solution strategies.

Analyzing the L-band only solution, the first remarkable observation is the lowest formal error in the modelling scenario 2. Here the analysis estimates a three times per revolution parameter in B, in addition to two and four times per revolution in D and constant terms in all directions. This is the term, which is least beneficial for orbit modelling, according to the analysis of the *best possible* orbit. In this SRP modelling scenario very high cross track errors occur. Estimating B1 (scenario 1) instead of B3 is slightly worse and estimating both or even more parameters is not possible within L-band only. Comparing the solution for seven ground stations with the one of the full network shows a rise in the formal error of a factor of 2–3. Looking at the changing precision of the L-band analysis from *code*, via *float*, to the *ambiguity fixed* solution, we see an expected steep improvement in the precision.

Next, we compare the L-band-only simulations with the different OISL scenarios. Fig. 6 shows the relative decrease in the formal error for the modelling scenario 1, estimating B1, compared to L-band only. The gain factor for all optical two-way tracking schemes is approximately the same for all Galileo analysis strategies. For any-to-any it is around 10–12 and for the ring scenarios between 7 and 8. The open ring configurations are slightly better than the closed ring, but for the closed ring configuration, the variation within the satellite constellation is very small compared to any-to-any.

The difference in SRP modelling does not lead to much variability in the gained precision for phase measurements. In a relative sense, scenario 2 would gain less as L-band-only favored this scenario. In the *code* analysis, the second SRP modelling strategy leads to worse orbit precisions compared to the other models. From this observation, we can conclude that the enhanced geometry with inter-satellite tracking prefers a good modelling of the cross-track component. As the formal error does not rise with the number of SRPs estimated, we conclude, that in OISL scenarios the modelling of solar radiation pressure gains a lot. The formal errors show only small degradation with the reduction of the number of ground stations, independent from the GNSS analysis strategies.

Comparing the different any-to-any measurements, we observe an increase in the precision with the number of observations. The any-to-any analysis with 30 s shows an

Table 3
Optimal relative weighting of the ISL measurements in respect to the Galileo L-band measurements $\frac{\sigma^2_{L-band}}{\sigma^2_{ISL}}$.

Weighting	Code 7 Stations	Phase float 7 Stations	Phase fixed 7 Stations	Code 16 Stations	Phase float 16 Stations	Phase fixed 16 Stations
Any-to-any	2.5	1.0	0.5	5.0	2.5	1
Open ring 30 min	2.5	7.5	5.0	1	7.5	2.5
Open ring 2 h	2.5	10	10	25	10	5.0
Closed ring	250	25	75	250	50	50

Table 4
Summary of the 10 days and three component mean formal orbit error of all simulation scenarios.

Scenario 1	7 Stations						16 Stations					
Formal errors [mm]	Code		Phase float		Phase fixed		Code		Phase float		Phase fixed	
L-band 60 s/30	1174	830	78	57	20	14	625	438	29.7	21	10.6	7.5
Any-to-any 60/30 s	56	40	2.5	1.8	1.4	1.0	50	35	2.3	1.6	1.1	0.8
Open ring 30 min/2h	108	107	4.3	4.3	2.2	2.3	85	85	3.6	3.6	1.7	1.7
Closed ring	271		6.1		3.3		158		4.8		2.0	
16 Stations	Scenario 1			Scenario 2			Scenario 3			Scenario 4		
Formal errors [mm]	Phase float			Phase float			Phase float			Phase float		
L-band	29.7			26.3			36.4			40.8		
Any-to-any 60s	2.3			2.8			2.3			2.3		
Open ring 30min/2h	3.6		3.6	3.6		3.6	3.9		3.9	4.0		4.1
Closed ring	4.8			4.6			5.2			5.4		

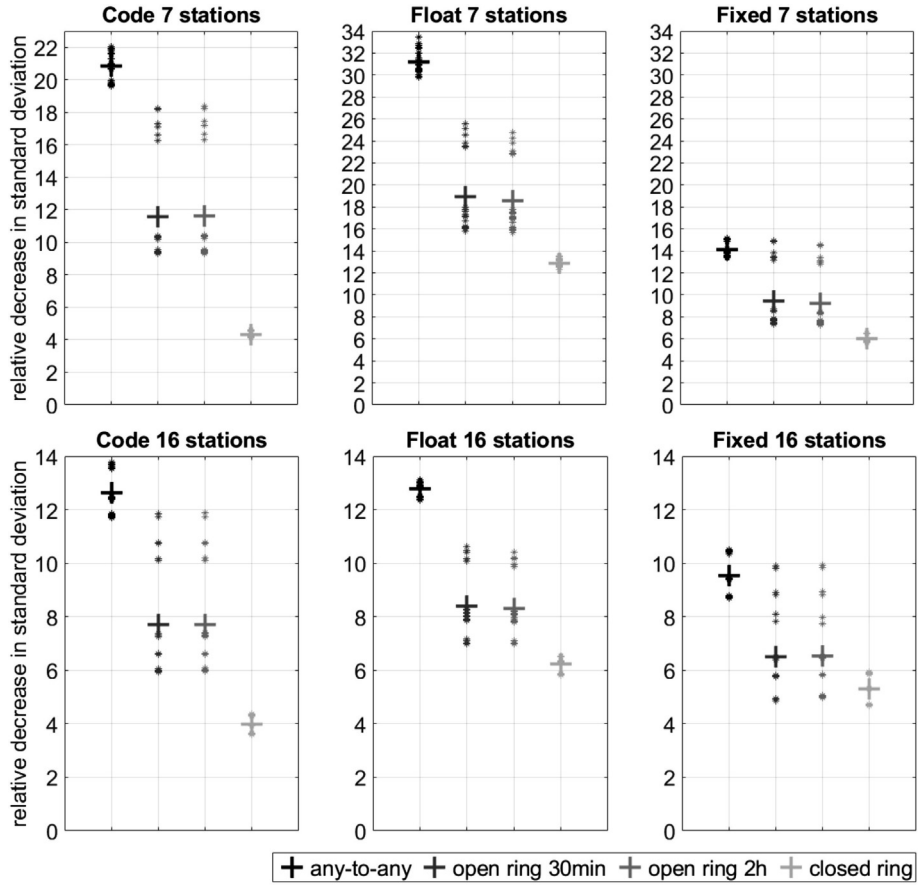

Fig. 6. Relative reduction of mean standard deviation of the orbit solutions in different scenarios in relation to L-band only solution with different analysis strategies in a 7 stations network (top) and 16 stations network (bottom). Individual satellites are marked with stars and the mean value as a big cross.

increase of about 30%, in the same way the L-band-only solution also increases by about 30% (relates to $\sqrt{2}$).

Fig. 7 shows the contribution of the different orbit components to the 3D RMS. In the L-band-only analysis, the along-track error is slightly higher than that in the other directions. With the additional any-to-any OISL measurements, the radial component benefits the most. A factor of about 30 is possible. The along-track error has neither variability with time, nor within the satellite constellation. Whereas the cross-track component has a twice per revolution time dependence. The closed ring constellation has a comparable gain in radial direction, but is slightly worse in along-track, and suffers by a factor of 10 in cross-track.

4.2. Orbit error

The formal errors analyzed above take into account only the contribution of stochastic noise and geometry. Orbit errors, i.e., the difference between *true* and *adjusted* orbit, on the other hand, also demonstrate the impact of systematic disturbances in measurements and modelling.

Table 5 summarizes the 3D error of the orbits. Starting again with L-band-only, the SRP modelling scenario 2 with a three times per revolution term in B direction estimated performs better than scenario 1 considering a once per revolution term. We have seen this already in the formal errors, where we discussed the reduced geometry of ground tracking observations as the limiting factor. Estimating more solar radiation parameters, like in scenario 3 and 4, degrades the orbit accuracy. The number of extractable SRPs limits the orbit accuracy for L-band tracking. Our solution for L-band only with 16 stations in the *ambiguity float* analysis shows an accuracy of the orbit of about 20 cm. This is about the expected accuracy of real Galileo orbits when evaluating tracking data of 16 ground stations with state-of-the-art models.

Fig. 8 compares the gain of the OISL constellations with the solutions using only ground station tracking. The largest gain is achieved when combining *code* with OISL measurements. This gain is even larger than the gain found for the formal errors. Here the high systematic errors in the *code* measurements, the phase center variations, play the dominant role. OISL measurements mitigate these errors to a high extent. The gain is lower for the *float* solution, but with a factor of 5–7 not negligible. The differences between the ring scenarios is marginal. The gain in the *ambiguity fixed* solution increases again, just as observed for the formal error.

The gain of OISL in the *float* solution increases when estimating more SRPs (compare Table 5). Scenario 2 drops off, significantly. Here the modelling error of solar radiation pressure gets the dominant error contribution. All scenarios have less accurate orbits within the reduced ground network. This reduction is higher than indicated by the formal errors. The systematic measurement offsets have a large contribution. The number of ground stations has no influence on the possibility of estimating additional SRPs with OISL. As the influence on L-band only is clearly observable, the possibility of ground network reduction with OISL is an appropriate way for reducing costs.

The ring structures show a clear gain, too, even though it is lower than in the case of any-to-any. The opening of the ring brings some benefit for the orbit accuracy. In Fig. 9 the *float* solution with 16 stations for the closed ring in scenario 1 is compared to the scenario where the ring is opened every 30 min. In both cases, the radial direction can be determined quite well. The error in cross-track and along-track is slightly higher in the case of the closed ring than in the open ring. In both scenarios, the variation in cross-track is for each satellite once per revolution. The error in along-track varies with the orbital plane in the closed ring scenario. Opening the ring can mitigate this variation.

Unfortunately, the orbit error does not decrease with increasing measurement rate in the any-to-any scenario. In the any-to-any scenario as well as L-band only nearly no changes are visible This behavior is contrary to the observations in the formal error. It is not clear why the variable offset introduced as a systematic error in the OISL measurement leads to a slight increase in the orbit errors. We had a closer look on the variation between the days and observed not negligible spreading of the solutions day by day. This variation is due to the variable bias and is not observable in the formal errors. There are days where the solution with higher measurement rate is better. Even though the mean is slightly worse.

5. Discussion and outlook

We have analyzed different scenarios of optical inter-satellite links and their influence on Galileo processing. We can conclude that the orbit accuracy suffers when arranging the OISL measurements in a ring structure. Opening of the ring from time to time does only slightly improve the orbit again. The decrease in orbit accuracy is moderate and may balance the benefit in synergetic use of the links in other ways. In a ring structure, the OISL measurements are high precision range-rate measurements with less systematic influences. In an any-to-any scenario, biases in the measurements can be estimated.

We have taken many systematic effects into account, link biases and their variability, colored noise on the OISL measurements and distance dependent effect. The orbit error of Galileo only solution in phase float processing leads to 20 cm orbit accuracy. A value quite expectable with 16 ground stations. These systematic errors manifest themselves in a difference in OISL scenarios between the *best possible* and the adjusted orbit. There is about a factor of 3 between these orbits. The difference between formal orbit errors and the adjusted orbit is a factor of 10. This indicates that quite a lot of the systematic errors stay in the orbit analysis. This is the reason why the any-to-any

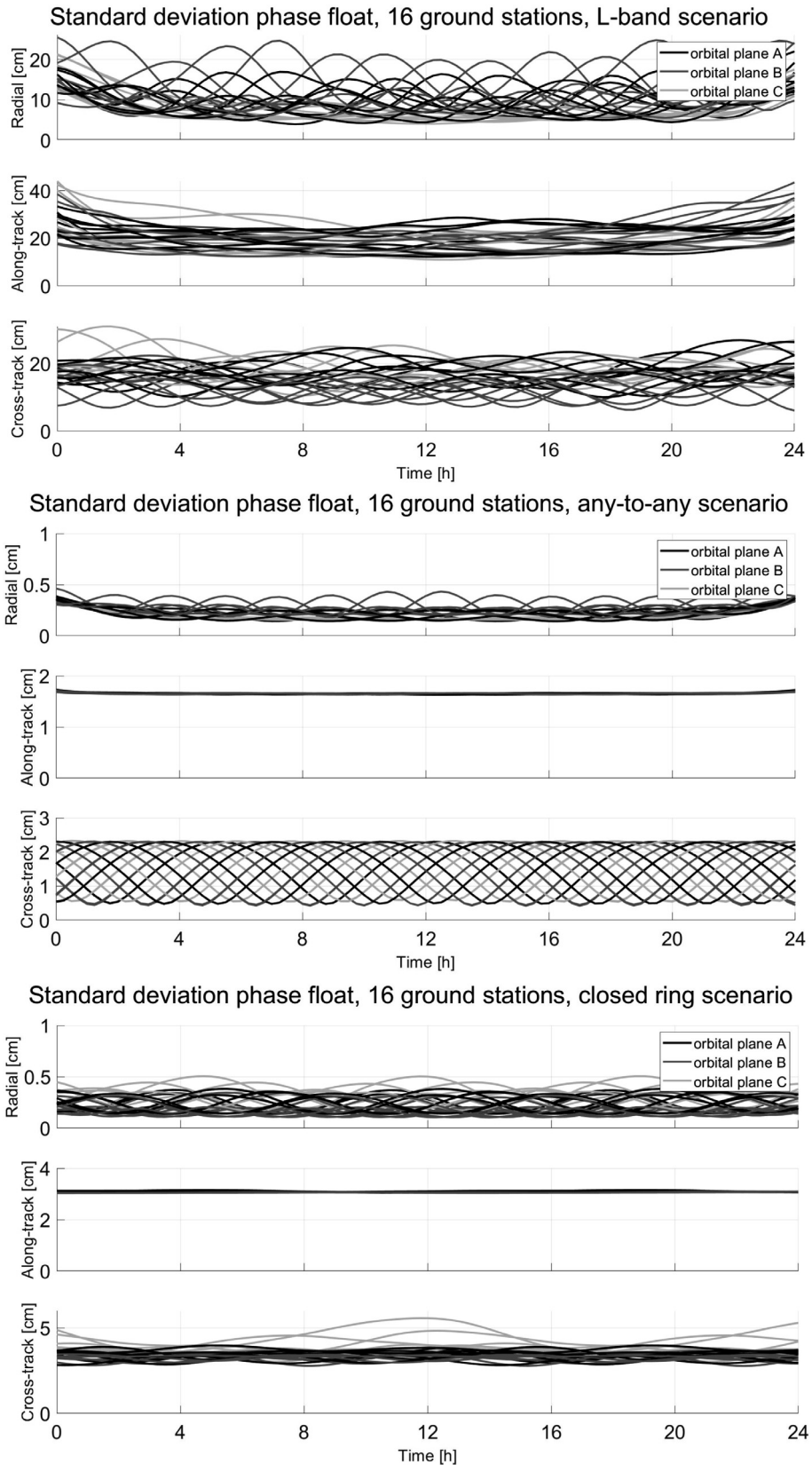

Fig. 7. Formal errors of the orbit solution for the ambiguity *float* phase observations with 16 ground stations without OISL in radial, cross-track, and along-track (top three plots) and with the any-to-any scenario (three plots in the middle), and in closed ring configuration (three plots on the bottom) over one day.

Table 5
Summary of the 10 days and three component mean orbit error of all simulation scenarios.

Scenario 1	7 Stations						16 Stations					
Orbit errors [mm]	Code		Phase float		Phase fixed		Code		Phase float		Phase fixed	
L-band 60 s/30	9110	8978	681	679	199	197	9758	9834	202	200	186	187
Any-to-any 60/30 s	212	210	30	31	8.5	8.5	173	174	28	29	8	8
Open ring 30 min/2h	949	954	50	51	24	23	616	611	42	43	15	15
Closed ring	1102		72		27		695		50		17	

16 Stations	Scenario 1		Scenario 2		Scenario 3		Scenario 4	
Orbit errors [mm]	Phase float		Phase float		Phase float		Phase float	
L-band 60s	202		184		262		277	
Any-to-any 60s	28		54		25		24	
Open ring 30min/2h	42	43	50	48	40	41	40	41
Closed ring	50		45		53		53	

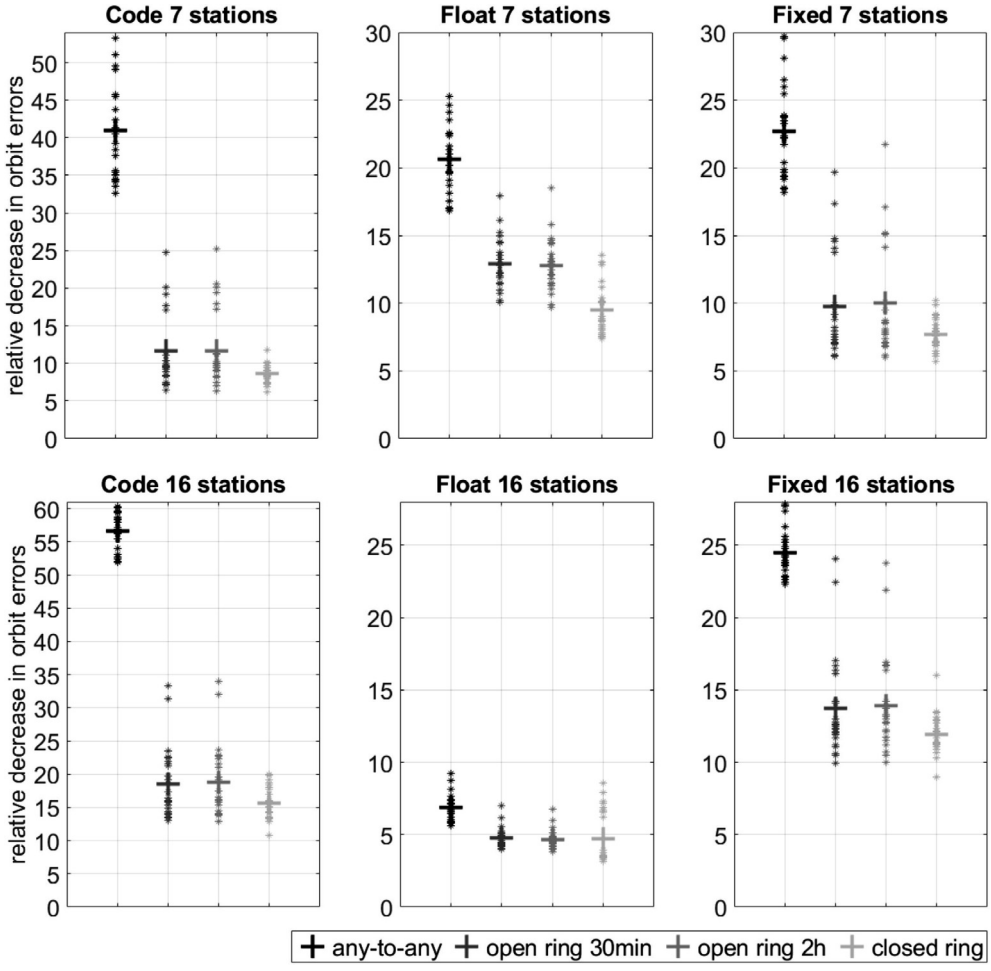

Fig. 8. Relative reduction of orbit errors in different scenarios compared to the Galileo only solution with different analysis strategies in a 7 stations network (top) or 16 stations network (bottom). Individual satellites are marked with stars and the mean value as a big cross.

scenario with twice as much observations does not lead to better orbits.

Inter-satellite links enhance the geometry of the measurements and allow a better estimation of orbit modelling parameters. We showed that it is possible to estimate more solar radiation pressure parameters in all scenarios allowing a more precise modelling of the orbit.

Inter- satellite links enhance the autonomy of the Galileo constellation and if cost reduction forces a reduction of ground stations, it is possible to do so without great decrease in orbit accuracy.

The great challenge when using real inter-satellite link data will be the weighting of the measurements in respect to the one-way measurements. Our analysis shows that a

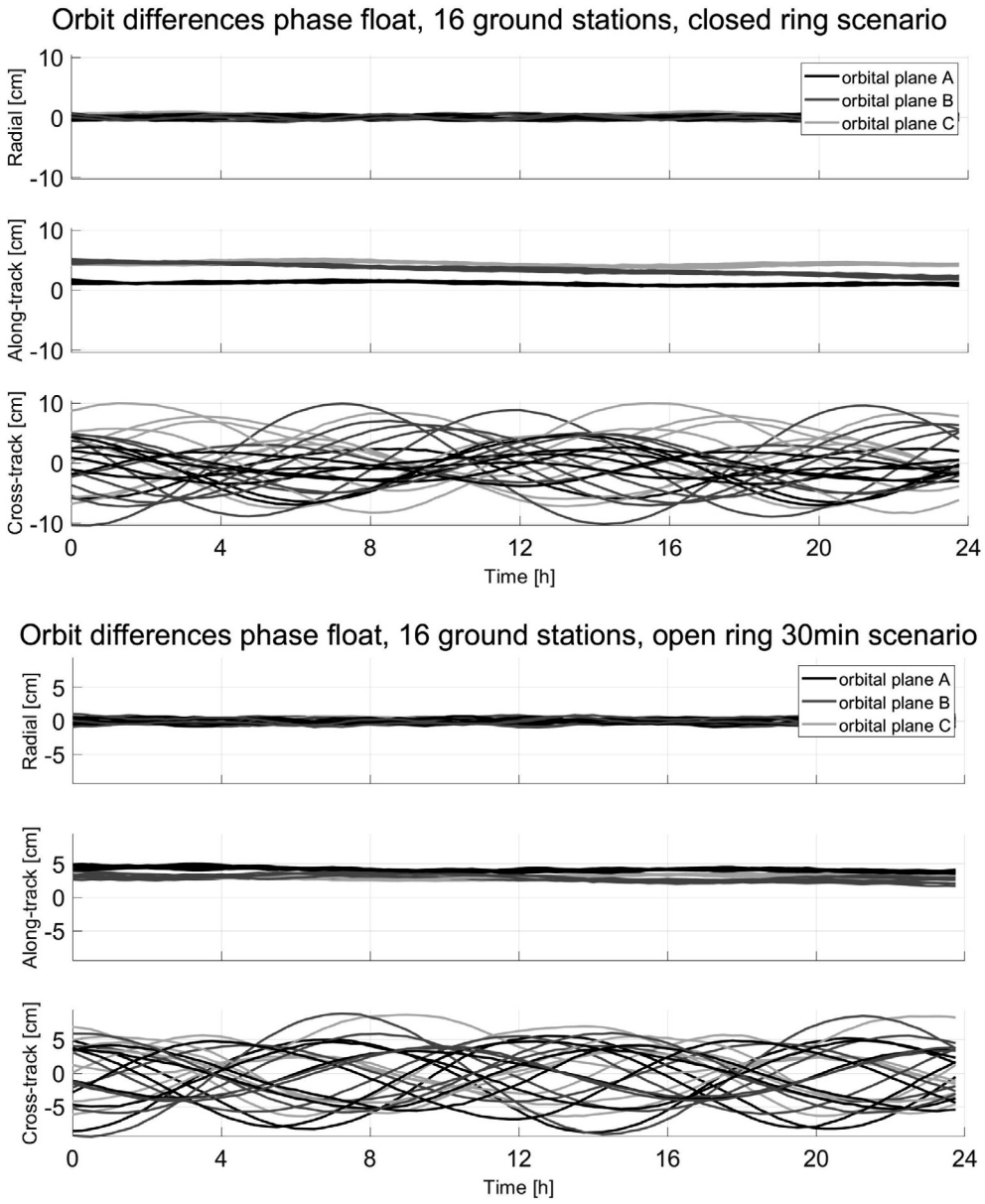

Fig. 9. Orbit errors of the orbit solution of the *ambiguity float phase* analysis with 16 ground stations in two ring scenarios: On top, the closed ring scenario, on bottom the ring is opened every 30 min. The plots separate the influences in the different directions: radial, along-track and cross-track.

weighting according to the noise is a good start for all any-to-any scenarios. In case of the rings a weighting as an accurate range-rate measurement is preferable and the tuning of this may need some experience.

Declaration of Competing Interest

The authors declare that they have no known competing financial interests or personal relationships that could have appeared to influence the work reported in this paper.

Acknowledgement

This work was supported by the Space Agency of the German Aerospace Center (DLR) with funds from the Federal Ministry of Economics and Technology (BMWi) based on a resolution of the German Bundestag under the code 50 NA 1508 and by the Deutsche Forschungsgemeinschaft – Project number SCHL 1973/1-2.

References

Abusali, P.A.M., Tapley, B.D., Schutz, B.E., 1998. Autonomous navigation of Global Positioning Systems using cross-link measurements. J. Guid. Control Dyn. 21 (2), 321–327.

Arnold, D., Meindl, M., Beutler, G., Dach, R., Schaer, S., Lutz, S., Prange, L., Sosnica, K., Mervart, L., Jäggi, A., 2015. ODE's new solar radiation pressure model for GNSS orbit determination. J. Geodesy 89 (775–791).

Boehm, J., Niell, A., Tregoning, P., Schuh, H., 2006. Global Mapping Function (GMF): A new empirical mapping function based on

numerical weather model data. Geophys. Res. Lett. 33, L07304. https://doi.org/10.1029/2005GL025546.

Dach, R., Lutz, S., Walser, P., Fridez, P. (Eds.), 2015. Bernese GNSS Software Version 5.2. User manual, Astronomical Institute, University of Bern, Bern Open Publishing. https://doi.org/10.7892/boris.72297; ISBN: 978-3-906813-05-9.

Degnan, J.J., 1993. Millimeter accuracy satellite laser ranging: A review. In: Geodynamics Series (25), Contribution of Space Geodesy to Geodynamics: Technology.

Duan, B., Hugentobler, U., Selmke, I., 2019. The adjusted optical properties for galileo/BeiDou-2/QZS-1 satellites and initial results on BeiDou-3e and QZS-2 satellites. Adv. Space Res. 63 (5), 1803–1812. https://doi.org/10.1016/j.asr.2018.11.007.

Fernández, F.A., 2011. Inter-satellite ranging and intersatellite communication links for enhancing GNSS satellite broadcast navigation data. Adv. Space Res. 47, 786–801.

Fernández, A., Sánchez, M., Beck, T., Amarillo, F., 2010. Future satellite navigation system architecture: inter-satellite ranging and orbit determination In: ION 2010 International Technical Meeting, San Diego.

Gill, E., 1999. Precise GNSS-2 satellite orbit determination based on inter-satellite-links. In: 14th International Symposium on Space Flight Mechanics, Iguassu, Brazil.

Han, S., Gui, Q., Li, J., 2011. Analysis of the connectivity and robustness of inter-satellite links in a constellation. Sci. China Phys. Mech. Astronomy 54 (6), 991–995.

Holmes, J.K., 1990. Coherent Spread-Spectrum Systems. Krieger Publishing Co., FL.

Lucchesi, D.M., Santoli, F., Peron, R., Fiorenza, E., Lefevre, C., Lucente, M., Magnafico, C., Iafolla, V.A., Kalarus, M., Zielinski, J., 2016. Non-gravitational accelerometer measurements by means of an on-board accelerometer for Second Generation Galileo Global Navigation Satellite System. In: 2016 IEEE Metrology for Aerospace, Florence. https://doi.org/10.1109/MetroAeroSpace.2016.7573253.

Michalak, G., Neumayer, K.H., Koenig, R., 2018. Precise orbit determination with inter-satellite links and ultrastable time for a future satellite navigation system. In: Proceedings of the 31st International Technical Meeting of the Satellite Devision of the Institute of Navigation (ION GNSS 2018), Long Beach, CA, pp. 1227–1232.

Rajan, J.A., 2002. Highlights of GPS II-R autonomous navigation. In: ION 58th Annual Meeting, Albuquerque.

Rajan, J.A., Orr, M., 2003. On-Orbit Validation of GPS IIR autonomous navigation In: ION 59th Annual Meeting, Albuquerque.

Riley, W., 2008. Handbook of Frequency Stability Analysis. NIST Special Publications 1065.

Samain, E., Vrancken, P., Guillemot, P., Fridelance, P., Exertier, P., 2014. Time transfer by laser link (T2L2): characterization and calibration of the flight instrument. Metrologia 51, 503–515. https://doi.org/10.1088/0026-1394/51/5/503.

Sánchez, M., Arona, L., Soualle, F., Pulido, J.A., 2008. "GNSSPLUS Final Report" in GNSSPLUS-DMSTECFIR01-11-E-R.

Schreiber, U., Prochazka, I., Lauber, P., Hugentobler, U., Schäfer, W., Cacciapuoti, L., Nasca, R., 2010. Ground-based demoinstration of the European laser timing (ELT) experiment. IEEE Trans. Ultrason., Ferrorelect. Freq. Control 57, 728–737.

Shargorodsky, V.D., Pasynkov, V.V., Sadovnikov, M.A., Chubykin, A. A., 2013. Laser Glonass: Era of Extended Precision. Glonass Herald J. Navig..

Vespe, F., 2014. On-board Accelerometry on Galileo Satellites: Technical Note. https://doi.org/10.13140/RG.2.1.2718.7048.

Wang, D., Ni, S., Liu, W., Yong, S., 2012. Compass satellite orbit determination based on inter-satellite and satellite-to-station ranging In: ION 25th International Technical Meeting of the Satellite Division, Nashville, Tennessee.

Wang, D., Zhao, J., Liu, C., 2014. Inter-satellite links study for GEO/MEO satellite networks. In: ION 27th International Technical Meeting of the Satellite Division, Tempa, Florida.

Xu, Y., Chang, Q., Yu, Z., 2012. On new measurement and communication techniques of GNSS inter-satellite links. Sci. China Technol. Sci. 55 (1), 285–294.

Yang, Y., Xu, Y., Li, J., Yang, C., 2018. Progress and performance evaluation of BeiDou global navigation satellite system: Data analysis based on BDS-3 demonstration system. Sci. China Earth Sci. 61, 614–624. https://doi.org/10.1007/s11430-017-9186-9.

Zhou, Y., Wang, Y., Huang, W., Yang, J., Sun, L., 2018. In-orbit performance assessment of BeiDou intersatellite link ranging. GPS Solut. 22, 119. https://doi.org/10.1007/s10291-018-0784-0.

Journal of Geodesy (2021) 95:85
https://doi.org/10.1007/s00190-021-01534-4

ORIGINAL ARTICLE

Galileo precise orbit determination with optical two-way links (OTWL): a continuous wave laser ranging and time transfer concept

Stefan Marz[1] · **Anja Schlicht**[1] · **Urs Hugentobler**[1]

Received: 14 October 2020 / Accepted: 13 June 2021 / Published online: 2 July 2021

Abstract
In this simulation study we analyze the benefit of ground-space optical two-way links (OTWL) for Galileo precise orbit determination (POD). OTWL is a concept based on continuous wave laser ranging and time transfer with modulated signals from and to ground stations. The measurements are in addition to Global Navigation Satellite System (GNSS) observations. We simulate the measurements with regard to 16 Galileo Sensor Stations. In the simulation study we assume that the whole Galileo satellite constellation is equipped with terminals for OTWL. Using OTWL together with Galileo L-band, in comparison with an orbit solution calculated with L-band-only, demonstrates the advantage of combining two ranging techniques with different influences of systematic errors. The two-way link allows a station and satellite clock synchronization. Furthermore, we compare the ground-space concept with the satellite-to-satellite counterpart known as optical two-way inter-satellite links (OISL). The advantage of OTWL is the connection between the satellite system and the solid Earth as well as the possibility to synchronize the satellite clocks and the ground station clocks. The full network, using all three observation types in combination is simulated as well. The possibility to estimate additional solar radiation pressure (SRP) parameters within these combinations is a clear benefit of these additional links. We paid great attention to simulate systematic effects of all observation techniques as realistically as possible. For L-band these are measurement noise, tropospheric delays, phase center variation of receiver and transmitter antennas, constant and variable biases as well as multipath. For optical links we simulated colored and distance-dependent noise, offsets due to the link repeatability and offsets related to the equipment calibration quality. In addition, we added a troposphere error for the OTWL measurements. We discuss the influence on the formal orbit uncertainties and the effects of the systematic errors. Restrictions due to weather conditions are addressed as well. OTWL is synergetic with the other measurement techniques like OISL and can be used for data transfer and communication, respectively.

Keywords Galileo · POD · Optical two-way link · Inter-satellite link

1 Introduction

Since the invention of the laser, optical communication links have been considered for space applications. In the last decades, laser technology in space experienced growing importance for future satellite missions. Optical links are perfect for point-to-point connection and can be used for communication, data transfer, clock synchronization and ranging, or synergetically for all applications. Due to a shorter wavelength compared to microwaves, a higher modulation rate is possible, which leads to a higher data rate for communication or higher precision in ranging applications. However, the operation of optical links from ground to a satellite with the same precision as microwave links or better was a difficult task in the past years. Due to the turbulence in the troposphere the development of adaptive optics was necessary (Weyrauch and Vorontsov 2004). An overview of the development and operation of optical communication links in space is given in Hemmati (2020). Giorgi et al. (2019) reviews possible optical communication and timing technologies for space-based clock synchronization.

The GRACE-FO (Gravity Recovery And Climate Experiment—Follow On) mission (Abich et al. 2019) and LISA Pathfinder (McNamara et al. 2008) are examples of inter-satellite optical frequency ranging applications. The European

✉ Stefan Marz
s.marz@tum.de

[1] Forschungseinrichtung Satellitengeodäsie, Technical University of Munich, Munich, Germany

Data Relay Satellites (EDRS) operate optical data transfer from the Sentinel satellites in low Earth orbits to geostationary satellites with a data rate of up to 1.8 Gbit/s (Zech et al 2015; Calzolaio et al. 2020). Many authors put a lot of effort into the inter-satellite link (ISL) concept for Global Navigation Satellite System (GNSS) (Gill 1999; Fernández et al. 2010; Fernández et al. 2010; Shargorodsky et al. 2013; Michalak et al. 2021; Zhang et al. 2021). In this context, Giorgi et al. (2019) and Schlicht et al. (2020) discuss optical inter-satellite links (OISL) in particular. The satellite orbit precision and handling of systematic errors will benefit from such OISL and a highly accurate satellite clock synchronization is possible as well. Inter-satellite links determine the relative positions of the satellites, but the constellation can be freely rotated around the geocenter (Schlicht et al. 2020). A high-precision optical link with the connection to the Earth surface would reduce this rotational freedom.

For this reason, authors discuss optical ranging and time transfer from the ground (Prochazka et al. 2011; Meng et al. 2013; Zhang et al. 2019). In the T2L2 (Time Transfer by Laser Link; Samain et al. 2014) project an optical ground-to-space time transfer link was tested. Exertier et al. (2019) describe the performance of state-of-the-art time and laser ranging as well as analyze the sources of limitation. In the upcoming ESA (European Space Agency) mission ACES (Atomic Clock Ensemble in Space; Cacciapuoti and Salomon 2009; Cacciapuoti et al. 2020) advanced ground-to-space time transfer links will be operated. The first link is a two-way microwave link (MWL) in the Ku-band (Delva et al. 2012). This acts like an asynchronous transponder and uses a phase-modulated signal with a rate of up to 100 MHz (Hess et al. 2011). An additional S-band downlink supports the characterization of ionospheric influences. The second link is the optical European Laser Timing (ELT; Schreiber et al. 2010) experiment. The laser link uses short pulses with a repetition rate of up to 2 kHz.

Furthermore, many authors discuss the combination of Satellite Laser Ranging (SLR) and GNSS measurements (Urschl et al. 2007; Thaller et al. 2011; Sośnica et al. 2015; Bury et al. 2021). The difficulty of this observation techniques combination is the treatment of the systematic errors of both systems. As SLR is not a standardized system, it has a complex error budget due to systematic biases of the different tracking stations (Schreiber and Kodet 2018; Luceri et al. 2019; Zajdel et al. 2019). For this reason, the potential of GNSS Precise Orbit Determination (POD) using a combination of GNSS and optical two-way ground-space measurements is still limited using SLR.

In this study, we analyze the optical two-way links (OTWL) (Schlicht et al. 2019) concept which is based on the use of modulated optical links between Galileo satellites and ground stations. OTWL encompasses two-way continuous wave laser ranging and time transfer. The signals use phase modulation. The module onboard of the satellites can be seen as an active retroreflector which acts similarly as a synchronous or asynchronous transponder. As an optical link has a shorter wavelength compared to microwaves, the use of higher modulation rates up to 10 GHz is possible. Optical terminals that offer Gbit/s rates over distances of 45000 km are already operative, as for example the TESAT-Spacecom terminal used for EDRS (European Data Relay Satellites) (Zech et al 2015; Calzolaio et al. 2020). An overview of active, tested and planned optical transmitters is given in Pribil and Hemmati (2020). These terminals operate with wavelengths of 1064 nm or 1550 nm.

OTWL (Optical Two-Way Links) is a theoretical concept that assumes the existence of these optical ground links to Galileo Sensor Stations. These L-band Galileo Sensor Stations are established to collect ranging measurements of Galileo navigation signals, to perform orbit determination and time synchronization as well as to monitor the signal in space (Falcone et al. 2017). The final Galileo Sensor Station network is planned to encompass about 40 sites. Fifteen Galileo Sensor Stations were active as of 2018. In June 2020, Wallis and Futuna (GWAL) successfully completed the infrastructure implementation for an additional Galileo Sensor Station. For our study, we use a Galileo Sensor Station network which is built-up of these 16 stations. In this work, the network is assumed—this is not planned up to now—to be fully equipped with laser ranging terminals to perform OTWL measurements. The hardware—the clock and the laser terminal for transmitting and receiving signals—is assumed to be the same at each site. This provides a standardized station network. At each OTWL observation epoch, a ground station can connect to one satellite and switches to another satellite at the next epoch. OTWL thus observes one satellite at a time while GNSS navigation signals connect multiple satellites to one stations. To classify the OTWL concept, a comparison in terms of the technical realization and the accuracies of different ranging techniques introduced above is given in Sect. 2.

The aim of this simulation study is to quantify the benefit of additional OTWL measurements for Galileo POD. We added a variety of systematic errors for all observation techniques and we investigated a possible expansion of the number of estimated empirical solar radiation pressure (SRP) parameters for the POD solution.

This study consists of three key parts: simulation, estimation and evaluation, which are addressed as follows:

- We simulate Galileo L-band, OTWL (Optical Two-Way Link) and OISL (Optical Inter-Satellite Link) observations for a ground network of 16 Galileo Sensor Stations and the Galileo constellation with 24 satellites.
- Five different scenarios are considered, accounting for different combinations of observations: L-band-only,

L-band+OTWL, L-band+OISL, L-band+OTWL+OISL and OTWL+OISL.
– Each scenario is analyzed by estimating typical geodetic parameters in order to assess the impact of OTWL and OISL observations.

In this paper, we characterize the error budget with three different consecutive scenarios:

– The use of true ground station coordinates in the measurements simulation and then for the estimation of the coordinates in the least-squares adjustment—only the coordinates of one station are fixed. This allows the coordinates to absorb link errors. Additionally, this shows the weakness of OISL in a solution with a one-station-fixed geodetic datum.
– The use of true ground station coordinates for the measurements simulation and then for the fixing of all station coordinates in the least-squares adjustment. This forces the adjustment to distribute the errors into the orbit and the clocks, or in the best case into the residuals.
– The fixing of all ground stations in the least-squares adjustment to biased coordinates. This shows the impact of errors in the station coordinates on the orbit solution.

These analysis steps allow a conclusion on how different aspects affect the orbit solution and how OTWL and other measurement types drive the estimation process.

The study is structured as follows: In Sect. 2 we compare different ranging techniques to classify OTWL and OISL. In Sect. 3 we first describe the satellite constellation used and the simulation of the measurement types. Second, we explain the estimation procedure and the scenarios using different link combinations. As we took great attention to the modeling of SRP parameters in the estimation process, we give a detailed explanation on this in Sect. 4. This also includes the definition of different orbit types, needed in a simulation procedure, as their generation is highly dependent on different SRP models. The SRP analysis defines further scenarios in terms of the estimation of different empirical SRP parameters in the least-squares adjustment. Section 5 discusses the results of this study following the analysis steps described above. A conclusion and an outlook is given in Sect. 6.

2 Classification of the OTWL and OISL ranging concepts

In the following, we compare the ranging techniques GNSS, MWL (microwave link; Delva et al. 2012), SLR/ELT (European Laser Timing; Schreiber et al. 2010), OTWL (Optical Two-Way Link) and OISL (Optical Inter-Satellite Link) in terms of their technical realization and their accuracies. Table 1 gives an overview.

GNSS is a space-ground oriented one-way ranging technique based on signals in the L-band. GNSS uses a phase-modulated signal with a rate of about 10 MHz. Code and phase can be analyzed. The achieved ranging precision is at about 1.5 mm for the phase.

In comparison with GNSS, the MWL is a two-way link which operates in the Ku-band (Delva et al. 2012) and uses a phase-modulated signal with a rate of up to 100 MHz (Hess et al. 2011). Time transfer is possible as it is a two-way link (Delva et al. 2012). The achieved chipping rate is about ten times higher than for GNSS. The microwave link has a time transfer precision of 300 fs and a ranging precision of 100 µm at 300 s integration time (Cacciapuoti and Salomon 2009), limited by the maser stability. Compared to the up-to-date used optical links, the phase can be evaluated using

Table 1 Comparison of different ranging techniques

	GNSS	MWL	SLR/ELT	OISL	OTWL
Frequency	MW L-band 1.5 GHz Modulation 10 MHz	MW Ku-band 14 GHz Modulation 100 MHz	Optical Repetition 2 kHz	Optical Modulation 0.1–10 GHz	Optical Modulation 0.1–10 GHz
Ranging technique	Phase modulated, one-way	Phase modulated, two-way	Pulsed, round trip / one-way	Phase modulated, two-way	Phase modulated, two-way
Analysis	Code + Phase	Code + Phase	Single photon	Code	Code
Precision	1.5 mm phase	0.2 mm phase, at 30 s integration time (Cacciapuoti and Salomon 2009)	1 mm for normal point (Schreiber et al. 2010; Luceri et al. 2019)	Potentially higher than MWL	Potentially higher than MWL
Capability of routine calibration	No	No	Yes, on ground, not in space	Yes, in any-to-any scenario	Yes, on ground and in combination with any-to-any OISL also in space

a MWL. This is not yet possible with an optical link in conditions of large relative movements. This leads to a much higher ranging and time transfer precision than a SLR/ELT link can achieve.

SLR/ELT operates with short laser pulses with a repetition rate of up to 2 kHz. This is a much lower repetition rate than used for the MWL. Using single-photon detectors for ELT onboard of the satellite and on ground allows an accurate signal detection, but 90% of the measurements are lost due to the detection mode. European Laser Timing has an expected time transfer precision of 3 ps at 300 s and a ranging precision of 1 mm (Schreiber et al. 2010). An advantage of an optical link compared to a link using microwaves is the capability of performing a routine calibration. ELT can be calibrated with an accuracy of less than 25 ps for time transfer and about 7.5 mm for ranging, while the MWL can be calibrated to around 3 cm. The advantages of both links can be combined as well, e.g., the optical link can be used to calibrate the microwave link (Leute et al. 2018).

Compared to SLR/ELT, the OISL and OTWL concepts use phase modulation and continuous waves instead of short laser pulses. Therefore, the laser terminals used for OTWL have to provide this tracking technique. The OISL and OTWL ranging technique is generally comparable to MWL. But due to the shorter wavelength of an optical link compared to a microwave link, the use of modulation rates of up to 10 GHz is possible. Such or even higher modulation rates can already be technically realized. Therefore, OISL and OTWL have the potential to achieve an even higher precision than a microwave link.

As mentioned in Sect. 1, the SLR station network is not a standardized system. The Galileo Sensor Station network used for OTWL is assumed to be equipped with the same hardware at each site to reduce systematic errors. In space, SLR/ELT use retroreflectors and single photon detectors, while OISL and OTWL need active transponders onboard of the satellites, similar to those used for the European Data Relay Satellites (EDRS) for example. Furthermore, OTWL and OISL can easily be used for data transfer, which is not yet common with SLR/ELT. On the other hand, SLR/ELT has the advantage that also the ITRF stations can contribute to the tracking and no scheduling onboard of the satellites is required for this type of measurement.

A ground-space oriented optical link is restricted by weather conditions—an optical signal cannot penetrate clouds. Hence, OISL has an advantage over OTWL and SLR/ELT since the troposphere is not involved. A ground-space oriented microwave link does not have these observation restrictions due to clouds as well. However, microwaves are sensitive to the delay caused by the wet part of the troposphere, which cannot always be properly modeled.

The synergetic aspects of both link types addressing different systematic effects, as well as the calibration aspects, are arguments for a combination of microwave-based and laser-based observation techniques, for instance GNSS and OTWL. OTWL is also of great interest when combined with OISL. Furthermore, in an any-to-any—each satellite tracks all other satellites in the constellation within one scheduling period—inter-satellite link scenario a continuous calibration of the space segment is achievable. The inter-satellite link terminals on a satellite have the capability to point to each other for calibration (Koepf et al. 2002).

Having the comparison of the different ranging techniques as a base, we now can classify the precision and accuracy of the OTWL and OISL observations used in this study. For our simulations we require an OTWL link to provide a ranging precision of at least 1 mm at an integration time of 30 seconds. This is a very moderate assumption. We require OTWL to provide a ranging accuracy like SLR/ELT, as we estimate biases with no constraints. Very important for the estimation is a long time stability of the bias, at least 1 mm within one day. The same applies for the OISL measurements in this study. Additionally, it is of utmost importance that the eccentricity of both instruments be known precisely, in space and on ground—on ground with less than about 1 mm in total Three-Dimensional (3D)—Root Mean Square (RMS). We use this fact as we only estimate one-station coordinate, to which all observation types refer to. The local ties and the stability of the connection of a common clock are a prerequisite in combining different links. In this way, the Galileo system equipped with OTWL would represent a good testing ground for a Global Geodetic Observing System (GGOS; Plag and Pearlman 2009) station in space.

3 Simulation setup

For this paper, we evaluate the impact of additional OTWL (Optical Two-Way Link) observations in a typical Galileo orbit solution. Furthermore, we compare the results to the impact of OISL (Optical Inter-Satellite Link) observations. For both, simulation and analysis, we used a modified version of the Bernese GNSS Software (Dach et al. 2015). We processed four time periods, each with ten successive days as 24 hours of observations—the days 043–052, 102–111, 132–143 and 163–172 of the year 2019—to cover a relatively large range of beta angles. The beta angle is defined as the sun elevation angle above the orbital plane. The solar radiation, acting on a satellite, changes with varying beta angle. SRP is the largest non-gravitational force disturbing GNSS satellite orbits (Fliegel et al. 1992; Springer et al. 1999; Montenbruck and Gill 2005). In Sect. 4 we present further analysis results regarding the modeling of SRP parameters.

3.1 Constellation and measurement schedule

The Galileo constellation that we used consisted of 24 satellites, with 21 Full Operational Capability (FOC) satellites—including the satellites E14 and E18 in eccentric orbits—and three IOV (Initial Orbit Validation) satellites (E11, E12, E19). We obtained the orbits from MGEX CODE products of the International GNSS Services (IGS). A Galileo Sensor Station network of 16 ground stations (see Fig. 1) was used in this simulation study for both, the two frequency code- and phase-observations and the OTWL observations. We created a measurement schedule for the OTWL observations for each of the four 10-day time periods. This measurement schedule is yet not optimized for a mission deployment, but serves as a good baseline to determine the potential of OTWL observations. The minimum elevation for observations above horizon is set to 30°. The time between two observation epochs is 60 seconds, with a measurement sampling rate of 30 seconds and 30 seconds for the telescope to move to the next satellite. The schedule builds up as follows:

- Each satellite is allowed to be connected to just one station per epoch.
- The first satellite assigned to each ground station is the next free satellite which is descending and closest to the minimum elevation.
- Then that satellite is assigned to each station which is the closest in azimuth and elevation direction to avoid excessive slewing.
- In case this satellite is already connected to another station, the next nearest satellite is chosen.
- For the order of selection, a ground station priority list is generated according to the number of Galileo satellites visible for a station above the minimum elevation. The list is adapted every epoch.

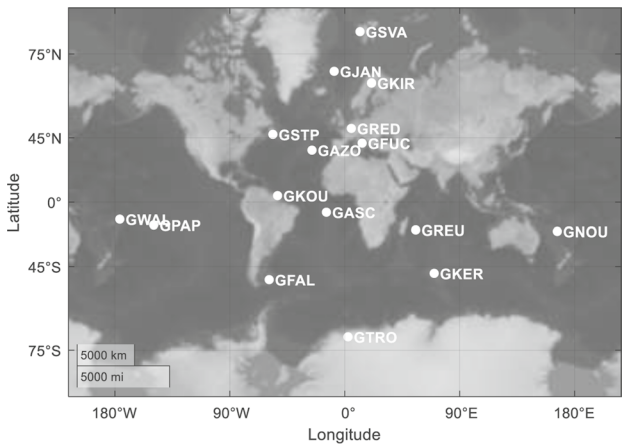

Fig. 1 The Galileo Sensor Station network used in this study

- An observation period is finished when a station once was connected to all visible satellites in the period time span.
- In case a station does not have a free satellite left in an observation period, double observations or a suspending of the station for one epoch is allowed, but is avoided as much as possible.
- When a station finished an observation period, the next observation period starts for this station.

3.2 Simulation

The OTWL observations are two-way continuous wave laser ranges as well as clock differences. The measurement errors used to simulate laser observations are given in Table 2. A more detailed description and equations of the errors can be found in Schlicht et al. (2020). To be congruent with the OTWL observations, the sampling rate of the GNSS and OISL observations is 60 seconds as well. The GNSS observations were simulated as dual frequency code and phase measurement for E1 and E5. Effects due to the ionosphere were eliminated to a great extent by forming the ionosphere free linear combination. A summary of the simulated microwave link measurement errors is shown in Table 3. The OISL laser technology is based on EDRS (European Data Relay Satellites) data transfer links. We generated the observation schedule for an any-to-any scenario with bidirectional links between the satellites. Schlicht et al. (2020) show that this scenario offers the best results. The OISL observation schedule was derived from the connectivity scheme by Fernández (2011). We simulated two-way range measurements and clock differences. For the OISL measurements we simulated the errors analogously to the OTWL observations but without troposphere delay errors. This is an advantage for OISL observations as no signal path is disturbed by the troposphere. The measurement errors for OISL are collected in Table 2 as well.

The simulated satellite clocks are hydrogen masers. This leads to a mean satellite clock error of about 24 ns after ten days. Ground station clocks are assumed to be simple quartz oscillators and are simulated based on polynomials of order four with respect to time. The station clock error is smaller than 0.1 μs. Each satellite and each ground station is equipped with one clock, assuming that all observation techniques are connected to the same clock in each satellite and each station. We simulated inter-system biases: a once per revolution variable bias per satellite in case of L-band, emulating a temperature dependency, biases affecting the clock offsets and ranges in case of OISL and biases affecting the clock offsets and ranges in case of OTWL. Hence, each observation technique has its own biases, resulting from different cable lengths and delays on the signal path between the corresponding receiving terminal and the clock.

Table 2 Simulated measurement errors for the laser based observation techniques OTWL and OISL

Optical link measurement errors		Description/Remark
Measurement noise	Flicker-phase noise (Riley 2008)	Occurs in all electronic devices Induced by various effects (e.g., trapping of charge carriers in semiconductors) Selected noise level up to 0.5 mm
	Jitter of the Phase Locked Loop (PLL) (Holmes 1990)	Error is ranging distance dependent: Selected maximum distance for OTWL 31 000 km, for OISL 60 000 km Noise at maximum ranging distance: OTWL 1.4 mm, OISL 1.5 mm
Troposphere offset (for OTWL only)		Simulated error: Half the difference between the models of Marini and Murray (1973) and Mendes and Pavlis (2004): (Marini-Murray—Mendes-Pavlis)/2 Air pressure and temperature information from GPT (Boehm et al. 2007) Relative humidity was set individually per ground station: min. 75%, max. 90%. Varies randomly per station and epoch reaching up to around ± 6% Max. error at 30° elevation 5 mm, min. error at 90° elevation 0.4 mm
Offset due to the repeatability of the link		Uniformly distributed for each transmitter–receiver-pair between ± 0.5 mm
Offset related to the equipment calibration quality		Offset per satellite, randomly distributed between -0.5 and 0.5 mm inter-system bias which affects the clock (bias difference between receiver and transmitter) and the range (bias sum of receiver and transmitter) includes a variability due to the Phase Locked Loop (Schlicht et al., 2020)

A detailed description of the different errors can be found in Schlicht et al. (2020)

Table 3 Measurement errors which were simulated for L-band in this study

L-band measurement errors		Description/remark
Measurement noise		White noise of 15 cm for code and 1.5 mm for phase measurements for each frequency
Troposphere modeling errors	Simulation	Gridded VMF1 (Boehm et al. 2006a) model as an accurate model This model is based on real weather model data
	Solution	GMF model (Boehm et al. 2006b) as a less accurate model The difference VMF1-GMF gives an error of about 2.2 cm at 15° elevation and about 4 mm at 80° elevation
Phase center variations (PCV)		For receiver and transmitter: different pattern for each of the 16 ground stations and satellites For receiver and transmitter code measurements: multiplication by factor 50 represents a worst case scenario The signatures are comparable to multipath
Constant bias		Different bias per satellite, randomly distributed up to 5 mm
Variation with once per revolution		Different variation per satellite, randomly distributed up to 5 mm emulates temperature-dependent inter-technique bias per satellite

The error free force model in the simulations includes the Earth gravity field up to degree and order 12, ocean and solid Earth tides, influences from third bodies (Sun, Moon, Venus, Mars and Jupiter). For SRP we applied a modeling error (see Sect. 4).

3.3 Estimation

In the solution, we parameterized the satellite orbits with six osculating elements and nine or more empirical SRP parameters (see Sect. 4). Furthermore, we estimated station specific piecewise linear tropospheric zenith delays every

two hours (L-band), ground station coordinates per 24 hours (L-band and OTWL), epoch-wise satellite and ground station clocks (L-band, OTWL and OISL) as well as L-band phase ambiguities per pass (float). In addition, we estimated daily range and clock biases for each satellite (OISL and OTWL) as well as each ground station in case of OTWL. We simulated inter-technique biases affecting the clock and the range. However, we estimated only one bias per clock and one per range, representing the bias between L-band and the optical techniques. The estimation of biases per observation technique would be the next step, but is only relevant for the scenarios L-band + OTWL + OISL and OTWL + OISL. Regarding the ground station coordinates, we assumed small coordinate eccentricities errors of about 0.5 mm (3D) between L-band and OTWL. However, we estimate only one reference coordinate per station, to which all observation techniques refer to. An overview of the estimated parameters regarding each observation technique can be found in Table 4. Following the OTWL observation schedule, for 16 ground stations and 24 satellites around 42560 OTWL observations were simulated per day. In comparison, around 403890 GNSS observations in code and phase as well as around 32300 OISL observations were simulated per day.

In the analysis procedure we defined the geodetic datum by fixing the coordinates and the clock of one ground station (GASC) for L-band and OTWL. For comparison, we performed a second procedure fixing another station (GKOU). The analysis shows that fixing another station does not affect the behavior of the results.

Having only 16 ground stations in the estimation, an all-stations-fixed scenario would be chosen in the real world to stabilize the solution since the coordinates are assumed as well known. For this reason, we did another analysis with fixing all 16 ground station coordinates in the estimation (shown at the end of Sect. 5)—still only one ground station clock is fixed. In a first scenario we did not assume station coordinate errors. A second scenario takes station coordinate errors into account. A comparison of both scenarios shows the impact of the coordinate errors on the orbit solution. Defining an all-stations-fixed geodetic datum, the additional constraints added may on the one hand stabilize the solution due to the strong tie to the reference frame, and on the other hand they may distort the solution as systematic errors can no longer be absorbed in the station coordinates. The results in this paper show that a L-band + OISL scenario benefits a lot from an all-stations-fixed geodetic datum, while for a L-band + OTWL scenario the orbits can be adjusted with high accuracy in a system with a one-station-fixed or an all-stations-fixed geodetic datum.

4 Solar radiation pressure modeling

Doing simulations, one faces two typical problems: First, one can only take already known modeling or systematic measurement errors into account. Second, the analysis is future oriented and, hence, it is difficult to specify the utmost precision and accuracy of the measurements. In this study, the main modeling issue in orbit determination of Galileo satellites is SRP. We just focus on this modeling error. Furthermore, we assume a moderate accuracy and precision for the optical ranging techniques. Other non-gravitational forces, like thermal radiation, radiators, thruster leakage and attitude biases, can be taken into account in future work.

Table 4 Estimated parameters regarding each observation technique

Estimated parameters	L-band	OTWL	OISL
Station specific tropospheric zenith delays	✓ Every two hours	-	-
Ground station coordinates	✓/–	✓/–	–
	Both observation techniques refer to the same reference coordinates at each site with a known eccentricity		
Epoch-wise satellite and ground station clocks	✓	✓ One clock for each satellite and each ground station	✓
Phase ambiguities	✓	–	–
Range biases	–	✓ One bias for each satellite and ground station, respectively (also in scenarios with L-band + OTWL + OISL and OTWL + OISL)	✓
Clock biases	–	✓ One bias for each satellite and ground station, respectively (also in scenarios with L-band + OTWL + OISL and OTWL + OISL)	✓

Two strategies are possible when modeling SRP:

- The physical approach is to describe the absorption and reflection properties of the main surfaces of the satellite. For instance, a box-wing model is a physical model that approximates the general shape of the satellite (Bury et al. 2019; Duan et al. 2019).
- The empirical approach is to estimate periodic accelerations of the satellite in an appropriate coordinate system, described by models like the Empirical CODE Orbit Model 2 (ECOM2) (Arnold et al. 2015).

ECOM2 (see Eq. (1)) is one of the commonly used empirical SRP models in the IGS community for the processing of GNSS solutions. Generally, the SRP parameters are estimated in the Sun-Satellite-Earth frame (SSE): D points from the satellite to the Sun, Y is in the direction along the solar panels and B completes the right-handed orthogonal system. The accelerations in each of the DYB directions encompass a constant term as well as sine and cosine terms with selected frequencies that are integer multiples of once per revolution. ECOM2 covers constant terms in all DYB directions, as well as two and four times per revolution terms in D direction and a once per revolution term in B direction (see Eq. (1) with the argument of latitude with respect to the sun Δu). The per revolution parameters are divided into a sine and cosine parameter. In the further context, we name the parameters related to the direction with the corresponding letter D, Y or B and append the per revolution term by its number. For example, the D2 parameters are related to direction D with a frequency of twice per revolution. A subscript c names the cosine, s the sine parameter and 0 the constant parameters.

Two SRP model types following different modeling strategies is an appropriate starting point for orbit determination simulations:

- We can define the simulation truth (*true* orbit) with a physical model.
- We introduce a slightly wrong physical model representing the a priori modeling error (*mismodeled* orbit), used as input for the orbit adjustment.
- Fitting empirical accelerations to realistic measurements with observation errors using a least-squares adjustment results in an *adjusted* orbit. As the empirical parameters cannot compensate the modeling errors perfectly in total, the *adjusted* orbit includes a corresponding a posteriori modeling error.
- Calculating a *best possible* orbit, we can quantify this a posteriori modeling error (see below).

Hence, this procedure defines four different orbit types that are generally relevant in a simulation study: *true*, *mismodeled*, *adjusted* and *best possible* orbits. Figure 2 gives a scheme how these orbit types are generated in our study. The following subsections describe the generation of the orbits by guiding through the scheme (Fig. 2), followed by an analysis of the introduced modeling error.

4.1 True orbit

To get as realistic Galileo orbits as possible, we retrieved MGEX CODE orbits of the IGS (Prange et al. 2020) and

$$\begin{aligned} D &= D_0 + D2_c \cos(2\Delta u) + D2_s \sin(2\Delta u) + D4_c \cos(4\Delta u) + D4_s \sin(4\Delta u) \\ Y &= Y_0 \\ B &= B_0 + B1_c \cos(\Delta u) + B1_s \sin(\Delta u) \end{aligned} \tag{1}$$

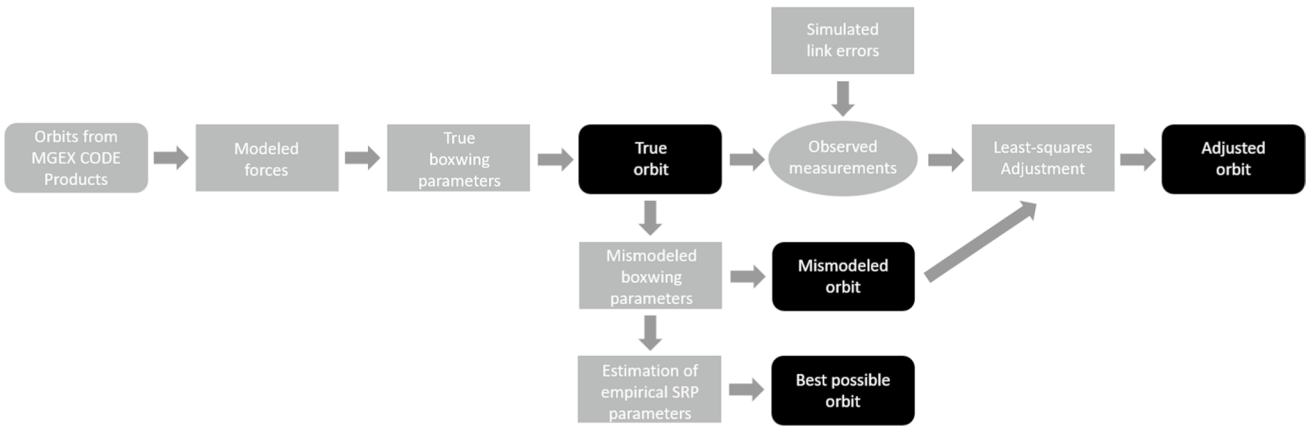

Fig. 2 Scheme of the orbit generation procedure of this simulation study

adjusted them with models. To get the simulation truth for our study, we used the box-wing model by Duan et al. (2019) as a physical model. The box-wing model considers the surfaces of a satellite in $\pm x$, $\pm y$ and $\pm z$ body-fixed directions (box) and the solar panel area (wings). The physical optical parameters of absorbed α, reflected ρ and diffusely reflected δ photons are modeled for each satellite surface. Integrating the Galileo orbits with a box-wing parameter set assumed as *true* leads us to the simulation truth, represented by the *true* orbit that is used to simulate the observations. The FOC and IOV satellites are integrated with slightly different box-wing parameters.

4.2 Mismodeled orbit

To get the *mismodeled* orbit, the input orbit for the least-squares adjustment, the *true* orbit was integrated with a modified box-wing parameter set to introduce an orbit with an a priori modeling error. We generated two *mismodeled* orbits with different SRP modeling errors to analyze the influence of different modeling errors to the solution. The following models are identically used for FOC and IOV satellites, which leads to a slightly higher modeling error for the IOV satellites as the *true* box-wing parameters have a slightly larger difference.

First, we modified the three optical parameters of absorbed α, reflected ρ and diffusely reflected δ photons in the directions $\pm x$, $\pm y$ and $\pm z$ by 10–20% (see the equations shown in Table 5). Box surfaces and solar panel sizes remained unchanged. Thus, generated *mismodeled* orbits are wrong by around 15 cm on average (*true—mismodeled* orbit). We further call this the *mismodeled orbit* according to *modeling error 1*. This *mismodeled* orbit was mainly used in this simulation study.

Second, we modified the box surface in $\pm x$ direction by +4% (Table 6). The solar panel sizes as well as the three optical parameters remained unchanged for all directions for this simulation. We further call this the *mismodeled* orbit according to *modeling error 2*.

The satellite producer and ESA do not publish errors for the physical optical parameters, but discussed uncertainties are at a level of about 10%. A study analyzed the error of a box-wing model compared to a CAD (Computer-Aided Design) model and concluded that the satellite surfaces are wrong by 7% for GPS and 2% for Galileo on average for all beta angles (Li and Ziebart 2020). As we analyzed individual errors for the physical optical parameters and the satellite box, our assumed modeling errors fit well to the total acceleration errors due to SRP.

Table 6 Modification of box-wing parameters used to generate the *mismodeled orbit* (*modeling error 2*)

	$\pm x$	$\pm y$	$\pm z$
$\alpha_{\text{mismodeled}} =$	α_{true}	α_{true}	α_{true}
$\rho_{\text{mismodeled}} =$	ρ_{true}	ρ_{true}	ρ_{true}
$\delta_{\text{mismodeled}} =$	δ_{true}	δ_{true}	δ_{true}
$\text{boxsurface}_{\text{mismodeled}} =$	$1.04\,\text{boxsurface}_{\text{true}}$	$\text{boxsurface}_{\text{true}}$	$\text{boxsurface}_{\text{true}}$
$\text{wingsize}_{\text{mismodeled}} =$	$\text{wingsize}_{\text{true}}$	$\text{wingsize}_{\text{true}}$	$\text{wingsize}_{\text{true}}$

4.3 Adjusted orbit

The resulting orbit from the least-squares adjustment of the measurements is the *adjusted* orbit. Using the *mismodeled* orbit as the a priori orbit, the *adjusted* orbit is based on *modeling error 1 or 2*, respectively, with additionally adjusted empirical parameters.

4.4 Best possible orbit

The *best possible* orbit delivers the maximum achievable accuracy from the introduced modeling errors. This orbit is retrieved by adjusting the *true* orbit positions using an orbit model based on the *mismodeled* box-wing parameter set and additionally adjusting empirical parameters. The difference of the *best possible* orbit and the *adjusted* orbit thus is the fact that the former is adjusted to the *true* orbit positions while the latter is adjusted to the observations simulated using the *true* orbit. In comparison with the *mismodeled* orbit, empirical parameters are estimated for both of them.

4.5 Modeling error analysis

Empirical orbit models like ECOM2 (Eq. (1)) use different per revolution-dependent terms. In a pre-simulation analysis, we investigated the influence of such once per revolution-dependent terms and their multiples, caused by the a priori

Table 5 Modification of box-wing parameters used to generate the *mismodeled orbit* (*modeling error 1*)

	$\pm x$	$\pm y$	$\pm z$
$\alpha_{\text{mismodeled}} =$	$1.2\alpha_{\text{true}}$	$0.9\alpha_{\text{true}}$	$1.1\alpha_{\text{true}}$
$\rho_{\text{mismodeled}} =$	$1-\left(1.2\alpha_{\text{true}}+\delta_{\text{true}}\right)$	$1-\left(0.9\alpha_{\text{true}}+\delta_{\text{true}}\right)$	$1-\left(1.1\alpha_{\text{true}}+\delta_{\text{true}}\right)$
$\delta_{\text{mismodeled}} =$	δ_{true}	δ_{true}	δ_{true}
$\text{boxsurface}_{\text{mismodeled}} =$	$\text{boxsurface}_{\text{true}}$	$\text{boxsurface}_{\text{true}}$	$\text{boxsurface}_{\text{true}}$
$\text{wingsize}_{\text{mismodeled}} =$	$\text{wingsize}_{\text{true}}$	$\text{wingsize}_{\text{true}}$	$\text{wingsize}_{\text{true}}$

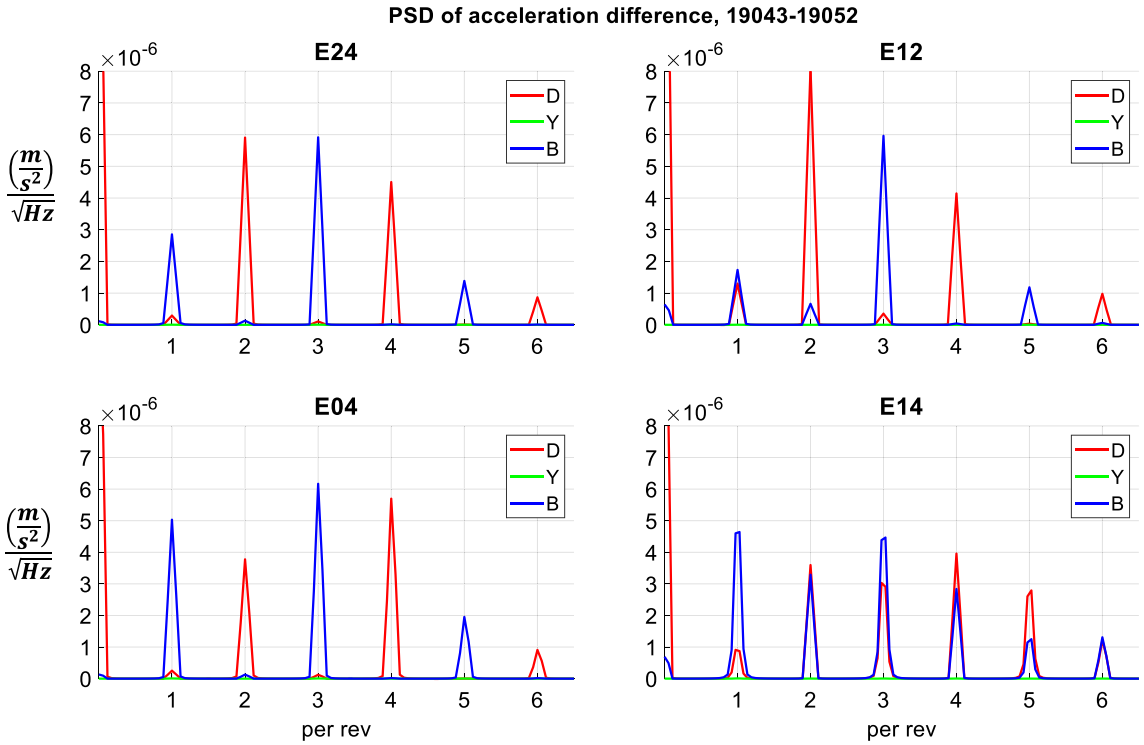

Fig. 3 PSD of the acceleration difference extracted from the *true* and *mismodeled* box-wing model for the time period 19,043–052 with respect to *modeling error 1* (Table 5). The results are computed for one satellite of each of the four Galileo planes. Satellite E24 relates to plane A, E12 to B, E04 to C. For the more eccentric satellites like E14 we define the plane D as the fourth plane. The *x*-axis shows the per revolution terms, the *y*-axis the amplitude of the acceleration

box-wing model errors. We extracted the computed SRP accelerations from the *true* and the *mismodeled* orbit in the SSE frame and computed the differences (*true—mismodel*). We processed SRP accelerations for the same four 10-day time periods used in the simulation study. The analysis was done for one satellite of each of the four Galileo planes A-D as the beta angle is the same for all satellites in the same orbital plane. The planes A-C refer to the regular Galileo orbital planes. Plane D was defined for the satellites E14 and E18 in eccentric orbits.

Figure 3 shows the Power Spectral Density (PSD) of the acceleration difference *true—mismodeled* according to *modeling error 1* (Table 5) for the days 043–052 from 2019 (19043-052). The following discussion is transferable to the other three simulation time periods as well. In Y direction there is overall no influence. The even per revolution terms are dominant in D direction, while the odd terms are dominant in B direction, as expected. This is less obvious for the satellites E14 and E18 in eccentric orbits for which additional harmonic terms are required because Δu is no longer linear with time. For some beta angles, the three times per revolution term is more dominant than the once per revolution term. Figure 4 shows the PSD of the acceleration difference *true—mismodeled* according to *modeling error 2* (Table 6) for the period 19043-052. The results are again transferable to the other three time periods. In this case, the main terms are up to twice per revolution for all planes. The influence of higher per revolution terms is negligibly small.

From this analysis we can conclude that the influence of certain per revolution terms is dependent on different modeling errors and the resulting impact on SRP accelerations. The ECOM2 model was developed by reviewing direct SRP models for GNSS satellites (Arnold et al. 2015). We analyzed the SRP influence by modifying box-wing parameters. In case of a SRP influence with respect to the *modeling error 1* (Table 5), we identify in addition to B1, D2 and D4 also a strong influence of B3 parameters, which are not taken into account by the ECOM2 model. In this regard, we would expect an effect on the orbit adjustment with the estimation of additional B3 parameters as well. We mainly use the *mismodeled* orbit according to *modeling error 1* (Table 5) in this simulation study. However, for the discussion of the results in Sect. 5, we compared the *adjusted* orbits resulting from both *mismodeled* box-wing models—according to *modeling error 1* (Table 5) and *modeling error 2* (Table 6)—to show if it is possible to estimate higher per revolution terms to improve the *adjusted* orbit, independently from the accelerations acting on the satellite.

Furthermore, we analyzed the beta angle dependence of the estimated B as well as the D acceleration parameters for

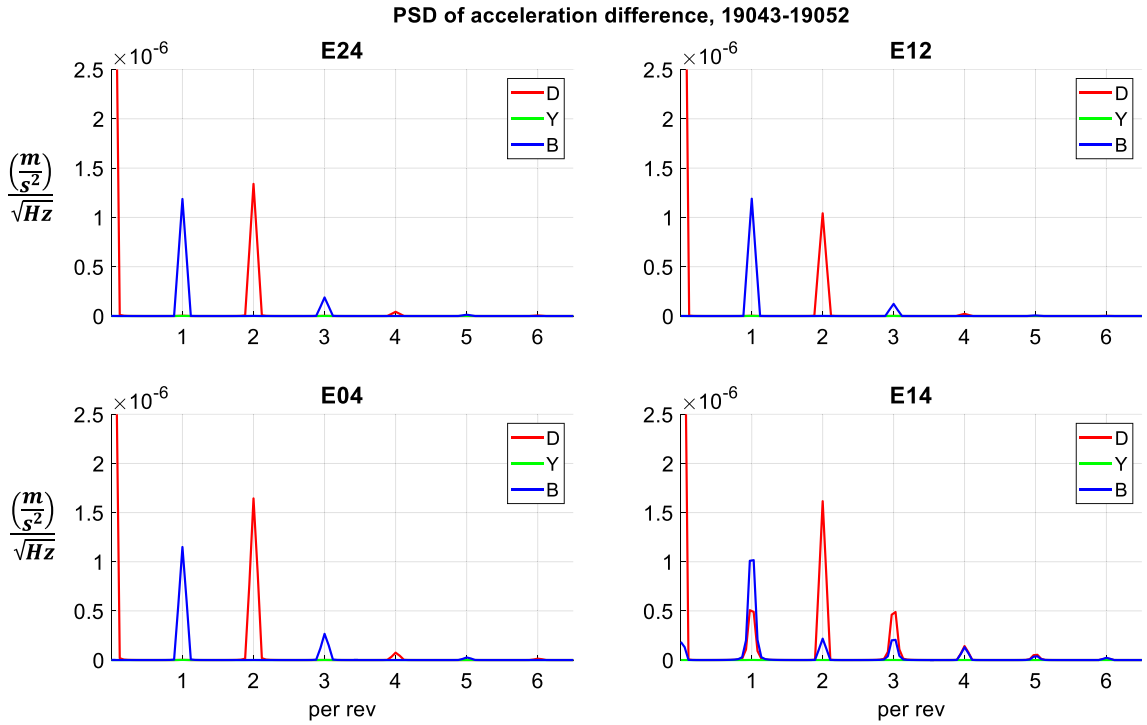

Fig. 4 PSD of the acceleration difference extracted from the *true* and *mismodeled* orbit for the time period 19,043–052 with respect to *modeling error 2* (Table 6). The *x*-axis shows the per revolution terms, the *y*-axis the amplitude of the acceleration. Satellite E24 relates to plane A, E12 to B, E04 to C. For the satellites in eccentric orbits, like E14, we define the plane D as the fourth plane

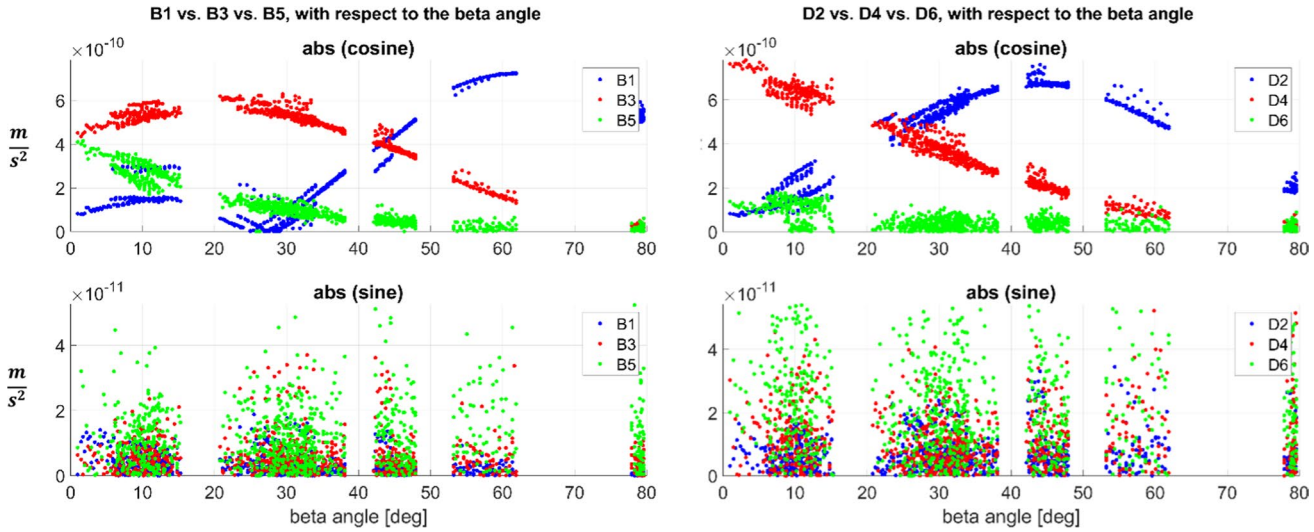

Fig. 5 Dependence of the B1, B3, B5 parameters (top and bottom left graphics) and D2, D4, D6 (top and bottom right graphics) with respect to the beta angle. The analysis was done for the four time periods 19,043–052, 19,012–111, 19,132–141 and 19,163–172 and 24 Galileo satellites. The top graphics show the absolute value of the cosine parameters, the bottom graphics the sine parameters

all four analysis periods and all 24 satellites of the constellation. The parameters—sine and cosine of B1, B3 and B5 as well as D2, D4 and D6—which are estimated when generating the *best possible* orbit, show which of the individual SRP parameters absorb the introduced *modeling error 1* (Table 5). Figure 5 shows the absolute value of the obtained empirical accelerations as a function of the beta angle. Generally, in the sine terms no significant beta angle dependence can be found. This is expected as the accelerations from the box-wing model are symmetric with respect to the satellite

position along the orbit relative to the Sun. However, in the cosine parameters a clear beta angle dependency is recognizable. The impact on B1 and B3 is relatively large, while for B5 the accelerations are negligibly small for beta angles larger than 40°. Beta angle dependence can be found for D2 and D4 parameters as well. The acceleration related to D6 are, however, relatively small for all beta angles compared to D2, D4 and the B parameters. These results show the varying projection of the accelerations induced by the box-wing modeling error into the SSE coordinate directions as a function of the beta angle.

When estimating the terms D6, no improvement was recognizable. In a scenario with ECOM2 and estimating terms B3+B5+D6, the *best possible* mean 3D-RMS error even increased again. For this reason, we investigated in the following only the influence of up to five times per revolution terms. We defined four SRP scenarios for this simulation study: the first scenario relates to the commonly used ECOM2 model given in Eq. (1), in the second we replaced the B1 parameters with B3, see Eq. (2), in the third we extended ECOM2 by B3, Eq. (3), and in the fourth we extended ECOM2 by B3 and B5, Eq. (4).

$$\begin{aligned} D &= D_0 + D2_c \cos(2\Delta u) + D2_s \sin(2\Delta u) + D4_c \cos(4\Delta u) + D4_s \sin(4\Delta u) \\ Y &= Y_0 \\ B &= B_0 + B3_c \cos(3\Delta u) + B3_s \sin(3\Delta u) \end{aligned} \tag{2}$$

$$B = B_0 + B1_c \cos(\Delta u) + B1_s \sin(\Delta u) + B3_c \cos(3\Delta u) + B3_s \sin(3\Delta u) \tag{3}$$

$$B = B_0 + B1_c \cos(\Delta u) + B1_s \sin(\Delta u) + B3_c \cos(3\Delta u) + B3_s \sin(3\Delta u) + B5_c \cos(5\Delta u) + B5_s \sin(5\Delta u) \tag{4}$$

Furthermore, we had a look at the error of the *best possible* orbits resulting from the different SRP parameter estimates. When estimating per revolution terms in B and D directions up to order five in the orbit adjustment, a decrease of the mean 3D-RMS orbit error could be determined.

Figure 6 shows the error of the *best possible* orbit as a function of the beta angle for the four SRP estimation scenarios. The mean orbit error results in 3.4 mm for scenario (1), 7.0 mm for (2), 1.0 mm for (3) and 0.9 mm for (4). The large mean error for scenario (2) is due to a continuously

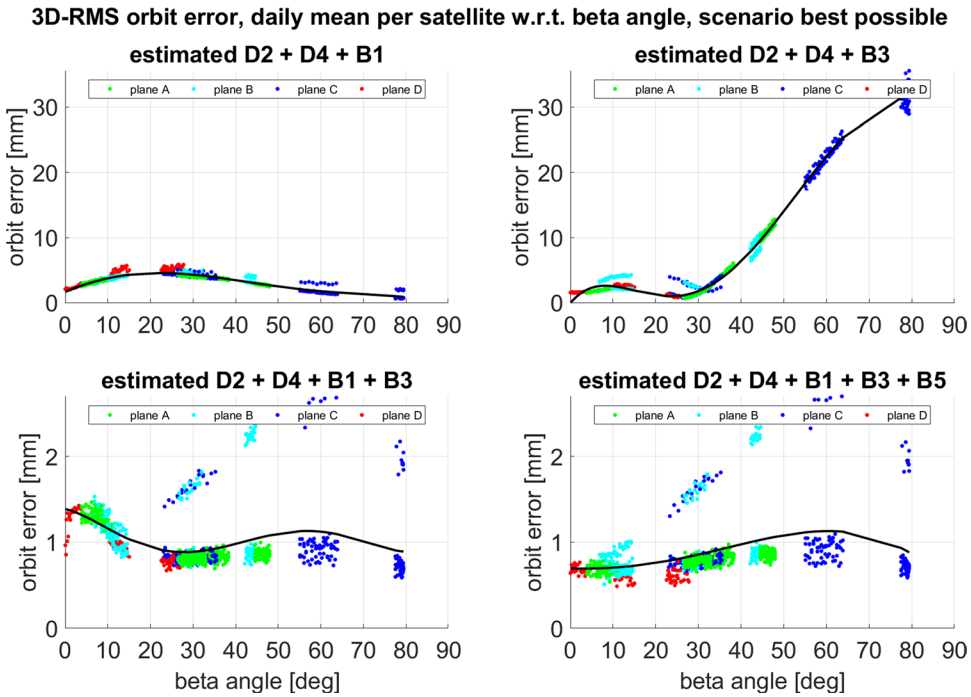

Fig. 6 Orbit errors of the *best possible* orbit with respect to the beta angle. The top left figure relates to the SRP modeling according to Eq. (1), the top right to Eq. (2), the bottom left to Eq. (3) and the bottom right to Eq. (4). The black line is a polynomial fit of the data with order five to guide the eyes. The planes A to C are the three regular Galileo satellite planes. Plane D consists of the more eccentric E14 and E18 satellites. The IOV satellites have slightly larger orbit errors regarding the mean value, due to the slightly larger modeling error

increasing error for increasing beta angles above 30°. This result is consistent to the result presented in Fig. 5. The course of the polynomial fit of scenario (2) shown in Fig. 6 is similar to the accelerations represented by the cosine B1 in Fig. 5, which is not estimated in scenario (2). The same is recognizable for scenario (1) in Fig. 6 and the accelerations of B3 in Fig. 5. In scenario (3) shown in Fig. 6 both B1 and B3 were estimated, resulting in orbit errors in the range of around 1 mm for all beta angles, showing the importance of estimating these terms. It should be noted that the three IOV satellites (two in plane B and one in C) show slightly larger discrepancies from the mean value, due to the slightly larger simulated SRP modeling error (see Sects. 3.1 and 3.2). However, we have to consider that the overall orbit error is already quite small with maximum values up to around 2.5 mm. The two satellites in eccentric orbits (plane D), however, fit very well with the mean value, although the argument of latitude is not optimal as argument of the harmonic expansion of the SRP accelerations for these satellites. When we compare scenario (4) with (3), a decrease of the orbit errors for small beta angle is recognizable. This behavior coincides with that of the B5 accelerations of Fig. 5. Comparing Fig. 5 and 6, the residuals of the *best possible* orbit fit show the signature of the not estimated parameter.

5 Results

We now discuss the results of this simulation study. We evaluate the influence of a combined Galileo L-band and OTWL (Optical Two-Way Links) scenario for Galileo POD using 16 Galileo Sensor Stations. The results are compared to an L-band-only scenario. Furthermore, we compare the influence of OTWL in contrast to OISL (Optical Inter-Satellite Link) measurements in addition to Galileo L-band. We evaluate the full network with L-band, OTWL and OISL observations as well as a solution without L-band, making only use of both optical observation techniques. For all observation technique combinations, we additionally show the influence of a B3 SRP parameter estimated in addition to the regular ECOM2 parameter set. Therefore, we compare four scenarios with SRP modeling according to Eqs. (1), (2), (3) and (4). We further also call these the scenarios (1), (2), (3) and (4). The following results were computed using the *mismodeled* orbit based on *modeling error 1* (Table 5). Comparisons to the results generated using *mismodeled* orbits according to *modeling error 2* (Table 6) are added to the discussion.

With two or more different observation techniques in combination, the weighting of the different measurements can significantly affect the results. To find the weights which best represent the real-world observation precision is a critical task. Table 7 collects the weighting (variance factor) for the different analysis scenarios. In this simulation study, we weighted L-band, OTWL and OISL in each combination such that the resulting difference of the *true* and *adjusted* orbit is minimized. The result shows that in case of L-band + OTWL and L-band + OISL the L-band phase measurements have to be down-weighted with respect to the more precise OTWL and OISL measurements. In the L-band + OTWL + OISL scenario a different weight leads to negligible differences in the results. Therefore, we weighted L-band, OTWL and OISL equally. For the OTWL + OISL scenario we weighted OISL measurements with respect to the OTWL measurements. In this case, the measurements have to be weighted equally. This is expected since both links have similar systematic errors.

Our analysis encompasses the following four parts:

- In a first analysis we compare the formal orbit uncertainties. These represent the stochastic measurement errors as well as the observation geometry. We took the information from the covariance matrix of the *adjusted* orbit parameters propagated in radial, along- and cross-track directions and averaged along the orbit.
- Second, we analyze the orbit differences between the *true* and *adjusted* obits in contrast to the formal orbit uncertainties. The orbit differences include the effects of the systematic modeling errors on the orbits. The analysis of both formal orbit uncertainties and orbit errors was done

Table 7 Weighting (variance factor) of OTWL and OISL measurements with respect to Galileo L-band measurements ($\frac{\sigma^2_{L-band}}{\sigma^2_{OTWL/OISL}}$) for the different observation technique combinations

Weighting within observation technique combination					
SRP modeling according to	L-band + OTWL	L-band + OISL	L-band + OTWL + OISL		OTWL + OISL
	OTWL	OISL	OTWL	OISL	OISL
Equation (1)	25	5	1	1	1
Equation (2)	100	5	1	1	1
Equation (3)	100	100	1	1	1
Equation (4)	100	100	1	1	1

In case of the OTWL + OISL combination the OISL measurements are weighted with respect to the OTWL measurements

for solutions based on 16 Galileo Sensor Stations, with coordinates of just one ground station fixed.

- In a third analysis step, we gradually reduce the number of ground stations for OTWL observations to simulate possible cloudy weather conditions or a Galileo Sensor Station network which is not fully equipped with optical terminals. In this regard, ground stations tracking Galileo L-band signals are not reduced.
- The fourth analysis step compares the results of solutions with coordinates of just one ground station fixed—for both L-band and OTWL—and with all 16 stations fixed. In doing so, we analyze a first scenario in which no ground station coordinate errors are assumed. In a second scenario, we use wrong coordinates for the simulation of L-band and OTWL observation, with small eccentricity errors between L-band and OTWL. We evaluate the impact of the station coordinate errors on the orbit solutions.

5.1 Formal orbit uncertainty

The formal orbit uncertainty focuses the analysis on the stochastic errors and the geometrical configuration of the measurements. Figure 7 gives the formal orbit uncertainty of all four SRP modeling scenarios for L-band with respect to the beta angle. Shown are the daily mean formal orbit uncertainties per satellite, adjusted by a polynomial of fifth order. No beta angle dependence can be found for the SRP scenarios (1) and (2). However, the scenarios (3) and (4) show a strong increase of the formal orbit uncertainty for beta angles below 15°. Interestingly, for L-band the lowest formal orbit uncertainty of around 27 mm is achievable with SRP scenario (2). This means that this SRP model performs better for our orbit modeling error than the commonly used ECOM2 model with a mean formal orbit uncertainty of around 31 mm. We noticed this behavior already in Schlicht et al. (2020). Estimation of more than nine empirical parameters leads to larger formal orbit errors in an L-band-only solution, compared to the nine

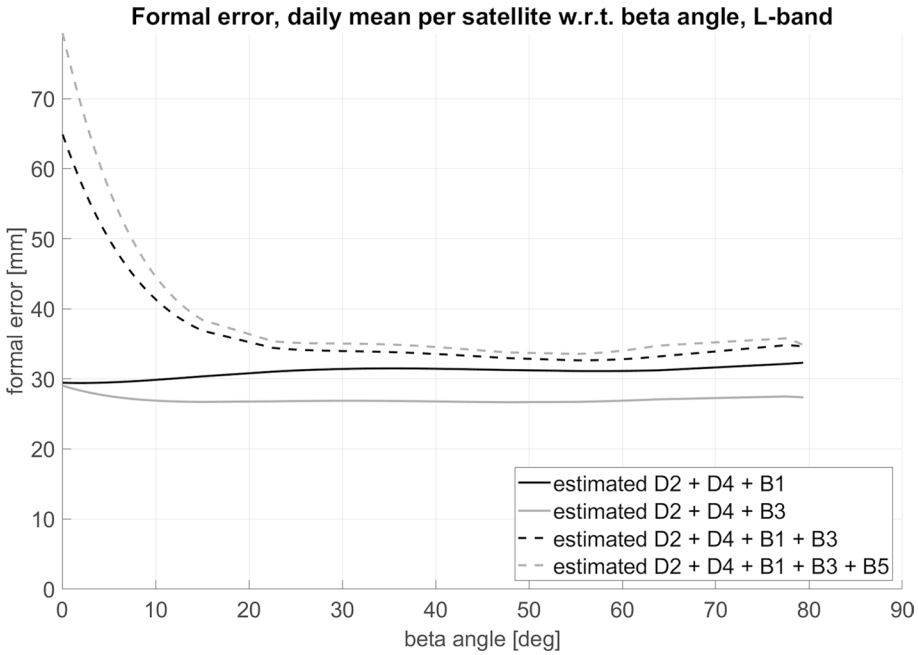

Fig. 7 Formal orbit uncertainties of the L-band solution with respect to the beta angle. The lines represent polynomial adjustments of order five to the daily mean per satellite. The four SRP modeling scenarios according to Eqs. (1), (2), (3) and (4) are compared to each other

Table 8 Formal orbit uncertainty with respect to the SRP modeling scenarios for each simulated observation technique combination in millimeters

SRP modeling according to	L-band-only (mm)	L-band + OTWL (mm)	L-band + OISL (mm)	L-band + OTWL + OISL (mm)	OTWL + OISL (mm)
Equation (1)	31.0	1.2	2.4	1.1	0.3
Equation (2)	26.9	0.8	2.7	1.2	0.3
Equation (3)	36.4	0.8	2.6	1.2	0.4
Equation (4)	38.3	0.9	2.5	1.2	0.4

The formal orbit uncertainty is a 3D mean for all 40 days of the simulation time periods. There is no noticeable beta angle dependence for the formal orbit uncertainties of these observation technique combinations

parameter models. The mean formal orbit uncertainty is at around 36 mm for scenario (3) and 38 mm for scenario (4). Table 8 collects the simulated scenarios for combined observation technique solutions.

The given formal orbit uncertainty is a 3D mean over the four simulation time periods since no significant beta angle dependence was noticeable for these cases. With L-band + OISL formal uncertainties down to 2.4 mm and with L-band + OTWL down to 0.8 mm are achievable. While for L-band + OISL the best result can be achieved with SRP model (1), model (2) is at the lower end. For L-band + OTWL it is opposite. With a formal orbit uncertainty of around 1.1 mm, the L-band + OTWL + OISL scenario achieves slightly worse results compared to L-band + OTWL. The combination of the optical techniques OTWL + OISL reaches 0.3 mm and represents the best scenario. Overall, the formal orbit uncertainty improvement with respect to the best L-band-only solution is at around 91% for L-band + OISL, around 96 % for L-band + OTWL + OISL, around 97 % for L-band + OTWL and around 99 % for OTWL + OISL. Using the *mismodeled* orbit according to *modeling error 2* (Table 6) gives the same results.

5.2 Orbit error

The analysis of the orbit errors, the difference between the *true* and *adjusted* orbits, focuses on the systematic effects in the measurements. In this regard, modeling errors gain importance as well. Figure 8 collects the results for the four SRP models for the L-band-only solution as a function of the beta angle. The results are polynomial adjustments of order five of the daily mean 3D-RMS orbit errors per satellite. The results for the different SRP model solutions resemble the formal orbit uncertainties. Again, with a mean 3D-RMS of around 217 mm, the SRP model (2) gives the best results. In comparison, with ECOM2 a mean orbit error of around 235 mm can be achieved. The main impact of the systematic errors on the POD with L-band is from phase center variations (PCV) errors, which are also intended to cover multipath in our simulations. The error contribution of the PCV is larger than the troposphere delay error, which can be

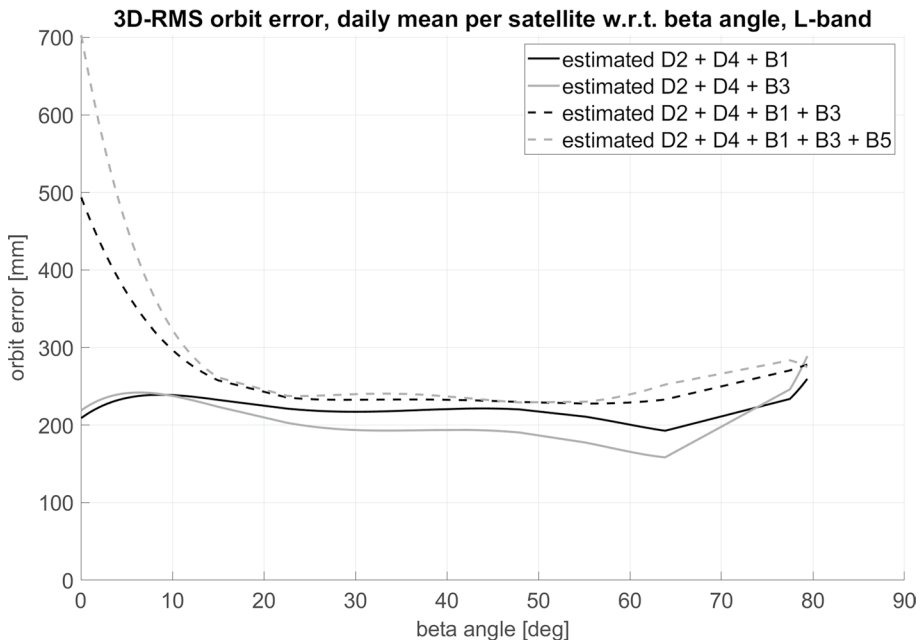

Fig. 8 Orbit errors (3D-RMS) of the L-band solution with respect to the beta angle. The results are polynomial adjustments of order five of the daily mean per satellite. The four SRP modeling scenarios according to Eqs. (1), (2), (3) and (4) are compared to each other

Table 9: 3D-RMS orbit error of the orbit difference *true—adjusted* for each SRP modeling scenarios and each simulated observation technique combination in millimeters

SRP modeling according to	L-band-only (mm)	L-band + OTWL (mm)	L-band + OISL (mm)	L-band + OTWL + OISL (mm)	OTWL + OISL (mm)
Equation (1)	234.8	13.3	25.4	6.2	11.2
Equation (2)	216.8	17.1	35.1	14.3	18.3
Equation (3)	275.1	3.6	21.6	3.4	10.6
Equation (4)	294.9	3.6	21.9	3.4	10.8

The orbit error is a mean of the 3D-RMS for all 40 days of the simulation time periods

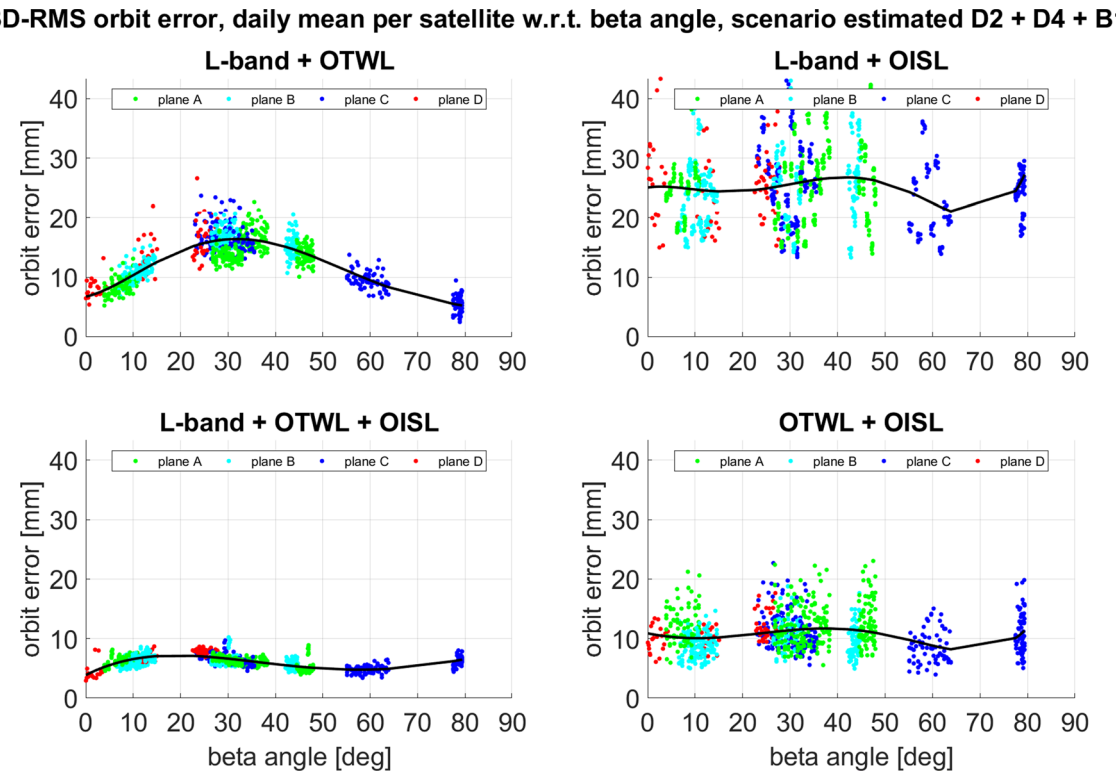

Fig. 9 Orbit errors (3D-RMS) of the solutions related to the different observation technique combinations with respect to the beta angle. The comparison is for SRP modeling according to Eq. (1). The black lines are polynomial adjustments of order five of the daily mean per satellite to guide the eyes

compensated well by estimating station specific piecewise linear tropospheric zenith delays (see Table 4).

Table 9 collects the 3D-RMS orbit errors as a mean of the 40 days of the analysis periods. Figures 9, 10 and 11 give an overview of the 3D-RMS orbit errors as a function of the beta angle for the observation technique combinations. The results regarding SRP modeling according to Eq. (4) are not shown since they are not significantly different from (3).

Figure 9 relates to SRP scenario (1). For the L-band + OTWL scenario a beta angle dependency is recognizable, while the other observation technique combinations do not show a significant beta angle dependence. In analogy to the analysis regarding the *best possible* orbits (see Fig. 6), the shape of the polynomial adjustment is comparable to the B3 acceleration in Fig. 5 suggesting that it is caused by the not estimated B3 parameters in case (1). The orbit errors for the L-band + OTWL scenario are generally lower than for L-band + OISL, while L-band + OTWL + OISL achieves the best results (see Table 9). The noise in the L-band + OTWL + OISL scenario is extremely small compared to the other combinations. However, still small systematic discrepancies are visible for some satellites at certain times in this case. In the other three scenarios such systematic effects disappear in the noise. The OTWL + OISL scenario overall achieves better results than the L-band + OISL scenario. This means that OTWL can fix the satellite constellation to the solid Earth more effectively than L-band, despite the smaller number of observations per epoch.

For the L-band + OTWL solution with the SRP modeling according to Eq. (2), shown in Fig. 10, an identical behavior is noticeable: the shape of the polynomial adjustment is similar to the B1 accelerations in Fig. 5. In case of scenario (2), the other observation technique combinations show beta angle dependences as well. The L-band + OISL scenario has the weakest beta angle dependency. The influence of not estimated B1 parameters on the results is in total much larger than for not estimated B3 parameters. The achievable orbit quality with L-band + OTWL is again generally superior to L-band + OISL (see Table 9). L-band + OTWL + OISL is still the best scenario, but much closer to the results from L-band + OTWL.

From the analysis to this point it can be concluded that the orbit accuracy related to the OTWL is highly beta angle dependent due to the not estimated SRP parameters B1 or B3. However, when both B1 and B3 parameters are estimated (see Fig. 11), the beta angle dependence disappears. In this case, the other scenarios again do not show this either. This SRP scenario is overall the best for all observation technique combinations. Looking at Table 9, with a mean orbit error of around 3.6 mm, the L-band + OTWL scenario is

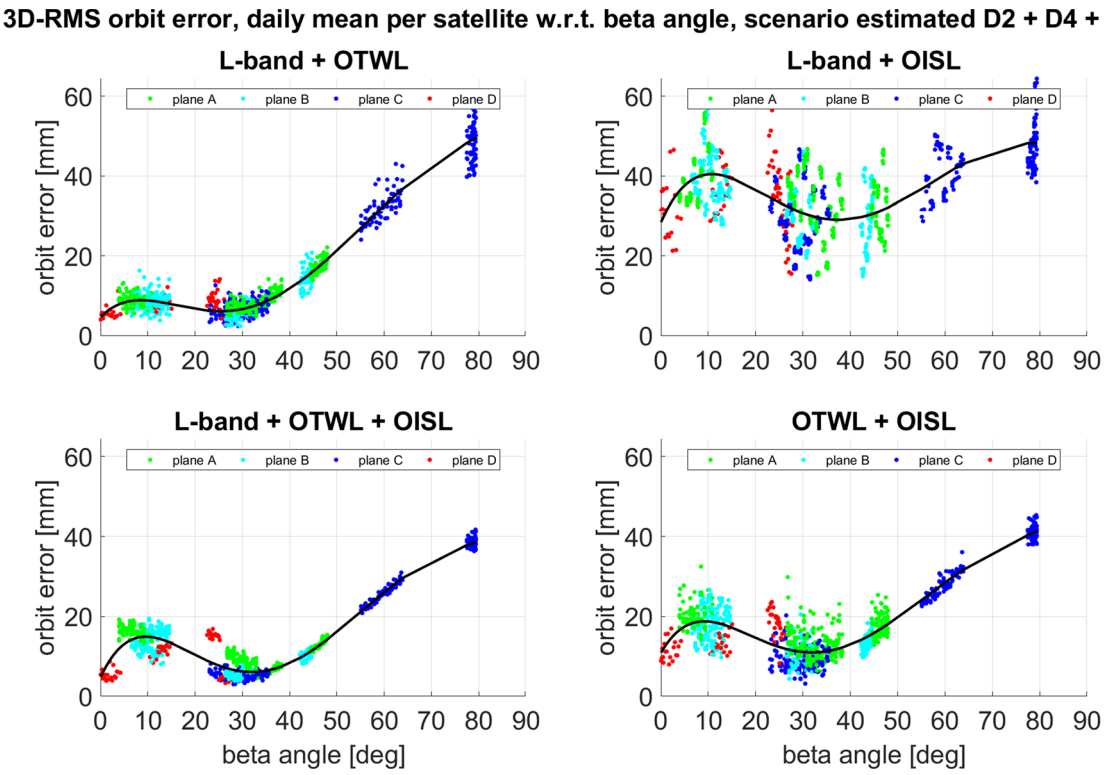

Fig. 10 Orbit errors (3D-RMS) of the solutions related to the different observation technique combinations with respect to the beta angle. The comparison is for SRP modeling according to Eq. (2). The black lines are polynomial adjustments of order five of the daily mean per satellite to guide the eyes

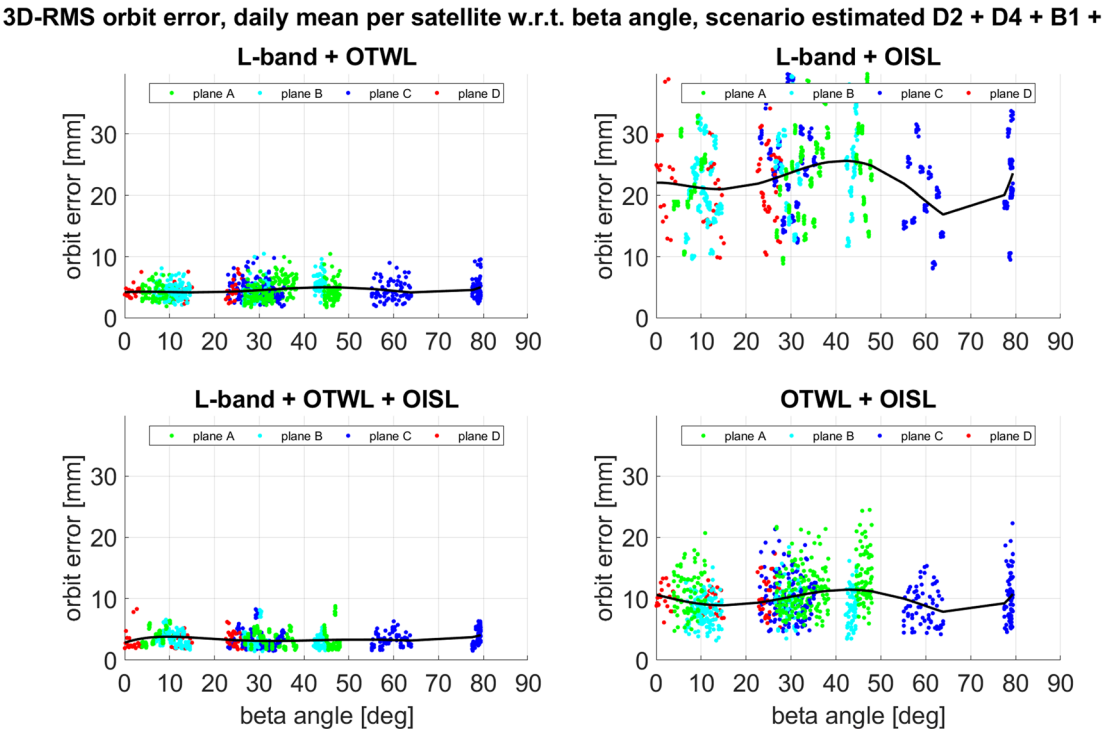

Fig. 11 Orbit errors (3D-RMS) of the solutions related to the different observation technique combinations with respect to the beta angle. The comparison is for SRP modeling according to Eq. (3). The black lines are polynomial adjustments of order five of the daily mean per satellite to guide the eyes

Table 10: 3D-RMS orbit error of the orbit difference *true—adjusted* with respect to the SRP modeling scenarios for each simulated observation technique combination in millimeters

SRP modeling according to	L-band-only (mm)	L-band + OTWL (mm)	L-band + OISL (mm)	L-band + OTWL + OISL (mm)	OTWL + OISL (mm)
Equation (1)	235.4	3.7	23.0	3.2	10.3
Equation (2)	218.1	4.9	23.5	4.7	10.5
Equation (3)	275.1	3.3	22.0	3.2	10.6
Equation (4)	294.9	3.5	22.0	3.2	10.8

The table shows the results computed with the *mismodeled* orbit according to *modeling error 2* (Table 6). The orbit error is a mean of the 3D-RMS for all 40 days of the simulation time periods

Table 11 Selected OTWL ground stations for reduced station scenarios (compare to Fig. 1)

	Selected OTWL ground stations
7	GASC, GKIR, GKER, GNOU, GPAP, GSTP, GTRO
5	GASC, GKIR, GNOU, GPAP, GTRO
4	GASC, GKIR, GNOU, GTRO
3	GASC, GKIR, GNOU
2	GASC, GNOU | GASC, GKIR
1	GASC

In case 2 for two stations, we compared a North–South (GASC, GKIR) and an East–West (GASC, GNOU) configuration. The E-W configuration is slightly superior and was, hence, used in the analysis

similar to the L-band + OTWL + OISL scenario (3.4 mm). In this regard, the influence of additional OISL observations would be negligibly small. The orbit error improvement with L-band + OTWL is around 83 % with regard to L-band + OISL and around 98 % with regard to the best L-band-only solution (SRP scenario (2)). The advantage of the ground-space link, in contrast to a satellite-to-satellite link, comes from the possibility to synchronize the ground station clock as well. With OISL, only the satellite clocks are synchronized. Furthermore, the high-precision ground-space oriented OTWL helps with the orbit adjustment in a system with a one-station-fixed geodetic datum (coordinates and clock of just one ground station fixed). As already mentioned, the purely optical scenario OTWL + OISL generally achieves better results than L-band + OISL. However, the good results from the formal orbit uncertainty do not transfer to the orbit error solution. This means that the systematic effects and clock errors cannot be mitigated completely in the OTWL + OISL scenario. The L-band measurements are supportive in this case (see L-band + OTWL + OISL scenario). When we compare these results with the results using the *mismodeled* orbits according to *modeling error 2* (Table 6), the general behavior is the same. These results are summarized in Table 10. The scenario estimating B1 and B3 (SRP scenario (3)) does not negatively affect the results, compared to an estimation with ECOM2 (SRP scenario (1)). Rather, the combinations L-band + OTWL and L-band + OISL show a slight improvement of the 3D-RMS orbit error. This means that all parameters of the SRP scenario (3) with both parameters B1 and B3 could be estimated in an analysis based on these observation technique

Fig. 12 Relative orbit error improvement with respect to the L-band-only scenario in percent. The *x*-axis displays the number of used OTWL ground stations for each scenario (compare with Table 11). Stations for L-band measurements are unchanged and use the full 16 Galileo Sensor Station network. The results are related to the SRP modeling according to Eq. (1)

combinations—independent of the SRP accelerations acting on the satellites.

5.3 Reduced station scenarios for OTWL observations

The reduction in the number of ground stations with OTWL observations simulates possible cloudy weather conditions or a Galileo Sensor Station network which is not fully equipped with optical terminals. However, this analysis also identifies the number of ground stations required to achieve a certain level of orbit improvement with respect to the L-band-only scenario. The number of OTWL ground stations is gradually reduced. Table 11 shows the selected stations for the different scenarios. Figure 12 collects the relative improvement of the orbit error with respect to the L-band-only solution. The shown orbit error improvements are related to the SRP modeling according to Eq. (1), but the behavior is similar for the other SRP modeling scenarios as well. The number of ground stations used for L-band measurements is not reduced in all cases. This means that the result for the L-band + OISL scenario stays unchanged and is just shown for comparison. The L-band + OISL scenario gives a maximum orbit error improvement of around 89% with respect to the L-band-only scenario.

Reducing the number of stations in an L-band + OTWL scenario, the orbit error improvement decreases continuously. However, the L-band + OTWL orbit error improvement is superior to the L-band + OISL scenario using more than five OTWL stations. Using three OTWL stations, an orbit error improvement of around 74% is possible and still around 31% with one station, with respect to L-band-only.

It is highly remarkable that the results for the L-band + OTWL + OISL scenario do not significantly change when reducing OTWL observation stations. The orbit error improvement remains constant at around 97.5 % with respect to L-band-only. This means that additional OTWL observations from only a single ground station already give a further orbit error improvement of around 8.5 % with respect to the L-band + OISL scenario. It is very important to note that this one ground station has fixed coordinates and clocks. Signal biases and modeling errors are simulated for the OTWL observations with regard to this fixed station.

In a scenario without L-band, just using OTWL + OISL observations, the orbit error improvement varies slightly with a reduction of the number of ground stations. This is a reminder that the simulation is built on different types of random errors.

5.4 Fixing the ground station coordinates

In a further analysis we compare the results with fixing the coordinates of just one station (GASC) in the estimation, as for the results presented above, and the scenario with fixing the coordinates of all 16 Galileo Sensor Stations for L-band and OTWL. The clocks of the stations, except for one station (GASC), were estimated in any case. Such a scenario also represents a real-world application since the coordinates of grounds stations are generally assumed as well known.

Table 12 shows the results for the scenario with fixed station coordinates for the whole Galileo Sensor Station network of 16 stations. We used no ground station coordinate errors in this scenario. Comparing Table 12 with Table 9, the orbit errors from the L-band-only (1), (3) and (4) scenarios are worse compared to the results of the one-station-fixed scenarios due to station-related modeling errors. As we do not estimate a bias for L-band, all systematic errors are shifted to the station coordinates, clocks or the orbits. When all stations are fixed, we remove some of the freedoms for the least-squares adjustment. Again scenario (2) is the best and, interestingly, is the only scenario which improves compared to the one-station-fixed scenario (see Table 9). A large improvement can be achieved for L-band + OISL for all SRP modeling scenarios. Especially the scenarios with more than 9 SRP parameters estimated ((3) and (4)) profit from the fixing. This improvement for OISL is due to the strong tie of the constellation to the solid Earth in an all-stations-fixed reference frame. With just one fixed station, the satellite constellation has more degrees of freedom in the adjustment to the OISL observations. The fixing of all coordinates, however, ties the orbits to the solid Earth at multiple sites. The

Table 12: 3D-RMS orbit error of the orbit difference *true*—*adjusted* with respect to the SRP modeling scenarios for each simulated observation technique combination in millimeters

SRP modeling according to	L-band-only (mm)	L-band + OTWL (mm)	L-band + OISL (mm)	L-band + OTWL + OISL (mm)	OTWL + OISL (mm)
Equation (1)	260.4	12.8	10.8	5.8	10.4
Equation (2)	203.3	16.8	21.1	13.2	16.2
Equation (3)	311.9	4.3	5.8	3.0	9.6
Equation (4)	329.5	4.5	5.9	2.9	9.8

The table shows the 3D-RMS orbit error without estimating ground station coordinates. The *true* station coordinates were used for the observation simulation and for parameter estimation. The orbit error is a mean of the 3D-RMS for all 40 days of the simulation time periods

Table 13: 3D-RMS orbit error of the orbit difference *true—adjusted* with respect to the SRP modeling scenarios for each simulated observation technique combination in millimeters

SRP modeling according to	L-band-only (mm)	L-band + OTWL (mm)	L-band + OISL (mm)	L-band + OTWL + OISL (mm)	OTWL + OISL (mm)
Equation (1)	260.9	13.1	10.7	5.7	10.4
Equation (2)	203.8	17.0	21.0	13.2	16.2
Equation (3)	312.3	5.1	5.7	2.8	9.7
Equation (4)	329.7	5.4	5.8	2.8	9.9

The table shows the 3D-RMS orbit error without estimating ground station coordinates. Slightly different station coordinates were used for the observation simulation and parameter estimation. The orbit error is a mean of the 3D-RMS for all 40 days of the simulation time periods

L-band + OTWL scenario shows slightly worse results with a fixed station network, comparing the best SRP scenario (3) in Tables 9 and 12. Nevertheless, the 3D-RMS orbit error is still smaller than for the L-band + OISL scenario. Both the L-band + OTWL + OISL and the OTWL + OISL scenarios profit from the all-stations-fixed geodetic datum. In case of the scenarios (3) and (4), L-band + OISL is superior to OTWL + OISL in this all-stations-fixed scenario.

To get the results shown in Table 13 we again fixed all station coordinates in the estimation process, but in this scenario we included station coordinate errors for the measurements simulation, based the coordinate accuracies provided by the ITRF. The 3D station coordinate errors for L-band are 1.1 mm on average. For OTWL observations we assumed small eccentricity errors to L-band up to about 0.5 mm per station in 3D. The resulting 3D station coordinate errors for OTWL are 1.2 mm on average. The analysis shows the impact of errors in the station coordinates on the orbit solutions. In the L-band-only scenario, the wrong station coordinates affect the orbit solution by up to 0.5 mm. Analyzing L-band + OTWL, the scenarios with a SRP modeling error according to Eqs. (1) and (2) are only affected by 0.3 mm, while scenarios with an estimation of more than 9 SRP parameters (scenario (3) and (4)) are affected by up to 0.9 mm. This is almost the full 3D station coordinate error. In contrast, scenarios including OISL measurements are not influenced by using wrong station coordinates instead of the true coordinates in the simulation. The satellites themselves are tied to each other by the OISL observations as well as tied to the solid Earth at multiple sites by fixing the station coordinates. For these reasons, small station coordinate errors average out for scenarios with OISL, similar to the comparatively large systematic errors of L-band.

6 Conclusions and outlook

In this simulation study we have analyzed the impact of ground-space optical two-way links for Galileo precise orbit determination. The optical two-way link (OTWL) observations are in addition to L-band measurements. The L-band and OTWL observations were simulated with regard to 16 Galileo Sensor Stations. We compared the L-band + OTWL solution to a solution with optical inter-satellite links (OISL) (L-band + OISL). We further analyzed the observation technique combinations L-band + OTWL + OISL and the optical-only OTWL + OISL scenario. We performed an analysis regarding the estimation of additional solar radiation parameters in these scenarios. Many systematic effects were taken into account: link biases and their variability, distance-dependent effects, colored noise and a troposphere error for OTWL measurements. We simulated inter-technique clock biases while estimating only one bias for each clock.

We can conclude that the Galileo processing can highly benefit from the use of additional OTWL measurements. The improvements in the orbit solution using L-band + OTWL observations can be attributed to the two main advantages of OTWL compared to L-band measurements. First the higher ranging accuracy and precision. This helps for a better compensation of systematic errors. Second, the two-way link gives the possibility to synchronize the station and satellite clock. We did not study the influence of the clock synchronization on the orbit determination in this paper, but analyzed it in Schlicht et al. (2019). The impact of the clock synchronization is small compared to the impact of the range measurements.

From the results of this work, the following conclusions can be drawn for OTWL:

- The high-precision ground-space oriented links help with the orbit adjustment of a system with a one-station-fixed geodetic datum. This is due to the tie of the satellite constellation to the terrestrial reference frame through the high-precision ground-space links and the additional synchronization of the ground clocks.
- OTWL is dependent on the number of available ground stations. In case that less than seven ground stations are available for OTWL observations, while the other stations are restricted, for instance due to cloudy weather conditions, the L-band + OISL solution achieves smaller three-dimensional (3D)—root mean square (RMS) orbit error results than L-band + OTWL.

- A L-band + OTWL scenario cannot profit from the ground station coordinate fixing (all-stations-fixed geodetic datum) anymore as the L-band systematic errors are already compensated to a great extent by OTWL.
- Applying in addition station coordinate errors, only scenarios using L-band + OTWL and with estimation of more than nine solar radiation pressure (SRP) parameters have a significant relative increase of the orbit error. The impact on the 3D-RMS orbit error is about 0.9 mm, starting from an a priori 3D station coordinate error of about 1.2 mm on average.

For OISL, the following conclusions can be drawn:

- In a system with a one-station-fixed geodetic datum, the resulting orbit error from L-band + OISL is six times worse compared to the solution from L-band + OTWL. The reason is that OISL measurements can only constrain the internal geometry of the satellite constellation, while L-band does not provide a strong tying to the solid Earth due to the large systematic errors and the one-way nature of the technique.
- In a system with an all-stations-fixed geodetic datum, a huge improvement for L-band + OISL can be achieved. This is due to the tying of the satellite constellation to the solid Earth. The orbit error resulting from L-band + OISL is almost at the same level as for L-band + OTWL.
- Applying in addition station coordinate errors, scenarios including OISL measurements achieved the same results as for the scenario without coordinate errors.

The addition of OISL observations to L-band + OTWL improves the measurement geometry and fixes the internal geometry of the satellite constellation. Generally, this is the best solution, especially in case of less than 16 stations available for OTWL measurements. An optical-only scenario—OTWL + OISL—achieved worse 3D-RMS orbit errors compared to the results from scenarios including L-band and OTWL. This means, L-band is supportive for the OTWL bias estimation.

For the SRP analysis we can conclude that a combination of two or more observation techniques allows the estimation of more than nine orbit modeling parameters. Schlicht et al. (2020) already showed this for an inter-satellite link scenario, we can confirm this for an L-band + OTWL as well as the L-band + OTWL + OISL scenario. For the latter it would have been even possible to estimate 13 empirical parameters—Empirical CODE Orbit Model 2 (ECOM2; Arnold et al. 2015) + B3 + B5. However, there is no further benefit with estimating B5 parameters. Nevertheless, the possibility to estimate more SRP parameters allows a more precise orbit modeling. The overall best results could be achieved for an ECOM2 + B3 parameter model.

With the possibility to get better modeled orbits, the geodetic parameters will not contain signals with a draconitic period. This would be a huge step forward to reach the goals of GGOS (Global Geodetic Observing System; Plag and Pearlman 2009) of a precise terrestrial reference frame with 1 mm accuracy and a stability of 0.1 mm/year as well as improving the precision of the societal and scientific applications of GNSS (Global Navigation Satellite System) (Plag and Pearlman 2009; Johnston et al. 2017).

Furthermore, the combination of different observation techniques is one of the next important steps in improving satellite orbits as well as space geodesy. Especially the combination of OTWL and OISL is of great interest for future application. As previously mentioned, a general advantage of the OTWL concept, in contrast to OISL, is the tight tie to the terrestrial reference frame. Not only the satellite orbits but also both the satellite and ground station clock can be synchronized. From a future aspect, compared to OISL we would expect an improved estimation of Earth Rotation Parameters (ERPs) as well as the possibility to optimize the ITRF (International Terrestrial Reference Frame) with the OTWL measurements due to the tight connection of precise GNSS orbits to the terrestrial frame. Hence, the influence of L-band + OTWL on the ERPs as well as the ITRF is a very interesting question.

We paid considerable attention to the simulation of systematic effects, but of course there are still systematic errors in the orbit determination which were not taken into account in this paper. These errors will be studied in future work, but on the other hand, there is still more potential using a high-precision optical two-way link we did not take into account in our simulations. This is, for example, the calibration of the L-band, which was already shown for T2L2 (Time Transfer by Laser Link; Samain et al. 2014) and GNSS (Leute et al. 2018). The calibration provides great support for the ambiguity resolution with integer ambiguities. Thus, a calibrated L-band can provide support when the optical link cannot operate due to cloudy weather conditions. Furthermore, with the possibility to estimate more parameters in general, a potential for the estimation of other non-gravitational forces, like thruster leakage or radiator properties, can be expected.

The weighting of the different measurement types concerning the L-band measurements in observation technique combinations is a challenging task and may need some more experience: which weights optimally represent the real-world precisions? We weighted the measurement according to the best achievable orbit accuracies as a start. This gives an indication for the potential of the measurement combinations.

In the end it is worth to mention that the synergy to use the same link as a data transfer link is an option that should not be ignored. Such a link can work as a backup or even an alternative to microwave data downlinks. This provides

increased security, too, as an optical connection cannot be eavesdropped.

Acknowledgements The German Research Foundation (DFG) is gratefully acknowledged for funding the Project AOBJ:638291.

Author contributions SM and AS designed the study. SM performed the data processing, compiled the figures and wrote the paper with the assistance from AS and UH. All authors reviewed the paper.

Funding Open Access funding enabled and organized by Projekt DEAL.

Data availability All models and assumptions used for the simulation of all observations used in this study are provided in the paper.

References

Abich K, Abramovici A, Amparan B, Baatzsch A, Okihiro BB et al (2019) In-orbit performance of the GRACE follow-on laser ranging interferometer. Phys Rev Lett 123(3):031101. https://doi.org/10.1103/PhysRevLett.123.031101

Arnold D, Meindl M, Beutler G, Dach R, Schaer S, Lutz S, Prange L, Sosnica K, Mervart L, Jäggi A (2015) CODE's new solar radiation pressure model for GNSS orbit determination. J Geod 89:775–791. https://doi.org/10.1007/s00190-015-0814-4

Boehm J, Werl B, Schuh H (2006a) Troposphere mapping functions for GPS and very long baseline interferometry from European Centre for Medium-Range Weather Forecasts operational analysis data. J Geophys Res 111:B02406. https://doi.org/10.1029/2005JB003629

Boehm J, Niell A, Tregoning P, Schuh H (2006b) Global mapping function (GMF): a new empirical mapping function based on numerical weather model data. Geophys Res Lett 33:L07304. https://doi.org/10.1029/2005GL025546

Boehm J, Heinkelmann R, Schuh H (2007) Short note: a global model of pressure and temperature for geodetic applications. J Geod 81(10):679–683. https://doi.org/10.1007/s00190-007-0135-3

Bury G, Zajdel R, Sośnica K (2019) Accounting for perturbing forces acting on Galileo using a box-wing model. GPS Solut 23:74. https://doi.org/10.1007/s10291-019-0860-0

Bury G, Sośnica K, Zajdel R, Strugarek D, Hugentobler U (2021) Determination of precise Galileo orbits using combined GNSS and SLR observations. GPS Solut 25:11. https://doi.org/10.1007/s10291-020-01045-3

Cacciapuoti L, Salomon Ch (2009) Space clocks and fundamental tests: The ACES experiment. Eur Phys J Spec Top 172(1):57–68. https://doi.org/10.1140/epjst/e2009-01041-7

Cacciapuoti L, Armano M, Much R, Sy O, Helm A, Hess MP, Kehrer J, Koller S, Niedermaier T, Esnault FX, Massonnet D, Goujon D, Pittet J, Rochat P, Liu S, Schaefer W, Schwall T, Prochazka I, Schlicht A, Schreiber U, Delva P, Guerlin C, Laurent P, Le Poncin-Lafitte C, Lilley M, Savalle E, Wolf P, Meynadier F, Salomon C (2020) Testing gravity with cold-atom clocks in space. Eur Phys J D 74:164. https://doi.org/10.1140/epjd/e2020-10167-7

Calzolaio D, Curreli F, Duncan J, Moorhouse A, Perez G, Voegt S (2020) EDRS-C—The second node of the European Data Relay System is in orbit. Acta Astronaut 177:537–544. https://doi.org/10.1016/j.actaastro.2020.07.043

Dach R, Lutz S, Walser P, Fridez P (2015) Bernese GNSS Software Version 5.2. User manual, Astronomical Institute, University of Bern, Bern Open Publishing. ISBN: 978-3-906813-05-9. https://doi.org/10.7892/boris.72297

Delva P, Meynadier F, Wolf P, Le Poncin-Lafitte C, Lauraent P (2012) Time and frequency transfer with a microwave link in the ACES/PHARAO mission. 2012 European Frequency and Time Forum, pp 28–35. https://doi.org/10.1109/EFTF.2012.6502327

Duan B, Hugentobler U, Selmke I (2019) The adjusted optical properties for Galileo/BeiDou-2/QZS-1 satellites and initial results on BeiDou-3e and QZS-2 satellites. Adv Space Res 63(5):1803–1812. https://doi.org/10.1016/j.asr.2018.11.007

Exertier P, Belli A, Samain E, Meng W, Zhang H, Tang K, Schlicht A, Schreiber U, Hugentobler U, Prochazka I, Sun X, McGarry JF, Mao D, Neumann A (2019) Time and laser ranging: a window of opportunity for geodesy, navigation, and metrology. J Geod 93:2389–2404. https://doi.org/10.1007/s00190-018-1173-8

Falcone M, Hahn J, Burger T (2017) Galileo. In: Teunissen PJ, Montenbruck O (eds) Springer handbook of global navigation satellite systems. Springer Handbooks. Springer, Cham. ISBN: 978-3-319-42926-7. https://doi.org/10.1007/978-3-319-42928-1_9

Fernández FA (2011) Inter-satellite ranging and inter-satellite communication links for enhancing GNSS satellite broadcast navigation data. Adv Space Res 47:786–801. https://doi.org/10.1016/j.asr.2010.10.002

Fernández A, Sánchez M, Beck T, Amarillo F (2010) Future satellite navigation system architecture: inter-satellite ranging and orbit determination. In: Proceedings of the 2010 international technical meeting of the institute of navigation, San Diego, CA, pp 872–879

Fliegel HF, Gallini TE, Swift ER (1992) Global positioning system radiation force model for geodetic applications. J Geophys Res 97(B1):559–568. https://doi.org/10.1029/91JB02564

Gill E (1999) Precise GNSS-2 satellite orbit determination based on inter-satellite-links. In: 14th international symposium on space flight mechanics, Iguassu, Brazil

Giorgi G, Schmidt TD, Trainotti C, Mata-Calvo R, Fuchs C, Hoque MM, Berdermann J, Furthner J, Günther C, Schuldt T, Sanjuan J, Gohlke M, Oswald M, Braxmaier C, Balidakis K, Dick G, Flechtner F, Ge M, Glaser S, König R, Michalak G, Murböck M, Semmling M, Schuh H (2019) Advanced technologies for satellite navigation and geodesy. Adv Space Res 64:1256–1273. https://doi.org/10.1016/j.asr.2019.06.010

Hemmati H (2020) Near-Earth laser communications. In: Hemmati H (ed) Near-Earth laser communications, 2nd ed. CRC Press, Boca Raton. ISBN: 978-1-498-77740-7

Hess MP, Stringhetti L, Hummelsberger B, Hausner K, Stalford R, Nasca R, Cacciapuoti L, Much R, Feltham S, Vudali T, Leger B, Picard F, Massonnet D, Rochat P, Goujon D, Schäfer W, Laurent P, Lemonde P, Clairon A, Wolf P, Salomon C, Procházka I, Schreiber U, Montenbruck O (2011) The ACES mission: System development and test status. Acta Astronaut 69:929–938. https://doi.org/10.1016/j.actaastro.2011.07.002

Holmes JK (1990) Coherent spread-spectrum systems. Krieger Publishing Co., FL. ISBN: 978-0-89464-468-9

Johnston G, Riddell A, Hausler G (2017) The international GNSS service. In: Teunissen PJ, Montenbruck O (eds) Springer handbook of global navigation satellite systems. Springer Handbooks. Springer, Cham. ISBN: 978-3-319–42926-7. https://doi.org/10.1007/978-3-319-42928-1_33

Koepf GA, Marshalek RG, Begley DL (2002) Space laser communications: a review of major programs in the United States. Int J Electron Commun 56(4):232–242. https://doi.org/10.1078/1434-8411-54100103

Leute J, Petit G, Exertier P, Samain E, Rovera D, Uhrich P (2018) High accuracy continuous time transfer with GPS IPPP and T2L2. 2018 European Frequency and Time Forum, pp 249–252. https://doi.org/10.1109/EFTF.2018.8409043.

Li Z, Ziebart M (2020) Uncertainty analysis on direct solar radiation pressure modelling for GPS IIR and Galileo FOC satellites. Adv Space Res. https://doi.org/10.1016/j.asr.2020.04.050

Luceri V, Pirri M, Rodríguez J, Appleby G, Pavlis EC, Müller H (2019) Systematic errors in SLR data and their impact on the ILRS products. J Geod 93:2357–2366. https://doi.org/10.1007/s00190-019-01319-w

Marini JW, Murray CW (1973) Correction of laser range tracking data for atmospheric refraction at elevations above 10 degrees. NASA GSFC X-591-73-351.

McNamara P, Vitale S, Danzmann K (on behalf of the LISA Pathfinder Science Working Team 2008) (2008) LISA pathfinder. Class Quant Grav 25(11). https://doi.org/10.1088/0264-9381/25/11/114034.

Mendes VB, Pavlis EC (2004) High-accuracy zenith delay prediction at optical wavelengths. Geophys Res Lett 31:L14602. https://doi.org/10.1029/2004GL020308

Meng W, Zhang H, Huang P, Wang J, Zhang Z, Liao Y, Ye Y, Hu W, Wang Y, Chen W, Yang F, Prochazka I (2013) Design and experiment of onboard laser time transfer in Chinese Beidou navigation satellites. Adv Space Res 51:951–958. https://doi.org/10.1016/j.asr.2012.08.007

Michalak G, Glaser S, Neumayer KH, Koenig R (2021) Precise orbit and Earth parameter determination supported by LEO satellites, inter-satellite links and synchronized clocks of a future GNSS. Adv Space Res. J Pre-proof, Available online 18 March 2021 (**in Press**). https://doi.org/10.1016/j.asr.2021.03.008.

Montenbruck O, Gill E (2005) Satellite orbits—models, methods, applications. Springer, Berlin, ISBN: 3-540-67280-X.

Plag H-P, Pearlman M (2009) Global geodetic observing system: meeting the requirements of a global society on a changing planet in 2020. Springer, Berlin. https://doi.org/10.1007/978-3-642-02687-4. ISBN: 978-3-642-02686-7.

Prange L, Villiger A, Siderov D, Schaer S, Beutler G, Dach R, Jäggi A (2020) Overview of CODE's MGEX solution with the focus on Galileo. Adv Space Res 66(12):2786–2798. https://doi.org/10.1016/j.asr.2020.04.038

Pribil K, Hemmati H (2020) Laser transmitters: coherent and direct detection. In: Hemmati H (ed) Near-Earth laser communications, 2nd ed. CRC Press, Boca Raton. ISBN: 978-1-498-77740-7

Prochazka I, Schreiber U, Schäfer W (2011) Laser time transfer and its application in the Galileo programme. Adv Space Res 47(2):239–246. https://doi.org/10.1016/j.asr.2010.02.008

Riley W (2008) Handbook of frequency stability analysis. NIST Special Publications, Boca Raton, p 1065

Samain E, Vrancken P, Guillemot P, Fridelance P, Exertier P (2014) Time transfer by laser link (T2L2): characterization and calibration of the flight instrument. Metrologia 51:503–515. https://doi.org/10.1088/0026-1394/51/5/503

Schlicht A, Hugentobler U, Marz S, Seel S, Biller P (2019) Concept for continuous wave laser ranging and time transfer to Galileo using optical two-way links. In: Proceedings of the 7th international colloquium on scientific and fundamental aspects of GNSS, Zurich

Schlicht A, Marz S, Stetter M, Hugentobler U, Schäfer W (2020) Galileo POD using optical inter-satellite links: a simulation study. Adv Space Res 66(7):1558–1570. https://doi.org/10.1016/j.asr.2020.06.028

Schreiber KU, Kodet, j. (2018) The application of coherent local time for optical time transfer and the quantification of systematic errors in satellite laser ranging. Space Sci Rev 214:22. https://doi.org/10.1007/s11214-017-0457-2

Schreiber KU, Prochazka I, Lauber P, Hugentobler U, Schäfer W, Cacciapuoti L, Nasca R (2010) Ground-based demonstration of the European Laser Timing (ELT) experiment. IEEE Trans Ultrason Ferroelectr Freq Control 57(3):728–737. https://doi.org/10.1109/TUFFC.2010.1471

Shargorodsky VD, Pasynkov VV, Sadovnikov MA, Chubykin AA (2013) Laser glonass: era of extended precision. Glonass Herald J Navig 14:22–26

Sośnica K, Thaller D, Dach R, Steigenberger P, Beutler G, Arnold D, Jäggi A (2015) (2015) Satellite laser ranging to GPS and GLONASS. J Geod 89:725–743. https://doi.org/10.1007/s00190-015-0810-8

Springer TA, Beutler G, Rothacher M (1999) A new solar radiation pressure model for GPS. Adv Space Res 23(4):673–676. https://doi.org/10.1016/S0273-1177(99)00158-1

Thaller D, Dach R, Seitz M, Beutler G, Marayen M, Richter B (2011) Combination of GNSS and SLR observations using satellite co-locations. J Geod 85:257–272. https://doi.org/10.1007/s00190-010-0433-z

Urschl C, Beutler G, Gurtner W, Hugentobler U, Schaer S (2007) Contribution of SLR tracking data to GNSS orbit determination. Adv Space Res 39(10):1515–1523. https://doi.org/10.1016/j.asr.2007.01.038

Weyrauch T, Vorontsov MA (2004) Free-space laser communications with adaptive optics: atmospheric compensation experiments. In: Majumdar AK, Ricklin JC (eds) Free-space laser communications. Optical and fiber communications reports, vol 2. Springer, New York. ISBN: 978-0-387-28652-5. https://doi.org/10.1007/978-0-387-28677-8_5

Zajdel R, Sośnica K, Drożdżewski M, Bury G, Strugarek D (2019) Impact of network constraining on the terrestrial reference frame realization based on SLR observations to LAGEOS. J Geod 93:2293–2313. https://doi.org/10.1007/s00190-019-01307-0

Zech H, Heine F, Tröndle D, Seel S, Motzigemba M, Meyer R, Philipp-May S (2015) LCT for EDRS: LEO to GEO optical communications at 1,8 Gbps between Alphasat and Sentinel 1a. In: Proceedings of SPIE 9647, unmanned/unattended sensors and sensor networks XI; and advanced free-space optical communication techniques and applications, 96470J (29 October 2015). https://doi.org/10.1117/12.2196273.

Zhang H, Cheng Z, Long M, Deng H, Meng W, Wu Z, Zhao G, Zhang Z (2019) Applications of satellite laser ranging and laser time transfer in BeiDou navigation satellite system. Optik 188:251–262. https://doi.org/10.1016/j.ijleo.2019.04.131

Zhang R, Tu R, Zhang P, Fan L, Han J, Lu X (2021) Orbit determination of BDS-3 satellite based on regional ground tracking station and inter-satellite link observations. Adv Space Res Corrected Proof Available online 1 March 2021 (**in Press**). https://doi.org/10.1016/j.asr.2021.02.027.

Available online at www.sciencedirect.com

ScienceDirect

Advances in Space Research 71 (2023) 624–644

ADVANCES IN SPACE RESEARCH (a COSPAR publication)

www.elsevier.com/locate/asr

Geosynchronous satellites expanding a future GNSS satellite constellation: A precise orbit determination study

Stefan Marz *, Anja Schlicht, Urs Hugentobler

Forschungseinrichtung Satellitengeodäsie, Technical University of Munich, Munich, Germany

Received 14 April 2022; received in revised form 4 November 2022; accepted 5 November 2022
Available online 12 November 2022

Abstract

The integration of geosynchronous orbit (GSO) satellites in Global Navigation Satellite Systems (GNSS) is mostly discussed to enable a regional enhancement for tracking. But how do GSO satellites affect the orbit determination of the rest of the constellation? How accurately can these orbits be determined in a future GNSS tracking scenario with optical links? In this simulation study we analyze the benefit of GSO satellites as an expansion of a MEO (Medium Earth Orbit) satellite constellation – we selected the Galileo satellite constellation – for MEO Precise Orbit Determination (POD). We address not only the impact on POD of MEO satellites but also the possibility to precisely determine the GSO satellites – geostationary orbits (GEO) and inclined geosynchronous orbits (IGSO) – in such an expanded MEO constellation. In addition to GNSS microwave observations, we analyze the influence of different optical links between the participating entities: Optical two-way Inter-Satellite Links (OISL) and ground-space oriented Optical Two-Way Links (OTWL). These optical measurements together with the GNSS microwave observations give a remarkable benefit for the POD capability. In the case of GNSS and OTWL, we simulate the measurements with regard to a network of 16 ground stations. We pay great attention to the simulation of systematic effects of all measurement techniques. We discuss the influence on the systematic errors as well as the formal orbit uncertainties. A MEO constellation expanded with GSO satellites as well as the use of optical links together with GNSS observations not only improves the MEO satellite orbits but also the GSOs to a great extent.

Keywords: GEO; IGSO; MEO; POD; Optical two-way link; Inter-satellite link

1. Introduction

Today, geosynchronous orbit (GSO) satellites within GNSS (Global Navigation Satellite System) constellations are mainly used to provide a regional enhancement within the tracking system as well as to increase the accuracy and reliability of user positioning. The BeiDou satellite navigation system has embedded geostationary orbit (GEO) and inclined geosynchronous orbit (IGSO) satellites in its GNSS constellation. Regional navigation satellite systems like QZSS and IRNSS are built entirely on GSO satellites. Satellite Based Augmentation Systems (SBAS; Walter, 2017), such as the European Geostationary Navigation Overlay Service (EGNOS; Ventura-Traveset et al., 2015) or the US-American Wide Area Augmentation System (WAAS; Walter et al., 2018), were built to support GNSS systems with additional regional services and information provided by GSO satellites. Furthermore, GSO satellites are used for data transfer and communication to near Earth satellites or ground stations. For instance, the European Data Relay System (EDRS) uses GSO satellites for data communication with laser in its 'SpaceDataHighway' (ESA, 2013).

* Corresponding author.
E-mail addresses: s.marz@tum.de (S. Marz), anja.schlicht@tum.de (A. Schlicht), urs.hugentobler@tum.de (U. Hugentobler).

https://doi.org/10.1016/j.asr.2022.11.009
0273-1177/

Table 1
Simulated measurement errors for L-band.

L-band measurement errors		Description / Remark
Measurement noise		- White noise of 15 cm for code and 1.5 mm for phase measurements for each frequency.
Troposphere modeling errors	Simulation	- Gridded VMF1 (Boehm et al., 2006a) model as an accurate model.
	Solution	- GMF model (Boehm et al., 2006b) as a less accurate model.
Phase Center Variations (PCV)		- A different pattern for each of the 16 ground stations and satellites, for transmitter and receiver. - Multiplication by factor 50 for receiver and transmitter code measurements; represents a worst case scenario. - The signatures are with resemblance to multipath.
Constant bias		- Different bias per satellite, randomly distributed up to 5 mm.
Variation with once per revolution		- Different variation per satellite, randomly distributed up to 5 mm; represents a temperature dependent inter-technique bias per satellite.

Table 2
Simulated measurement errors for the optical observation techniques OTWL and OISL. A detailed description of the different errors is given in Schlicht et al. (2020).

Optical link measurement errors		Description / Remark
Measurement noise	Flicker-phase noise	- Induced by various effects (e.g. trapping of charge carriers in semiconductors) and occurs in all electronic devices.- Selected noise level up to 0.5 mm.
	Jitter of the Phase Locked Loop (PLL)	- A ranging distance dependent error. - Noise when varying between minimum and maximum ranging distance: - OTWL 1.2–1.4 mm (MEO) and 1.7–1.9 mm (GSO) - OISL 0.1–1.5 mm
Troposphere offset (for OTWL only)		- Simulated error: Half the difference between the models of Marini and Murray (1973) and Mendes and Pavlis (2004). - Air pressure and temperature information from GPT (Boehm et al. 2007). - Relative humidity was set individual by ground station: min. 75 %, max. 90 %. Varies randomly per station and epoch each up to around ± 6 %. - Max. error at 30° elevation 5 mm, min. error at 90° elevation 0.4 mm.
Offset due to the repeatability of the link		- Uniformly distributed for each transmitter–receiver-pair between ± 0.5 mm.
Offset related to the equipment calibration quality		- Offset per transmitter and receiver, randomly distributed between −0.5 and 0.5 mm; represents an inter-system bias, which affects the clock and the range.

Table 3
Estimated parameters regarding each observation technique.

Estimated parameters	L-band	OTWL	OISL
Station specific tropospheric zenith delays	Yes every-two hours	no	no
Ground station coordinates	no	no	no
Satellite initial state vectors and solar radiation pressure parameters	yes	yes	yes
Epoch-wise satellite and ground station clock parameters	yes	yes	yes
	One clock for each satellite and each ground station		
Phase ambiguities	yes	no	no
Range and clock biases	no	yes	yes
		One transmitter and one receiver bias per participating entity, (also in scenarios with L-band + OTWL + OISL)	

Table 4
Modified box-wing parameters used to generate the MEO *mismodeled orbit*.

	$\pm x$	$\pm y$	$\pm z$
$\alpha_{mismodeled} =$	$1.2\alpha_{true}$	$0.9\alpha_{true}$	$1.1\alpha_{true}$
$\rho_{mismodeled} =$	$1-(1.2\alpha_{true}+\delta_{true})$	$1-(0.9\alpha_{true}+\delta_{true})$	$1-(1.1\alpha_{true}+\delta_{true})$
$\delta_{mismodeled} =$	δ_{true}	δ_{true}	δ_{true}
$boxsurface_{mismodeled} =$	$boxsurface_{true}$	$boxsurface_{true}$	$boxsurface_{true}$
$wingsize_{mismodeled} =$	$wingsize_{true}$	$wingsize_{true}$	$wingsize_{true}$

Table 5
Modified box-wing parameters used to generate the GSO *mismodeled orbit*.

	$\pm x$	$\pm y$	$\pm z$
$\alpha_{mismodeled} =$	$1.2\alpha_{true}$	$0.9\alpha_{true}$	$1.1\alpha_{true}$
$\rho_{mismodeled} =$	$1-(1.2\alpha_{true}+\delta_{true})$	$1-(0.9\alpha_{true}+\delta_{true})$	$1-(1.1\alpha_{true}+\delta_{true})$
$\delta_{mismodeled} =$	δ_{true}	δ_{true}	δ_{true}
$boxsurface_{mismodeled} =$	$1.2boxsurface_{true}$	$1.2boxsurface_{true}$	$1.2boxsurface_{true}$
$wingsize_{mismodeled} =$	$wingsize_{true}$	$wingsize_{true}$	$wingsize_{true}$

Table 6
Best possible 3D-RMS orbit error with respect to the SRP modeling scenarios in millimeters. The results are means over the 10-days of the first simulation period. For IGSO and GEO satellites the 3D-RMS is given separately for each of the four satellites. For MEO satellites the best possible value is a mean for the 24 MEO satellites. IGSO and GEO satellites are numbered the same as in Fig. 1.

Best possible 3D-RMS orbit error SRP modeling according to	MEO [mm]	IGSO 1 [mm]	IGSO 2 [mm]	IGSO 3 [mm]	IGSO 4 [mm]	GEO 1 [mm]	GEO 2 [mm]	GEO 3 [mm]	GEO 4 [mm]
Eqn. (1)	3.4	2.5	2.1	2.3	1.6	10.7	17.7	6.5	16.8
Eqn. (2)	1.0	1.9	1.2	1.8	1.1	10.3	17.4	6.1	16.6
Eqn. (3)	0.8	1.9	1.1	1.8	1.1	10.2	17.4	6.1	16.6
Eqn. (4)	–	–	–	–	–	1.9	1.1	1.3	1.0

Table 7
Weighting of OTWL and OISL measurements with respect to Galileo L-band measurements ($\frac{\sigma^2_{L-band}}{\sigma^2_{OTWL/OISL}}$) for the different observation technique combinations.

Weighting	with IGSO satellites			with GEO satellites		
SRP modeling according to	L-band + OTWL	L-band + OISL	L-band + OTWL + OISL	L-band + OTWL	L-band + OISL	L-band + OTWL + OISL
Eqn. (1)	25	2.5	2.5	1000	2.5	2.5
Eqn. (2)	25	25	25	100	10	10
Eqn. (3)	25	25	25	100	10	10
Eqn. (4)	–	–	–	100	100	10

Future applications consider to use GSO satellites to link to satellites in the far Earth environment as well. As an extension of the Space Service Volume (Bauer et al., 2006; UNNOSA, 2021), geosynchronous satellites can be used in future constellations as a ranging and data relay interface between the Earth and highly elliptical orbit satellites, which are discussed to receive GNSS signals up to lunar distances (Winternitz et al., 2017; Ashman et al., 2018).

The concept of a Geodesy and Time Reference in Space (GETRIS) (Schäfer et al., 2013; Schlicht et al., 2014) aims to synergistically use GNSS L-band and EDRS-like optical links for ranging. Carrying high-precision clocks and equipped with two-way high-low satellite-to-satellite high-precision optical links between the GSO and Low Earth Orbit (LEO) satellites, GSO satellites have the central role in the GETRIS project. The concept assumes a globally distributed GSO network to enable a global tracking between the LEO and GSO satellites. With the aim to have GSO accuracies at the low mm-level – hence, the same accuracy to which ground stations can be determined – this geodesy and time reference in space shall be realized for providing high precision services to users, e.g., through optical links. However, the current common methods of geosynchronous orbit determination are far from delivering GSO accuracies of a few millimeters.

Today, tracking of GSO satellites is mainly performed using transponder two-way range measurements from a few ground stations. The currently best possible GSO determination is in the range of several decimeters to up to one meter. The difficulty is the poor observation geometry with respect to the Earth's surface. Lei et al. (2011) demonstrated a 1 m orbit precision for GEO satellites using the ranging technique SATRE (SATellite Time and Ranging Equipment). Using a network based on six BeiDou capable GNSS receivers, Steigenberger et al. (2013) achieved 1–2 dm for IGSO and several decimeters for GEO satellites by one-way L-band tracking. Some works analyzed new SRP models for BeiDou GEO satellite, achieving a Root Mean Square (RMS) of less than 10 cm in radial direction (Liu et al., 2016; Wang et al., 2019). Knogl et al. (2011) discussed a concept using one-way communications links from LEO to GEO satellites, resulting in a centimeter level positioning accuracy for the GEO satellites. Combining

ground station data with GPS (Global Positioning System) and BeiDou data of the LEO Feng-Yun 3C, Zhao et al. (2017) improved BeiDou orbit and clock products including the BeiDou GEO satellites. The use of beyond Earth signals from GNSS satellites is a further method discussed by several groups to improve the GSO accuracy (Moreau et al., 2002; Bauer et al., 2006; Jing et al., 2015; Enderle et al., 2018; Parker, et. al., 2018; Guan et al., 2022). The challenge is the weakness of such beyond Earth signals, mainly side-lobe signals with a low signal-to-noise ratio. GNSS antennas are directed to the Earth. For this reason, the GNSS signals can only be received by a GSO satellite at the far side of the Earth.

In this simulation study, we discuss the integration of GSO satellites into a future Galileo system, which is equipped with terminals to perform Optical dual one-way Inter-Satellite Link (OISL) measurements. As an additional measurement type, the same dual one-way ranging technique is used to stations on the ground, called OTWL (Optical Two-Way Link; Marz et al., 2021). The proposed ranging signal is a pseudo random noise code modulated on an optical carrier with a precision of 1 mm. A high-precision optical technique for the ground link has the advantage to complement the L-band measurements. We use the synergy between continuous wave dual one-way OISL and OTWL in this study.

Inter-satellite links are one of the most discussed concepts for future GNSS constellations (Gill, 1999; Fernández et al., 2010; Schlicht et al., 2020; Michalak et al., 2021). The BeiDou-3 satellite constellation shows already that inter-satellite links enhance the orbit accuracy (Yang et al. 2020).

As an alternative or complement to OISL, ground-space oriented OTWL measurements (Schlicht et al., 2019; Marz et al., 2021) can be used as well. Two-way ranging additionally supports this GNSS system with accurate time transfer by an optical measurement LTT (Laser Time Transfer; Meng et al., 2013) and a two-way microwave technique TWSTFT (Two-way Satellite Time Frequency Transfer; Tang et al., 2016). Ranging and time transfer techniques like the pulsed one-way/two-way European Laser Timing (ELT; Schreiber et al., 2010) or T2L2 (Time Transfer by Laser Link; Samain et al., 2014) are also able to achieve 1 mm ranging and time transfer precision (Marz et al. 2021).

In a simulation study (Marz et al., 2021) we show that combinations of observation techniques as well as an enhanced Solar Radiation Pressure (SRP) parameter modeling allow to achieve MEO orbit accuracies at the low millimeter level. Such observation technique combinations are GNSS microwave observations together with OISL and/or OTWL measurements.

In this study we adapt these findings to GEO and IGSO satellites. Integrating geosynchronous orbit (GSO) satellites into the MEO satellite constellation, is it possible to achieve GSO accuracies at the same level as for the Medium Earth Orbit (MEO) satellites? Do GSO satellites in a MEO satellite constellation improve the MEO satellite orbits themselves? To answer these questions, we analyzed the formal error and orbit accuracy of all satellite types in a possible future Galileo constellation. We show the contribution of each ranging technique by studying the error in POD performing different combinations of these techniques. Our intention is to directly compare POD results from a L-band-only scenario to the results from the observation technique combinations and additional SRP parameter estimation. In addition, we added a short analysis of the effect of a centre of mass error for the scenario with the best POD. Regarding the presented absolute POD results, we want to indicate again that this work is a simulation study. Although, we take many systematic effects for L-band and optical measurement as well as for orbit modeling into account, the complexity of the physical reality cannot be fully transported into a simulation environment. Therefore, the POD results which are reported in this work are to be regarded as indicative values that need confirmation and tuning based on real ranging data.

We structured the analysis in the following way: First, we introduce the set-up of the simulations in chapter 2 before we introduce the error in orbit modeling due to wrong solar radiation pressure parameters in chapter 3. Chapter 4 presents the results in form of formal errors and accuracy of the orbit determination process. Each satellite type is discussed separately before we summarize the outcome in chapter 5.

2. Simulation set-up

For this paper, we evaluate the impact of geosynchronous satellites as an expansion to a MEO GNSS satellite constellation in a typical orbit solution. We selected the Galileo satellite constellation for our simulation study. We compare the results using expanded Galileo MEO constellations with GEO or IGSO satellites to the solution using the intended Galileo MEO constellation consisting of 24 MEO satellites. In the first scenario we assume the geosynchronous satellites to be equipped with GNSS microwave (L-band) transmitters that offer the same signal-to-noise ratio at the Earth surface as the Galileo MEO satellites. In the second scenario we use OISL together with L-band. The third scenario combines ground-space oriented OTWL measurements with L-band. A further scenario analyzes a L-band + OTWL + OISL combined solution for POD. The L-band and OTWL measurements are performed with respect to 16 ground stations as a typical GNSS ground station network (see Fig. 1 left). In this work, we do not consider cloudy weather conditions for OTWL measurements. Hence, our L-band + OTWL scenario results presented in this work are for optimal conditions. L-band-only, L-band + OISL and L-band + OTWL + OISL results are not affected. An analysis on the influence of station failures due to weather conditions was performed in Marz et al. (2021) for MEO POD.

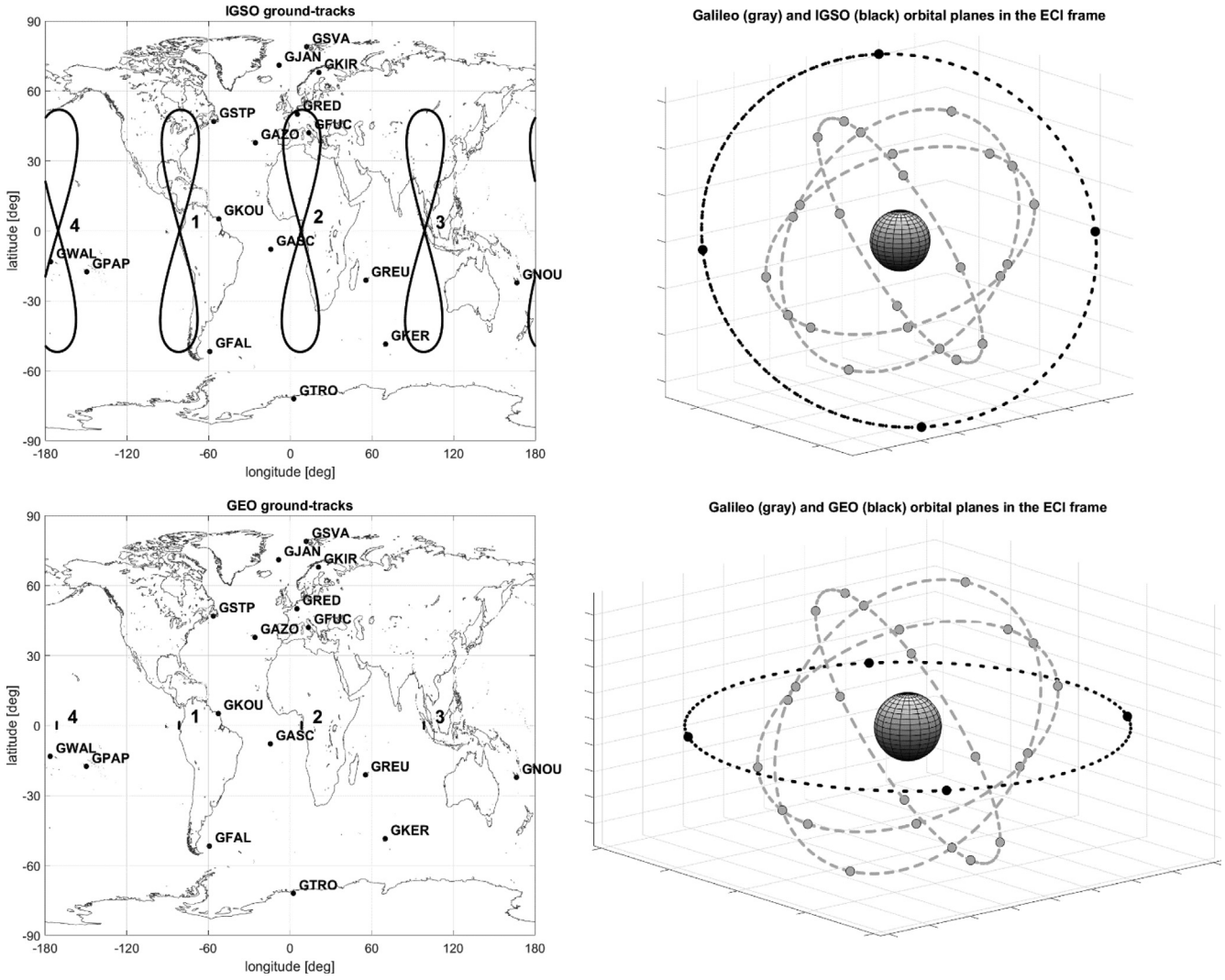

Fig. 1. Ground-tracks of the four IGSO (top) and GEO (bottom) satellites in the ECEF (Earth-centered Earth-fixed) frame as well as 16 ground stations, as a typical GNSS ground station network, are shown on the left side, the Galileo MEO and IGSO (top) as well as Galileo MEO and GEO (bottom) orbital planes in the ECI (Earth-centered inertial) frame on the right side.

We used a modified version of the Bernese GNSS Software version 5.2 (Dach et al., 2015) for simulation and analysis. We processed 24 h observations of ten consecutive days, the Galileo MEO repeat cycle. The analysis was simulated for the period 12th – 21st Feb. 2019 (days of year: 043–052). This is further called the first simulation period. Furthermore, we analyze the orbit error for a second period, 12th – 21st May 2019 (days of year: 132–141). The reason is to proof the validity of the conclusions we made for the first simulation period as well as the dependence on the beta angle and different systematic effects of the measurements. The beta angle is defined as the sun elevation angle above the orbital plane.

SRP is the largest non-gravitational force disturbing MEO and GSO satellites (Fliegel et al., 1992; Springer et al.,1999; Montenbruck and Gill, 2005). In Schlicht et al. (2020) and Marz et al. (2021) we analyzed the use of additional SRP parameters to the commonly used empirical SRP model ECOM2 (Empirical CODE Orbit Model 2) (Arnold et al., 2015). Especially, using combinations of observation techniques like microwave + optical, the POD solution gains a huge benefit. In chapter 3 we give an overview regarding the modeling of SRP parameters.

The following simulation and estimation procedures are overall similar as those presented in Marz et al. (2021). Improvements concern in particular the simulation and estimation of clock and range biases. For this paper we simulate and estimate a range and a clock bias for each transmitter and receiver. As this leads to a rank-deficient normal equation matrix, constraints for the bias estimation need to be introduced. For the first scenarios we assume constraints of 1 mm for all biases. This is within the range of the expected precision of the optical links. For comparisons, we perform another scenario using five times looser

constraints. We also considered a solution where no ground station clock biases were estimated and no constraints were used.

2.1. Satellite constellations

The simulated satellite constellation consists of 24 MEO satellites and is intended to represent the final Galileo MEO satellite constellation. The Galileo MEO orbits were simulated as a Walker constellation (56°:24/3/1). The used satellite properties are based on the 1st generation Galileo satellites. To get as realistic orbits as possible, we adjusted the orbits with a force model including the Earth gravity field up to degree and order 12, ocean and solid Earth tides as well as direct tides from third bodies (Sun, Moon, Venus, Mars and Jupiter) and SRP.

Each of the GSO satellite constellations consists of four GEO or four IGSO satellites. GEO and IGSO constellations are used separately with the MEO satellite constellation to account for the impact of the different GSO types. We used the previously described conservative forces consistently for the GSO satellites as for the Galileo MEO satellites. Both, the GEO and IGSO satellites were placed at the longitudes 10°, 100°, 190° and 280° to get a homogeneous distribution around the Earth. To have a globally distributed GSO satellite network is also the aim of the GETRIS project (Schäfer et al., 2013; Schlicht et al., 2014). We are aware that GSO satellites in a future Galileo constellation would be optimized for use across Europe, however, one goal of this work is to analyze the POD capabilities regarding the number of available ground stations for each GSO satellite for L-band and OTWL measurements.

The IGSOs have an inclination of 52°. A pre-simulation analysis showed that this inclination gives a very good visibility coverage with 16 ground stations as a typical GNSS ground station network. Fig. 1 left top/bottom shows the IGSO/GEO satellite ground-tracks of one day in the Earth-centered Earth-fixed (ECEF) frame, Fig. 1 right top/bottom the IGSO/GEO and Galileo MEO orbital planes in the Earth-centered inertial (ECI) frame. For GEO satellites we used an orbit normal attitude mode, for IGSO and MEO satellites a nominal yaw-steering attitude, affecting SRP modeling.

The beta angles in the first simulation period are between about −9° and −13° for GEO and about 38° and 41° for IGSO satellites, in the second period between about 18° and 20° for GEO and about 15° and 20° for IGSO satellites. As all GEO and IGSO satellites are on the same orbital plane (see Fig. 1), respectively, all GEO or IGSO satellites thus have the same beta angles.

2.2. Simulation

GNSS L-band measurements were simulated as two-frequency code and phase measurements in E1 and E5a with 60 s sampling rate. Building the ionosphere free linear combination, effects due to the ionosphere can be eliminated to a great extent. The simulated microwave measurement errors are a measurement noise as white noise of 15 cm for code and 1.5 mm for phase measurements for each frequency. Furthermore, we simulated troposphere modeling errors and phase center variations for receivers and transmitters which give signatures with resemblance to multipath. Furthermore, we simulated different randomly distributed constant biases of up to 5 mm for each satellite as well as randomly distributed once per revolution variations up to 5 mm for each satellite simulating a temperature dependent inter-technique bias. An overview of the used microwave measurement errors is given in Table 1.

OISL observations – two-way range measurements and clock differences – are simulated in an any-to-any scenario with bidirectional links. In the simulation of these measurements, we used the connectivity scheme from Fernández (2011) and adapted the scheme according to 24 or 28 satellites. The sampling rate of the OISL measurements is 60 s. We integrated the following measurement errors for the optical link: a flicker-phase noise (Riley, 2008) with a level up to 0.5 mm, a ranging distance dependent jitter of the phase locked loop (Holmes, 1990; compare Schlicht et al., 2020) – about 0.1–1.5 mm when varying between the minimum (about 5250 km) and maximum ranging distance (about 60000 km) –, an offset due to the repeatability of the link, uniformly distributed for each transmitter–receiver-pair between ± 0.5 mm, as well as a randomly distributed offset per transmitter and receiver between −0.5 and 0.5 mm. The latter simulates the calibration uncertainty of hardware biases that affect the clock and range measurements. Again, an overview of the used OISL measurement errors is given in Table 2. In the case of GSO satellites, the maximum ranging distance is set to 60000 km to avoid the low signal-to-noise ratio long distance signals. This means, in the case of longer ranging distances, the observation is not taken into account for the estimation for this epoch. In a pre-simulation analysis, we compared the POD results to the solution calculated in a scenario without a ranging distance limit to GSO satellites. As the resulting orbit differences from the adjustment have been negligibly small, we performed the measurement simulation with the distance limit in this simulation study. It is assumed that the OISL tracking instrument can point towards the geocenter with a maximum nadir angle allowing to track the satellites' direct neighbors on the same orbital plane.

The OTWL measurements were simulated as two-way range measurements and clock difference observations as well. The measurement schedule was simulated according to Marz et al. (2021), with a minimum observation elevation of 30° seen from ground stations and a sampling rate of 60 s. Within a measurement epoch, each ground station connects with one satellite. For the next epoch, the scheduling takes into account that always the satellite reached with the shortest ground station telescope movement is tracked and which has no ground station partner yet. A station does not track the same satellite in successive epochs.

The measurement errors are used analogously to OISL, however, with an additional error due to the impact of the troposphere to the ground-space link (see Table 2). The maximum error at 30° elevations is 5 mm, the minimum error in the zenith is 0.4 mm. For OTWL, the noise at MEO distances is at about 1.2–1.4 mm and at GSO distances at about 1.7–1.9 mm, when varying between the minimum and maximum ranging distance.

All satellites are assumed to carry one terminal to perform either OTWL or OISL measurements. For the L-band + OTWL + OISL scenario, the satellites carry two terminals to be able to perform OTWL and OISL measurements at the same time and independently. Furthermore, we assume all satellite types to be equipped with hydrogen masers. The ground station clocks are based on polynomials of order four. We assume that each satellite and ground station is equipped with only one clock. This means, all observation techniques refer to the same clock at each participating entity. However, each observation technique is affected by individual hardware biases.

2.3. Estimation

We estimated satellite orbits with six osculating elements and nine or more empirical SRP parameters. A detailed description of the estimated SRP parameters is given in chapter 3. We estimated epoch-wise ground station and satellite clock parameters (L-band, OTWL and OISL), one transmitter and one receiver bias for each participating entity per day (OISL and OTWL) representing the inter-system bias to L-band, station specific tropospheric wet zenith delays with two hours sampling (L-band) and L-band phase ambiguities. An overview is given in Table 3. All ground station coordinates were fixed to have a well-defined geodetic datum. In Marz et al. (2021) we showed that especially a L-band + OISL scenario can benefit from having a well-defined geodetic datum. Furthermore, we fixed one ground station clock (GKOU).

In scenarios without GSO satellites, we simulated around 408740 GNSS observations for code and phase, around 43400 OTWL and around 32290 OISL observations per day. With IGSO/GEO satellites in the constellation we have around 482830/478900 GNSS, around 45040/44950 OTWL and around 33900/33890 OISL observations per day. The OTWL observations are evenly distributed over a day.

3. Solar radiation pressure modeling

The selected SRP model parameters have a huge impact on the POD results. For the processing of GNSS solutions, ECOM2 (Arnold et al., 2015) with a total of nine SRP parameters is one of the commonly used empirical SRP models in the International GNSS Services (IGS) community. In the case of MEO and IGSO satellites, the SRP parameters of the model are defined in the DYB coordinate system with D pointing from the satellite to the Sun, Y the direction along the solar panels and B completing the right-handed orthogonal system. In orbit normal mode the orientation of the solar panel is not perpendicular to the Sun-satellite direction. Therefore, for GEO satellites a different orientation of the DYB frame is used, named $\bar{D}\bar{Y}B$. In this frame, $\bar{Y}$ is perpendicular to the orbital plane, $\bar{B}$ perpendicular to $\bar{Y}$ and the Sun-satellite direction, and $\bar{D}$ completes the right-handed orthogonal system.

The SRP parameters are estimated as constant as well as periodic sine and cosine terms with multiples of once per revolution in all three directions. In the following equation, DYB and $\bar{D}\bar{Y}B$ directions are consistently named D,Y and B. In the case of ECOM2 (Eqn. (1)) these are a once per revolution term in B as well as two and four times per revolution terms in direction D each with a sine and cosine term. Δu is the argument of latitude with respect to the sun. In the further context, the constant parameters are given with a subscript 0, the sine parameter with a s and the cosine parameter with a c. The per revolution term is named with its number following the corresponding directions D, Y, or B.

$$D = D_0 + D_{2c}\cos(2\Delta u) + D_{2s}\sin(2\Delta u) + D_{4c}\cos(4\Delta u) + D_{4s}\sin(4\Delta u)$$
$$Y = Y_0 \qquad B = B_0 + B_{1c}\cos(\Delta u) + B_{1s}\sin(\Delta u) \tag{1}$$

In Marz et al. (2021) we showed that it is possible to estimate up to 13 SRP parameters in a MEO POD process when using measurements of two or more different observation techniques. This extended SRP model allows for a significantly improved accuracy of the estimated MEOs. The selection of the SRP parameters was done performing a direct analysis of the modeled accelerations acting in D, Y and B directions. Scenarios with different initial SRP modeling all gained from the additional SRP parameter estimates. Therefore, we recommended to use additional SRP parameters for MEO POD solutions estimated using measurements of two or more different observation techniques. In this study the analysis is applied to GSO satellites. Performing a simulation study, four different orbit types are relevant: *true*, *mismodeled*, *adjusted* and *best possible* orbits. An explanation of these orbit types is given in the following.

3.1. True orbit

The simulated real world orbit is represented by the further called *true* orbit. Therefore, we simulated orbits of MEO, GEO and IGSO satellites as described in chapter 2 and adjusted them with models to get as realistic orbits as possible. We used the box-wing model by Duan et al. (2019) which models physical optical parameters of absorbed α, reflected ρ and diffusely reflected δ photons for all satellites surfaces – the surfaces of a satellite in the directions ± x, ±y and ± z (box) as well as the solar panel area (wing). We used three different sets of parameters for

MEO, GEO and IGSO satellites, each assumed to be *true* and adapted for the corresponding satellite system in terms of mass, size and physical conditions. We did not estimate empirical parameters in the generation process of *true* orbits. The *true* orbit is used to simulate the measurements.

3.2. Mismodeled orbit

For the least-squares adjustment an orbit with a modeling error is needed. This orbit is in the following called *mismodeled* orbit. The *mismodeled* orbit is based on the same initial orbit as the *true* orbit, however, a modified set of box-wing parameters is used in the orbit generation process. Only initial state vectors but no empirical parameters are estimated. The difference of the *true* and *mismodeled* orbit represents the orbit modeling error. For MEO satellites, we modified the three optical parameters α, ρ and δ in the directions ± x, ±y and ± z according to Table 4. Satellite surface areas and solar panel sizes remained unchanged. Thus generated *mismodeled* MEO orbits are wrong by around 14 cm on average (*true* – *mismodeled* orbit). Uncertainties for the physical optical parameters are not published by the satellite manufacturers. However, uncertainties at a level of about 10 % are discussed. Furthermore, Li and Ziebart (2020) studied the error of a box-wing model by comparing it to a CAD (Computer-Aided Design) model. The outcome was a satellite surface error of 7 % for GPS and 2 % for Galileo on average for all beta angles. We analyzed individual errors for the physical optical parameters and the satellite box. The total acceleration errors from SRP fit well to our assumed modeling errors.

For GSO satellites we expect that the optical parameters can be determined to a similar level as for the MEO satellites. In addition, we assume that the GSOs have more functionalities and, hence, carry additional antennas and hardware. This would lead to a more difficult estimation of the optimal box-wing model parameters. Therefore, we introduce an additional error which we tuned to the state-of-the-art GEO and IGSO orbit determination accuracy. The used model for GSO satellites is given in Table 5. The solar panel sizes remained unchanged. On average, thus generated *mismodeled* IGSO orbits are wrong by around 71 cm and the GEO orbits by around 82 cm (*true* – *mismodeled* orbit).

3.3. Adjusted orbit

The further called *adjusted* orbit is the resulting orbit from the least-squares adjustment of the measurements. The *adjusted* orbit is based on the corresponding MEO, GEO or IGSO modeling error. In addition to the initial state vector, empirical parameters are adjusted to the measurements.

3.4. Best possible orbit

In a simulation, the *best possible* orbit is very important to quantify the modeling error. It represents the maximum achievable accuracy given by the introduced modeling errors. The *best possible* orbit is generated similarly to the *mismodeled* orbit, however, in addition to the state vector the respective empirical parameters are additionally adjusted to the true satellite trajectory. To generate the *best possible* orbit thus no measurements are used but true orbit positions are adjusted. Hence, the difference between the *true* and *best possible* orbit gives the errors from the introduced orbit modeling, the difference between the *adjusted* and the *best possible* orbit shows the remaining errors from the measurements after the least-squares adjustment.

3.5. Empirical parameter analysis

We analyzed the direct impact of the introduced modeling errors from the difference (*true* – *mismodeled*) of the computed SRP accelerations in the corresponding DYB frame, each extracted from the *true* and the *mismodeled* orbit generation process.

In Marz et al. (2021) we already performed this analysis for MEO satellites. Using the same modeling errors for MEO satellites in this study (see Table 4), we can transfer the results. In the case of measurements from two or more different observation techniques used in the estimation process, the adjustment of additional sine and cosine B_3 (see Eqn. (2)) as well as B_5 (see Eqn. (3)) parameters to the nine ECOM2 parameters improves the MEO POD accuracy to a great extent.

Fig. 2 left shows the Power Spectral Density (PSD) of the acceleration difference *true* – *mismodeled* for the IGSO satellites and Fig. 2 right for the GEO satellites. For each of the four IGSO or GEO satellites the results are the same, respectively. The analysis was done for both 10-days simulation periods. The y-axis is the amplitude of the acceleration difference in $\left(\frac{m}{s^2}\right)/\sqrt{Hz}$, the x-axis the per-revolution terms in the D, Y and B or $\bar{D}$, $\bar{Y}$ and $\bar{B}$ directions, respectively.

The accelerations for the IGSO satellites (see Fig. 2 left) are similar to the results of the analysis for the MEO orbits (see Marz et al. (2021)). The even per revolution terms dominate in the D direction and the odd per revolution terms in B direction. These are the harmonics which are taken into account in ECOM2 (Eqn. (1)). The main terms are up to four times per revolution. A pre-analysis showed that the additional use of D_6 parameters gives similar POD results as using B_5 parameters in the estimation process. The additional use of B_5 and D_6 parameters together does not give a further improvement for POD as well. Resulting from the analysis, we performed three scenarios with SRP modeling according to ECOM2 (Eqn. (1)), Eqn. (2) and Eqn. (3) for the study of IGSO and MEO POD.

In the case of GEO satellites, the result of the analysis (see Fig. 2 right) differs from ECOM2 as well as from the analysis for IGSO and MEO satellites. For each per revolution term, the accelerations are quite large in all directions $\bar{B}$, $\bar{D}$ as well as $\bar{Y}$. This result means that for GEO

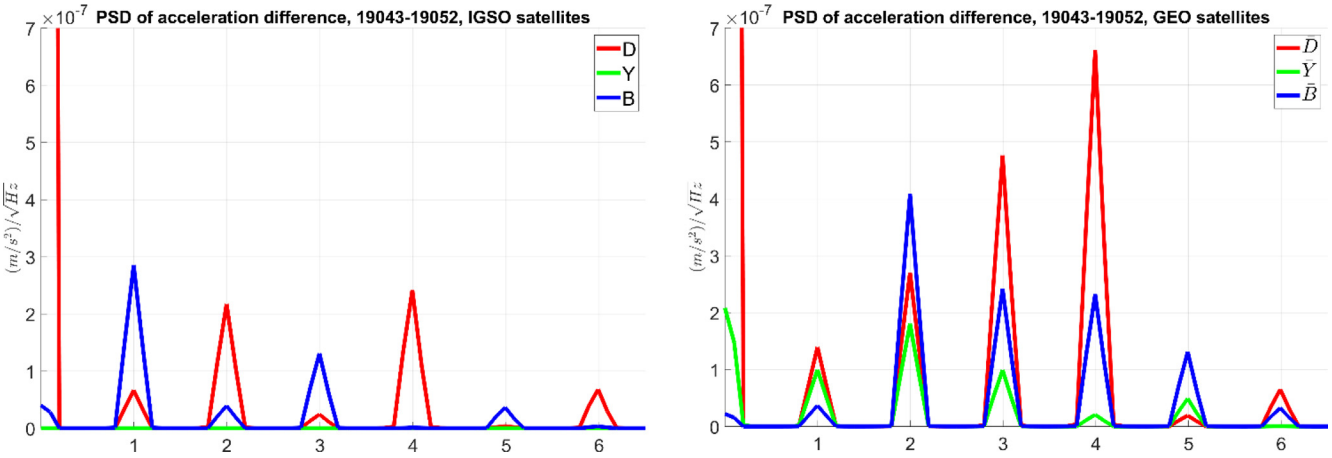

Fig. 2. PSD of the acceleration difference extracted from the true and mismodeled IGSO (left) and GEO (right) orbits with respect to the modeling error according to Table 5. The y-axis gives the amplitude of the accelerations; the x-axis shows the per revolution terms. For IGSO satellites, in D direction the even parameters are dominant, in B direction the odd parameters. There is no influence in Y direction. For GEO satellites, disturbing periods cannot be covered by ECOM2 and differ from the disturbances on IGSO and MEO orbits. For each per revolution term the influence is quite large in all directions B, D and Y.

satellites many empirical SRP parameters have to be estimated to compensate for the perturbing accelerations. To avoid parameter correlations using a large number of parameters, we performed a pre-analysis to identify the influence of the different SRP parameters terms. The analysis showed, that dependent on the direction only the sine or the cosine term has a large influence, while the other can be compensated by another term. In $\bar{D}$ direction, the sine terms of the odd per revolution terms are dominant, while the cosine terms are dominant for the even per revolution terms. The same behavior can be found in $\bar{Y}$ direction. In $\bar{B}$ direction it is reversed. The resulting model is given in Eqn. (4). The maximum number of SRP parameters is still 13 which is the same as in Eqn. (3). We used the SRP modeling according to Eqn. (4) for the study of GEO POD, however, for comparisons we performed scenarios for GEO POD using SRP modeling according to ECOM2 (Eqn. (1)), Eqn. (2) and Eqn. (3) as well. In the MEO + GEO constellation and the scenario with the SRP modeling according to Eqn. (4) for GEO satellites, the MEO satellites are still modeled according to Eqn. (3).

$$D = D_0 + D_{2c}\cos(2\Delta u) + D_{2s}\sin(2\Delta u) + D_{4c}\cos(4\Delta u) + D_{4s}\sin(4\Delta u)$$

$$Y = Y_0$$

$$B = B_0 + B_{1c}\cos(\Delta u) + B_{1s}\sin(\Delta u) + B_{3c}\cos(3\Delta u) + B_{3s}\sin(3\Delta u) \quad (2)$$

$$B = B_0 + B_{1c}\cos(\Delta u) + B_{1s}\sin(\Delta u) + B_{3c}\cos(3\Delta u) + B_{3s}\sin(3\Delta u) + B_{5c}\cos(5\Delta u) + B_{5s}\sin(5\Delta u) \quad (3)$$

$$\bar{D} = \bar{D}_0 + \bar{D}_{1s}\sin(\Delta u) + \bar{D}_{2c}\cos(2\Delta u) + \bar{D}_{3s}\sin(3\Delta u) + \bar{D}_{4c} \times \cos(4\Delta u)$$

$$\bar{Y} = \bar{Y}_0 + \bar{Y}_{1s}\sin(\Delta u) + \bar{Y}_{2c}\cos(2\Delta u)$$

$$\bar{B} = \bar{B}_0 + \bar{B}_{1c}\cos(\Delta u) + \bar{B}_{2s}\sin(2\Delta u) + \bar{B}_{3c}\cos(3\Delta u) + \bar{B}_{4s}\sin(4\Delta u) \quad (4)$$

After establishing the different scenarios which are performed in this study, we look at the *best possible* achievable POD accuracy for MEO, IGSO and GEO satellites. Table 6 gives the best possible Three-Dimensional (3D) -RMS orbit error – computed as the square 3D error for each satellite at each epoch, then the mean thereof over all satellites and epochs, followed by the square-root – in millimeters as a mean for the 24 MEO satellites and separately for each of the four IGSO and GEO satellites. For MEO and IGSO satellites an improvement for the *best possible* orbit accuracy can be achieved using SRP modeling according to Eqn. (2) and (3). The *best possible* 3D-RMS orbit error is at around 1–2 mm for MEO and IGSO satellites. The comparatively large values of around 10–18 mm for GEO satellites with SRP modeling according to Eqn. (1), (2) and (3) can mainly be attributed to the cross-track component. With the SRP model optimized for GEO satellites (Eqn. (4)), however, similar results as for IGSO satellites can be achieved. In this regard, the additionally estimated Y parameters improve the accuracy in cross-track the most. Some IGSO and GEO satellites do not reach the same low *best possible* values as the other satellites. These satellites have larger modeling errors at the beginning and end of each simulated day which cannot be fully compensated. This indicates that the daily processing has a different influence on these satellites.

4. Results

We now discuss the results of this simulation study analyzing the formal orbit uncertainty and the orbit error. We evaluate the influence of IGSO or GEO satellites in a Galileo MEO constellation for MEO POD as well as the impact on the achievable IGSO and GEO accuracy itself. We performed scenarios using different observation techniques in combinations – L-band + OTWL, L-band + OISL and L-band + OTWL + OISL– and compared the results to the L-band-only scenario. For L-band and OTWL, we simulated the measurements based on the 16 ground stations (compare Fig. 1). Furthermore, we varied the SRP modeling for each scenario according to Eqn. (1), (2), (3) or (4). Using combinations of different observation techniques, the weighting of the different measurement types to each other is a critical task: Which weights represent the real observation errors best? In this simulation study, we optimized the weights of all measurement combinations to achieve the best orbit accuracies (*true* – *adjusted* orbits). Tables with the weights with respect to L-band ($\frac{\sigma^2_{\text{L-band}}}{\sigma^2_{\text{OTWL/OISL}}}$) are given in Table 7.

In the case of IGSO or GEO satellites in the constellation, the quality of the GSO POD solution in the L-band-only and L-band + OTWL scenarios is highly dependent on the number of ground stations the corresponding GSO satellite can connect to. Fig. 3 shows the visible ground stations (left) as well as the total number of OTWL observations (right) for ten days for each of the four IGSO satellites. The same is shown in Fig. 4 for the four GEO satellites.

All IGSO satellites (see Fig. 3) can connect to more than four ground stations. IGSO-2 has the best ground coverage as the total number of OTWL observations shows. Although IGSO-3 tracks in total more ground stations than IGSO-4, the number of total observations is slightly lower. This is due to the fact, that only two stations, namely GREU and GKER, account for around 50 % of the observations. With around 1500 observations for each of the two stations, the total observation number of the most frequently visible station is more than 25 % lower than for the other three IGSO satellites. For instance, IGSO-4 has around 2000 observations to each of the stations GWAL, GPAP and GNOU. For the GEO satellites the ground station visibility is generally lower than for IGSO satellites using the 16 ground stations network (see Fig. 4). While GEO-2 can still connect to five stations, the other three GEO satellites can connect to less than four stations. For GEO-1 only two stations are visible, for GEO-3 only one station. As the normal equation matrix in the estimation of the scenarios L-band-only and L-band + OTWL is singular for these two satellites, no POD results for these two GEO satellites are shown in this study for these two scenarios. Scenarios including OISL observations deliver reliable results. In the case of GEO-4, having three stations visible, only the normal equation matrix of the L-band-only scenario estimation is singular. In the case of L-band + OTWL observations, the clocks can be synchronized having two-way observations. Hence, three visible ground stations are necessary to get a reasonable and stable solution in our case.

In the following we show the formal orbit uncertainties and orbit errors for MEOs with respect to all SRP modeling scenarios. For the analysis of IGSO and GEO POD, in each case we compare the results according to the ECOM2 modeling (see Eqn. (1)) with the results of the overall best scenario using a SRP modeling with more than nine SRP parameters. For the results shown in the following sections, we set up constraints of 1 mm for the estimated range and

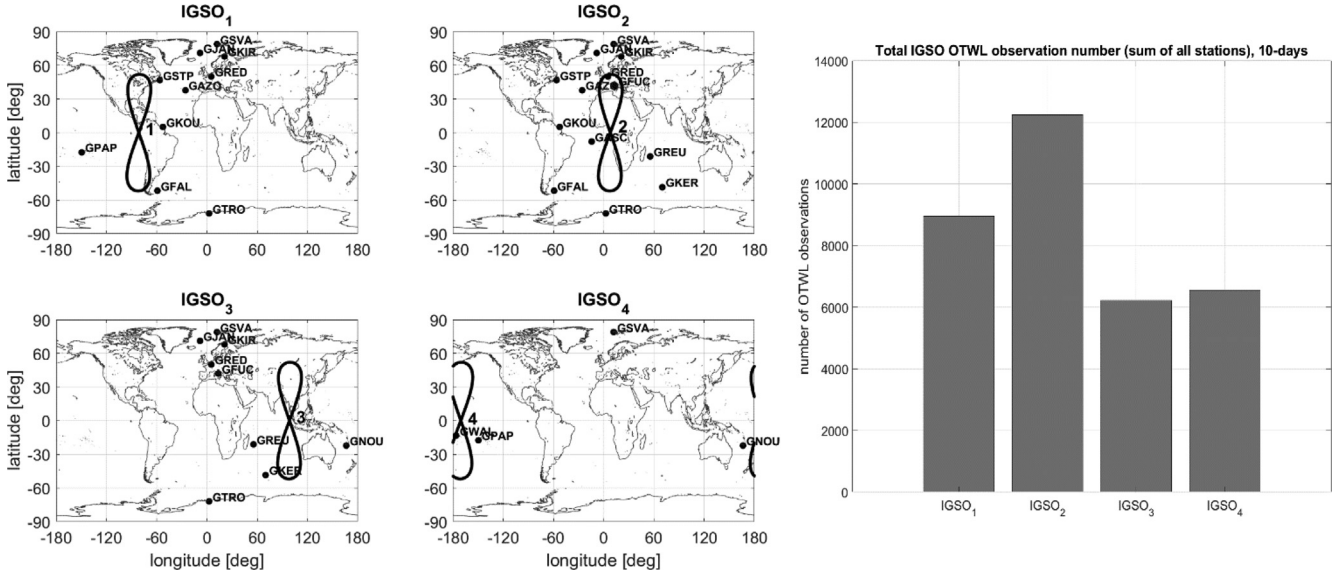

Fig. 3. Visible ground stations for each of the four IGSO satellites (left) as well as the total number of OTWL observations regarding each IGSO satellite for the 10-days of the first simulation period (right). The IGSO satellites are numbered with 1–4.

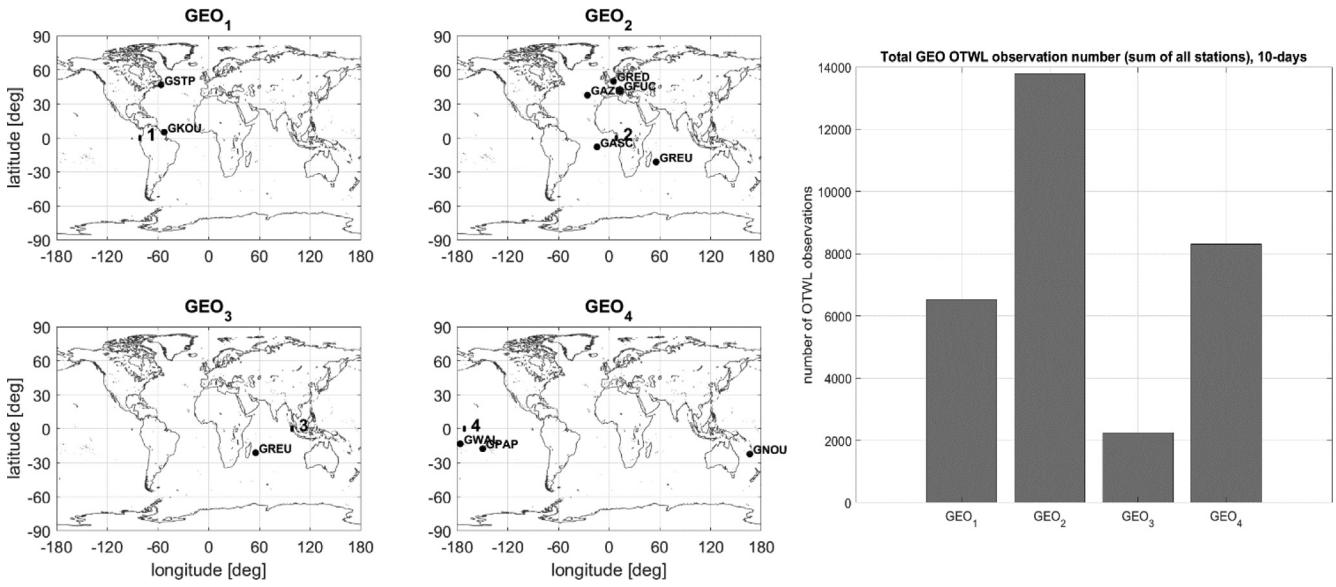

Fig. 4. Visible ground stations for each of the four GEO satellites (left) as well as the total number of OTWL observations regarding each GEO satellite for the 10-days of the first simulation period (right). The GEO satellites are numbered with 1–4.

1 mm for the clock biases. For comparisions, we also generated orbit error results with five times weaker constraints as well as a solution where no ground station clock biases were estimated and no constraints were used for ranging biases. The differences between these solutions and the results calculated with 1 mm constraints are in the range of around 0.1 mm for all scenarios including OISL measurements. For L-band + OTWL the differences can reach 0.5 mm for the GEO or IGSO satellites with the lowest OTWL observations. As the orbit error differences are rather small, we finally continued to use the solution with 1 mm constraints for the results shown in this paper. The clock biases, however, are much more affected by a less tight constraining and, therefore, the clock estimates as well. Results for the clocks will be discussed in another research and are not shown in this work.

4.1. MEO formal orbit uncertainty

A simulation should not only analyze the modeling errors which we studied by the best possible orbit, but also the influence of the stochastic errors and the geometrical configuration of the measurements, represented by the formal orbit uncertainty. This also allows an analysis of the observability. Fig. 5 shows the formal orbit uncertainties for MEO satellites comparing a MEO-only, a MEO + IGSO and a MEO + GEO constellation for all types of simulated scenarios. The presented formal orbit

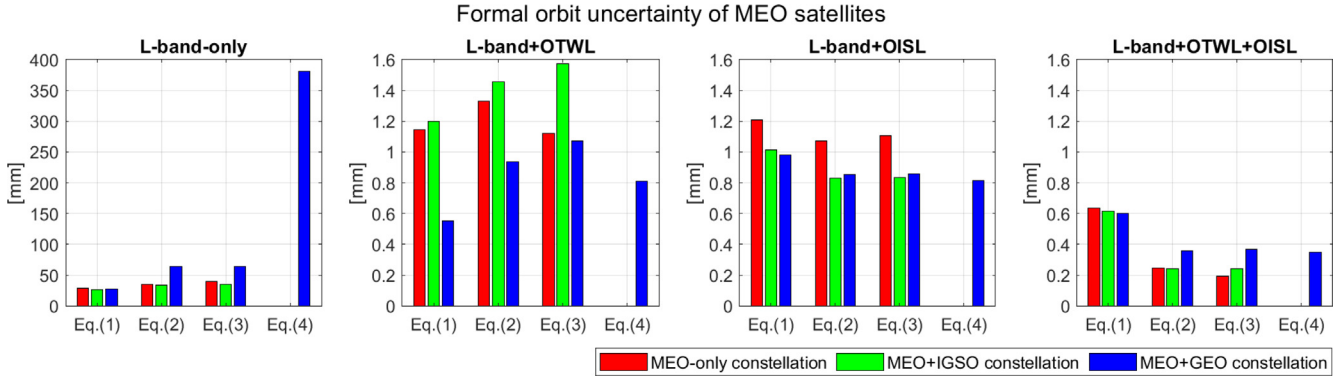

Fig. 5. Formal orbit uncertainties of MEO satellites in millimeters, resulting from a MEO-only, a MEO + IGSO and a MEO + GEO constellation. The values are averaged over the 24 MEO satellites as well as the 10-days of the first simulation period (12th – 21st Feb. 2019; days of year: 043–052). The results are with respect to the different SRP modeling according to Eqn. (1), (2), (3) and additionally (4) for GEO satellites.

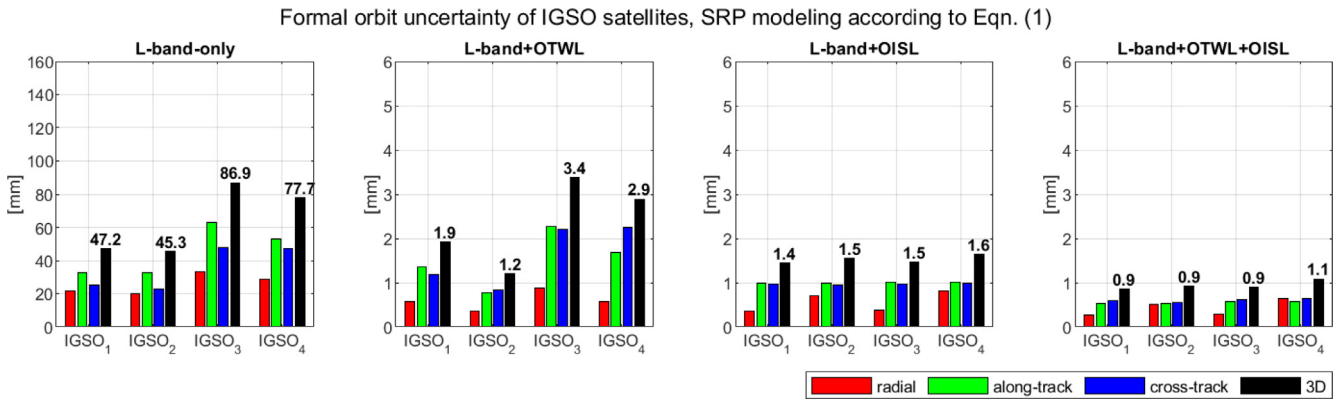

Fig. 6. Radial, along- and cross-track as well as 3D formal orbit uncertainties for each of the four simulated IGSO satellites in millimeters. The results are for a SRP modeling according to Eqn. (1). The values are averaged over the 10-days of the first simulation period (12th – 21st Feb. 2019; days of year: 043–052).

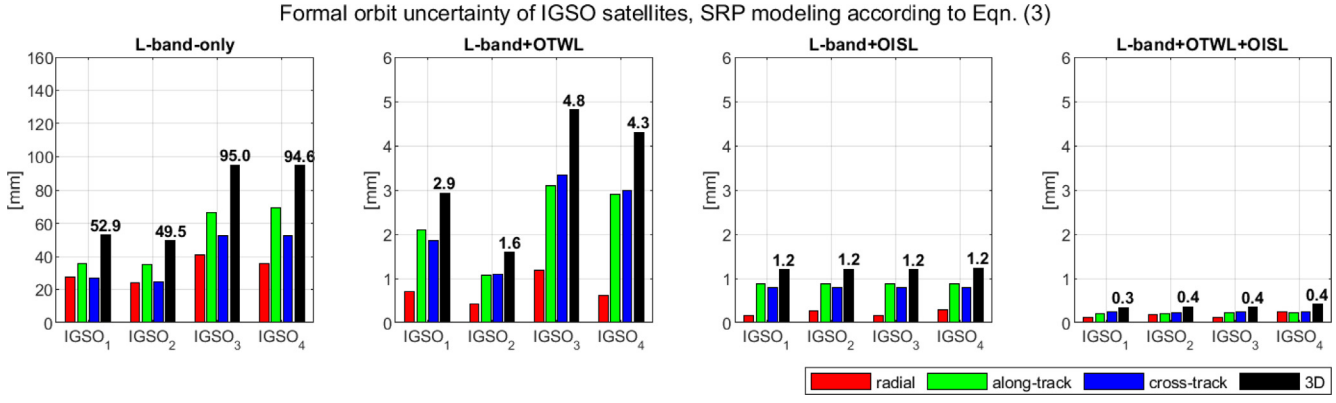

Fig. 7. Radial, along- and cross-track as well as 3D formal orbit uncertainties for each of the four simulated IGSO satellites in millimeters. The results are for a SRP modeling according to Eqn. (3). The values are averaged over the 10-days of the first simulation period (12th – 21st Feb. 2019; days of year: 043–052).

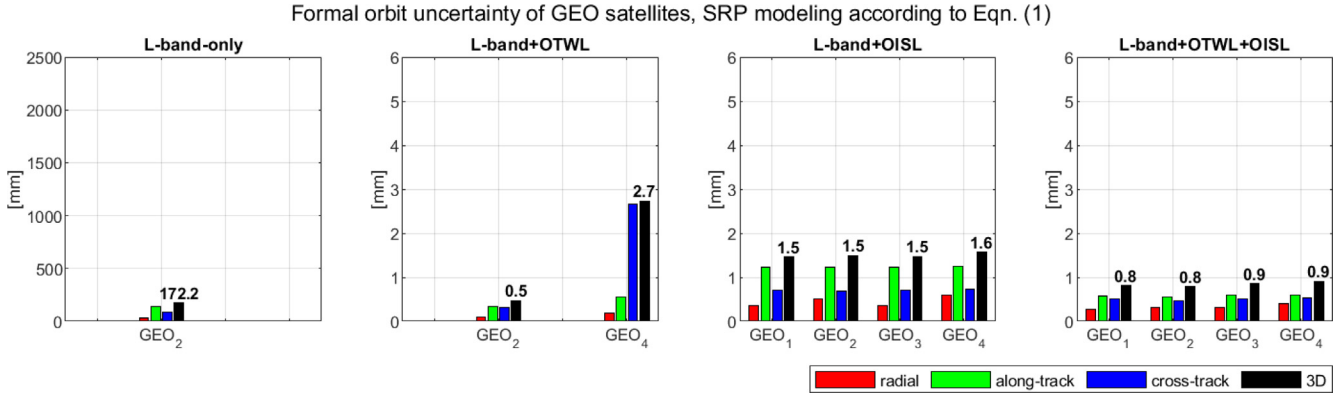

Fig. 8. Radial, along- and cross-track as well as 3D formal orbit uncertainties for each of the four simulated GEO satellites in millimeters. The results are for a SRP modeling according to Eqn. (1). The values are averaged over the 10-days of the first simulation period (12th – 21st Feb. 2019; days of year: 043–052).

uncertainties – computed as the mean over one day – are averaged over the 10-days of the first simulation period. The behavior of the results is similar for the second simulation period.

In an L-band-only scenario a SRP modeling according to ECOM2 (Eqn. (1)) gives the best results. This was expected as the results in Marz et al. (2021) also showed that a single measurement technique used for the estima-

tion process cannot handle the adjustment of more SRP parameters so well. Achieving around 27–29 mm, all constellations are on a similar level. Using combinations of observation techniques in the estimation process, the formal orbit uncertainty is for almost all simulated scenarios in the range of around one millimeter down to sub-millimeters.

In the L-band + OTWL scenario, the MEO-only and MEO + IGSO constellations achieve formal orbit uncertainties of around 1.1–1.2 mm. The MEO + GEO constellation achieves far better results, with values of around 0.6 mm. This can be traced back to a continuous ground clock synchronization with the same GEO satellite clock. This leads to a more continuous satellite clock with less jumps. Here, we see the huge benefit of the combination of a one-way link with a two-way link. The clock synchronization from the two-way measurement minimizes the variability between the range and time synchronization of a one-way measurement.

Having OISL measurements in a scenario, the estimation of more than 9 SRP parameters generally improves the formal orbit uncertainty results. Using L-band + OISL, around 0.8–1.1 mm can be achieved for MEO-only, MEO + IGSO and MEO + GEO constellations. For L-band + OTWL + OISL, we achieve around 0.2–0.4.

4.2. IGSO formal orbit uncertainty

The formal orbit uncertainty for each IGSO satellite in a MEO + IGSO constellation is shown in Fig. 6 in radial, along- and cross-track directions as well as the 3D value, using SRP modeling according to Eqn. (1). Fig. 7 shows the same for a SRP modeling according to Eqn. (3). Generally, the achievable IGSO formal orbit uncertainties in the L-band-only and L-band + OTWL scenarios are not equal for the IGSO satellites. This is due to the visibility of the IGSO satellites with respect to the ground station network as previously shown in Fig. 3. In this simulation study, we use a very limited number of 16 ground stations. However, such an analysis can show the dependence on the number of ground stations that track an IGSO during its one-day orbit as well as the distribution of these stations.

Analyzing the L-band-only results shown in Fig. 6 and Fig. 7, IGSO-1 and −2 have lower formal orbit uncertainties than IGSO-3 and −4. The best achievable values are at around 45–47 mm using SRP modeling according to Eqn. (1) (see Fig. 6). A similar behavior can be found using L-band + OTWL which is almost inversely proportional to the total number of OTWL observations (see Fig. 3). The values are already in the low millimeter level for this scenario. IGSO-2 achieves the lowest values of around 1.2 mm (see Fig. 6). In the scenarios L-band + OISL and L-band + OTWL + OISL, all four simulated IGSO satellites achieve similar formal orbit uncertainties with respect to each scenario. This means that additional OISL observations can compensate the connectivity limitations regarding L-band and/or OTWL. Using SRP modeling according to Eqn. (3) (see Fig. 7), around 1.2 mm for L-band + OISL and around 0.3–0.4 mm for L-band + OTWL + OISL can be achieved.

4.3. GEO formal orbit uncertainty

Furthermore, we evaluate the formal orbit uncertainties for GEO satellites. Fig. 8 shows the formal orbit uncertainties in radial, along- and cross-track directions as well as the 3D value separately for the four GEO satellites using SRP modeling according to Eqn. (1). Fig. 9 shows the same for a SRP modeling according to Eqn. (4). Similar to the MEO + IGSO constellation, MEO + GEO L-band-only and L-band + OTWL scenarios are limited by the ground station network of 16 stations as shown in Fig. 4. As previously described, in the case of the L-band-only scenario no results for GEO-1, −3 and −4 and in the case of L-band + OTWL no results for GEO-1 and −3 are given due to the poor geometry of the visible ground stations. The GEO-2 formal orbit uncertainty resulting from the L-band-only scenario and using the ECOM2 SRP modeling (Eqn. (1)) is at around 17 cm (see Fig. 8). In the L-band + OTWL scenarios, the best formal orbit uncertainties are at around 0.5 mm for GEO-2. Hence, the best achievable GEO formal orbit uncertainty is even lower than the best for the IGSO satellites in the L-band + OTWL scenario. The results of all further scenarios including OISL measurements are similar to the IGSO results in terms of the achievable formal uncertainty level and are almost the same for all GEO satellites in each scenario.

4.4. MEO orbit error

The difference between the *true* and *adjusted* orbits gives the orbit errors. The orbit error analysis focuses on the systematic effects in the measurements as well as the orbit modeling errors, which we analyze based on one-day-arcs. Fig. 10 shows the resulting 3D-RMS orbit errors for MEO satellites comparing a MEO-only, a MEO + IGSO and a MEO + GEO constellation for all types of simulated scenarios. The 3D-RMS values – computed as the square root of the mean of the quadratic orbit differences over all satellites and all epochs per day – are averaged over the 10-days of the first simulation period.

Using only L-band measurements in a scenario, modeling according to ECOM2 (Eqn. (1)) generally gives the best results. Again, this was expected from the results discussed in Marz et al. (2021). We can add that this is also valid for the simulated MEO + IGSO and MEO + GEO constellations. With around 25 cm for MEO + IGSO and around 24 cm for MEO + GEO, both constellations give a slight improvement compared to the MEO-only constellation (around 26 cm).

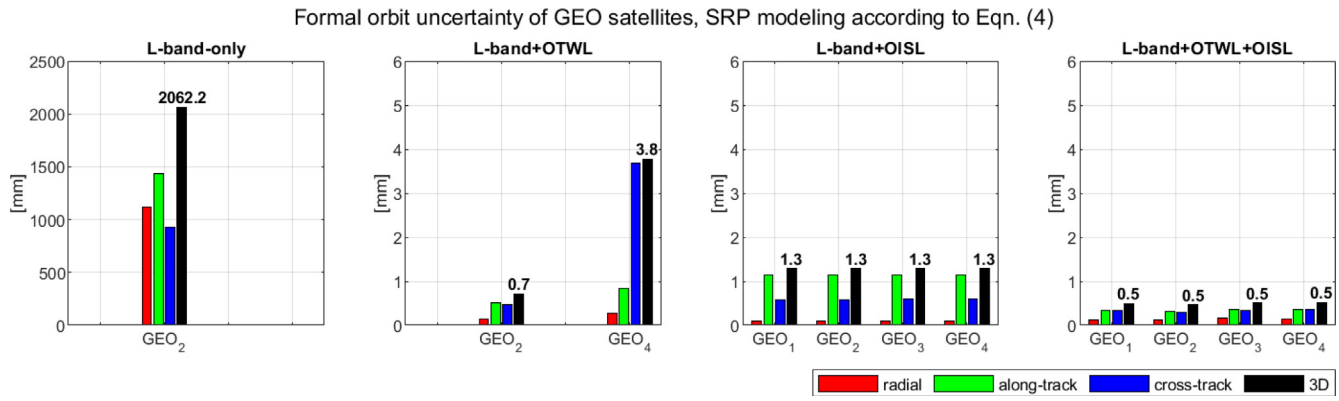

Fig. 9. Radial, along- and cross-track as well as 3D formal orbit uncertainties for each of the four simulated GEO satellites in millimeters. The results are for a SRP modeling according to Eqn. (4). The values are averaged over the 10-days of the first simulation period (12th – 21st Feb. 2019; days of year: 043–052).

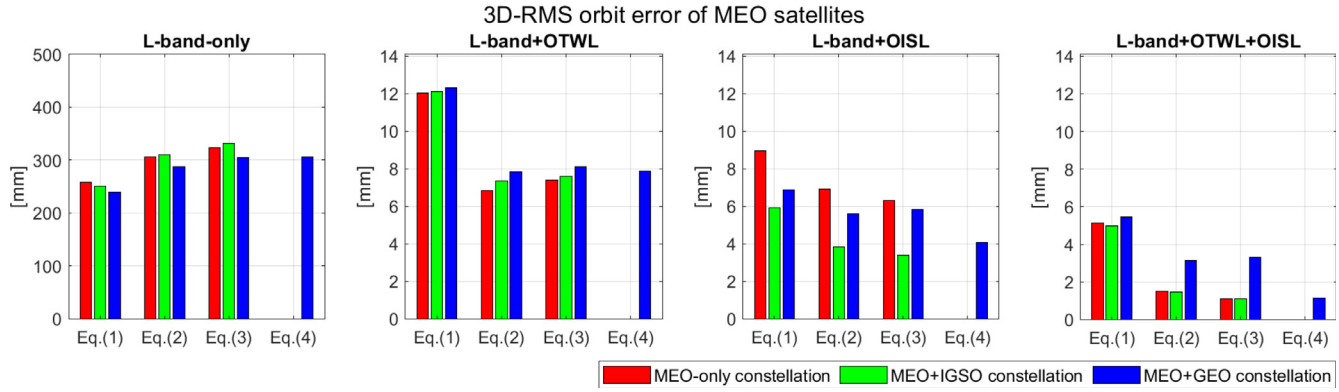

Fig. 10. 3D-RMS orbit errors (*true – adjusted* orbits) of MEO satellites in millimeters, resulting from a MEO-only, a MEO + IGSO and a MEO + GEO constellation. The values are averaged over the 24 MEO satellites as well as the 10-days of the first simulation period (12th – 21st Feb. 2019; days of year: 043–052). The results are with respect to the different SRP modeling according to Eqn. (1), (2), (3) and additionally for GEO satellites Eqn. (4).

For scenarios with observation technique combinations, estimation of more than 9 SRP parameters generally improves the MEO POD. For the MEO + GEO constellation, the optimized SRP modeling according to Eqn. (4) gives the best results. The L-band + OISL scenario shows improvements for MEO POD using additional IGSO or GEO satellites in the constellation as well, with around 3.4 mm for MEO + IGSO and around 4.1 mm for MEO + GEO, compared to around 6.3 mm for MEO-only. This mean that a constellation with additional IGSO satellites gives a slight improvement for MEO POD compared to using additional GEO satellites.

A similar behavior with regard to the SRP modeling shows the L-band + OTWL + OISL scenario, however, with a 3D-RMS MEO orbit errors of around 1.1 mm the MEO-only, MEO + IGSO and MEO + GEO are all on the same level. Scenarios with L-band + OTWL measurements do not show improvements using additional IGSO or GEO satellites in the constellation. Here, the best achievable orbit error values are for a MEO-only constellation (around 6.8 mm).

For MEO POD the orbit accuracies behave similar for the second simulation period.

4.5. IGSO orbit error

In a further analysis we evaluate the impact on IGSO POD in a constellation together with Galileo MEO satellites. Fig. 11 shows the resulting radial, along- and cross-track directions as well as the 3D-RMS orbit errors separately for the four IGSO satellites using SRP modeling according to Eqn. (1). Fig. 12 shows the same for a SRP modeling according to Eqn. (3).

As already noticed for the formal orbit uncertainty, the achievable IGSO orbit accuracy in the L-band-only and L-band + OTWL scenarios is not equal for the IGSO satellites due to the visibility of the IGSO satellites with respect to the ground station network (see Fig. 3).

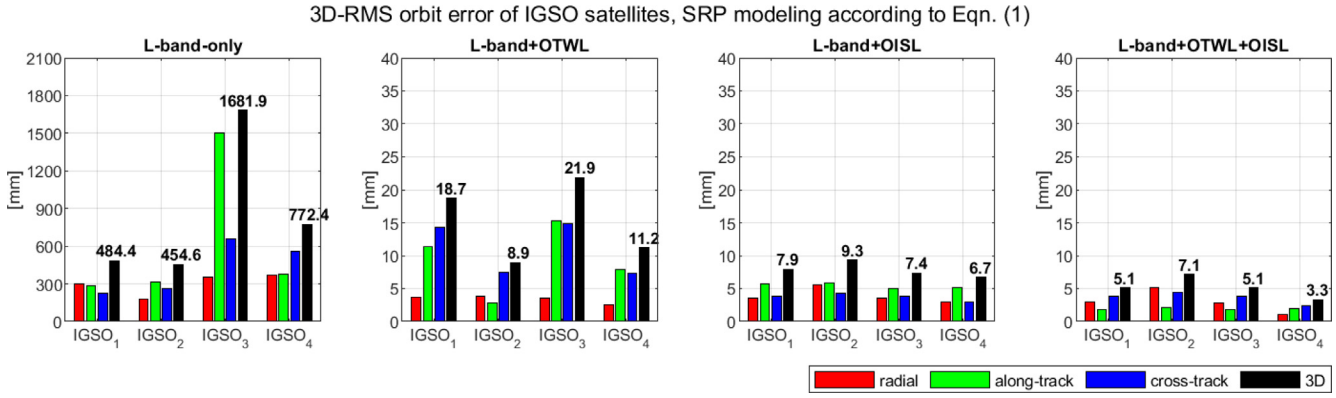

Fig. 11. Radial, along- and cross-track as well as 3D-RMS orbit errors (*true – adjusted* orbits) for each of the four simulated IGSO satellites in millimeters. The results are for a SRP modeling according to Eqn. (1). The values are averaged over the 10-days of the first simulation period (12th – 21st Feb. 2019; days of year: 043–052).

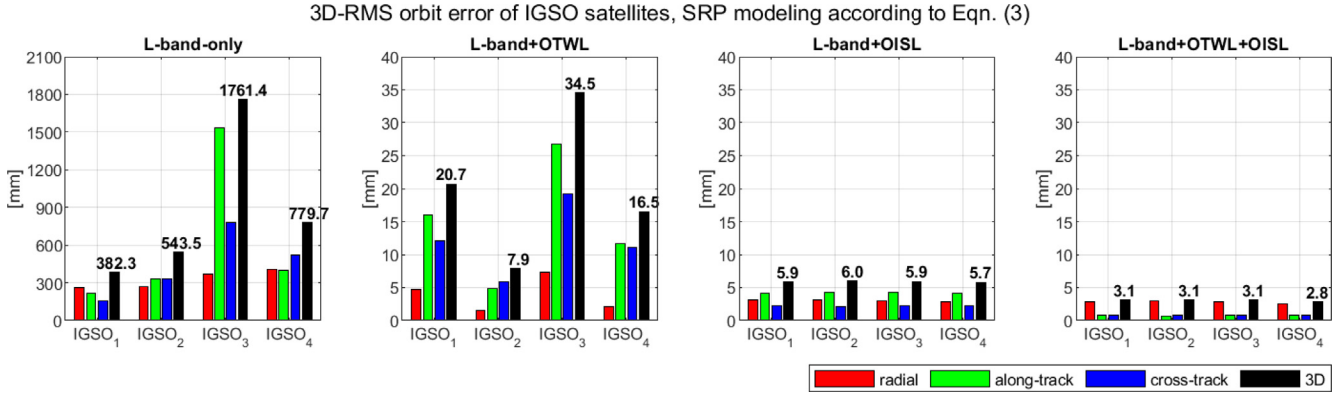

Fig. 12. Radial, along- and cross-track as well as 3D-RMS orbit errors (*true – adjusted* orbits) for each of the four simulated IGSO satellites in millimeters. The results are for a SRP modeling according to Eqn. (3). The values are averaged over the 10-days of the first simulation period (12th – 21st Feb. 2019; days of year: 043–052).

Analyzing the L-band-only scenario, IGSO-1 and −2 can be determined the best, while IGSO-3 is the worst. This is valid for both scenarios shown in Fig. 11 and Fig. 12. Especially the IGSO-3 along-track component suffers from having sparse observations mainly on the northern hemisphere. The best achievable IGSO POD 3D-RMS is at around 38 cm for IGSO-1 with SRP modeling according to Eqn. (3) (see Fig. 12).

In the L-band + OTWL scenario, in comparison to the formal orbit uncertainty results, the orbit errors behave not inversely to the total number of OTWL observations (see Fig. 3). This is typical for systematic errors, which do not influence the formal orbit uncertainty. Using SRP modeling according to Eqn. (3), IGSO-2 can be determined the best with a 3D-RMS of around 7.9 mm (see Fig. 12) and even 7.0 mm using a modeling according to Eqn. (2).

The L-band-only and L-band + OTWL scenarios analyzed above show a dependence on the ground stations network, even though this does not hold for IGSO-1, which is observed quite often by OTWL but the orbit accuracy is

Table 8
Biases of the orbit error results shown in Fig. 12. The values are averaged over the 10-days of the simulation period (12th – 21st Feb. 2019; days of year: 043–052).

Orbit error Bias [mm]	L-band + OTWL			L-band + OISL			L-band + OTWL + OISL		
	Radial	Along-track	Cross-track	Radial	Along-track	Cross-track	Radial	Along-track	Cross-track
IGSO-1	−4.4	1.2	−5.5	3.0	3.9	−0.6	2.8	−0.3	−0.3
IGSO-2	1.2	2.0	−2.0	3.0	4.1	−0.2	2.8	−0.03	0.1
IGSO-3	−6.4	8.2	−12.4	2.8	4.1	−0.2	2.8	0.1	0.1
IGSO-4	−1.0	8.1	−2.6	2.7	4.0	−0.5	2.4	−0.03	−0.2

not better than IGSO-3 and far worse than IGSO-4. Therefore, only one or two IGSO satellites can be determined with higher accuracy in our case.

This is less prominent in scenarios using additional OISL measurements. Furthermore, additional OISL measurements help to reduce the orbit errors in cross-track direction to a great extent. Using a SRP modeling according to Eqn. (3) (see Fig. 12) the 3D-RMS values are at around 6 mm for all four IGSO satellites.

Analyzing the L-band + OTWL + OISL scenario, the orbit errors behave similar to those of the L-band + OISL scenario, however, with a further improvement for each IGSO. In the scenario with SRP modeling according to Eqn. (3) (see Fig. 12) a 3D-RMS of around 3 mm is achievable for all IGSO satellites. The along-track and cross-track components largely improve compared to the L-band + OISL scenario, while the radial component orbit error does not gain from additional OTWL measurements. When we explicitly analyze the orbit errors in radial direction for the L-band + OTWL + OISL scenario, an offset is noticeable for all four IGSO satellites. The offset within the 10-days simulation period is at around 2.4–2.8 mm on average, the standard deviation is at around 0.6 mm for all four IGSO satellites. Therefore, we can conclude that the systematic errors and their correlations with range biases, clock biases and the troposphere delays in the least squares adjustment are one reason for larger orbit errors. Table 8 gives an overview of the biases in radial, along-track and cross-track directions for all observation technique combination scenarios. For the L-band + OTWL scenario, the biases of all three directions are in the range of several millimeters. However, the quality of the bias estimation is again dependent on the number of visible ground stations for each IGSO. In the L-band + OISL scenario, the biases in radial and along-track directions are in the range of several millimeters while no significant bias is present in cross-track. In the L-band + OTWL + OISL scenario only in the radial component a significant bias can be found.(See Table 9.)

From the comparison of the L-band + OISL and L-band + OTWL + OISL scenarios, once again the synergy of the L-band and OTWL measurement techniques is illustrated. The great benefit of L-band is the epoch-wise crosslinking of several satellites and stations. The epoch-wise combination of L-band and OTWL measurements stabilizes the OTWL measurements and allows the use of OTWL for the clock synchronization which supports the bias estimation, while OTWL observations calibrate L-band measurements.

For the second simulation period, Fig. 13 shows the IGSO orbit error results with SRP modeling according to Eqn. (1), Fig. 14 shows the same for SRP modeling according to Eqn. (3). In the L-band + OTWL scenario, IGSO-1 can be estimated much better compared to the first period.

Table 9
Biases of the orbit error results shown in Fig. 14. The values are averaged over the 10-days of the second simulation period (12th – 21st May 2019; days of year: 132–141).

Orbit error Bias [mm]	L-band + OTWL			L-band + OISL			L-band + OTWL + OISL		
	Radial	Along-track	Cross-track	Radial	Along-track	Cross-track	Radial	Along-track	Cross-track
IGSO-1	−0.1	−0.5	0.04	0.8	2.2	0.9	0.7	−0.3	0.1
IGSO-2	−0.1	2.2	−2.7	1.8	2.2	1.1	1.8	−0.3	0.1
IGSO-3	−3.8	−6.0	−1.6	1.2	2.1	0.7	0.9	−0.2	0.03
IGSO-4	−2.1	5.6	4.4	2.0	2.2	0.4	1.1	−0.3	−0.1

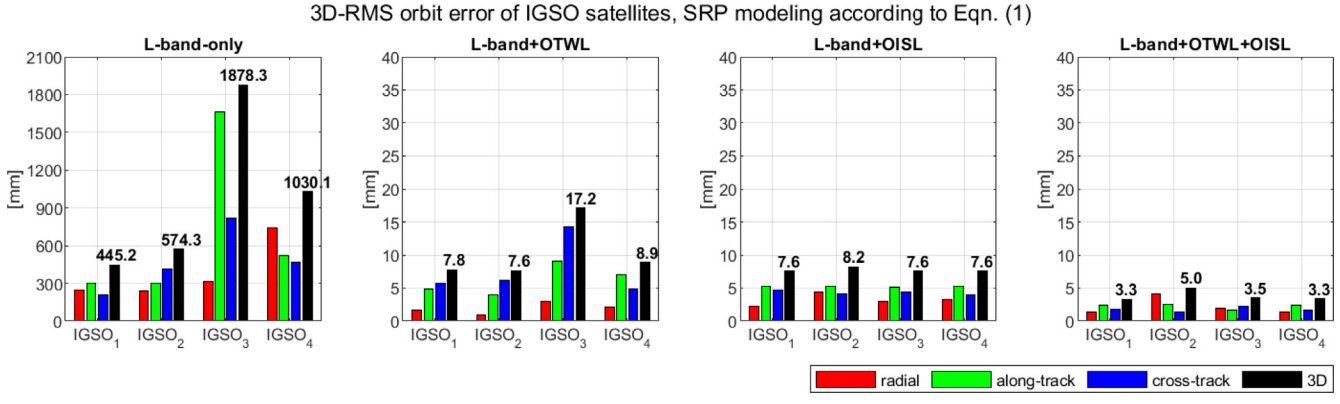

Fig. 13. Radial, along- and cross-track as well as 3D-RMS orbit errors (*true – adjusted* orbits) for each of the four simulated IGSO satellites in millimeters. The results are for a SRP modeling according to Eqn. (1). The values are averaged over the 10-days of the second simulation period (12th – 21st May 2019; days of year: 132–141).

Estimating more than 9 SRP parameters in scenario (3) shown in Fig. 14, the orbit error of IGSO-1 is even slightly lower than that of IGSO-2.

For the L-band + OISL and L-band + OTWL + OISL, the radial and cross-track component orbit errors are overall slightly smaller compared to the first simulation period. This is particularly noticeable for the L-band + OTWL + OISL scenario with SRP modeling according to Eqn. (3) (compare Fig. 12 and Fig. 14). With the radial component orbit error clearly being dominant in the first period, all three components are on a similar level for the second simulation period.

Table 9 gives an overview of the biases per direction of the results shown in Fig. 14. Comparing Table 9 with Table 8 it is noticeable that in the second period the biases could overall be estimated better. IGSO-1 in the L-band + OTWL scenario shows even no significant biases in the orbit error results.

While in some scenarios the orbits of certain IGSO satellites, especially of IGSO-1, can be estimated better compared to the other IGSO satellites, differently to the first simulation period, the overall values of the orbit errors of both periods are in about the same order of magnitude for all scenarios. This means that the IGSO satellites are not only dependent on the total number and distribution of the ground stations each IGSO can connect to, but also systematic effects of different links can have an influence on the final orbit determination results. As all IGSO satellites have the same beta angle, respectively, a clear dependence on the beta angle could not be found in the results. The variation of the results in both simulation periods do largely depend on the systematic effects and the bias estimation.

4.6. GEO orbit error

Furthermore, we evaluate the impact on GEO POD in a constellation together with Galileo MEO satellites. Fig. 15 shows the resulting radial, along- and cross-track directions as well as the 3D-RMS orbit errors separately for the four GEO satellites using SRP modeling according to Eqn. (1). Fig. 16 shows the same for a SRP modeling

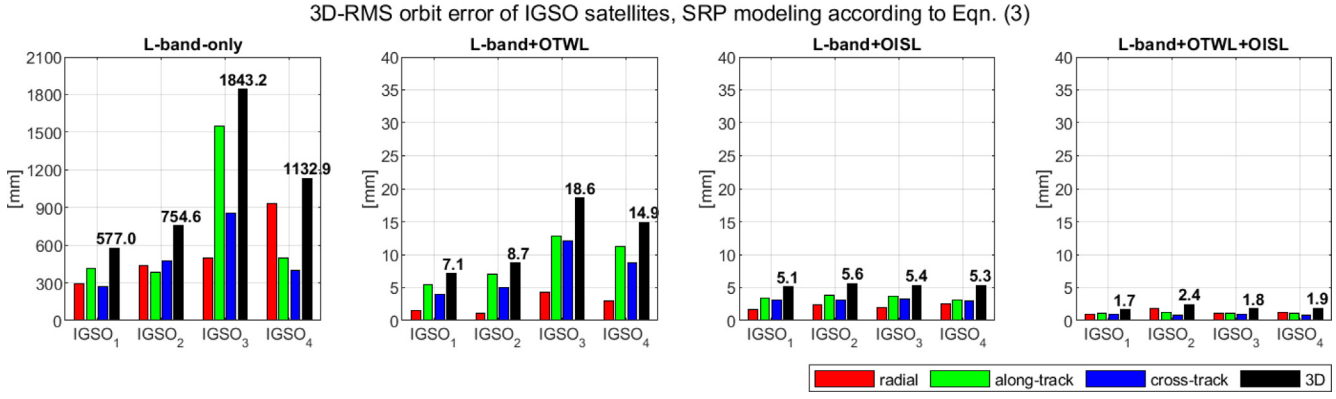

Fig. 14. Radial, along- and cross-track as well as 3D-RMS orbit errors (*true – adjusted* orbits) for each of the four simulated IGSO satellites in millimeters. The results are for a SRP modeling according to Eqn. (3). The values are averaged over the 10-days of the second simulation period (12th – 21st May 2019; days of year: 132–141).

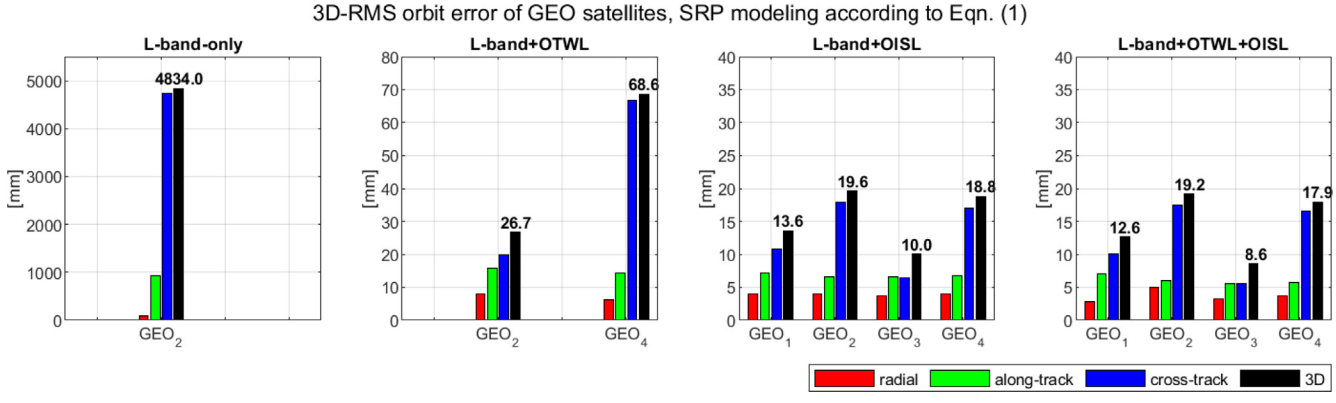

Fig. 15. Radial, along- and cross-track as well as 3D-RMS orbit errors (*true – adjusted* orbits) for each of the four simulated GEO satellites in millimeters. The results are for a SRP modeling according to Eqn. (1). The values are averaged over the 10-days of the first simulation period (12th – 21st Feb. 2019; days of year: 043–052).

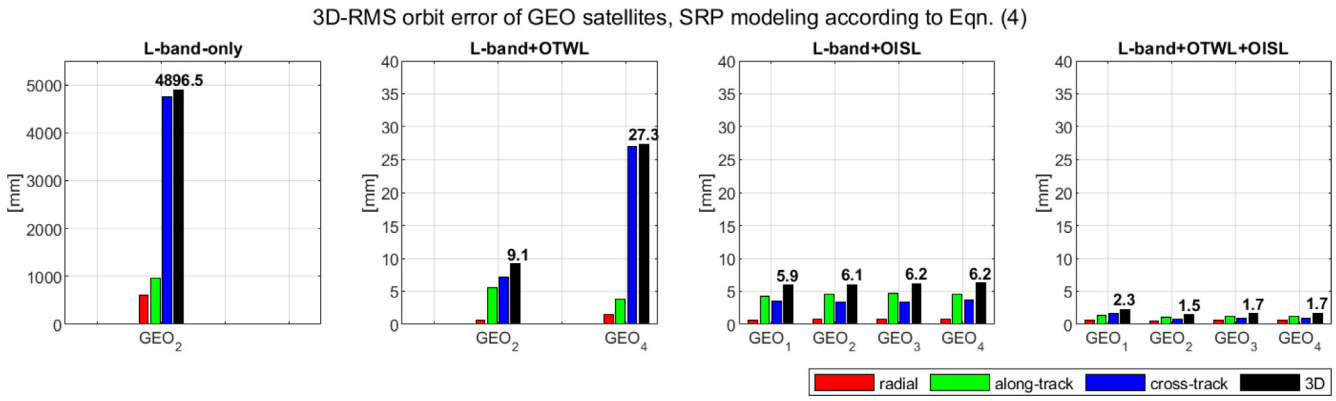

Fig. 16. Radial, along- and cross-track as well as 3D-RMS orbit errors (*true – adjusted* orbits) for each of the four simulated GEO satellites in millimeters. The results are for a SRP modeling according to Eqn. (4). The values are averaged over the 10-days of the first simulation period (12th – 21st Feb. 2019; days of year: 043–052).

according to Eqn. (4). As already seen in the GEO formal orbit uncertainty analysis and similar to the IGSO constellation, GEO POD is limited by the ground station network of 16 stations when using L-band-only and L-band + OTWL. Especially due to a worse estimation in cross-track direction, the GEO POD errors from a L-band-only scenario are huge compared to the other scenarios with additional measurement types and all the IGSO related scenarios. The 3D-RMS orbit error for GEO-2 is at around 4–5 m for both shown scenarios (see Fig. 15 and Fig. 16). This means in our case, using the 16 ground stations network, the number of ground stations distributed around the equator is not enough to perform orbit determination at the same level as for IGSO satellites using only L-band measurements in the solution. For the GEO satellites the limitation due to the number of ground stations can be compensated using further observation techniques, as shown in the following.

Analyzing the results given in Fig. 15, the main limitation of all these scenarios using the ECOM2 SRP model (Eqn. (1)) is the bad estimable cross-track component. SRP modeling according to Eqn. (4) optimizes the GEO POD using observation technique combinations (shown in Fig. 16). In a scenario with L-band + OTWL measurements around 9.1 mm can be achieved for GEO-2. Similar to the results with IGSO satellites, additional OISL measurements help to reduce the orbit errors in cross-track direction in this SRP modeling scenario. The L-band + OISL scenario gets the 3D-RMS orbit accuracy down to around 6 mm equally for all four GEO satellites. This is the same accuracy level which can be achieved for IGSO satellites (see Fig. 12). Using L-band + OTWL + OISL between around 1.6–2.3 mm are achievable for the four GEO satellites. These orbit errors are even slightly lower than those for IGSO satellites (see Fig. 12). The main reason is that the GEO radial component orbit errors are better determined compared to the IGSO results (compare Fig. 12 and Fig. 16). The biases in radial direction could be estimated much better in all scenarios.

For the second simulation period the GEO orbit accuracies behave similar to the first period.

4.7. Centre of mass error influence

In the previous chapters we discussed the orbit error for different scenarios. Our intention was to directly compare L-band-only POD results with those from observation technique combinations as well as different SRP modeling. Although, we took many systematic errors into account, we did not account for all errors that influence the measurement techniques in the same way. Such errors are for example attitude and center of mass (CoM) errors. In future it is expected that such errors can be controlled quite well as they are related to the modeling and manufacturing quality of the industry and space agencies. If this is not the case, it should be possible to estimate these errors to a great extent, especially when ISL measurements are included providing a much improved observation geometry.

The L-band + OTWL + OISL scenarios with SRP modeling according to Eqn. (3) for MEO and IGSO satellites and Eqn. (4) for GEO satellites achieve the overall best POD results from all our simulation. With errors at the level of 1–3 mm for MEO, IGSO and GEO satellites, these scenarios are our references and represent the prerequisite for a concept like GETRIS.

As an addition to our work, we performed a further simulation with an additional CoM error in a L-band + OT WL + OISL scenario. Therefore, we assumed an CoM error of 2 mm (3D-RMS), which is right within our POD accuracy.

For MEO satellites, the additional influence of the assumed CoM error to the POD accuracy is at about 1 mm. This leads to an absolute POD performance of

2 mm for the MEO satellites. For the IGSO and GEO satellites, the effect of the CoM error to the POD accuracy is at the sub-millimeter level.

5. Conclusions and outlook

In this simulation study we have analyzed the impact of geostationary orbit (GEO) or inclined geosynchronous orbit (IGSO) satellites as a potential expansion of the regular Galileo Medium Earth Orbit (MEO) constellation for MEO Precise Orbit Determination (POD) as well as the potential for IGSO and GEO POD having a MEO + IGSO or MEO + GEO constellation. We compared solutions estimated using L-band measurements with scenarios using observation technique combinations: L-band + OTWL (Optical Two-Way Links), L-band + OISL (Optical Inter-Satellite Links) and L-band + OTWL + OISL. We took many systematic effects into account for the optical links: a colored measurement noise, distance dependent effects, link biases and their variability as well as a troposphere error for OTWL measurements. Furthermore, we analyzed the influence of additional empirical SRP parameters in the estimation process for MEO, IGSO and GEO POD.

We systematically analyzed the different error contributions starting from orbit modeling errors, the best possible orbits – these show us how to improve the SRP modeling –, followed by an analysis of the influence of the geometry by discussing the formal orbit uncertainties and, finally, discussing the orbit POD solutions – including modeling errors, geometry and systematic errors. We are aware that this work is still far from a realistic project study, because the complexity of physical reality cannot be fully transported into a simulation environment. Therefore, the reported absolute performances are to be regarded as indicative, and will need confirmation/tuning based on real ranging data.

The combination of Galileo MEO with IGSO or GEO satellites to a common constellation improves the inclined geosynchronous and geostationary orbit accuracy as well. Starting from *mismodeled* geosynchronous orbits which were wrong by around 71 cm (IGSO) and 82 cm (GEO) on average, the orbit accuracy of IGSO and GEO can be improved to the same accuracy level as the Galileo MEO satellite orbits in some scenarios. Using a ground station network which consists only of the 16 ground stations is not sufficient to get the same POD results for all four IGSO or GEO satellites in the simulated constellation using L-band-only or L-band + OTWL measurements. In the L-band-only scenario, improvements of up to around 36–46 % with respect to the *mismodeled* orbits can be achieved at least for some IGSO satellites. Determination of inclined geosynchronous and geostationary orbits with sub-centimeter accuracy is possible in a L-band + OTWL scenario. In these scenarios the OTWL measurements stabilize the variability of L-band measurements, resulting from systematic errors of this measurement technique such as tropospheric delay variations and multipath, and on the other hand the great amount of GNSS measurements, which connect many satellites at the same epoch, help estimating the OTWL biases. In our case, estimating orbit parameters and clocks, there is no difference between fixing ground station clock biases and constraining them. If more parameters would be estimated, it might be better to calibrate the optical links as good as possible and not to estimate the biases. Especially the IGSO satellite orbit accuracies depend heavily on the measurement geometry, so the ground network has to be configured accordingly. The observed variability of the IGSO POD indicates that it could be worth to perform an analysis on the number and distribution of ground stations an IGSO can connect to. OISL measurements together with L-band observations compensate the variable number of L-band and OTWL observations for each IGSO or GEO satellite and homogenizes the orbit error of different geosynchronous orbit (GSO) satellites. All GSO satellites achieved the same orbit accuracy at around 6 mm in an L-band + OISL scenario. The overall best results were achieved in the L-band + O TWL + OISL scenario with *adjusted* orbits which were only wrong by around 1.5–3 mm.

Comparing the results of this paper with the POD results achieved for BeiDou IGSO and GEO satellites, with 38–45 cm orbit accuracy for some IGSO satellites using only L-band measurements, our results are a few decimeters behind those in Steigenberger et al. (2013). For GEO satellites using only L-band observations, with a RMS of 9 cm in radial and 93 cm in along-track direction we get results similar to Lei et al (2011) for these components and similar to e.g. Liu et al. (2016) and Wang et al. (2019) for the radial component. Furthermore, we are at a similar level as Steigenberger et al. (2013), but the results in cross-track direction cannot hold this accuracy level. However, as described before, the addition of OTWL observations to the L-band measurements improves the IGSO and GEO POD accuracy to a few centimeters. Comparing the L-band + OISL scenario to the LEO-GEO one-way communication link concept discussed in Knogl et al. (2011), we achieved a centimeter GEO orbit accuracy as well, using the ECOM2 SRP modeling (see Eqn. (1)). A SRP modeling according to Eqn. (4) reduced the GEO POD results to a 3D-RMS of 6 mm, showing that the modeling of solar radiation pressure gains from the additional precise measurements.

For Galileo MEO POD we can conclude that additional IGSO and GEO satellites in the satellite constellation improve the Galileo MEO satellite orbits using only L-band or L-band + OISL measurements. In the best L-band-only scenario we achieved around 3 % improvement with IGSO satellites and around 7 % with GEO satellites through jointly estimated common station parameters, in particular receiver clocks. These are rather minor improvements and would not economically justify expanding a GNSS constellation with GSO satellites, but it is an interesting side effect for MEO satellites when expanding the

constellation with GSO satellites. The improvement using L-band + OISL measurements is much larger: around 46 % with additional IGSO satellites and around 35 % with GEO satellites in the constellation. MEO POD did not achieve further improvements from additional IGSO and GEO satellites using OTWL observations together with L-band as the clocks are synchronized in the two-way measurement.

Considering that this work is a simulation study and the reported values have to be confirmed and tuned based on real ranging data, it is a step towards a Geodesy and Time Reference in Space (GETRIS), which aims to achieve GEO and IGSO POD accuracy in the same level as ground station coordinates can be determined (around 2 mm). This would also allow an accurate POD for altimetry or gravity field missions using autonomous dual one-way measurements from higher altitude satellites. Furthermore, with low millimeter level POD accuracy, e.g. draconitic errors in the station coordinates originating from orbit mismodeling can be reduced, leading eventually to a further improvement of the stability of the International Terrestrial Reference Frame (ITRF). Moreover, novel possibilities will be offered for using GSO satellites as connection to highly elliptical orbit satellites or satellites in Lunar transfer orbits, especially in combination with dual one-way observations.

Declaration of Competing Interest

The authors declare that they have no known competing financial interests or personal relationships that could have appeared to influence the work reported in this paper.

Acknowledgement

The German Research Foundation (DFG) is gratefully acknowledged for funding the project AOBJ:638291.

Appendix A. Supplementary material

Supplementary data to this article can be found online at https://doi.org/10.1016/j.asr.2022.11.009.

References

Arnold, D., Meindl, M., Beutler, G., Dach, R., Schaer, S., Lutz, S., Prange, L., Sosnica, K., Mervart, L., Jäggi, A., 2015. CODE's new solar radiation pressure model for GNSS orbit determination. J. Geod. 89, 775–791. https://doi.org/10.1007/s00190-015-0814-4.

Ashman, B. W.; Parker, J. J. K.; Bauer, F. H.; Esswein, M. (2018) Exploring the Limits of High Altitude GPS for Future Lunar Missions. 41st Annual AAS Guidance & Control Conference (AAS/GNC 2018), Breckenridge, Colorado, USA, February 2-7th, 2018. https://ntrs.nasa.gov/search.jsp?R=20180001247.

Bauer, F.H.; Moreau, M.C.; Dahle-Melsaether, M.E.; Petrofski, W.P.; Stanton, B.J.; Thomason, S.; Harris, G.A.; Sena, R. P.; Temple, L. P. III (2006): The GPS Space Service Volume. In: Proceedings of the ION GNSS 2006, Fort Worth, Texas, USA. 2503–2514.

Boehm, J., Werl, B., Schuh, H., 2006a. Troposphere mapping functions for GPS and very long baseline interferometry from European centre for medium-range weather forecasts operational analysis data. J. Geophys. Res. 111, B02406. https://doi.org/10.1029/2005JB003629.

Boehm, J., Niell, A., Tregoning, P., Schuh, H., 2006b. Global Mapping Function (GMF): a new empirical mapping function based on numerical weather model data. Geophys. Res. Lett. 33, L07304. https://doi.org/10.1029/2005GL025546.

Boehm, J., Heinkelmann, R., Schuh, H., 2007. Short note: a global model of pressure and temperature for geodetic applications. J. Geod. 81 (10), 679–683. https://doi.org/10.1007/s00190-007-0135-3.

Dach, R.; Lutz, S.; Walser, P.; Fridez, P. (Eds) (2015) Bernese GNSS Software Version 5.2. User manual, Astronomical Institute, University of Bern, Bern Open Publishing. doi: , ISBN: 978-3-906813-05-9.

Duan, B., Hugentobler, U., Selmke, I., 2019. The adjusted optical properties for Galileo/BeiDou-2/QZS-1 satellites and initial results on BeiDou-3e and QZS-2 satellites. Adv. Space Res. 63 (5), 1803–1812. https://doi.org/10.1016/j.asr.2018.11.007.

Enderle, W.; Gini, F.; Boomkamp, H.; Parker, J. J.K.; Ashman, B. W.; Welch, B. W.; Koch, M.; Sands, O. S. (2018) Space User Visibility Benefits of the Multi-GNSS Space Service Volume: An Internationally-Coordinated, Global and Mission-Specific Analysis. Proceedings of the 31st International Technical Meeting of the Satellite Division of The Institute of Navigation (ION GNSS+ 2018), Miami, Florida, USA, September 2018, pp. 1191-1207. doi: 10.33012/2018.15966.

ESA (2013) European Data Relay System: the SpaceDataHighway. esamultimedia.esa.int/docs/telecom/EDRS_factsheet.pdf.

Fernández, F.A., 2011. Inter-satellite ranging and inter-satellite communication links for enhancing GNSS satellite broadcast navigation data. Adv. Space Res. 47, 786–801. https://doi.org/10.1016/j.asr.2010.10.002.

Fernández, A.; Sánchez, M.; Beck, T.; Amarillo, F. (2010) Future Satellite Navigation System Architecture: Inter-Satellite Ranging and Orbit Determination. Proceedings of the 2010 International Technical Meeting of The Institute of Navigation, San Diego, CA, USA, pp. 872-879.

Fliegel, H.F., Gallini, T.E., Swift, E.R., 1992. Global positioning system radiation force model for geodetic applications. J. Geophys. Res. 97 (B1), 559–568. https://doi.org/10.1029/91JB02564.

Gill, E. (1999) Precise GNSS-2 Satellite Orbit Determination Based on Inter-Satellite-Links. In 14th International Symposium on Space Flight Mechanics, Iguassu, Brazil.

Guan, M., Xu, T., Li, M., Gao, F., Mu, D., 2022. Navigation in GEO, HEO, and Lunar Trajectory Using Multi-GNSS Sidelobe Signals. Remote Sens. 14 (2), art. 318. https://doi.org/10.3390/rs14020318.

Holmes, J.K., 1990. Coherent Spread-spectrum Systems. Krieger Publishing Co., FL.

Jing, S., Zhan, X., Lu, J., Feng, S., Ochieng, W., 2015. Characterisation of GNSS space service volume. J. Navig. 68 (1), 107–125. https://doi.org/10.1017/S0373463314000472.

Knogl, S. J.; Henkel, P.; Günther, Ch. (2011): Precise Positioning of a Geostationary Data Relay using LEO Satellites. Proceedings of the 53rd International Symposium ELMAR-2011, Zadar, Croatia, 14-16th September 2011, pp. 325-328.

Lei, H., Li, Z., Yang, X., Wu, W., Cheng, X., Yang, Y., Feng, C., 2011. Geostationary orbit determination using SATRE. Adv. Space Res. 48 (5), 923–932. https://doi.org/10.1016/j.asr.2011.05.005.

Li, Z., Ziebart, M., 2020. Uncertainty analysis on direct solar radiation pressure modelling for GPS IIR and Galileo FOC satellites. Adv. Space Res. 66 (4), 963–973. https://doi.org/10.1016/j.asr.2020.04.050.

Liu, J., Gu, D., Ju, B., Shen, Z., Lai, Y., Yi, D., 2016. A new empirical solar radiation pressure model for BeiDou GEO satellites. Adv. Space Res. 57 (1), 234–244. https://doi.org/10.1016/j.asr.2015.10.043.

Marini, J. W., and Murray, C. W. (1973) Correction of Laser Range Tracking Data for Atmospheric Refraction at Elevations Above 10 Degrees. NASA GSFC X-591-73-351

Marz, S., Schlicht, A., Hugentobler, U., 2021. Galileo precise orbit determination with optical two-way links (OTWL): a continuous wave

laser ranging and time transfer concept. J. Geod. 95, art. 85. https://doi.org/10.1007/s00190-021-01534-4.

Mendes, V. B., and Pavlis, E. C. (2004) High-accuracy zenith delay prediction at optical wavelengths. Geophys. Res. Lett. 31, art. L14602. doi:10.1029/2004GL020308.

Meng, W., Zhang, H., Huang, P., Wang, J., Zhang, Z., Liao, Y., Ye, Y., Hu, W., Wang, Y., Chen, W., Yang, F., Prochazka, I., 2013. Design and experiment of onboard laser time transfer in Chinese Beidou navigation satellites. Adv. Space Res. 51, 951–958. https://doi.org/10.1016/j.asr.2012.08.007.

Michalak, G., Glaser, S., Neumayer, K.H., Koenig, R., 2021. Precise orbit and Earth parameter determination supported by LEO satellites, inter-satellite links and synchronized clocks of a future GNSS. Adv. Space Res. 68 (12), 4753–4782. https://doi.org/10.1016/j.asr.2021.03.008.

Montenbruck, O., Gill, E., 2005. Satellite Orbits – Models, Methods. Applications, Springer, Berlin Heidelberg.

Moreau, M. C.; Bauer, F. H.; Carpenter, J. R.; Davis, E. P.; Davis, G. W.; Jackson, L. A. (2002) Preliminary Results of the GPS Flight Experiment on the High Earth Orbit AMSAT-OSCAR 40 Spacecraft. 25th Annual AAS Guidance and Control Conference, Breckenridge, CO, USA, Feb. 06-10.

Parker, J. J. K.; Bauer, F. H.; Ashman, B. W.; Miller, J. J.; Enderle, W.; Blonski, D. (2018) Development of an Interoperable GNSS Space Service Volume. Proceedings of the 31st International Technical Meeting of the Satellite Division of The Institute of Navigation (ION GNSS+ 2018), Miami, Florida, USA, September 2018, pp. 1246-1256. doi: 10.33012/2018.15968.

Riley, W. (2008) Handbook of Frequency Stability Analysis. NIST Special Publications 1065.

Samain, E., Vrancken, P., Guillemot, P., Fridelance, P., Exertier, P., 2014. Time transfer by laser link (T2L2): characterization and calibration of the flight instrument. Metrologia 51, 503–515. https://doi.org/10.1088/0026-1394/51/5/503.

Schäfer, W.; Flechtner, F.; Nothnagel, A.; Bauch, A.; Hugentobler, U. (2013) Geodesy and Time Reference in Space – GETRIS. ESA Study AO/1-6311/2010/F/WE Final Report GETRIS-TIM-FR-0001.

Schlicht, A.; Hugentobler, U.; Stetter, M.; Schäfer, W. (2014) Concept for a Geodetic and Time Reference in Space. Proceedings of the International Laser Ranging Service, Annapolis, USA.

Schlicht, A.; Hugentobler, U.; Marz, S.; Seel, S.; Biller, P. (2019) Concept for continuous wave laser ranging and time transfer to Galileo using optical two-way links. Proceedings of the 7th International Colloquium on Scientific and Fundamental Aspects of GNSS, Zurich, Switzerland.

Schlicht, A., Marz, S., Stetter, M., Hugentobler, U., Schäfer, W., 2020. Galileo POD using optical inter-satellite links: a simulation study. Adv. Space Res. 66 (7), 1558–1570. https://doi.org/10.1016/j.asr.2020.06.028.

Schreiber, K.U., Prochazka, I., Lauber, P., Hugentobler, U., Schäfer, W., Cacciapuoti, L., Nasca, R., 2010. Ground-based demonstration of the European Laser Timing (ELT) experiment. IEEE Trans. Ultrason., Ferroelectr. Frequency Control 57 (3), 728–737. https://doi.org/10.1109/TUFFC.2010.1471.

Springer, T.A., Beutler, G., Rothacher, M., 1999. A new solar radiation pressure model for GPS. Adv. Space Res. 23 (4), 673–676. https://doi.org/10.1016/S0273-1177(99)00158-1.

Steigenberger, P., Hugentobler, U., Hausschild, A., Montenbruck, O., 2013. Orbit and clock analysis of compass GEO and IGSO satellites. J. Geod. 87, 515–525. https://doi.org/10.1007/s00190-013-0625-4.

Tang, C., Hu, X., Zhou, S., et al., 2016. Improvement of orbit determination accuracy for Beidou navigation satellite system with two-way satellite time frequency transfer. Adv. Space. Res. 58 (7), 1390–1400. https://doi.org/10.1016/j.asr.2016.06.007.

UNNOSA (2021) The Interoperable Global Navigation Satellite Systems Space Service Volume (2nd edition). ISBN: 9789211304367.

Ventura-Traveset, J., López de Echazarreta, C., Lam, J.P., Flament, D., 2015. An Introduction to EGNOS: The European Geostationary Navigation Overlay System. In: Nurmi, J., Lohan, E., Sand, S., Hurskainen, H. (Eds.), GALILEO Positioning Technology. Signals and Communication Technology, vol. 182. Springer, Dordrecht, pp. 323–358. https://doi.org/10.1007/978-94-007-1830-2_14.

Walter, T., 2017. Satellite Based Augmentation Systems. In: Teunissen, P. J., Montenbruck, O. (Eds.), Springer Handbook of Global Navigation Satellite Systems. Springer Handbooks. Springer, Cham. https://doi.org/10.1007/978-3-319-42928-1_12.

Walter, T., Shallberg, K., Altshuler, E., Wanner, W., Harris, C., Stimmler, R., 2018. WAAS at 15. J. Inst. Navig. 65 (4), 581–600. https://doi.org/10.1002/navi.252.

Wang, C., Huo, J., Zhao, Q., Lui, J., 2019. Empirically derived model of solar radiation pressure for BeiDou GEO satellites. J. Geod. 93, 791–807. https://doi.org/10.1007/s00190-018-1199-y.

Winternitz, L. B.; Bamford, W. A.; Price, S. R. (2017): New High-Altitude GPS Navigation Results from the Magnetospheric Multiscale Spacecraft and Simulations at Lunar Distances. Proceedings of the 30th International Technical Meeting of The Satellite Division of the Institute of Navigation (ION GNSS+), Portland, Oregon, September 25th, pp. 1114-1126, 2017. https://ntrs.nasa.gov/search.jsp?R=20170009487.

Yang, Y., Yang, Y., Hu, X., et al., 2020. Inter-satellite link enhanced orbit determination for BeiDou-3. J. Navig. 73 (1), 115–130. https://doi.org/10.1017/S0373463319000523.

Zhao, Q., Wang, C., Guo, J., Yang, G., Liao, M., Ma, H., Liu, J., 2017. Enhanced orbit determination for BeiDou satellites with FengYun-3C onboard GNSS data. GPS Solut. 21 (3), 1179–1190. https://doi.org/10.1007/s10291-017-0604-y.

geosciences

MDPI

Article

Toward a Geodesy and Time Reference in Space (GETRIS): A Study of Apparent Satellite Clocks of a Future GNSS Satellite Constellation

Stefan Marz *, Anja Schlicht * and Urs Hugentobler

Forschungseinrichtung Satellitengeodäsie, Technical University of Munich, 80333 Munich, Germany
* Correspondence: s.marz@tum.de (S.M.); anja.schlicht@tum.de (A.S.)

Abstract: Today, concepts within the Global Geodetic Observing System (GGOS) aim a Terrestrial Reference System (TRS) with 1 mm accuracy and long-term stability of 0.1 mm/year. GETRIS (Geodesy and Time Reference In Space) is a concept that aims to realize a relativistic reference system based on satellites as an extension to the TRS. This helps with another goal of the GGOS, namely, the connection of different satellite layers with the TRS. For a valuable contribution to the GGOS's goals, we would expect to achieve precise determined satellite orbits at the level of 1–3 mm and satellite clocks with a picosecond accuracy. The use of increasingly precise links helps to improve the satellite precise orbit determination (POD) and is necessary to synchronize the clocks in the satellite/station network. We analyze a complementary use of high-precision optical dual one-way links at the level of 1 mm precision together with the L-band. In previous studies, we analyzed the benefit for satellite POD, achieving Medium Earth Orbit (MEO) as well as geosynchronous orbit (GSO) accuracies at the low-millimeter level. In this work, we analyze the capabilities for clock synchronization. We compare two different clock types for estimation and prediction. We analyze different satellite constellations and different combinations of measurement links.

Keywords: GEO; IGSO; MEO; clock estimation; optical two-way link; inter-satellite link

Citation: Marz, S.; Schlicht, A.; Hugentobler, U. Toward a Geodesy and Time Reference in Space (GETRIS): A Study of Apparent Satellite Clocks of a Future GNSS Satellite Constellation. *Geosciences* **2023**, *13*, 173. https://doi.org/10.3390/geosciences13060173

Academic Editors: Mimmo Palano and Jesus Martinez-Frias

Received: 13 April 2023
Revised: 2 June 2023
Accepted: 5 June 2023
Published: 8 June 2023

1. Introduction

The aims for the future Terrestrial Reference System (TRS) are driven by the goals of the Global Geodetic Observing System (GGOS) [1]: 1 mm accuracy and long-term stability of 0.1 mm/year. The GGOS wants to achieve these goals by the collocated use of different observation techniques such as GNSS (Global Navigation Satellite System) measurements, VLBI (Very Long Baseline Interferometry), SLR (Satellite Laser Ranging), LLR (Lunar Laser Ranging), radar observations, ISL (Inter-Satellite Links) and gravity acceleration measurements. Furthermore, it is important for the GGOS to closely connect the different satellite layers from the Low Earth Orbit (LEO), via the Medium Earth Orbit (MEO), to the geosynchronous orbit (GSO).

The concept of a Geodesy and Time Reference in Space (GETRIS) was first discussed by [2,3]. The goal of GETRIS is to extend the TRS by a space-based relativistic reference system to contribute to the GGOS for the connection of the near Earth environment and deep space—the moon and beyond. With the complementary use of GNSS L-band measurements and dual one-way high-precision optical links between GSO and MEO satellites, a 1 mm orbit precision as well as a clock synchronization at the picosecond level shall be achieved. Dual one-way links are two one-way links that simultaneously measure between two entities, where both are transmitters and receivers. From a technical perspective, the optical links are comparable to the European Data Relay System (EDRS; [4,5])'s links, which are used for data communication with geostationary (GEO) satellites. Due to its high modulation rate, the EDRS link would technically allow ranging and time transfer with

high precision. To move toward a GETRIS, such optical links have to be adapted to perform calibrated ranging and time transfer.

The GENESIS satellite mission [6] has a similar approach as the one we follow with the GETRIS concept. By a collocated use of geodetic techniques in space—GNSS, SLR, VLBI and DORIS (Doppler Orbitography and Radiopositioning Integrated by Satellite)—the time and space reference systems on Earth are aimed to be improved and homogenized. GENISIS also intends to equip the satellite with a high-stability clock. The goal is to realize a TRS with accuracy of 1 mm and long-term stability of 0.1 mm/year, which also matches the GGOS's [1] goal. A GENESIS-like concept on GNSS satellites would even enhance the contribution to the GGOS and GETRIS.

The development of high-stability clocks has been rapidly growing in the recent past. The Cesium atomic clock (frequency stability in the low 10^{-13} region at one day), the Rubidium Atomic Frequency Standard (RAFS) (frequency stability in the low 10^{-14} region at one day) and the Passive Hydrogen Maser (PHM) (frequency stability in the high 10^{-15} region at one day) are clock types that are already used in satellites of different GNSSs. Satellite missions to test clocks with a significantly increased precision are already in preparation. These high-stability clock concepts are, e.g., clocks based on iodine cells and using optical frequency standards with a targeted frequency stability in the low 10^{-15} region for sample intervals between 100 s and 10,000 s [7–9]. The Deep Space Atomic Clock (DSAC; [10]), a trapped-ion atomic clock developed by the National Aeronautics and Space Administration (NASA), already demonstrated stability of 2×10^{-15} at 1 day and 3×10^{-15} at 23 days [10,11]. Along with the ESA mission Atomic Clock Ensemble in Space (ACES; [12,13]), a new clock concept is tested, which combines an Active Hydrogen Maser (AHM) and a laser-cooled Cesium clock, called the Project d'Horloge Atomique à Refroidissement d'Atomes en Orbite (PHARAO) [12–14]. The expected frequency stability and precision is at the level of 3×10^{-15} at 300 s, 3×10^{-16} at 1 day and 1×10^{-16} at 10 days. The main challenges of such future clock types are still the high costs and the complex manufacturing to be able to be carried by a satellite. For real-time processing and, thus, for clock prediction, it is important to have stable clocks. However, with an epoch-wise clock processing, a more stable clock does not give an improvement for clock estimation. To achieve improvements in the estimation, a possibility is to optimize the algorithm for clock modeling.

Optical two-way Inter-Satellite Links (OISL) is one measurement technique to perform high-precision dual one-way satellite-to-satellite tracking with a laser [8,15–17]. The impact of different ISL connectivity schemes was simulated in [15,18]. An alternative to OISL is optical two-way/dual one-way ground-to-satellite links. European Laser Timing (ELT; [19]), as part of the ACES mission, and T2L2 (Time Transfer by Laser Link; [20]) are two of the ground-to-satellite ranging and time transfer techniques. BeiDou already involved an optical measurement technique for two-way ranging, named Laser Time Transfer (LTT; [21]), and a two-way microwave technique, named Two-way Satellite Time and Frequency Transfer (TWSTFT; [22]), to achieve accurate time transfer. In [16,23], we introduced the Optical Two-Way Link (OTWL) measurement concept for a future GNSS MEO satellite constellation. This concept builds on dual one-way measurements and is the ground-to-space counterpart of OISL. In [16], we compared the OISL and OTWL measurement techniques and showed the benefits of synergistically using both techniques with Galileo L-band measurements for the POD of MEO satellites. In [17], we expanded the MEO satellite constellation by using inclined geosynchronous orbit (IGSO) and GEO satellites and analyzed the orbit errors. The resulting orbit errors from [17] showed that combinations of these measurement techniques also increase the orbit accuracy of IGSO and GEO satellites to the millimeter level.

While we only analyzed the orbit errors in [16,17], in this study we focus on the analysis of the satellite clocks from the simulation scenarios, which are identical to [17]. Our target is to estimate the satellite clocks, with respect to the reference clock, with an accuracy at the picosecond level. We assumed that all satellites in the constellation each

carry a PHM. The clocks were estimated epoch-wise using a least-squares adjustment. We analyzed the results of the clock estimation by the mean error and standard deviation of the estimated (apparent) clocks as well as the Allan deviation [24]. For comparison, we performed a further simulation using the ACES clock as an example of a clock with high stability for the future. Last, we performed the prediction of the estimated clocks for all scenarios up to one day. We analyzed the influence of the OTWL and/or OISL measurements being used in addition to the GNSS L-band observations as well as the expansion of the MEO constellation with either the IGSO or GEO satellites for the clocks' estimation and prediction. We want to indicate that this work is a simulation study and is still far from a realistic project study. We take many systematic errors for the observations' simulation and the orbit modeling into account, but the complexity of physical reality cannot be fully transported into a simulation environment.

The work is structured as follows. In Section 2, we described the simulation setup and initialize the simulation and estimation parameters. Section 3 presents the results of the clock analysis. Our conclusions are given in Section 4.

2. Simulation Setup and Estimation

For this paper, we evaluate the impact of different high-precision observation techniques used by a future GNSS satellite constellation for the estimation of satellite clocks. The whole simulation and estimation procedure is equal to [17]. For the simulations and analysis, we used a modified version of Bernese GNSS Software 5.2 [25]. Next, we describe the satellite constellations used (Section 2.1), the simulated observation techniques (Section 2.2) and the measurement errors (Section 2.3) as well as the parameters estimated in the least-squares adjustment (Sections 2.4 and 2.5).

2.1. Satellite Constellations and Ground Station Network

We selected the Galileo MEO satellite constellation—the satellite properties are based on the first-generation Galileo satellites—as a typical GNSS satellite constellation and expanded the constellation by either four GEO or IGSO satellites. Analogous to the scheme of the GETRIS concept, we globally distributed the GSO satellites around the Earth [2,3]. An overview of the three satellite types used in this work is given in Table 1. We analyzed the results for the MEO-only, MEO+IGSO and MEO+GEO constellations. As the ground station network used for the L-band and OTWL measurements consists of 16 ground stations (see Figure 1), the GSO satellites had a different total number of visible ground stations. This allowed for an analysis of the necessary ground station visibility as well.

Table 1. Simulated satellite types.

Satellite Types	MEO	IGSO	GEO
Number of satellites in constellations	24	4	4
Constellation details	Walker constellation (56°: 24/3/1).	Equatorial passes of the IGSOs at the geographical longitudes 10°, 100°, 190° and 280° to obtain a homogeneous distribution around the Earth; inclination 52°. With respect to the Earth-centered inertial frame, all IGSO satellites are on the same orbital plane.	Placed at the geographical longitudes 10°, 100°, 190° and 280° to obtain a homogeneous distribution around the Earth. With respect to the Earth-centered inertial frame, all GEO satellites are on the same orbital plane.
Attitude mode	Nominal yaw-steering attitude.	Nominal yaw-steering attitude.	Orbit normal attitude mode.
Force models	Earth gravity field up to degree and order 12; ocean and solid Earth tides; direct tides from third bodies (Sun, Moon, Venus, Mars and Jupiter).		
Solar radiation pressure	Box-wing model according to [26].		

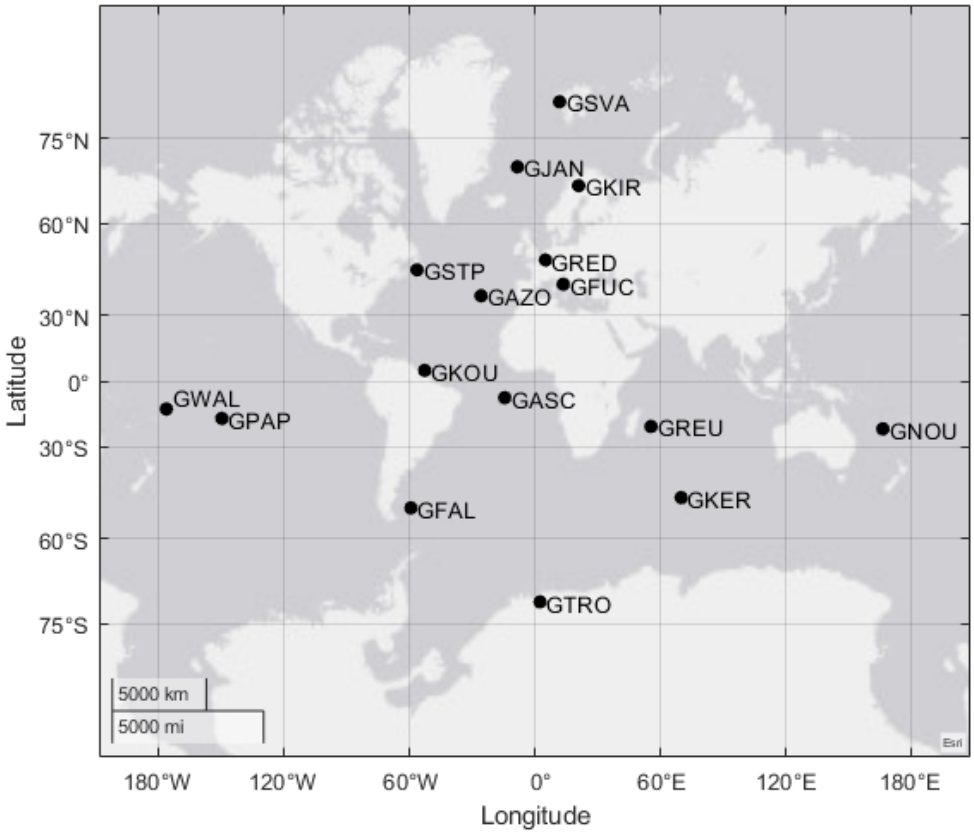

Figure 1. Ground station network used in this study.

Our analysis was based on a period of 10 days, the Galileo MEO repeat cycle. We processed 24 h observations, and the results were taken from one-day arcs. All satellites were each equipped with one clock, to which all the observations types refer to. For the first analysis, we emulated a PHM clock on each satellite. The PHM clocks were simulated with white frequency noise at the level of 1×10^{-12} and random walk at the level of 3.9×10^{-16} when integrating over one second. A quadratic phase drift was not simulated. For comparison, we performed further simulations with the ACES clocks, carried by all satellites in the constellation, representing a high-stability clock. We simulated the AHM of the ACES clock with flicker phase noise at the level of 1.4×10^{-13}, white frequency noise at the level of 3×10^{-14} and flicker frequency noise at the level of 1.35×10^{-15}, when integrating over one second. PHARAO was simulated with white frequency noise at the level of 1×10^{-13} when integrating over one second. The ACES clock noise is composed in such a way that the lowest noise always dominates. As PHARAO is a frequency standard, the ACES clock is expected to have no quadratic phase drift. We are aware that high-stability clock types such as the ACES clock will not be used as a standard GNSS satellite clock in the near future. Nevertheless, in this work we want to analyze the benefit when using the ACES clocks for GSO and MEO satellites.

2.2. Simulated Obervation Techniques

The simulated observation types for the study are the common GNSS L-band as well as optical ranging and time transfer measurements: OISL, as a dual one-way satellite-to-satellite measurement concept, and OTWL, as the dual one-way ground-to satellite counterpart. An overview of the different links and their simulation procedures is given in Table 2.

Table 2. Simulated measurement techniques.

Measurement Techniques	L-Band	OTWL	OISL
Simulation	Two-frequency code and phase measurements in E1 and E5a.	Dual one-way range measurements and clock differences' observations.	
Simulation details	Ionosphere free linear combination.	Scheduling according to [16]: one OTWL terminal per satellite; a ground station can connect to one satellite per epoch; long distance telescope movements for the ground stations are avoided when switching to the next satellite; minimum observation elevation is 30°, seen from ground stations.	Scheduling adapted from the connectivity scheme by [27]. Any-to-any scenario with bidirectional links. One OISL terminal per satellite.
Sampling rate in seconds	60	60	60
Number of used satellites	24 MEO satellites, optionally 4 additional IGSO or GEO satellites.		
Number of used ground stations	16	16	-
Number of simulated measurements per day: MEO-only constellation	408,740, in code and phase.	43,400	32,290
Number of simulated measurements per day: MEO+IGSO/GEO constellation	482,830/478,900, in code and phase.	45,040/44,950	33,900/33,890

In our simulations, it is assumed that each satellite is equipped with one terminal to perform OTWL measurements in the L-band+OTWL scenario. For OTWL, a ground station can, thus, connect with one satellite per epoch. In the following epoch, the ground station tracks the nearest available satellite by its elevation and azimuth to avoid long-distance telescope movements. The OTWL scheduling algorithm is optimized to avoid a ground station connecting with the same satellite in consecutive epochs. The minimum OTWL measurement elevation, as seen from the ground stations, is 30°. A more detailed description of the OTWL scheduling algorithm is given in [16].

Furthermore, we assumed that each satellite is equipped with one terminal to perform OISL measurements in the L-band+OISL scenario. The scheduling was an any-to-any scenario. The connectivity scheme was adapted from [27]. In the case of MEO+IGSO and MEO+GEO constellations, the IGSO or GEO satellites were integrated alongside the MEO satellites in the any-to-any link connectivity scheme, such that no GSO satellite connects to another GSO satellite in successive epochs.

For the L-band+OTWL+OISL scenario, the satellites were assumed to be equipped with two optical terminals: one to exclusively perform OISL measurements and the other to exclusively perform OTWL measurements.

In this study, we combined the three observation techniques in several ways, such as the L-band+OTWL, L-band+OISL and L-band+OTWL+OISL scenarios, and compared the results to the L-band-only scenario. We also performed the optical-only measurement technique scenario OTWL+OISL; however, in this scenario the clocks are singular [17]. Therefore, we do not consider the OTWL+OISL scenario in this work. Furthermore, we neglect relativistic effects on the clocks. No full recovery of the relativistic influences of the orbit may further disturb clock synchronization.

2.3. Simulated Measurement Errors

The simulated measurement errors for the L-band are collected in Table 3 and for the optical links in Table 4. A more detailed description of the simulation of the measurement techniques and the measurement errors is given in [15,17]. For the L-band, we only simulated white noise, while for the optical measurement types, we also accounted for other noise types. Furthermore, we used different troposphere models in the simulation and the further analysis. In the case of the L-band, we simulated Phase Center Variations (PCV) as an elevation-dependent error. Tables 3 and 4 show that we separated the inter-technique bias into a phase bias contribution and an optical bias contribution. Hence, for our simulations we assumed that these biases remain from the calibration with the optical links.

Table 3. Simulated L-band measurement errors.

L-Band Measurement Errors		Description/Remark
Measurement noise		White noise of 15 cm for code and 1.5 mm for phase measurements for each frequency.
Troposphere modeling errors	Simulation	Gridded VMF1 [28] model as an accurate model.
	Solution	GMF model [29] as a less accurate model.
Phase Center Variations (PCV)		A different pattern for each of the 16 ground stations and satellites, for transmitter and receiver. Multiplication by factor 50 for receiver and transmitter code measurements represents the worst-case scenario. The signatures are with resemblance to the multipath.
Constant phase bias		A different phase bias per satellite, randomly distributed up to 5 mm. This represents hardware delays in the phase.
Variation with once per revolution		A different variation in the phase bias per satellite, randomly distributed up to 5 mm; represents a temperature-dependent inter-technique bias per satellite.

Table 4. Simulated OTWL and OISL measurement errors. A detailed description of the different errors is given in [15].

Optical Link Measurement Errors		Description/Remark
Measurement noise	Flicker-phase noise	Induced by various effects (e.g., trapping of charge carriers in semiconductors) and occurs in all electronic devices. Selected noise level up to 0.5 mm.
	Jitter of the Phase Locked Loop (PLL)	A ranging distance-dependent error. Noise when varying between minimum and maximum ranging distance: - OTWL: 1.2–1.4 mm (MEO) and 1.7–1.9 mm (GSO). - OISL: 0.1–1.5 mm.
Troposphere offset (for OTWL only)		Simulated error: half the difference between the models of [30,31]. - Air pressure and temperature information from GPT [32]. - Relative humidity was set individually per ground station: min. 75%, max. 90%. Varies randomly per station and epoch, each up to around ±6%. - Max. error at 30° elevation 5 mm; min. error at 90° elevation 0.4 mm.
Bias due to the repeatability of the link		Uniformly distributed for each transmitter–receiver pair within ±0.5 mm.
Bias related to the equipment calibration quality		Bias per transmitter and receiver, randomly distributed between −0.5 and 0.5 mm; represents an inter-system bias, which affects the clock and the range.

2.4. Estimated Parameters

An overview of the estimated parameters, with respect to each measurement technique, is given in Table 5. The estimated Solar Radiation Pressure (SRP) parameters are discussed in more detail in Section 2.5. Furthermore, we estimated station-specific tropospheric wet zenith delays for the L-band (two-hour sampling), but we did not estimate troposphere parameters with respect to the OTWL measurements. We did not estimate ground station

coordinates. Satellite and ground station clock parameters were estimated epoch-wise. For the optical measurements, we estimated a daily range and clock synchronization bias for each transmitter and receiver. As we also simulated variable biases for the optical links, the estimation of daily biases did not fully represent the model. The simulated inter-technique bias also had a phase bias contribution, but for the L-band we did not estimate range and clock synchronization biases. We estimated phase ambiguities (float) for the L-band. The phase biases are absorbed by the ambiguity estimation to a great extent.

Table 5. Estimated parameters with respect to each observation technique.

Estimated Parameters	L-Band	OTWL	OISL
Station specific tropospheric zenith delays	Yes, every two hours.	No.	-
Ground station coordinates	No.	No.	-
Satellite initial state vectors and solar radiation pressure parameters	Yes.	Yes.	Yes.
Phase ambiguities (float)	Yes.	-	-
Epoch-wise satellite and ground station clock parameters	Yes.	Yes.	Yes.
	One clock for each satellite and each ground station.		
Daily range and clock synchronization biases	No.	Yes.	Yes.
		One transmitter and one receiver bias per entity, each for OTWL and OISL (also in scenarios with L-band+OTWL+OISL).	

Overall, the estimation of the biases leads to a rank-deficient normal equation matrix in our simulations. Therefore, we introduced constraints for the bias estimation in different scenarios: constraints within the range of the expected precision of the optical links (1 mm) and a solution with five times looser constraints.

2.5. Estimated SRP Parameters

SRP is the largest non-gravitational force disturbing the orbits of MEO and GSO satellites [33–35]. To include an SRP error in the procedure, we used the box-wing (BW) model from [26] when generating the orbits for the simulation. For the GNSS solutions, we used empirical SRP parameters in the least-squares adjustment. No BW parameters were estimated. ECOM2 [36], with a total of nine SRP parameters, was selected as the basic empirical SRP model. The model was defined in the DYB coordinate system: D points from the satellite to the Sun, Y is the direction along the solar panels and B completes the right-handed orthogonal system. The ECOM2 (Equation (1)) SRP parameters were estimated as constant as well as periodic sine and cosine terms, including a once per revolution term in B as well as two and four times per revolution terms in D. Δu is the argument of latitude with respect to the Sun. In the further context, the constant parameters had a subscript 0. A subscript s was used for the sine parameter and a c for the cosine parameter. The per revolution term was numbered following the corresponding directions: D, Y or B.

As discussed in [16], it is possible to estimate up to 13 SRP parameters in a POD process when using measurements of two or more different observation techniques. The L-band-only measurement scenario could not benefit from estimating more than nine SRP parameters. Therefore, for the results shown in this work, we used ECOM2 (Equation (1)) for scenarios only using the L-band.

$$\begin{aligned} D &= D_0 + D_{2c}\cos(2\Delta u) + D_{2s}\sin(2\Delta u) + D_{4c}\cos(4\Delta u) + D_{4s}\sin(4\Delta u), \\ Y &= Y_{0,} \\ B &= B_0 + B_{1c}\cos(\Delta u) + B_{1s}\sin(\Delta u), \end{aligned} \quad (1)$$

For scenarios using combinations of measurement techniques, we used an extended SRP model containing more than nine parameters. While the estimated parameters for D and Y stay the same, we extended further, per the revolution terms, for B. First, we extended the ECOM2 by the B_3 parameter (sine and cosine (Equation (2)).

$$B = B_0 + B_{1c} \cos(\Delta u) + B_{1s} \sin(\Delta u) + B_{3c} \cos(3\Delta u) + B_{3s} \sin(3\Delta u), \quad (2)$$

Second, we extended Equation (2) by the B_5 parameters (sine and cosine (Equation (3)). Again, the D and Y parameters are identical to ECOM2 (see Equation (1)) when using this SRP modeling.

$$B = B_0 + B_{1c} \cos(\Delta u) + B_{1s} \sin(\Delta u) + B_{3c} \cos(3\Delta u) + B_{3s} \sin(3\Delta u) + B_{5c} \cos(5\Delta u) + B_{5s} \sin(5\Delta u), \quad (3)$$

For each simulation scenario, we used the SRP modeling that is the best in the solution.

The DYB coordinate system is optimized for MEO and IGSO satellites but not for GEO satellites. As in orbit-normal mode, the orientation of the solar panel is not perpendicular to the Sun-satellite direction, so we used a different DYB orientation for the GEO satellites, named $\underline{D}\,\underline{Y}\,\underline{B}$. In this frame, $\underline{Y}$ is perpendicular to the orbital plane, $\underline{B}$ is perpendicular to $\underline{Y}$ and the Sun-satellite direction, and $\underline{D}$ completes the right-handed orthogonal system. In [17], we analyzed the modeling error introduced by the parameter differences of the true and mismodeled BW parameters for the GEO satellites. The result was a further optimized model, as shown in Equation (4). The maximum number of parameters is still 13.

$$\begin{aligned} \underline{D} &= \underline{D}_0 + \underline{D}_{1s} \sin(\Delta u) + \underline{D}_{2c} \cos(2\Delta u) + \underline{D}_{3s} \sin(3\Delta u) + \underline{D}_{4c} \cos(4\Delta u), \\ \underline{Y} &= \underline{Y}_0 + \underline{Y}_{1s} \sin(\Delta u) + \underline{Y}_{2c} \cos(2\Delta u), \\ \underline{B} &= \underline{B}_0 + \underline{B}_{1c} \cos(\Delta u) + \underline{B}_{2s} \sin(2\Delta u) + \underline{B}_{3c} \cos(3\Delta u) + \underline{B}_{4s} \sin(4\Delta u), \end{aligned} \quad (4)$$

3. Results

We discuss the results of this simulation study by analyzing the clock error (true—estimated clocks) for MEO satellites as well as IGSO and GEO satellites in the constellation. While we used PHM satellite clocks for the simulations performed in [17], all scenarios in this work are completed for two different clock types—the PHM and ACES clocks—carried by all satellites in the constellation. We analyze the clock error for the estimated period and discuss the clock prediction possibilities for the different scenarios. For each scenario, we select the SRP modeling according to the overall best solution—Equations (1)–(3) in the case of MEO and IGSO satellites and Equation (4) in the case of GEO satellites. The weights between the different observation techniques are shown in Table 6 and are selected in terms of the best orbit accuracies that could be achieved with a certain weighting. A variance component estimation was analyzed in [37].

Table 6. Weighting of OTWL and OISL observations with respect to L-band measurements $\sigma^2_{\text{L-band}} / \sigma^2_{\text{OTWL/OISL}}$.

	MEO-Only Constellation			**MEO+IGSO Constellation**			**MEO+GEO Constellation**		
SRP Modeling According to	**L-Band+ OTWL**	**L-Band+ OISL**	**L-Band+ OTWL+ OISL**	**L-Band+ OTWL**	**L-Band+ OISL**	**L-Band+ OTWL+ OISL**	**L-Band+ OTWL**	**L-Band+ OISL**	**L-Band+ OTWL+ OISL**
Equation (1)	25	2.5	2.5	25	2.5	2.5	-	-	-
Equation (2)	25	25	25	25	25	25	-	-	-
Equation (3)	25	25	25	25	25	25	-	-	-
Equation (4)	-	-	-	-	-	-	100	100	10

In the following, we first analyze the constraining of the clock synchronization biases in the case of OTWL measurements (Section 3.1), as this gives the constraining we use for all further analyses of the clock errors in this study. Then, we analyze the clock errors (Section 3.2) by a separate detailed analysis of the mean error (Section 3.2.1) and the standard deviation of the estimated clocks (Section 3.2.2) for the different scenarios. An analysis of the Allan deviation is given in Section 3.3. All the listed analysis steps are completed for the estimated period. Last, we analyze the possibilities of the clocks' prediction for all the simulated scenarios (Section 3.4). The results for the clock errors are mostly given in centimeters to relate to the positioning error that is analyzed in this work.

3.1. Analysis of the Constraining of the Clock Synchronization Biases

In different scenarios regarding OTWL observations, the clock synchronization biases are either hardly (at the level of the ranging precision of 1 mm) or loosely (five times looser constraints) constrained by introducing pseudo-observations. Scenarios without OTWL observations are not affected by the constraints' variations. In the following sections, we perform a separate detailed analysis on the mean error (see Section 3.2.1) as well as the standard deviation of the estimated clocks (see Section 3.2.2), but overall the different constraining types do not affect the standard deviation of the estimated clocks. Therefore, to analyze the effect of the constraining of the clock synchronization biases, we compute the mean error of the estimated clocks per satellite and per day of the simulation period. This leads to a total of 240 realizations for the MEO-only constellation and up to 280 realizations for the MEO+GSO constellation. These realizations are arranged in ascending order and the minimum, the 5%, the mean (average), the 95% and the maximum absolute values are extracted per scenario. Figure 2 shows the mean error of the estimated clocks as a function of the L-band+OTWL and L-band+OTWL+OISL scenarios as well as hard (left plot) or loose (right plot) constraining.

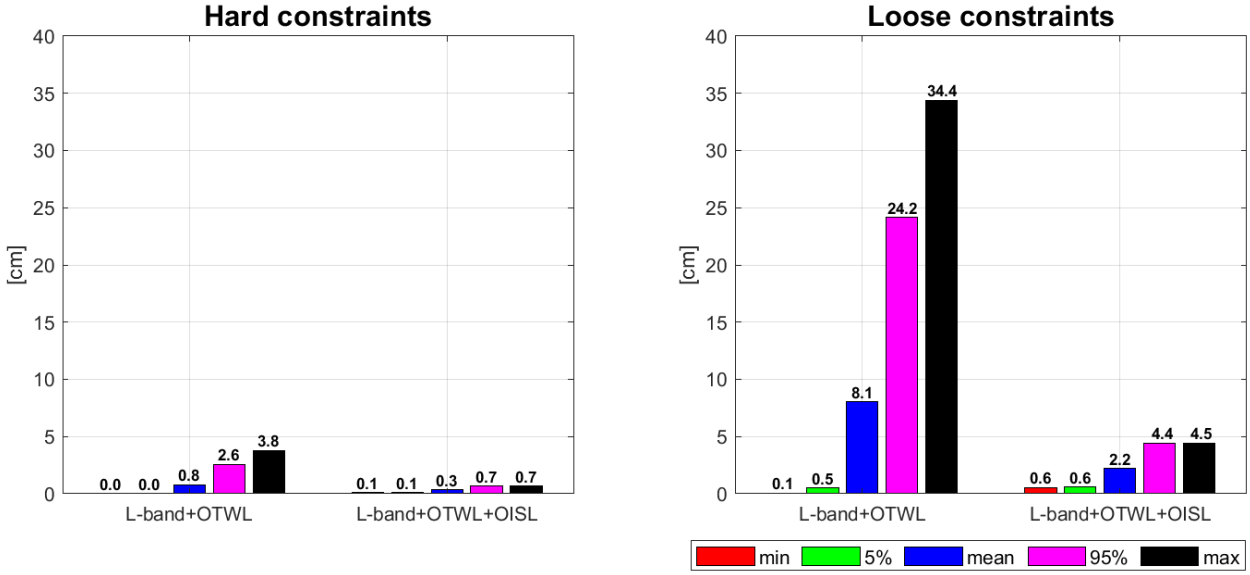

Figure 2. Analysis of the constraining of the clock synchronization biases in the case of OTWL observations. The plots show the mean error of the estimated clocks as a function of the type of observables used, and hard (**left plot**) or loose (**right plot**) constraining. The minimum, mean (average) and maximum values as well as the values bounding the 5% or 95% of the results are reported.

For the L-band+OTWL scenario, a large discrepancy between the minimum and maximum value is generally noticeable. The L-band+OTWL scenario with hard constraints gives a factor of about 10 lower mean errors than we obtain from the scenario with five times looser constraints. For the L-band+OTWL+OISL scenario, much lower maximum values as well as a much smaller discrepancy between the minimum and maximum values can be

achieved. This is due to the additional use of OISL observations. With the hard constraints, the mean error of the estimated clocks is on average at a factor of about 7.5 smaller than in the scenario with looser constraints. The same behavior can be found for results regarding the MEO+IGSO and MEO+GEO constellations. For our specific simulations, this leads us to use the hard constraints for all the further results presented in this work. Our goal is to realize a time and ranging reference. Therefore, hard constraining is needed, and for the optical link it is assumed that it is calibrated as good as possible.

3.2. Results of the Estimated Clocks

In this section, we analyze the results of the estimated clocks (true—estimated). Figure 3 shows the clock errors for different scenarios and 10 days of the simulation period from the MEO-only constellation. A similar behavior for the total error of the estimated clocks is achieved for the MEO+IGSO and MEO+GEO constellations. Referring to Figure 3, we provide a separate detailed analysis on the mean error and the standard deviation of the estimated clocks in the following subsections.

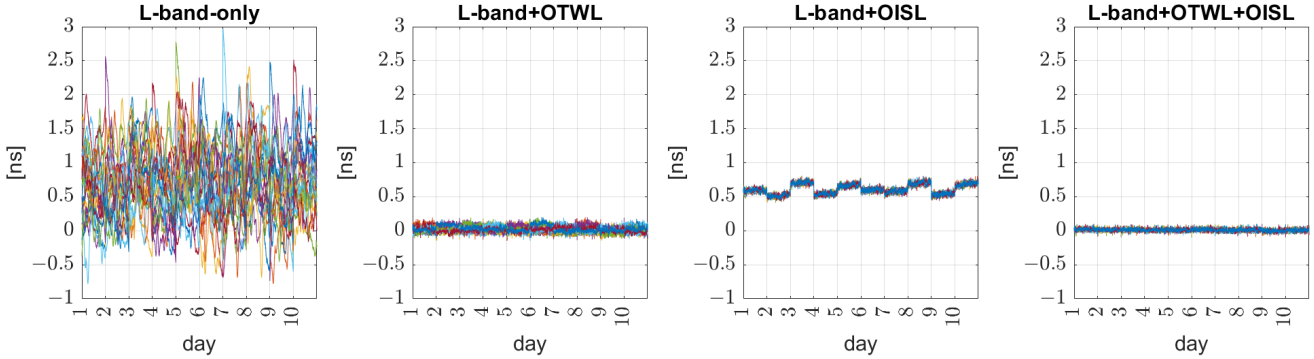

Figure 3. Total error of the estimated clocks for the different combinations of observation techniques and for the 10 days of the simulation period. Each color represents a different clock.

3.2.1. Mean Error of the Estimated Clocks

In this section, we analyze the mean error of the estimated clocks (true—estimated) for the different scenarios. The results shown in this section refer to simulations with the PHM clocks, but almost the same results are achieved for the ACES clocks. This is expected when estimating clocks epoch-wise. The advantage of a more stable clock is then only exploited in the prediction.

For the L-band-only scenario, a substantial mean error of the estimated clocks is noticeable (see Figure 3). Due to the epoch-wise clock estimation, errors from other sources—e.g., remaining orbit errors, errors due to a wrong bias estimation and dominant troposphere errors—are shifted to the clock. The optical observations support the L-band and prevent these errors from going into the clock. OISL does not allow for errors to be put into individual satellite clocks, as all satellite clocks are strongly connected. This is the huge benefit of OISL, as all satellites are synchronized with each other. The results for the clock errors are mostly given in centimeters to relate to the positioning error, which is analyzed in this work. Hence, the scenarios including OISL show the same mean error of the estimated clocks for all satellites for each daily solution, but the mean errors are still substantial. The reason is that OISL has no direct relation to the reference station on the ground, which only allows to uniformly distribute the clock synchronization biases for an average error. For the L-band-only or L-band+OTWL scenarios, the mean error of the estimated clocks varies for each satellite. However, for the scenarios including OTWL measurements, the estimated clock synchronization bias compensates for the systematic errors to a great extent. The reason is that OTWL has a direct relation to the reference station, and OTWL forces the solution toward the optical troposphere error—no model parameters are estimated for the optical troposphere delays, which are at the level of some millimeters. In the L-band+OTWL+OISL scenario, both the arguments of OISL and OTWL apply together.

Analogous to Section 3.1, we compute the mean error of the estimated clocks per satellite and per day of the simulation period, arranging the realizations in ascending order and extract the minimum, the 5%, the mean (average), the 95% and the maximum absolute values of all realizations. Figure 4 compares the mean error of the estimated clocks for the L-band-only, L-band+OTWL, L-band+OISL and L-band+OTWL+OISL scenarios in the MEO-only constellation. On average, the L-band-only scenario achieves a mean error of the estimated clocks of around 21 cm. The scatter of the mean error of the estimated clocks for the different realizations is substantial. For the L-band+OISL scenario, the average error reduces to around 18 cm. The minimum error is at 15 cm, and the maximum error is at around 21 cm. The scatter is from the daily variation in the estimated clock synchronization biases, as all satellites achieve an almost identical mean error of the estimated clocks per daily solution (see Figure 3). The L-band+OTWL scenario achieves an average error of 0.8 cm and 3.8 cm at the maximum. The L-band+OTWL+OISL scenario achieves the best results with an average error of 0.3 cm and a maximum error of 0.7 cm.

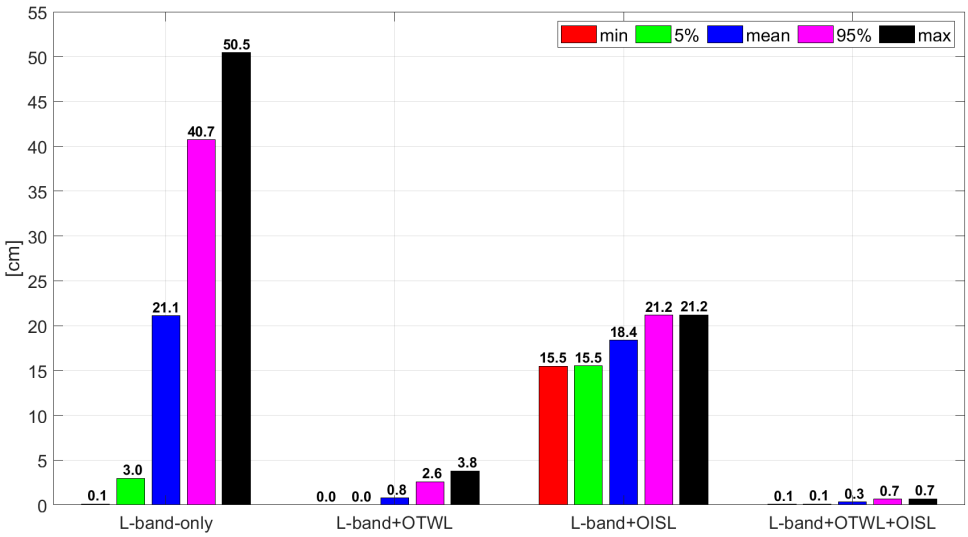

Figure 4. Analysis of the mean error of the estimated clocks, averaged for the 24 MEO satellites in the MEO-only constellation. The plot shows the mean error of the estimated clocks as a function of the type of observables used. The minimum, mean (average) and maximum values as well as the values bounding the 5% or 95% of the results are reported.

For additional IGSO satellites in the constellation, no significant changes in the mean errors of the estimated clocks are noticeable for the MEO satellites for all the scenarios compared to the MEO-only constellation.

For IGSO satellites, the mean errors of the estimated clocks behave similarly overall to the MEO satellites. However, due to the varying number of visible ground stations for each of the four IGSO satellites and, hence, the varying numbers of L-band observations, the scatter between the minimum and maximum values of the mean error of the estimated clock is much larger in the L-band-only scenario than for the MEO satellites. For L-band-only the best realization is at around 2 cm and the worst at around 70 cm. Although the number of OTWL observations varies with the number of visible ground stations for each IGSO, no significant degradation of the mean error of the estimated clocks shows up for the L-band+OTWL scenario, when analyzing the different realizations, compared to the results achieved for the MEO satellites. The same behavior is noticeable for the L-band+OISL scenario. However, the L-band+OTWL+OISL scenario shows about 1 cm worse mean errors of the estimated clocks for some realizations for the IGSO satellites. When averaging the mean errors of the estimated clocks per satellite over 10 days (see Figure 5), it is noticeable for the L-band+OTWL and L-band+OTWL+OISL scenarios that one IGSO satellite has a larger mean error of the estimated clock than the other IGSO satellite or all the MEO satellites.

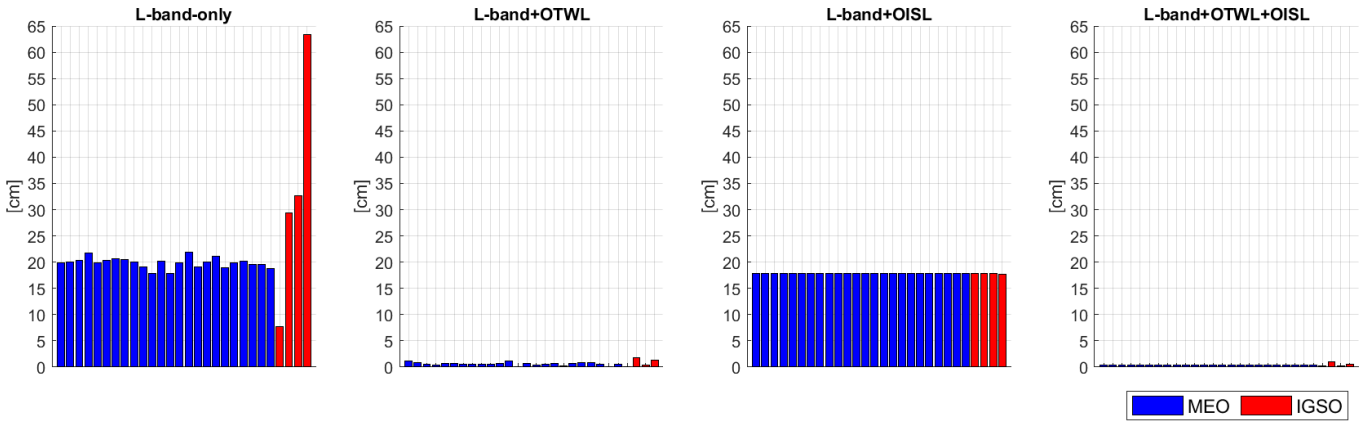

Figure 5. Analysis of the mean error of the estimated clocks by computing the mean per satellite per day and then averaging over the 10 days of the simulation period per satellite. Each blue bar is related to one of the 24 MEOs; the red bars relate to the IGSO satellites in the MEO+IGSO constellation.

For the MEO+GEO constellation, the L-band-only scenario achieves worse mean errors of the estimated clocks for the MEO satellites, compared to the MEO-only constellation. The degradation in the L-band-only scenario is at around 3 cm for the mean and the 95% values and 9 cm for the maximum value. For the scenarios with combinations of observation techniques, the mean errors of the estimated clocks are similar to the results from the MEO-only constellation.

For the GEO satellites, the coverage by the ground stations largely affects the results of the L-band-only and L-band+OTWL scenarios. While each IGSO satellite has visibility of at least four ground stations, some GEO satellites see less: GEO-1 sees two stations, GEO-2 sees five stations, GEO-3 sees one station, and GEO-4 sees three stations. Due to this, the normal equation matrix in the estimation is singular for some GEO satellites in the L-band-only and L-band+OTWL scenarios, as we estimate the orbit parameters in parallel to the clock parameters. Therefore, we have to exclude GEO-1, -3 and -4 from the L-band-only analysis. Due to the additional two-way observations in the L-band+OTWL scenario, the clocks can be synchronized with only three ground stations when estimating the orbit and clock parameters in parallel. Hence, we only exclude GEO-1 and -3 for the L-band+OTWL scenario. The mean clock errors of the estimated clocks, averaged over 10 days, are shown in Figure 6. For the GEO satellites, similar mean errors of the estimated clocks can be achieved compared to the MEO satellites, for all scenarios.

For MEO, IGSO and GEO satellites, the main outcome is that the OISL measurements homogenize the mean errors of the estimated clocks for all satellites, which is especially noticeable when averaging the results per satellite over several days. This is expected from OISL and underlines the advantage of having steady clock synchronizations between satellites at different altitudes. Although the OTWL observations in addition to the L-band measurements cannot synchronize satellite clocks to each other, the overall mean error of the estimated clocks is much smaller compared to the L-band+OISL scenario, as OTWL has a direct relation to the reference clock and, hence, helps to reduce the L-band's systematic errors. The L-band+OTWL+OISL scenario combines the advantages of OISL and OTWL.

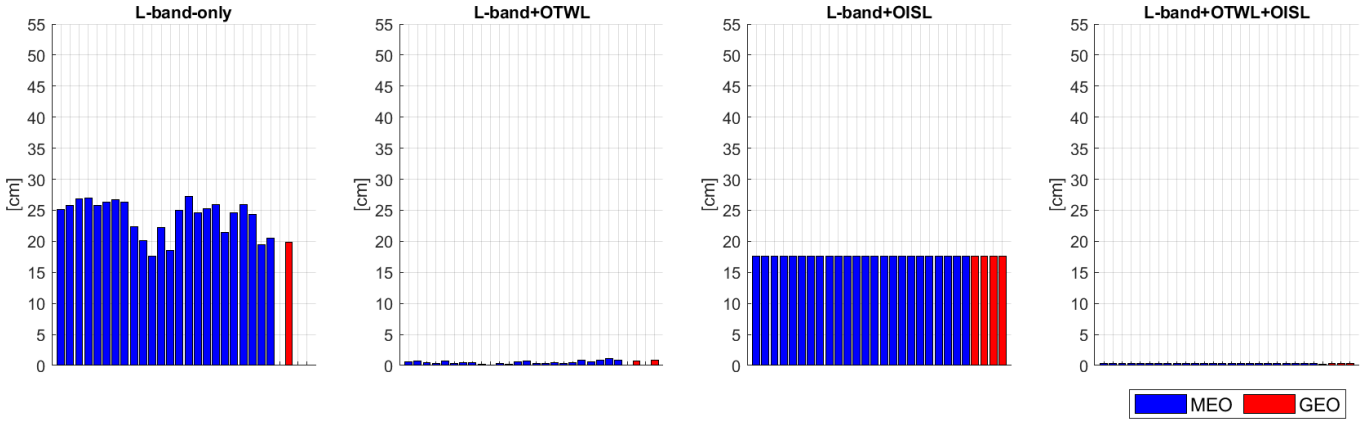

Figure 6. Analysis of the mean error of the estimated clocks by computing the mean per satellite per day and then averaging over the 10 days of the simulation period per satellite. Each blue bar is related to one of the 24 MEO; the red bars relate to the GEO satellites in the MEO+GEO constellation.

3.2.2. Standard Deviation of the Estimated Clocks

In this section, we analyze the standard deviation of the estimated clocks. The results shown in this section refer to the simulations with the PHM clocks but are analogous to the mean errors of the estimated clocks; the estimation results are similar when using the ACES clocks.

For the MEO satellites, the standard deviations of the estimated clocks are similar for the MEO-only and MEO+IGSO constellations. The results according to 240 realizations is shown in Figure 7 as an example for the MEO+IGSO constellation. The L-band-only scenario still has cm level standard deviations and a remarkable discrepancy between the minimum (around 2.7 cm) and maximum (around 18 cm) values. On the other hand, the standard deviations of the estimated clocks are at the mm level for the scenarios that include optical links (see also Figure 3). In addition, when the daily standard deviations per satellite are averaged over 10 days, the scatter of the results between the satellites is negligibly small with mean values of around 4–7 mm. The L-band-only scenario has a maximum scatter of about 4 cm and a mean of around 8 cm.

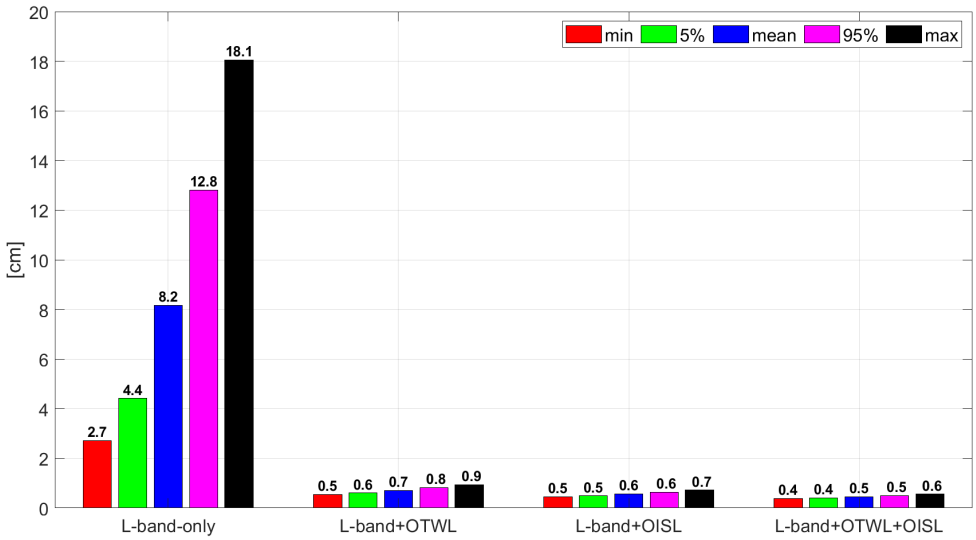

Figure 7. Analysis of the standard deviation of the estimated clocks for the 24 MEO satellites in the MEO+IGSO constellation. The plot shows the standard deviation of the estimated clocks as a function of the type of observables used. The minimum, mean (average) and maximum values as well as the values bounding the 5% or 95% of the results are reported.

For the MEO satellites in the MEO+GEO constellation, the daily results for the standard deviation of the estimated clocks are similar to the results of the MEO-only and MEO+IGSO constellations for the scenarios that include optical links. The L-band-only scenario shows worse results. Compared to the MEO-only and MEO+IGSO constellations, the degradation factor is around 1.8 for the mean value and around 2.7 for the 95% and the maximum value. The reason for the degradation in the L-band-only scenario is the correlation between the troposphere (visible in the estimated parameters of the tropospheric wet zenith delay) and clock parameters, as the final MEO orbit errors are rather smaller when adding the GEO satellites to the constellation (compare [17]).

Analyzing the scenarios with GSO satellites in the constellation, in the L-band-only scenario the best realization (minimum value) for the IGSO satellites is at around 5.7 cm, while the worst (maximum value) is at around 44 cm. Averaged over 10 days, the best IGSO achieves a standard deviation of the estimated clocks of around 15 cm and around 32 cm for the worst. The GEO satellite with good ground station coverage achieves around 26 cm for the best realization and around 114 cm for the worst. Averaged over 10 days, the standard deviation is at around 58 cm. Hence, the IGSO satellites achieve smaller standard deviations of the estimated clocks than the GEO satellites when having only L-band measurements. However, this can be traced back to the total number of visible ground stations.

For the scenarios with optical links included, the standard deviations of the estimated clocks for all IGSO satellites in the MEO+IGSO constellation as well as for all GEO satellites in the MEO+GEO constellation are at a similar level as for the MEO satellites. Hence, the optical links stabilize the clock errors of the MEO as well as the GSO satellites overall, to a great extent.

3.3. Allan Deviation

In this section, we analyze the frequency stability of the estimated clocks for the different scenarios. The frequency stability is defined as the variation in the frequency between two consecutive periods. Computing an Allan variance, the frequency stability is shown in the time spectrum. The square root of the Allan variance gives the Allan deviation. With the simulation period of 10 days, it is possible to determine the Allan deviation up to about 1 day.

Figure 8 (left) shows the Allan deviation for the estimated PHM clocks with respect to the true clocks for the L-band-only, L-band+OTWL, L-band+OISL and L-band+OTWL+OISL scenarios. The given results apply to the MEO satellite, as an example. The estimated clock from the L-band-only scenario does not reach the stability of the true clocks for the interval up to one day. On the other hand, the estimated clocks from the L-band+OISL, L-band+OTWL and L-band+OTWL+OISL scenarios are close to each other and reach the stability of the PHM for time intervals larger than about 1000 s. This indicates that the PHM is still limiting the potential of the combination of observation techniques. With a much more stable clock, the real potential of the combination of observation techniques can be investigated. The ACES clock is such a clock, which we use as an alternative clock in this work. While the L-band-only scenario mainly shows white noise, the downward slope of the L-band+OISL, L-band+OTWL and L-band+OTWL+OISL scenarios is larger for time intervals up to around 500 s. This is quantization noise, as the current International GNSS Service (IGS) clock's Receiver INdependent EXchange (RINEX) file—the file type we use to load our simulated clocks into the Bernese software—is primarily developed for GNSS, and, hence, the file accuracy is not quite sufficient for combinations of the observation techniques.

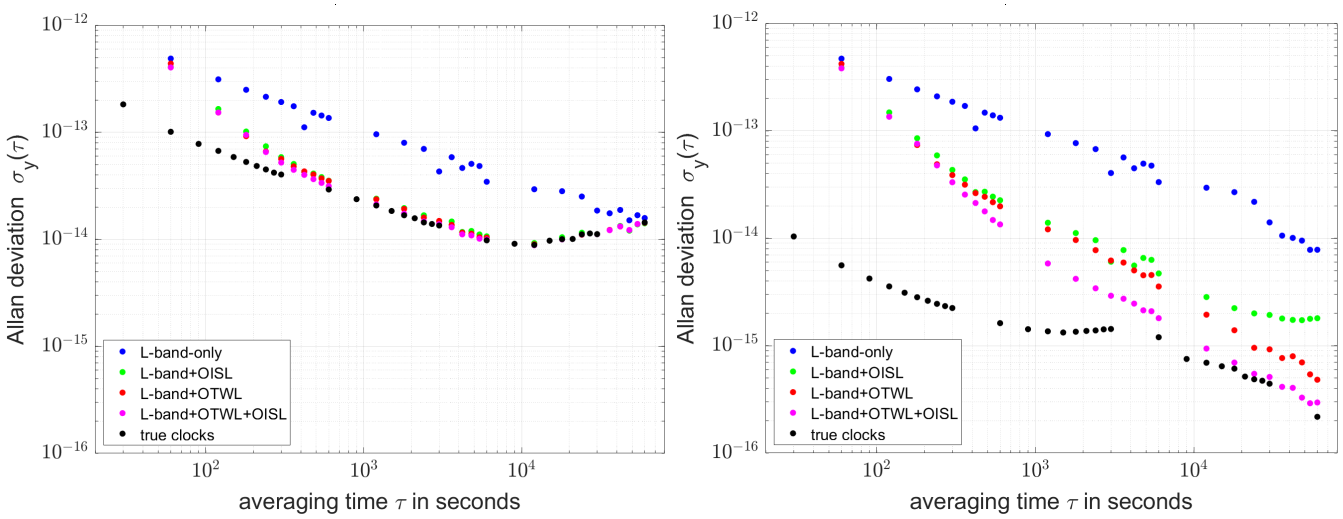

Figure 8. Allan deviation using PHM (**left**) and ACES (**right**) clocks in the simulation study. Results are for the MEO satellite with respect to the different combinations of observation techniques. The black dots refer to the true PHM and ACES clocks.

Figure 8 (right) shows the Allan deviation of the estimated clocks when using the ACES clocks in the simulation. For the L-band-only scenario, no improvement in frequency stability can be achieved compared to the use of the PHM clocks. In the L-band+OISL scenario, the frequency stability of the estimated clocks further improves but does not reach the frequency stability of the true clocks. The L-band+OTWL scenario behaves similarly to the L-band+OISL scenario up to intervals of 5000 s but achieves a minimal better frequency stability. For larger intervals, the L-band+OTWL scenario can gain from the long-term stability of the ACES clock. The L-band+OTWL+OISL scenario now achieves a far higher frequency stability compared to the estimated clocks from the L-band+OISL and L-band+OTWL scenarios. The estimated clocks even reach the stability of the true ACES clocks for intervals larger than about 20,000 s. This means that the L-band+OTWL+OISL scenario can completely benefit from the long-term stability of the ACES clock. On the other hand, there might still be potential for further improvements in the long-term stability when using even more stable clocks.

3.4. Clock Prediction

In this section, we analyze the possibilities for the prediction of clocks when using the different combinations of observation techniques. The prediction is performed for up to one day. The PHM clocks we use in this work are simulated from the noise taken from an Allan deviation (see the true clocks shown in Figure 8). We did not simulate a quadratic phase drift for the PHM clocks. We are aware that in reality the PHM also shows a quadratic phase drift, but for short prediction periods of up to about one day the effect of a quadratic phase drift is barely noticeable, as tested in a pre-analysis using the true clocks. On the other hand, the ACES clock is expected to have no quadratic phase drift, as PHARAO is a frequency standard. Hence, our clock prediction model reduces to a linear fitting model of the estimation interval of one day. We optimize the fit length for each scenario to achieve the overall best prediction results. For each scenario, we compute the 95the percentile from all realizations at different prediction times. As a comparative value, we also include the prediction results related to the true clocks. This value can also be seen as the best possible clock prediction value.

Figure 9 shows the 95% prediction values for the MEO satellites in the MEO-only constellation when using the PHM clocks in the simulation. Similar results can be achieved for the MEO satellites in the MEO+IGSO or MEO+GEO constellations. For the L-band-only scenario, a fit length of 12 h gives the best results, while the scenarios including

optical observation techniques as well as the true clocks achieved the best results for a fit length of 6 h.

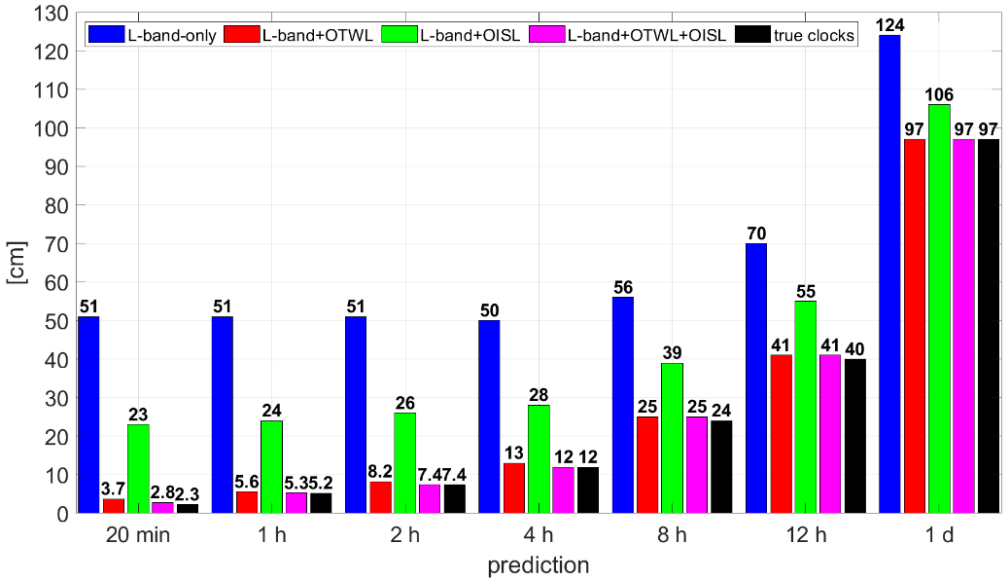

Figure 9. The 95th percentile at certain prediction times using PHM clocks. Results are for MEO satellites in the MEO-only constellation and for the different combinations of observation techniques. The black bars refer to the true PHM clocks.

After 20 min of prediction, the values are mainly dominated by the remaining mean errors of the estimated clocks. With the L-band+OISL scenario, around 51–55% of improvement was noticeable compared to the L-band-only scenario. The L-band+OTWL and L-band+OTWL+OISL scenarios achieve the best results by far, with an improvement of around 93–94% with respect to the L-band-only scenario and of around 84–88% in relation to the L-band+OISL scenario. The L-band+OTWL+OISL scenario is almost at the level of the true clock prediction errors. This is noticeable for all the prediction times shown and again underlines that the PHM is limiting the potential of the L-band+OTWL and L-band+OTWL+OISL scenarios for the clocks' prediction.

For longer prediction times, the percentage discrepancy between the different scenarios decreases. After a prediction of 8–12 h, the linear fitting starts to dominate the clock prediction errors. At a prediction time of one day, the L-band-only scenario achieves around 124 cm. The improvement when using the L-band+OISL scenario is at around 15% in relation to the L-band-only scenario. With a clock error of around 97 cm, the L-band+OTWL and L-band+OTWL+OISL scenarios improve by 22% compared to the L-band-only scenario.

For GSO satellites, the results concerning the L-band-only and L-band+OTWL scenarios are highly dependent on the number of ground stations each of the satellites can see. For the L-band-only scenario, the results are statistically not reliable. Furthermore, in the case of the L-band+OTWL scenario, there is a huge spread in the clock error of the prediction that does not give a reliable analysis foundation. Therefore, we only analyze the scenarios including OISL measurements, as those deliver more balanced prediction errors for the clocks and a better statistic. Almost the same results for the clock prediction are obtained for the IGSO and GEO satellites. The results are also quite similar to those of the MEO satellites for short prediction times. For long prediction times of around 12 h to one day, the clock error does not increase as much as for the MEO satellites, resulting in around a 22–27% lower clock error.

For the ACES clocks in the simulation, the fitting of a constant bias gives the best prediction results up to one day overall, as shown in Figure 10. The clock error barely decreases for the different combinations of observation techniques. Hence, all scenarios can

benefit from the high stability of the ACES clock. For the 20 min prediction, the clock errors from the different scenarios improve by about 1 cm compared to the scenarios with the PHM clocks. This is expected as, for short prediction times, the results are still dominated by the mean errors of the estimated clocks, which are similar to the ones from the scenarios with the PHM clocks in the simulation (see Section 3.2.1). For comparisons, the clock prediction errors at 20 min are at the low mm level for the true ACES clocks. After one day, the L-band-only scenario improves by a factor of around 2.4, and the L-band+OISL scenario improves by a factor of around 4–5, compared to the scenarios using the PHM clock. While the clock errors decrease by only a few millimeters for the different combinations of observation techniques, the true clock prediction error at one day is at around 1.7 cm. The L-band+OTWL scenario achieves a clock prediction error of 3.5 cm at one day. This is an improvement by a factor of about 28 compared to the scenario with the PHM clock. The L-band+OTWL+OISL scenario, which gives the best results, is at around 2.1 cm. This indicates that for this prediction interval, the L-band+OTWL+OISL scenario is approaching the stability of the ACES clock. Analogous to the PHM analysis, for the ACES clocks we only analyze the L-band+OISL and L-band+OTWL+OISL scenarios for the GSO satellites. Here, the IGSO and GEO satellites achieve almost the same clock prediction errors as the MEO satellites throughout the analyzed prediction interval.

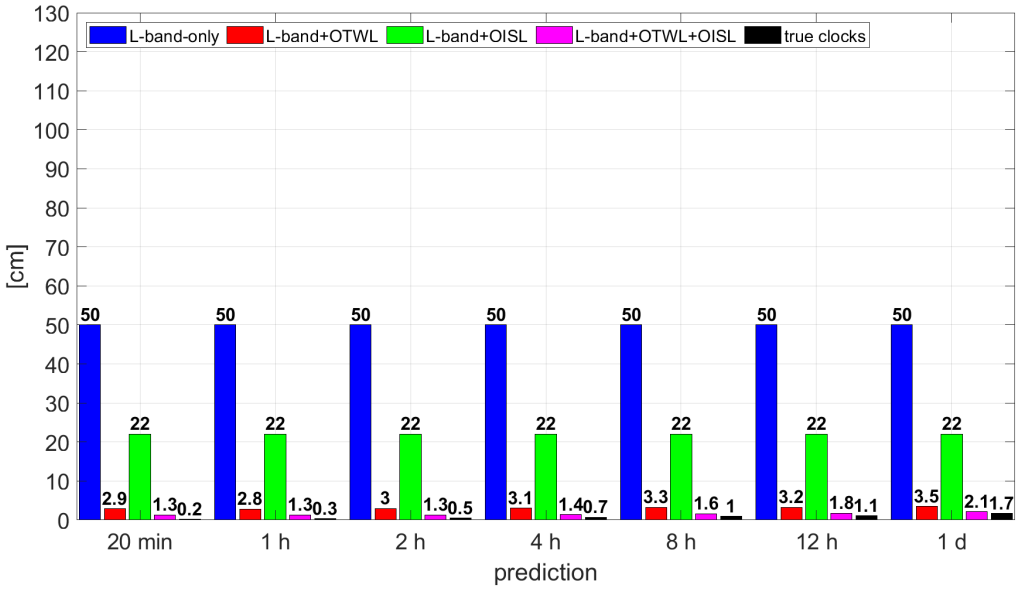

Figure 10. The 95th percentile at certain prediction times using ACES clocks. Results are for MEO satellites in MEO-only constellation and for the different combinations of observation techniques. The black bars refer to the true ACES clocks.

For today's procedures, performing clock synchronization from ground to space, the prediction results can be reduced by the mean, which is known from the last epoch of the estimated clocks. The mean clock error is still present when comparing the MEO system time with external time systems, but it cancels within the MEO system time and, hence, is irrelevant for the user. This leads to 35% lower clock prediction errors for the L-band-only scenario for short prediction times. The L-band+OTWL scenario only improves by about 13%. This indicates that the mean clock errors are already well-determined from the collocated use of the L-band and OTWL measurements. The L-band+OISL scenario achieves about the same results as the L-band+OTWL+OISL scenario. In the case of the PHM clocks, both scenarios reach the true clock prediction errors. For the ACES clocks, the L-band+OISL scenario's clock prediction errors are at around 10 mm, and the L-band+OTWL+OISL scenario's clock prediction errors are at around 6 mm, for short prediction times. Hence, the additional OTWL measurements help with further improvement, compared to the L-band+OISL scenario, when having the ACES clocks.

However, when a time system should be realized in space instead of on the Earth's surface, then the mean does not cancel, so having a small mean error of the estimated clocks is important.

4. Conclusions

In this simulation study, we analyzed the impact of optical dual one-way measurements—Optical Inter-Satellite Links (OISL) and ground–space-oriented Optical Two-Way Links (OTWL)—in addition to L-band measurements for clock estimation. We analyzed the capabilities for a pure Medium Earth Orbit (MEO) constellation as well as the MEO+IGSO (Inclined Geosynchronous Orbits) and MEO+GEO (Geostationary Orbit) constellations by the mean error of the estimated clocks, the standard deviation and the Allan deviation. Furthermore, we predicted the estimated clocks and analyzed the capabilities for predictions up to one day. All scenarios were computed for two different clock types: Passive Hydrogen Maser (PHM) and Atomic Clock Ensemble in Space (ACES). While the PHM clock represents a current standard clock type, the ACES clock is an example of a future high-stability clock.

We want to indicate that this work is a simulation study. Generally, the complexity of physical reality cannot be fully emulated in a simulation environment. Therefore, all the results discussed in this study are to be regarded as indicative and are not absolute performance results. With real data in the future, the presented results may be confirmed or need further tuning.

As we estimated a range bias and a clock synchronization bias for each transmitter and receiver, which led to a rank-deficient normal equation matrix, we had to introduce constraints in the case of the OTWL observations. In the analysis, we had to use hard constraints for the clock synchronization biases at the level of measurement precision of 1 mm. This allowed to achieve the clock error of the estimated clocks that need a time and ranging reference in space to be implemented. Five times looser constraints already led to 7–10 times worse clock errors.

In the case of the L-band+OISL scenario, the clock error is mainly dominated by the remaining mean errors of the estimated clocks. A collocated use of the L-band and OTWL in scenarios showed that the mean error of the estimated clocks can be estimated to a great extent. The L-band+OTWL scenario shows a smaller mean error of the estimated clocks on average than the L-band+OISL scenario by far. This is due to the direct relation of OTWL to the reference station, which allows for reducing the systematic effects from the L-band measurements. While the L-band-only and L-band+OTWL scenarios show a variation in the mean error for the different satellites, scenarios including the OISL measurements help to compensate for this discrepancy. This is the benefit of OISL: not only do all MEO satellites achieve about the same mean errors of the estimated clocks but also IGSO or GEO satellites do when included in the constellation. Achieving around 3 mm of the mean error of the estimated clocks on average, the L-band+OTWL+OISL scenario gives the best results by far, combining the advantages of OTWL and OISL. We could show that the L-band, OTWL and OISL are complementary. Moreover, all scenarios that include optical observations achieve the standard deviations of the estimated clocks at the mm level for the MEO, IGSO and GEO satellites.

Hence, concerning positioning accuracy, the clock error from the L-band+OTWL+OISL scenario is at a similar level as the orbit error, with 1–3 mm being achievable for the L-band+OTWL+OISL scenario (compare with [17]). The use of a high-stability clock does not give an improvement for the clock estimation as long as the clocks are estimated epoch-wise. Clock modeling in the estimation procedure helps to gain from a higher frequency stability, but this is not shown in this work. Furthermore, a common troposphere estimation for the L-band and OTWL might improve the results.

As the Allan deviation analysis shows, the potential of clock estimation is limited by the use of the PHM clocks for the scenarios using combinations of observation techniques. The use of the ACES clocks offers the possibility of the further improvement of the frequency

stability of the estimated clocks. The clocks' prediction profits as well. After one day of prediction, the clock error is at around 2.1 cm for the L-band+OTWL+OISL scenario when using the ACES clocks—compared to around 1.7 cm when using the true ACES clocks. With the PHM clocks, the clock prediction error worsens to around 97 cm—about the same as is achievable with the true clocks. This underlines the huge capability and potential of the combination of observation techniques with high-precision links in connection to a high-stability clock, as foreseen by the GETRIS (Geodesy and Time Reference In Space) concept.

Author Contributions: Conceptualization, S.M. and A.S.; methodology, S.M.; software, S.M.; validation, S.M., A.S. and U.H.; formal analysis, S.M.; investigation, S.M. and A.S.; data curation, S.M.; writing—original draft preparation, S.M.; writing—review and editing, S.M., A.S. and U.H.; visualization, S.M.; supervision, U.H. All authors have read and agreed to the published version of the manuscript.

Funding: This research received no external funding.

Data Availability Statement: Data sharing is not applicable.

Conflicts of Interest: The authors declare no conflict of interest.

References

1. Plag, H.-P.; Pearlman, M. (Eds.) *Global Geodetic Observing System: Meeting the Requirements of a Global Society on a Changing Planet in 2020*; Springer: Berlin/Heidelberg, Germany, 2009; ISBN 978-3-642-02686-7. [CrossRef]
2. Schäfer, W.; Flechtner, F.; Nothnagel, A.; Bauch, A.; Hugentobler, U. Geodesy and Time Reference in Space—GETRIS. ESA Study AO/1-6311/2010/F/WE Final Report GETRIS-TIM-FR-0001. 2013.
3. Schlicht, A.; Hugentobler, U.; Stetter, M.; Schäfer, W. Concept for a Geodetic and Time Reference in Space. In Proceedings of the International Laser Ranging Service, Annapolis, MD, USA, 27–31 October 2014.
4. Hauschildt, H.; Mezzasoma, S.; Moeller, H.L.; Witting, M.; Herrmann, J. European data relay system goes global. In Proceedings of the IEEE International Conference on Space Optical Systems and Applications (ICSOS), Naha, Japan, 14–16 November 2017; pp. 15–18. [CrossRef]
5. Calzolaio, D.; Curreli, F.; Duncan, J.; Moorhouse, A.; Perez, G.; Voegt, S. EDRS-C—The second node of the European Data Relay System is in orbit. *Acta Astronaut.* **2020**, *177*, 537–544. [CrossRef]
6. Delva, P.; Altamimi, Z.; Blazquez, A.; Blossfeld, M.; Böhm, J.; Bonnefond, P.; Boy, J.-P.; Bruinsma, S.; Bury, G.; Chatzinikos, M.; et al. GENESIS: Co-location of geodetic techniques in space. *Earth Planets Space* **2023**, *75*, 5. [CrossRef]
7. Schuldt, T.; Döringshoff, K.; Kovalchuk, E.; Keetman, A.; Pahl, J.; Peters, A.; Braxmaier, C. Development of a compact optical absolute frequency reference for space with 10^{-15} instability. *Appl. Opt.* **2017**, *56*, 1101–1106. [CrossRef]
8. Giorgi, G.; Schmidt, T.D.; Trainotti, C.; Mata-Calvo, R.; Fuchs, C.; Hoque, M.M.; Berdermann, J.; Furthner, J.; Günther, C.; Schuldt, T.; et al. Advanced technologies for satellite navigation and geodesy. *Adv. Space Res.* **2019**, *64*, 1256–1273. [CrossRef]
9. Schmidt, T.D.; Schlüter, S.; Schuldt, T.; Gohlke, M.; Calvo, R.M.; Lüdtke, D.; Dauth, M.; Lezius, M.; Michaelis, C.; Brzoska, A.; et al. COMPASSO: In-orbit Verification of Optical Key Technologies for Future GNSS. In Proceedings of the 53rd Annual Precise Time and Time Interval Systems and Applications Meeting, Long Beach, CA, USA, 25–27 January 2022; pp. 158–182. [CrossRef]
10. Tjoelker, R.L.; Prestage, J.D.; Burt, E.A.; Chen, P.; Chong, Y.J.; Chung, S.K.; Diener, W.; Ely, T.; Enzer, D.G.; Mojaradi, H.; et al. Mercury Ion Clock for a NASA Technology Demonstration Mission. *IEEE Trans. Ultrason. Ferroelectr. Freq. Control* **2016**, *63*, 1034–1043. [CrossRef] [PubMed]
11. Burt, E.A.; Prestage, J.D.; Tjoelker, R.L.; Enzer, D.G.; Kuang, D.; Murphy, D.W.; Robison, D.E.; Seubert, J.M.; Wang, R.T.; Ely, T.A. Demonstration of a trapped-ion atomic clock in space. *Nature* **2021**, *595*, 43–47. [CrossRef] [PubMed]
12. Cacciapuoti, L.; Salomon, C. Space clocks and fundamental tests: The ACES experiment. *Eur. Phys. J. Spec. Top.* **2009**, *172*, 57–68. [CrossRef]
13. Cacciapuoti, L.; Armano, M.; Much, R.; Sy, O.; Helm, A.; Hess, M.P.; Kehrer, J.; Koller, S.; Niedermaier, T.; Esnault, F.X.; et al. Testing gravity with cold-atom clocks in space. *Eur. Phys. J. D* **2020**, *74*, 164. [CrossRef]
14. Laurent, P.; Massonnet, D.; Cacciapuoti, L.; Salomon, C. The ACES/PHARAO space mission. *Comptes Rendus Phys.* **2015**, *16*, 540–552. [CrossRef]
15. Schlicht, A.; Marz, S.; Stetter, M.; Hugentobler, U.; Schäfer, W. Galileo POD using optical inter-satellite links: A simulation study. *Adv. Space Res.* **2020**, *66*, 1558–1570. [CrossRef]
16. Marz, S.; Schlicht, A.; Hugentobler, U. Galileo precise orbit determination with optical two-way links (OTWL): A continuous wave laser ranging and time transfer concept. *J. Geod.* **2021**, *95*, 85. [CrossRef]
17. Marz, S.; Schlicht, A.; Hugentobler, U. Geosynchronous satellites expanding a future GNSS satellite constellation: A precise orbit determination study. *Adv. Space Res.* **2023**, *71*, 624–644. [CrossRef]
18. Kur, T.; Kalarus, M. Simulation of Inter-Satellite Link schemes for use in precise orbit determination and clock estimation. *Adv. Space Res.* **2021**, *68*, 4734–4752. [CrossRef]

19. Schreiber, K.U.; Prochazka, I.; Lauber, P.; Hugentobler, U.; Schäfer, W.; Cacciapuoti, L.; Nasca, R. Ground-based demonstration of the European Laser Timing (ELT) experiment. *IEEE Trans. Ultrason. Ferroelectr. Freq. Control.* **2010**, *57*, 728–737. [CrossRef]
20. Samain, E.; Vrancken, P.; Guillemot, P.; Fridelance, P.; Exertier, P. Time transfer by laser link (T2L2): Characterization and calibration of the flight instrument. *Metrologia* **2014**, *51*, 503–515. [CrossRef]
21. Meng, W.; Zhang, H.; Huang, P.; Wang, J.; Zhang, Z.; Liao, Y.; Ye, Y.; Hu, W.; Wang, Y.; Chen, W.; et al. Design and experiment of onboard laser time transfer in Chinese Beidou navigation satellites. *Adv. Space Res.* **2013**, *51*, 951–958. [CrossRef]
22. Tang, C.; Hu, X.; Zhou, S.; Guo, R.; He, F.; Liu, L.; Zhu, L.; Li, X.; Wu, S.; Zhao, G.; et al. Improvement of orbit determination accuracy for Beidou Navigation Satellite System with Two-way Satellite Time Frequency Transfer. *Adv. Space. Res.* **2016**, *58*, 1390–1400. [CrossRef]
23. Schlicht, A.; Hugentobler, U.; Marz, S.; Seel, S.; Biller, P. Concept for continuous wave laser ranging and time transfer to Galileo using optical two-way links. In Proceedings of the 7th International Colloquium on Scientific and Fundamental Aspects of GNSS, Zurich, Switzerland, 4–6 September 2019.
24. Allan, D.W. Time and frequency (time-domain) characterization, estimation, and prediction of precision clocks and oscillators. *IEEE Trans. Ultrason. Ferroelectr. Freq. Control* **1987**, *34*, 647–654. [CrossRef]
25. Dach, R.; Lutz, S.; Walser, P.; Fridez, P. (Eds.) *Bernese GNSS Software Version 5.2*, User Manual; Astronomical Institute, University of Bern, Bern Open Publishing: Bern, Switzerland, 2015; ISBN 978-3-906813-05-9. [CrossRef]
26. Duan, B.; Hugentobler, U.; Selmke, I. The adjusted optical properties for Galileo/BeiDou-2/QZS-1 satellites and initial results on BeiDou-3e and QZS-2 satellites. *Adv. Space Res.* **2019**, *63*, 1803–1812. [CrossRef]
27. Fernández, F.A. Inter-satellite ranging and inter-satellite communication links for enhancing GNSS satellite broadcast navigation data. *Adv. Space Res.* **2011**, *47*, 786–801. [CrossRef]
28. Boehm, J.; Werl, B.; Schuh, H. Troposphere mapping functions for GPS and very long baseline interferometry from European Centre for Medium-Range Weather Forecasts operational analysis data. *J. Geophys. Res.* **2006**, *111*, B02406. [CrossRef]
29. Boehm, J.; Niell, A.; Tregoning, P.; Schuh, H. Global Mapping Function (GMF): A new empirical mapping function based on numerical weather model data. *Geophys. Res. Lett.* **2006**, *33*, L07304. [CrossRef]
30. Marini, J.W.; Murray, C.W. *Correction of Laser Range Tracking Data for Atmospheric Refraction at Elevations above 10 Degrees*; NASA Technical Rep. X-591-73-351; NASA/Goddard Space Flight Center: Greenbelt, Maryland, USA, November 1973.
31. Mendes, V.B.; Pavlis, E.C. High-accuracy zenith delay prediction at optical wavelengths. *Geophys. Res. Lett.* **2004**, *31*, L14602. [CrossRef]
32. Boehm, J.; Heinkelmann, R.; Schuh, H. Short Note: A Global model of pressure and temperature for geodetic applications. *J. Geod.* **2007**, *81*, 679–683. [CrossRef]
33. Fliegel, H.F.; Gallini, T.E.; Swift, E.R. Global positioning system radiation force model for geodetic applications. *J. Geophys. Res.* **1992**, *97*, 559–568. [CrossRef]
34. Springer, T.A.; Beutler, G.; Rothacher, M. A New Solar Radiation Pressure Model for GPS. *Adv. Space Res.* **1999**, *23*, 673–676. [CrossRef]
35. Montenbruck, O.; Gill, E. *Satellite Orbits—Models, Methods, Applications*; Springer: Berlin/Heidelberg, Germany, 2005; ISBN 3-540-67280-X.
36. Arnold, D.; Meindl, M.; Beutler, G.; Dach, R.; Schaer, S.; Lutz, S.; Prange, L.; Sosnica, K.; Mervart, L.; Jäggi, A. CODE's new solar radiation pressure model for GNSS orbit determination. *J. Geod.* **2015**, *89*, 775–791. [CrossRef]
37. Kur, T.; Liwosz, T. Simulation of the Use of Variance Component Estimation in Relative Weighting of Inter-Satellite Links and GNSS Measurements. *Remote Sens.* **2022**, *14*, 6387. [CrossRef]